

~~CONFIDENTIAL~~  
~~CONFIDENTIAL~~

Copy No. 1

MASS. INST. OF TECHNOLOGY  
APR 22 1960  
LIBRARY

ERRORS IN ANGLE RADAR SYSTEMS  
CAUSED BY COMPLEX TARGETS

DECLASSIFIED

*per*

by

*Letter DSC-42:GEC/4*

JAMES BROWNE ANGELL

*U.S. Navy*

*Bureau Navy Weapons*

S.B., Massachusetts Institute of Technology

*dated*

(1946)

*8 March 1960*

S.M., Massachusetts Institute of Technology

(1946)

**DECLASSIFIED**

SUBMITTED IN PARTIAL FULFILLMENT OF THE  
REQUIREMENTS FOR THE DEGREE OF  
DOCTOR OF SCIENCE

at the

MASSACHUSETTS INSTITUTE OF TECHNOLOGY

(1951)

Signature of Author .....

*J. B. Angell*  
Department of Electrical Engineering, Oct. 3, 1951

Certified by .....

*J. B. Angell*  
Thesis Supervisor

.....  
Chairman, Departmental Committee on Graduate Students

~~CONFIDENTIAL~~

~~CONFIDENTIAL~~

Abstract of Report on  
ERRORS IN ANGLE RADAR SYSTEMS CAUSED BY COMPLEX TARGETS

by James B. Angell

Submitted for the degree of Doctor of Science in the  
Department of Electrical Engineering on October 3, 1951

Direction-indicating radar systems that are used for determining the position of a target very precisely are subject to errors from a number of sources, any of which tends to decrease the accuracy of the indications. One of the principal causes of these errors when the target is close to the radar is the complex nature of the radar reflections from the target. In most cases the target does not have a simple configuration, such as an infinitesimal point or a sphere; as a result, the apparent center of reflection, which is the apparent target location as determined by a radar system with zero time of response, wanders about in the vicinity of the target, and can even pass outside the physical limits of the target. This wander of the apparent center of the target is quite apart from those errors produced in any of the various sequential-lobe-comparison systems by amplitude fluctuations; it is present with all types of radar systems.

Various analytical approaches, based on different sets of approximations, indicate that the wander of the apparent target center affects single-lobe, lobe-comparison, and phase-comparison systems to roughly the same extent. When a target is sufficiently far from a radar to span only a negligibly small portion of a lobe-width of the antenna pattern, the system, regardless of its type, indicates the target direction as the normal to the phase front at the antenna. At shorter ranges, the magnitudes of the errors with lobe-comparison systems and phase-comparison systems are somewhat different, although, for systems with the same receiving-antenna aperture, there is little to favor one type of system over the other. When other conditions are held fixed, the magnitude of wander almost always decreases, though not necessarily linearly, as the aperture size is increased. With a phase-comparison system, care must be taken in the design of the measurement sections to insure adequate bandwidth to prevent the system from going blind, due to

[REDACTED]

wander, when the target approaches close to the radar.

One of the analyses shows that no relation necessarily exists between the amplitude of the radar return and the wander of the apparent target center. This fact is demonstrated by proving that Maxwell's equations are satisfied by a two-dimensional field with any scattering pattern and a circular wave-front. Consequently, no conclusive data on wander can be obtained from records of amplitude fluctuations.

To obtain experimental data on wander and amplitude fluctuations, a series of tests were made with an X-band phase-comparison system and a variety of aircraft targets in flight. Voltage spectra of the wander data show that with large targets, frequency components above 40 cps can exist. However, for reasonably long sections of data, the upper half-voltage points of the spectra never occurred at frequencies above 20 cps. The zero-frequency ordinates of the wander spectra varied between 2.5 and 8 feet/ $\sqrt{\text{cps}}$ , with an average value of about 4.5 feet/ $\sqrt{\text{cps}}$  (the total rms wander in a 1-cps band). It was observed that the apparent center of reflection of a target consisting of two aircraft flying in close formation sometimes moves rapidly over distances greater than the aircraft separation. At other times, the mean of its position tends to lock on first one, then the other, target in a random manner, with the apparent center continuously oscillating about the average position.

[REDACTED]

**CONFIDENTIAL**

TABLE OF CONTENTS - I

List of Figures	page vi
List of Symbols	ix
Acknowledgment	xiii
1. Introduction	1
1.1 Sources of Angular Errors	2
1.2 Summary of Previous Studies	4
1.3 Scope of the Research Program	8
2. The Analysis of Wander	10
2.1 System Comparison from Signal Distribution at Receiver	14
2.11 Direction Indication of Single-lobe System	17
2.12 Direction Indication of Lobe-comparison System	17
2.13 Equivalence of Lobe-amplitude- and Simultaneous-lobe- Comparison Systems	18
2.14 Direction Indication of Phase-comparison Systems	20
2.15 Comparison of Systems with Target at Long Range	21
2.16 Comparison of Systems with Intermediate Target-ranges	22
2.2 Analysis of a Two-point Target	24
2.21 Wander of the Apparent Center of a Two-point Target	25
2.22 Error-detector Output with a Two-point Target	29
2.23 Comparison of Systems with a Two-point Target	34
2.3 Phase-detector Output with a Multi-point Target	35
2.31 Probability Density of Phase-detector Output	36
2.32 Average Magnitude and RMS of Output	41

**CONFIDENTIAL**



## TABLE OF CONTENTS - II

2.4	Relations Between Signal Amplitude and Wander	45
2.41	The Field at a Fixed Distance from a Target	46
2.42	Image Points in the w-plane	47
2.43	Minimum Phase for a Given Amplitude Pattern	49
2.44	Maximum Wander with a Given Amplitude Pattern	50
2.5	Further Studies of Wander with Phase-comparison Systems	52
2.51	Bandwidth Requirements with Targets at Short Range	53
2.52	Reduction of Large Errors with Partial Amplitude Limiting	57
3.	The Experimental Determination of Wander	62
3.1	X-band Wander Tests	63
3.11	Equipment for Obtaining Data	63
3.12	Description of Recorded Data	67
3.13	Method of Data Analysis	71
3.14	Spectra of Data on Single Targets	76
3.15	Multiple-target Data	89
3.16	Discussion of Spectra	94
3.2	S-band Tests	99
3.21	Data Recording Setup	101
3.22	Spectra of S-band Data	102
3.23	Discussion of S-band Data	107
4.	Conclusions	110

[REDACTED]

TABLE OF CONTENTS - III

5.	Recommendations for Further Research	113
5.1	Bandwidth Requirements of Phase-comparison Systems	113
5.2	Optimum Limiting Level	116
5.3	Properties of Wander in Wide-band Systems	117
5.4	Wander with Lobe-comparison Systems and Targets at Short Range	118
5.5	Doppler Frequencies in Target Echoes	119
5.6	Probability Density Distribution of Wander	120

APPENDICES

A	Pointing Errors Derived from Signal Distribution at Receiver	121
A-1	Direction Indication of Single-lobe System	121
A-2	Direction Indication of Lobe-comparison System	123
A-3	Direction Indication with First-order Aperture Illumination	125
B	Descriptions of Various Phase-comparison Systems	130
B-1	Nulling Servo System	130
B-2	Single-sideband-modulator System	130
B-3	Interferometer System	132
B-4	Doppler-difference System	132
C	Analysis of a Two-point Target	135
C-1	Position of Apparent Target Center	135
C-2	Error-detector Output with Radar Pointing at Stronger Point	139
D	Phase-detector Output with a Multi-point Target	150

[REDACTED]

## TABLE OF CONTENTS - IV

D-1	Phase-detector Output with Limiting	150
D-2	Average Magnitude and RMS of Output	153
D-3	Results for a Uniformly Distributed Target	154
D-4	Phase-detector Output with Errors in Aiming	155
E	General Expressions for the Signal Scattered by a Target	160
E-1	Fourier Series Representation of the Signal	160
E-2	Multiple Product Equivalent of Fourier Series	161
F	Radar Equipment for Recording Data	163
F-1	I-F Amplifier	163
F-2	Gater and Amplitude Detector	165
F-3	Automatic Gain Control	167
F-4	Automatic Frequency Control	167
F-5	Manually Tracked Range-gate Generator	167
F-6	Pregater	171
F-7	21-Mcps Oscillator	171
F-8	Mile Marker	171
F-9	Video Adder	174
F-10	12-Mcps Limiter and Amplitude Detector of Phase Measuring Unit	174
F-11	12-Mcps Pulse Phase Detector of Phase Measuring Unit	178
F-12	Pulse Stretcher and D-C Amplifier of Phase Measuring Unit	180
G	Spectrum Analyzer	182
G-1	Special Circuits	182
G-2	Operational Procedure	184



TABLE OF CONTENTS - V

H	Data Recording and Editing	188
H-1	Recording and Playback Equipment	188
H-2	Editing Procedure	192
J	Biographical Note	194
	References	195



## LIST OF FIGURES

<u>Number</u>	<u>Title</u>	<u>Page</u>
2-1	Signal Distribution at Uniform Aperture of Receiving Antenna	16
2-2	Errors in Radar Trackers - First Order Aperture Illumination	23
2-3	Position of Apparent Center, Two-point Target - Single-lobe Radar	26
2-4	Position of Apparent Center, Two-point Target - Lobe-comparison Radar	26
2-5	Position of Apparent Center, Two-point Target - Phase-comparison Radar	27
2-6	Average Magnitude and RMS of Wander - Two-point Target	28
2-7	Error-detector Output of Lobe-comparison Radar - Fast-acting AGC - Two-point Target	31
2-8	Error-detector Output of Lobe-comparison Radar - Slow-acting AGC - Two-point Target	31
2-9	Error-detector Output of Phase-comparison Radar with Limiting - Two-point Target	32
2-10	Error-detector Output of Phase-comparison Radar without Limiting - Two-point Target	32
2-11	Average Magnitude and RMS of Error-detector Output - Two-point Target	33
2-12	Multi-point Target	37
2-13	Vector Diagram of Received Signals	37
2-14	Average Magnitude and RMS of Error-detector Output of Phase-comparison Radar - Multi-point Target	42
2-15	Probability Density Function of Phase-detector Output - Multi-point Target	60
3-1	Block Diagram of Radar System for Recording Target Noise Data	64

## LIST OF FIGURES - II

3-2	Photograph of Receiving and Measuring Sections of Radar System	65
3-3	Wander of Apparent Radar Center of B-29 and AT-11 Aircraft	70
3-4	Block Diagram of Spectrum Analyzer	73
3-5	Photograph of Spectrum Analyzer and Playback Equipment	75
3-6	Spectra of Wander and Signal Amplitude with B-29 Target	78
3-7	Spectra of Wander and Signal Amplitude with AT-11 Target	79
3-8	Spectra of Wander and Signal Amplitude with C-46 Target	80
3-9	Spectra of Wander and Signal Amplitude with B-26 Target	81
3-10	Spectra of Wander and Signal Amplitude with AT-6 Target	82
3-11	Spectra of Wander and Signal Amplitude with F-84B Target	83
3-12	Spectra of Data from Successive Similar Runs	84
3-13	Spectra of Successive 3-second Sections of Data from Broadside B-29 Target	85
3-14	Spectra of Wander and Signal Amplitude with AT-6 Target and Circularly Polarized Receiving Antennas	87
3-15	Spectra of Data Recorded with no Limiting	88
3-16	Spectra of Data with B-29 Target at Various Ranges	90
3-17	Wander of Apparent Radar Center of Multiple Target	91
3-18	Spectra of Wander and Signal Amplitude with Multiple Target	92
3-19	Power Spectral Density of Radar Interference as a Function of Target Range	96
3-20	S-band Data Recording Setup	101
3-21	Spectra of S-band Data with PB4Y-2 Target	105
3-22	Spectra of S-band Data with F6F Target	106
A-1	Output Received Signal Strength for a Uniform Aperture - First Order Aperture Illumination	127

## LIST OF FIGURES - III

A-2	Error-detector Output for Lobe-comparison System - First Order Aperture Illumination	128
B-1	Block Diagram of System with Nulling Servo	131
B-2	Block Diagram of System with Single-sideband Modulator	131
B-3	Block Diagram of Interferometer System	133
B-4	Block Diagram of Doppler-difference System	133
C-1	Vector Diagram for Computing Error-detector Output - Lobe-comparison Radar - Two-point Target	142
F-1	Schematic of 33-12 Mcps. I-F Amplifier	164
F-2	Schematic of Balanced Gater	166
F-3	Schematic of AGC Amplifier and Filter	168
F-4	Schematic of Automatic Frequency Control	169
F-5	Schematic of Range-gate Generator	170
F-6	Schematic of Pregater	172
F-7	Schematic of Video Adder and 21-Mcps Oscillator	173
F-8	Schematic of Mile Marker	175
F-9	Schematic of Limiter, Linear Amplitude Detector, and Buffer of Phase Measuring Unit	177
F-10	Schematic of Phase Detector, Pulse Stretcher, and D-C Amplifier of Phase Measuring Unit	179
G-1	Schematic of 0-200 cps Spectrum Analyzer	183
H-1	Schematic of Frequency Modulator and Demodulator for Recording	189
H-2	Schematic of Power Supply for F-M Data Speedup System	190

## LIST OF SYMBOLS - I

<u>Symbol</u>	<u>Meaning</u>	<u>Section where First Used</u>
A	Ratio of signal strengths from a two-point target	C-1
$A_1, A_2$	Amplitudes of signals $S_1, S_2$ , respectively	2.31
$A_J$	Amplitude of any signal J	2.1
$a_n$	Coefficients in Fourier series for S	2.41
$A(x)$	Amplitude distribution along 'x'	2.1
$B_n$	Constants in Fourier series expansion of $A_S$	2.43
$b_n$	Constants in multiple-product expansion of $A_S$	2.43
$C_0, C_1$ , etc.	Constants for mathematical convenience	D-4
$c_k$	Coefficients in Maclaurin series expansion of $S(w)$	2.44
D	$S_2 - S_1$	2.31
d	Aperture size (antenna spacing for phase-comparison radar)	2.1
$D_p$	Component of D that is 90 degrees out of phase with $S_1$	2.31
g	Ratio of gains of two i-f amplifiers	C-2
$G(x)$	$\phi(x) + \frac{2\pi\beta}{\lambda} x$ , the phase distribution along an antenna aperture	2.1
H	Standardized angular error	2.16
$H_n^{(1)}$	Hankel function of the first kind	2.41
$H_p$	Standardized angle between the normal to a phase front and the direction of propagation	2.16
$H_q$	Standardized squint angle	C-1
$H_s$	Standardized angle subtended by a target	C-1
$I[ ]$	Imaginary part of a complex function	2.12
$I_b$	Average value of $i_b$	C-2
$i_b$	Plate current	C-2



## LIST OF SYMBOLS - II

j	$(-1)^{\frac{1}{2}}$	2.1
k	$2\pi d/\lambda R$	2.31
$K_1, K_2$	Constants in expression for S	C-1
L	Length of a uniformly distributed target	2.32
M	Difference between $S_a$ and $S_b$	2.13
$m_1, m_2$	Modulation coefficients	C-2
$M_p$	Component of M in phase with P	2.13
N	Limit of a summation or multiple product	2.31
P	Sum of $S_a$ and $S_b$	2.13
Q	Defined by the relation $Q^2 = \overline{ e^{jkyn} - 1 ^2}$	2.31
R	Range of a target from the radar receiver	2.21
R[ ]	Real part of a complex function	2.12
r	Magnitude of 'w'	2.41
$r_n$	Magnitude of $w_n$	2.41
S	Signal in complex notation	2.1
s	Spacing of the two points of a two-point target	2.21
S(w)	S as a function of the complex variable 'w'	2.41
$u_0, u_1, \text{etc.}$	Constants in the expansion of $\phi(x)$	2.15
$V_1, V_2$	Components of $V_n$ with a multi-point target	D-4
$v_0, v_1, \text{etc.}$	Constants in the expansion of A(x)	2.15
$V_m$	Phase-detector output with amplitude limiting	2.31
$V_n$	Phase-detector output without amplitude limiting	2.31
w	Complex variable	2.41
$w_n$	Constants in the multiple-product expansion of S(w)	2.41
x	Coordinate along an antenna aperture	2.1

## LIST OF SYMBOLS - III

$x_0, x_1$	Variables for mathematical convenience	D-4
$y$	Dummy variable for 'x'	2.11
$Z$	Error-detector output, referred to a linear coordinate at the target	2.22
$z$	Coordinate of the position of the apparent radar center of a target	2.21
$z_0$	Distance of the target center from the radar axis	2.52
$z_n$	Coordinate of the position of a point source 'n' on a multi-point target	2.31
$\beta$	Angle of antenna axis with respect to the direction of propagation	2.1
$\beta_p$	Angle of normal to phase front with respect to direction of propagation	2.1
$\beta_q$	Angle between antenna axis and either lobe axis of a lobe-comparison system, the squint angle	2.1
$\theta$	Angle about a target	2.41
$\theta_n$	Phase of $w_n$	2.41
$\theta'_n$	Phase constants in the Fourier series expansion of $A_s$	2.43
$\lambda$	Free-space wavelength of propagation	2.1
$\mu$	Phase difference of the signals from a two-point target	2.21
$\mu_n$	Relative phase of a point source 'n' on a multi-point target	2.31
$\phi_0$	Peak value of sinusoidal phase difference	2.51
$\phi_1, \phi_2$	Phases of signals $S_1, S_2$ , respectively	2.31
$\phi_d$	$\phi_2 - \phi_1$	2.31
$\phi_s$	Phase of the signal $S$	2.1
$\phi(x)$	Phase distribution along 'x'	2.1
$\psi$	Elementary wave function	2.41
$\omega_r$	Angular frequency of a reference carrier	2.51

## LIST OF SYMBOLS - IV

$\omega_w$	Angular frequency of sinusoidal wander	2.51
$\triangleq$	Equal by definition of some explicit quantity	2.1

## ACKNOWLEDGMENT

The author is indebted to many persons who gave assistance during the course of this research program. Particular appreciation is due Professor Henry J. Zimmermann for his help in planning the program, for his suggestions regarding many aspects of the research, and for his valuable criticism of the final report. Gratitude is also expressed to Professors L. J. Chu, Y. W. Lee, and S. J. Mason for their suggestions and advice on many phases of the analytical and experimental studies.

The author would also like to thank the many persons whose assistance made possible the two series of flight tests for obtaining the experimental data, including members of the guidance group of Project Meteor in the Research Laboratory of Electronics, the personnel of the Chincoteague Naval Air Ordnance Test Station, and the staff of the Bedford Flight Facility of the M. I. T. Instrumentation Laboratory. To Messrs. Charles Rowe and Dwight Brown the author is especially grateful, for their services in running the spectrum analyzer and tracking the X-band transmitting antenna on the open top of a tower during the middle of a Cambridge winter.

Finally, the author would like to make known his appreciation of the many facilities of the Research Laboratory of Electronics made available to him, and for the splendid cooperation extended by the drafting and photographic services in preparing the report.

ERRORS IN ANGLE RADAR SYSTEMS CAUSED BY COMPLEX TARGETS

1. INTRODUCTION

One of the principal functions of many types of radar systems currently being designed or in use is the accurate determination of the position of a specific target. The main applications of such systems are in the fields of gunfire control and guided missiles, where accuracies of the order of magnitude of a few yards are required.

The position of a target is determined by a radar set through the measurement of two quantities, the range and the direction to the target. The method used in determining range is considerably different from that used for finding direction. An active pulse-radar set is able to measure range by noting the time required for a pulse of radio-frequency energy to reach a target and return. The measurement of time, even the short intervals involved in radar ranging, is a very exact science, with the result that range can be determined with good precision.

The direction of a target is found with some radar systems by orienting an antenna with a narrow beam pattern so as to obtain maximum received signal from the target. A considerably more accurate direction indication is obtained by other systems in which the antenna has a pattern with two narrow, independent lobes, which are generated by essentially separate feeds and aimed in slightly different directions, for each measurement plane. With such a system, the antenna is oriented in the direction which gives equal signals in the two feeds for each measurement plane. In a third class of systems, the difference in phase of the signals received by adjacent, similar antennas is used as the basis for direction indication.

In many applications, it is desired that a radar set furnish the angular information with greater accuracy than that of the range data. A good example is the case of a homing missile flying a constant-true-bearing collision course towards its target. The basic information needed by the computer from the radar is the time rate-of-change of the angle between the line-of-sight from missile to target and the missile axis;<sup>1</sup> the accuracy requirements for any range data that might be needed by the computer are less severe than those for the angular information. There are a number of sources of error which are encountered in radar direction-finding, with the result that angular measurements, in terms of feet at the target, are apt to be less precise than range measurements. From these two facts it is evident that a good understanding of the various sources of angular errors is needed in designing radar systems with optimum performance as direction indicators.

#### 1.1 SOURCES OF ANGULAR ERRORS

Significant errors in direction-indicating radar systems can be produced by any one or more of four main sources.<sup>2</sup> These are:

- 1 - Thermal (Johnson) noise
- 2 - Tracking-servo noise, such as backlash, time lag, or dead spaces
- 3 - Amplitude modulation of the echo by the target
- 4 - Fluctuations in the direction of the normal to the phase-front of the reflected signal from a target.

The effects of thermal noise are well known. Its statistical properties have been thoroughly explored, and the errors it produces have been computed. The effects of thermal noise are important near maximum system range, where the echo from the target is weak.

The various types of servo noise give rise to angular errors whose magnitudes are independent of target range. They are a direct result of inadequacies of system design, and can probably be kept within any desired limits through sufficient care in design. Their properties can be studied with any particular system by means of an appropriate laboratory test setup.

Amplitude fluctuations of the return from a target may cause serious errors in certain types of direction-indicating systems. A system, such as a conical-scan radar, which makes sequential measurements of the signals received from a target by antennas pointed in different directions, is susceptible to errors from this source. Monopulse, or simultaneous-lobing, radars virtually eliminate errors from this source.

The errors produced by fluctuations in the normal to the phase front of the reflected signal appear to some extent in all systems and at any range. The magnitude and statistical properties of these errors are comparable in any type of system using a given transmitter frequency. These errors have been listed by various investigators studying them under the titles of angular scintillation, glint, variation in apparent angle of arrival, wander of apparent center of reflection, and possibly others. The concepts implied by the name 'wander of apparent center' seem to fit the actual phenomena most accurately, so that this phrase will be used subsequently in referring to errors from this cause.

Another possible source of errors, which might become serious in direction-indicating radar systems at very great target ranges, is inhomogeneity in the propagation medium between the radar and its target. Any nonuniformity could cause a refraction of the signal to or from the target, and displace the apparent target from its true position. Studies made of the

effects of such inhomogeneity on radio direction-finders indicate that the effects are unimportant for ranges that are generally used by fire-control and guided-missile radars.

This report is devoted primarily to the study of the wander of the apparent center of reflection of a radar aircraft target. The apparent center of reflection, which is the point to which an instantaneous radar tracker would point, moves about in a more or less random manner in the vicinity of the actual target. It does not necessarily remain within the physical limits of the target, but can occasionally pass well outside these limits. The speed of movement of the apparent center can be high; for aircraft targets, frequency components of the motion as high as 100 cps. or more are possible. When the angular deviations caused by wander are small compared with a lobe-width of the radar-antenna pattern, so that all operation is within the linear portion of the characteristic of the radar error-detector, the average magnitude of the deviations for a given target is inversely proportional to range. In other words, the average magnitude of the deviations, when referred to a linear dimension at the target, is approximately constant, regardless of range. As a result, the wander problem is most important at short range. It is of particular importance in the field of radar homing missiles, which require accurate information on target position in the final portion of their flight.

## 1.2 SUMMARY OF PREVIOUS STUDIES

The first studies of errors in electromagnetic direction-indicators were performed in connection with low-frequency radio direction-finders. Most of the errors in these low-frequency systems are such that they must be handled empirically. However, as early as 1923, an attempt at a mathematical



[REDACTED]

explanation of serious errors sometimes observed was made by Heiligtag.<sup>3, 4</sup> He explained the phenomenon now known as the Heiligtag effect by hypothesizing that when two waves of comparable amplitude from the same source arrive at the receiver from slightly different directions, one of them may be split into two components, one parallel to and one perpendicular to the other wave. When the parallel component and the other wave are of the same magnitude and opposite phase, they cancel, and only the perpendicular component remains.\*

Great increases in the effort put into the study of the nature of radar-target echoes have accompanied the rapid growth of radar techniques since 1940. One of the first of the characteristics of echoes to be investigated in detail was the amplitude of the return signal. The Radiation Laboratory Series presents examples of the range of amplitude fluctuations that might be expected from aircraft targets. Polar plots are included of the measured S-band return power reflected from various airplanes on the ground, plotted as a function of the azimuth viewing angle.<sup>5A</sup> For a B-26 aircraft, the power received often changed as much as 15 db. for a change of only 1/3 degree in aspect angle.<sup>5B</sup> There are also shown polar plots of the fractional modulation of the return signal caused by rotation of the propellers of the aircraft. Other studies have been concerned with the time dependence of the amplitude of echoes from aircraft in flight. Project Sambo at the Radiation Laboratory was concerned with the identification of aircraft by noting the principal frequency components in the modulation of the echo return.<sup>6, 7</sup> The amplitudes of successive pulses of radar target return have

---

\*Such an argument is valid only when the receiving antenna is of practically zero wavelengths dimensions, because it is not justifiable in general to split a wave into two components travelling at right angles.

[REDACTED]

been recorded photographically in various tests.<sup>8, 9</sup> The effects on tracking of a conical-scan radar produced by amplitude fluctuations have been computed by a number of writers.<sup>2, 10, 11</sup>

Experimental studies of the actual tracking performance of complete radar systems in actual use have been made for many systems.<sup>12, 13, 14</sup> Most such studies have been made with a bore-sighted motion-picture camera on the antenna mount. The analysis of such data gives the nature of the radar jitter as filtered by the tracking-servo system. The problem of tracking over water, where the presence of a fairly definite image can be very detrimental to performance, has also been investigated.<sup>15</sup> There exists a report on the theoretical and actual behavior of a conical-scan radar while tracking two aircraft in close formation.<sup>9</sup> The error-detector output is treated analytically as the algebraic sum of the outputs due to each aircraft individually. It is shown that this treatment gives a fair indication of the rms. value of an actual output. The results of both the experimental and the analytical studies show the radar pointing indecisively at or between the targets until their angular separation is sufficiently great that the radar can resolve them.

Although the study of wander has received considerable attention within the past six years, the results obtained have been by no means exhaustive. The general mathematical background for an analytical solution was established by Crout and Bothwell,<sup>16</sup> and some simple examples of the application of their method are shown in their report. In another report, Stibitz has determined the position of the apparent target center of a two-point target at long range with a linear lobe-comparison system.<sup>17</sup> Delano has performed an admirable statistical derivation of the wander of the apparent center of a target with

an infinite number of point reflectors, as determined at long range by a linear lobe-comparison radar.<sup>11</sup>

The experimental determination of wander associated with aircraft targets has been reported by few investigators up to the present. Some data on the output of the error detector of a conical-scan c-w radar optically aimed at the target are available in which sufficiently short ranges were used that the errors due to amplitude modulation were relatively small.<sup>18</sup> These data were filtered by a 0.1 second low-pass filter, so that the actual rms. wander cannot be evaluated. Meade has recorded and spectrum-analyzed the output of the error detector of a simultaneous-lobing radar. In this setup, the output which might result from tracking inaccuracy was removed by subtracting from the output the voltage from a second error detector operating on a beacon signal from the target. The results of this program promise to be extremely pertinent, although at present only a small amount of data has been published.<sup>2</sup>

The problem of reducing the errors produced in radar tracking systems by target echo fluctuations has been attacked in many ways. One method involves the use of improved methods for the detection of angular errors. An example of this method is the development of simultaneous lobing systems, a class of monopulse systems, in which the amplitudes of the signals received by two overlapping lobes of an antenna system are measured simultaneously, rather than sequentially.<sup>21, 22</sup> Such systems eliminate the errors resulting from pure amplitude modulation of the target echo return. Another illustration is the use of a multiple-antenna phase-comparison system.<sup>23, 24</sup> For example, a three-antenna system can be used to obtain correct data on the angle-of-arrival of two waves from different points, although it would be

inadequate for three waves. Such a system probably has its greatest use in multiple-target problems or in tracking low-flying targets over smooth surfaces, and is useless for reducing wander from a single target.

Another technique of error reduction is based on the use of a frequency filter in the output of the error detector of any type of system. In this method, the frequency characteristics of the filter, which may be the servo system of a tracker, are specified in accordance with some criterion for system performance, such as minimum mean-squared error or maximum hit probability.<sup>10B, 19, 20</sup> In order to determine the filter characteristics, it is necessary to know the statistical properties of the error-detector output caused by target-echo fluctuations and of the motion of the tracked target.

### 1.3 SCOPE OF THE RESEARCH PROGRAM

The research reported in this paper can be divided into three principal categories. In the first place, experimental data was taken to determine the nature of wander of the apparent radar center of actual aircraft targets in flight. Very little information of this sort has been available up to the present, and the demand for it is constantly growing. Of great interest are the rms. values and the frequency spectra of the wander of various types of aircraft, particularly the low-frequency ordinates of the spectral density curves. These data are required by those who are interested in optimizing the performance of radar tracking systems by specifying the filtering characteristic of the servo system.

Secondly, an analytical evaluation was made of the effects of wander on a phase-comparison system of radar direction-finding. cursory examination of the problem indicates that the response of such a system to wander cannot necessarily be predicted from the response of a more conventional system. The

use of this type of system in obtaining the experimental data, plus its use in the Meteor guided missile and other recent applications, have accentuated the need for such an evaluation.

Finally, a comparison is presented of the errors produced by wander in various types of radar direction-indicating systems, namely, single-lobe (searchlight), lobe-comparison, and phase-comparison systems. For the most part, the comparison is focussed on the inherent capabilities and limitations of the several methods of angular measurement, and not on particular system designs.

The analytical program is presented in Chapter 2. The analyses furnish a means for obtaining some idea as to the order of magnitude and properties of wander. They form the most important basis for comparing the effects of wander on the various systems. In addition, they indicate very clearly the quantity which should be measured to obtain the desired information on wander, thus providing the necessary justification for the methods actually used in obtaining data. The details of the more involved analyses are omitted from the chapter on analytical studies, and are presented in Appendices A through E at the end of the report.

The experimental program will be described in Chapter 3. The spectra of wander obtained with an X-band system and various aircraft constitute the most significant information in this chapter. A general description of the radar systems used for obtaining the data is included, although the details of actual circuitry and operation are left to Appendices F, G, and H.

## 2. THE ANALYSIS OF WANDER

Various analytical approaches can be made to the problem of determining the nature of the random wandering of the apparent center of reflection of a radar target. Because of the complexity of the processes in which any of the various approaches becomes involved, none of them can be conveniently carried through to exhaustive completion. Nevertheless, each of the approaches covers some aspects of the problem which the others do not, so that it is worth while to examine them all. Furthermore, by the time they all have been covered, a fairly thorough treatment of most of the aspects of wander has been made. Before proceeding with the analyses, a qualitative discussion of the phenomenon of wander will be presented.

Precise Description of Wander The apparent radar center of a target is defined as that point in the vicinity of a target to which an ideal radar tracking system would point. An ideal system is defined as a linear system perfect aiming, instantaneous response to angular changes, freedom from thermal noise, and complete insensitivity to amplitude modulation of the target echo. Expressed in another way, if the target were perfectly rigid and stationary, the apparent center is the point to which a radar system would point on the average. As the target moves, either as a unit or by slight changes in shape, the apparent center moves about. The mean value of the positions of the apparent center is most probably near the actual center of the target. It is the motion of the apparent radar center, relative to this mean value or to the geometrical center (it makes little difference which is considered), that is called wander.

The wander is a direct result of the complex shapes which are possessed

~~CONFIDENTIAL~~

by almost all actual targets. There is no wander at all with simple target shapes, such as a point reflector or an ideal spherical reflector.

Wander inherently affects all types of tracking systems, though not to exactly the same extent in all cases. At very long ranges, when actual antenna patterns can be replaced by linear approximations, the wander associated with a given target is the same, regardless of the type of system used. At shorter ranges, in those cases when antenna-pattern nonlinearities cannot be ignored, slight differences arise which may favor one system more than another.

At this point it is desirable to note the difference between wander and the output of the error detector of a linear system. The wander indicated by any system is almost independent of the type of system, while the error-detector outputs of various systems under identical conditions may be vastly different. This is well illustrated by some of the results of the two-point target analyses.

There are two different models of targets which can be used in explaining and analyzing wander, and unfortunately they do not lead to the same results. Either of the models represents a possible physical situation, though one is generally more feasible. The first model is constructed by replacing the actual target by a point source (probably amplitude modulated) which 'wanders' (from whence the term wander) about the target in the same fashion as the apparent center of the actual target. Such a model is suitable for representing specular reflection, or glint, off first one, then another, (and so on) predominant area of a target. This kind of model can never justifiably show the apparent center off the physical target.

The second, and usually more realistic, model can be explained if one

~~CONFIDENTIAL~~

~~CONFIDENTIAL~~

considers the target to be made up of two or more small reflecting areas distributed over the target, each having a relatively broad scattering pattern.\* The target can then be replaced, with some restraint on the magnitude of its rotations, by a number of point sources or reflectors, each fixed in position and giving a signal of constant amplitude. In this case, the wander results from interference of the various signals at the receiving antenna. With this model the apparent center can pass well outside the physical boundary of the target.

Other differences in the type of wander associated with either model will become apparent later on. For example, let there be constructed two models, one of each type, such that both give the same wander at very long range. At relatively short range, when the receiving antenna system spans a significant fraction of a lobe width of the target scattering pattern, the two models may give substantially different wander, both in magnitude and in spectral density. Such differences make caution necessary in interpreting the results derived from the assumption of either model.

Analytical Approaches There are four methods by which the analysis will be attacked. In each of the approaches, the angle-determining element will be considered to be the receiving antenna system; the target illumination is to be obtained by an external, independent means, and is to be the same for all systems. Such an assumption is made partly for mathematical convenience, and partly because it represents the actual situation in many homing-missile and gunfire radar systems. In cases where the same antenna

---

\*A report by Stibitz<sup>17</sup> contains a very plausible qualitative discussion of the basis for assuming a multi-point target model, and of reasons for its greater realism.



[REDACTED]

system is used for transmitting and receiving, effective beamwidths are smaller and the magnitudes of wander frequently less than in one-way systems. Nevertheless, at very long ranges, the average magnitudes of wander for both the two-way and the one-way systems are approximately the same for any given target.

It is assumed that the desired quantity to be measured by any system is the position of the target, and not some other function of position, such as the angular rate-of-change of the line-of-sight to the target. This is the quantity which lobe-comparison systems are able to determine most conveniently. Phase-comparison systems are somewhat better suited to measure the angular rate-of-change rather than position. However, if the ambiguities which can arise with the latter systems are not important, or are resolved by determining the initial conditions, the phase-comparison systems can be considered as position indicators, as is done in Appendix B.

The four analytical approaches are introduced here in the order in which they will be presented.

- a. Comparisons based on Signal Distribution at Receiver. The forms of amplitude and phase distributions of the signal reflected from a target are assumed over the aperture of a radar receiving-antenna system. The expressions for indicated direction can then be established for various systems. The expressions for various systems are compared for simple forms of the distributions, which correspond to long and intermediate target ranges. The results are useful in showing the similarity of the various systems. At short ranges, evaluation of the expressions becomes hopelessly complicated.
- b. Wander with a Two-point Target. From the assumption of a two-point

CONFIDENTIAL

target with a definite, fixed ratio of signal strengths of the two points, the wander can be computed for various systems. The solutions, obtained graphically, indicate the magnitude and form of wander which can be expected at different ranges. A comparison of the various systems is possible in to very short ranges. The outputs of the error detectors of phase-comparison and lobe-comparison systems are also studied.

- c. Phase-detector Output with a Multi-point Target. The target consists of an infinite number of point reflectors distributed at random over a target. The expressions for the output of the phase-detector of a phase-comparison radar are then derived for systems with amplitude limiting and without amplitude limiting. The long-range results for the system with limiting show some of the properties of the wander associated with such a target.
- d. Amplitude-phase Relations from Maxwell's Equations. A particular solution of Maxwell's equations shows that there is no necessary relation between the amplitude scattering pattern of a reflector and the shape of the phase-front of the reflected energy. It can be inferred that no definite information on wander can be obtained by measuring the amplitude of signal echoes from a target. However, the maximum possible phase-front distortion that can accompany a given amplitude pattern is derived.

### 2.1 SYSTEM COMPARISON FROM SIGNAL DISTRIBUTION AT RECEIVER

A comparison of three types of radar direction-indicating receivers will be presented in this section. The phase-comparison system indicates the direction to the apparent center of a target by orienting in such a way that

CONFIDENTIAL

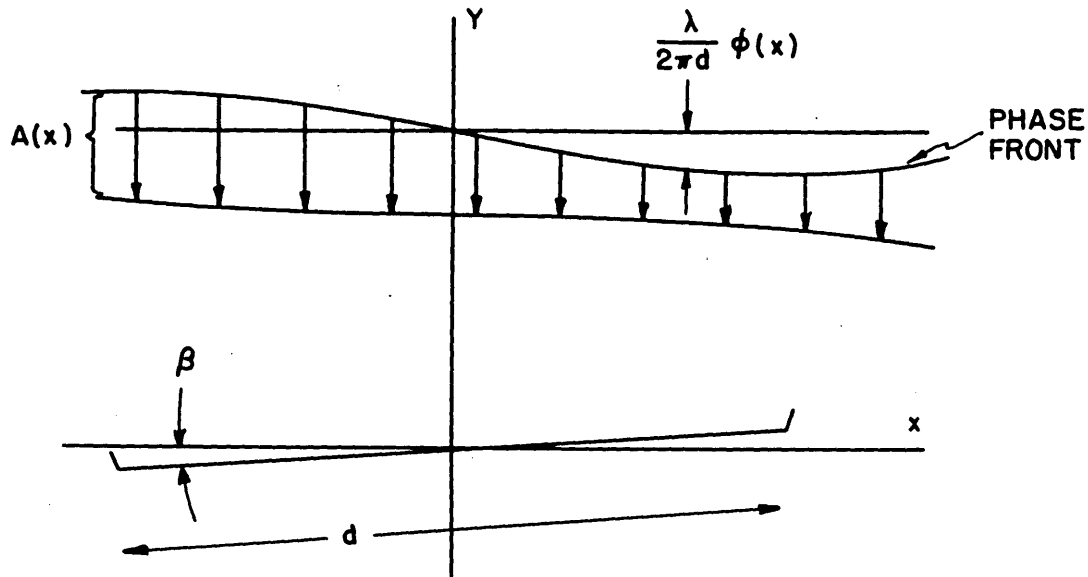
the phase difference of the signals received by two adjacent antennas is zero. The single-lobe system, sometimes referred to as a searchlight system, orients that lobe in the direction for maximum amplitude of received signal. The lobe-comparison system, which is assumed to have two overlapping lobes generated in the same aperture by separate feeds, equalizes the magnitudes of the signals in the two lobes for its direction indication. It is assumed that each of the latter two systems have a uniform aperture, which produces the well-known  $(1/H)\sin H$  lobe pattern.

The two antennas of the phase-comparison system are physically relatively small, so that they can be considered as omnidirectional. The phase and amplitude of the resultant signal received by either antenna are then equal to the phase and amplitude of the incident wave at the center of that antenna.

The expression for the signal received by the uniform aperture of the single-lobe system can be readily determined with the aid of Fig. 2-1. The uniform aperture is defined as one which transmits, with the same phase delay, to the antenna feed all the signal incident upon any infinitesimal portion of the aperture. As shown in Fig. 2-1, the direction of propagation is along the negative y-axis, the angle between the antenna axis and the y-axis is  $\beta$ , and the aperture dimension in this two-dimensional problem is  $d$ . The received signal  $S$  is then given by

$$S \triangleq A_s e^{j\phi_s} = \int_{-\frac{1}{2}d \cos \beta}^{\frac{1}{2}d \cos \beta} A(x) e^{j[\phi(x) + \frac{2\pi x}{\lambda} \sin \beta]} dx, \quad 2-1$$

where  $A(x)$  and  $\phi(x)$  are the distributions of amplitude and phase of the incident wave. In most applications, the lobe pattern is quite narrow, with the result that the maximum values of  $b$  that are of interest are small. No significant errors are introduced in these cases by writing



SIGNAL DISTRIBUTION AT UNIFORM APERTURE OF RECEIVING ANTENNA

Fig. 2-1

$$S = \int_{-\frac{1}{2}d}^{\frac{1}{2}d} A(x) e^{j[\phi(x) + \frac{2\pi\beta}{\lambda} x]} dx \triangleq \int_{-\frac{1}{2}d}^{\frac{1}{2}d} A(x) e^{jG(x)} dx, \quad 2-2$$

the second equality serving to define  $G(x)$ .

The signals in the two lobes of a lobe-comparison system are given by

$$S_{a,b} = \int_{-\frac{1}{2}d}^{\frac{1}{2}d} A(x) e^{j[\phi(x) + \frac{2\pi(\beta \pm \beta_q)}{\lambda} x]} dx \triangleq \int_{-\frac{1}{2}d}^{\frac{1}{2}d} A(x) e^{j[G_{a,b}(x)]} dx, \quad 2-3$$

where  $\beta_q$  is the angle between the antenna axis and the axis of either lobe, or the squint angle. This expression applies equally well to either simultaneous-lobing or sequential-lobing radar systems. For a conical-scan system,



it gives the received signals corresponding to both extreme positions of the lobe axis in a plane.

### 2.11 Direction Indication of Single-lobe System

When a single-lobe antenna is pointed in the direction for which the received signal has its maximum amplitude, the derivative of amplitude with respect to angle is zero. Therefore, if  $A_S$  is the magnitude of S,

$$\frac{dA_S}{d\beta} = 0 \quad 2-4$$

is the necessary condition for determining apparent direction. Of course, this condition could also indicate a minimum, but a study of the second derivative or of a plot of magnitude vs. angle will insure correct interpretation.

It is shown in Appendix A that this condition is fulfilled when

$$\int_{-\frac{1}{2}d}^{\frac{1}{2}d} A(x) \left[ \frac{d\phi_S}{d\beta} - \frac{2\pi}{\lambda} x \right] \sin [G(x) - \phi_S] dx = 0, \quad 2-5$$

where  $\phi_S$ , defined in Eq. 2-1, is itself a function of  $\beta$ . An equivalent expression, containing no such undetermined constant, is also derived in the appendix. It is

$$\int_{-\frac{1}{2}d}^{\frac{1}{2}d} \int_{-\frac{1}{2}d}^{\frac{1}{2}d} x A(x) A(y) \sin [G(y) - G(x)] dx dy = 0, \quad 2-6$$

where  $y$  is a dummy variable for  $x$ . To obtain any explicit data on  $\beta$ , contained in G, from either of these expressions is no trivial task when A and  $\phi$  are of order higher than the first.

### 2.12 Direction Indication of Lobe-comparison System

A lobe-comparison system is oriented in the direction of the apparent center of a target when  $\beta$  is such that

CONFIDENTIAL

$$A_{S_a} = A_{S_b} ,$$

2-7

where  $S_a$  and  $S_b$  are given in Eq. 2-3. If  $S_a$  and  $S_b$  are each separated into their real and imaginary components,  $S_a = R[S_a] + jI[S_a]$  and  $S_b = R[S_b] + jI[S_b]$ , the condition given by Eq. 2-7 is also given by

$$R^2[S_a] + I^2[S_a] = R^2[S_b] + I^2[S_b] .$$

2-8

It is shown in Appendix A that these relations are satisfied when

$$\int_{-\frac{1}{2}d}^{\frac{1}{2}d} A(x) \sin\left[G(x) - \frac{\phi_{S_a} + \phi_{S_b}}{2}\right] \sin\left[\frac{2\pi\beta_q}{\lambda} x + \frac{\phi_{S_a} - \phi_{S_b}}{2}\right] dx = 0 .$$

2-9

As  $\beta_q$  approaches zero,  $\frac{\phi_{S_a} - \phi_{S_b}}{2\beta_q}$  becomes merely  $\frac{d\phi_S}{d\beta}$ , and this equality degenerates into that given by Eq. 2-5. The equivalent double-integral expression containing no undetermined constants such as  $\phi_{S_a}$  and  $\phi_{S_b}$  is

$$\int_{-\frac{1}{2}d}^{\frac{1}{2}d} \int_{-\frac{1}{2}d}^{\frac{1}{2}d} A(x) \sin\left[\frac{2\pi\beta_q}{\lambda} x\right] A(y) \cos\left[\frac{2\pi\beta_q}{\lambda} y\right] \sin[G(y) - G(x)] dx dy = 0 .$$

2-10

It can be seen that this equality is the same as the one in Eq. 2-6 for small values of  $\beta_q$ . Therefore, the wander with a lobe-comparison system having a small squint angle is the same as with a single-lobe system. However, for values of  $\beta_q$  which give a crossover point of the lobes near their half-power points, and which are more realistic in practice, it is difficult to compare the wander in the two systems from cursory examination of these equations.

### 2.13 Equivalence of Lobe-amplitude- and Simultaneous-lobe- Comparison Systems

At this point it is desirable to demonstrate that, insofar as wander is concerned, two somewhat different types of lobe-comparison systems are equivalent. The first of these systems employs lobe-amplitude comparison, and orients for equal signal amplitudes in the two lobes. In the second system, the two antenna feeds associated with the separate lobes are fed into opposite

arms of a r-f magic-tee hybrid junction.<sup>21</sup> The outputs P and M of the sum and difference arms of the magic tee are amplified and applied to a phase detector. The direction to the apparent target center is indicated when the output of the phase detector is zero. The agc of the first system operates on the average of the amplitudes of the two lobe signals. The agc of the second system tends to keep the magnitude of P constant.

Assume that the error detector of the lobe-amplitude-comparison system has a linear characteristic. Its output is then

$$\frac{A_{S_a} - A_{S_b}}{\frac{1}{2}(A_{S_a} + A_{S_b})} = 2 \frac{(R^2[S_a] + I^2[S_a])^{\frac{1}{2}} - (R^2[S_b] + I^2[S_b])^{\frac{1}{2}}}{(R^2[S_a] + I^2[S_a])^{\frac{1}{2}} + (R^2[S_b] + I^2[S_b])^{\frac{1}{2}}} \quad 2-11$$

The phase detector in the second system, which is typical of present-day simultaneous-lobe comparers, is such that it measured the component of P in phase with M. Thus its output is proportional to the cosine of the phase difference.\* If we let  $M_p$  be defined as the component of M in phase with P, the output of the phase detector can be written as

$$\begin{aligned} \frac{M_p}{A_p} &= \frac{M P}{A_p^2} = \frac{R[M] R[P] + I[M] I[P]}{R^2[P] + I^2[P]} \\ &= \frac{R^2[S_a] + I^2[S_a] - (R^2[S_b] + I^2[S_b])}{R^2[S_a] + I^2[S_a] + R^2[S_b] + I^2[S_b]} = \frac{A_{S_a}^2 - A_{S_b}^2}{A_{S_a}^2 + A_{S_b}^2} \end{aligned} \quad 2-12$$

It is obvious that Eq. 2-12 goes to zero when and only when Eq. 2-11 goes to zero. In fact, if the linear error detector of the former system were replaced by a square-law one, the two expressions for error-detector

---

\*The phase detector in a phase-comparison system such as the one used in the experimental part of this research has an output which is approximately proportional to the sine of the phase difference. This characteristic is obtained by phase-shifting one signal through 90 degrees.

output would be the same, aside from the unimportant factor of 2. Therefore, it has been demonstrated that the two systems are equivalent.

#### 2.14 Direction Indication of Phase-comparison Systems

In a two-dimensional case, a phase-comparison system determines the direction of the apparent center of a target by measuring the phase difference of the signals received by two adjacent antennas.\* When the perpendicular bisector of the line joining the antennas is aimed at the apparent center, the phase difference is zero. It should be pointed out that this condition of zero phase difference is not wholly sufficient; ambiguities exist because there are many directions which give zero phase difference when the antennas are spaced many wavelengths apart. However, for the study of wander, these ambiguities can be ignored. In practice, they can be eliminated in various ways, or they may not be important, as in the case of angular rate measurement.

There are four somewhat different types of phase-comparison systems under consideration, but they indicate the same apparent center. The four systems are described in Appendix B. Their equivalence is shown on the diagrams in the appendix; in each case, the phase of a signal or a shaft rotation with respect to a reference is equal to the phase difference of the received signals.

Let the antenna spacing be  $d$ , the dimension of the aperture in Fig. 2-1. No loss of generality is involved; this assumption merely provides a convenient normalizing factor and a basis for comparing the various

---

\*Two pairs of antennas, arranged so that the lines joining the antennas of each pair are not parallel, are needed for three-dimensional direction indication.



systems. Using the notation introduced in Eq. 2-2, the condition for correct antenna-system orientation can be written

$$G(x = +\frac{1}{2}d) - G(x = -\frac{1}{2}d) = 0, \pm\pi, \quad 2-13$$

using 0 if  $A(x)$  has the same sign at  $+\frac{1}{2}d$  and  $-\frac{1}{2}d$ , or  $\pm\pi$  if the signs of  $A(x)$  are opposite at  $x = +\frac{1}{2}d$  and  $x = -\frac{1}{2}d$ .

### 2.15 Comparison of Systems with Target at Long Range

As the distance between target and radar system is increased, the largest fraction of a lobe of the target scattering pattern that is spanned by the radar aperture is correspondingly decreased. At very long range, this fraction approaches zero, with the result that the signal strength is constant across the aperture. Simultaneously, the higher order terms in the expression for  $\phi(x)$  diminish, until eventually the expression can be written

$$\phi(x) = u_0 + u_1 x. \quad 2-14$$

It will be assumed that, at long range,

$$A(x) = v_0, \quad \phi(x) = u_1 x, \quad 2-15$$

where  $u_0$  has been dropped because it is an irrelevant constant dependent on an arbitrary starting time of observation.

With these simplifying assumptions,  $G(x)$  is given by

$$G(x) = u_1 x + \frac{2\pi\beta}{\lambda} x = (u_1 + \frac{2\pi\beta}{\lambda}) x. \quad 2-16$$

The  $G$ 's are the only terms in Eq's. 2-6 and 2-10 that contain  $\beta$ . Therefore, the value of  $\beta$  for any  $u_1$  can be found from the value of  $\beta$  for  $u_1 = 0$  from the relation

$$\beta = (\beta_{u_1=0}) - \frac{u_1 \lambda}{2\pi}. \quad 2-17$$

It is well known that  $\beta_{u_1=0} = 0$ , because that is the case of an infinite

plane wave. Eq. 2-17 then shows that both the single-lobe and the lobe-comparison systems indicate direction in this case by orienting normal to the phase front, as does the phase-comparison system.

Two important conclusions can be drawn from these relations. First, the observed wander of the apparent center of reflection of a target at long range is independent of the type of radar system. Second, any system tends to orient its axis normal to the phase-front of the received signal, not parallel to the direction of propagation.

### 2.16 Comparison of Systems with Intermediate Target-ranges

At somewhat shorter ranges than those considered in Sec. 2.15, the amplitude distribution across the aperture can no longer be considered constant. The intermediate-range problem will be defined by assuming

$$\phi(x) = u_1 x, \quad A(x) = v_0 + v_1 x. \quad 2-18$$

As Sec. 2.15 might suggest, the quantity of interest to be studied here is the angular deviation from the normal to the phase-front that is produced by the amplitude distribution.

A graphical solution to this problem is given in Appendix A. The results of interest are shown in Fig. 2-2. The independent variable,  $x_{\text{null}}$ , is the point where  $A(x) = 0$ . When  $-\frac{1}{2}d < x_{\text{null}} < +\frac{1}{2}d$ , the zero-point is within the aperture. The quantity  $H$  used in defining the ordinates of these plots is the angular error normalized in terms of the lobe-width; the node-to-node beamwidth of the uniform aperture is  $2\pi$  radians, in terms of  $H$ . It is assumed that  $A(x)$  can have negative values, so that no 180-degree phase discontinuities are encountered. The plots show that the apparent direction is normal to the phase front for any system whenever the zero-point is outside the aperture. If a uniform motion of the zero-point across the aperture is

**CONFIDENTIAL**

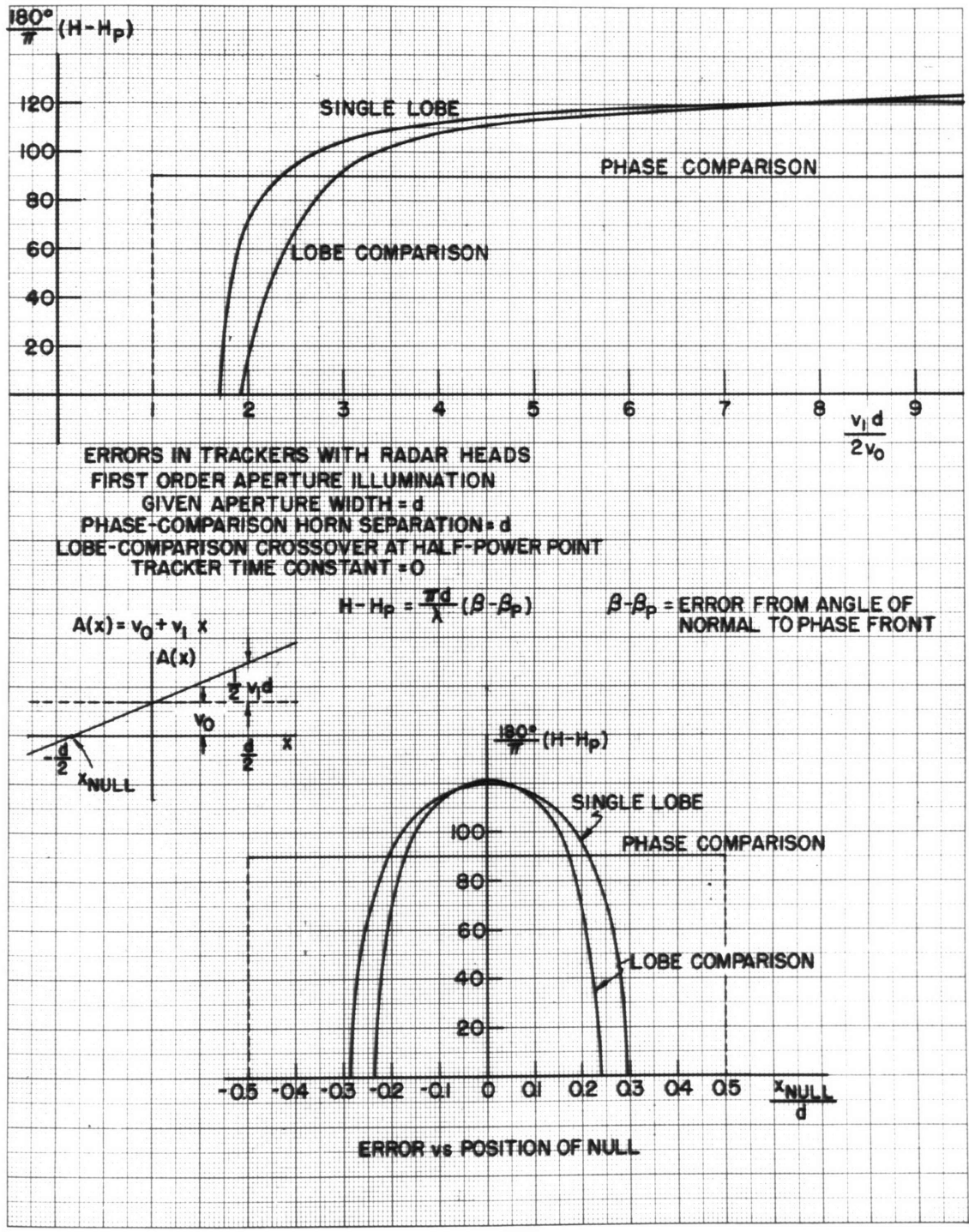


Fig. 2-2

**CONFIDENTIAL**

**CONFIDENTIAL**

assumed, it is apparent that the average error away from the normal to the phase-front is somewhat greater for the phase-comparison system than for the others.

The curves in Fig. 2-2 do not indicate the sign of the errors produced by the amplitude distribution. In the appendix it is shown that either sign of error is equally probably, and that the choice of either sign by any of the systems is a random one.

## 2.2 ANALYSIS OF A TWO-POINT TARGET

A particular two-point target was selected as a basis for the computations of this section. Such a target is sufficiently simple that explicit answers can be obtained graphically even for very short target ranges, where the receiving antenna aperture spans as much as a lobe-width of the target's scattering pattern.

Physically a two-point target is a highly justifiable configuration. Targets such as two aircraft in close formation or a single aircraft with a small body and two large nacelles, for example the Navy F7F, closely resemble the two-point target. In addition, many aircraft appear as essentially two-point reflectors when viewed from broadside, as some of the experimental work of this research illustrates. Apparently there are two predominant echoing areas, one the tail surface and one near the wing root, of a conventional aircraft when viewed from broadside.

A single value of 0.8 was chosen for the ratio of signal strengths of the two points. This value was chosen as a compromise between practical interest and accuracy of plotting. The larger the ratio, the greater are the spikes of wander, and the greater the difficulty in plotting and integrating the curves of wander.

**CONFIDENTIAL**

### 2.21 Wander of the Apparent Center of a Two-point Target

The position of the apparent center of a two-point target is shown as a function of the phase difference between the two points in Fig's. 2-3, 2-4, and 2-5 for the single-lobe, lobe-comparison, and phase-comparison systems respectively. The abscissa of these plots is the phase difference of the signals from the two points measured in each case at the center of the antenna system. The ordinate,  $w/s$ , is the coordinate of the apparent center measured from the stronger point source in a direction normal to the line-of-sight and normalized in terms of the point spacing  $s$ . The parameter of these curves,  $\frac{sd}{R\lambda}$ , where  $R$  is the range from radar to target, is an indication of the physical size of the antenna aperture in terms of the lobe-width of the target's scattering pattern. In fact, when  $\frac{sd}{R\lambda} = 1$ , the antenna aperture spans exactly one complete lobe of the scattering pattern.

It should be noted that  $s$  is measured normal to the line-of-sight. Furthermore, it has been implicitly assumed in the computation of these curves that changes in the angle of the line-of-sight as it follows the apparent center introduce only negligible second-order effects. This assumption is equivalent to stating that  $s/\lambda$  is very much greater than unity. Such an assumption is reasonable in the light of present-day radar practices.

A few points brought out by these curves are worthy of special mention. First, the large spikes of wander that occur at long range for all systems are substantially larger than the target, and are always off the target on the side of the stronger point. Secondly, the magnitude of the wander decreases very definitely with decreasing range. Finally, if the assumption is made that  $\mu$  changes uniformly with time, it is seen that the bandwidth of the spectrum of the wander does not increase with decreasing range.

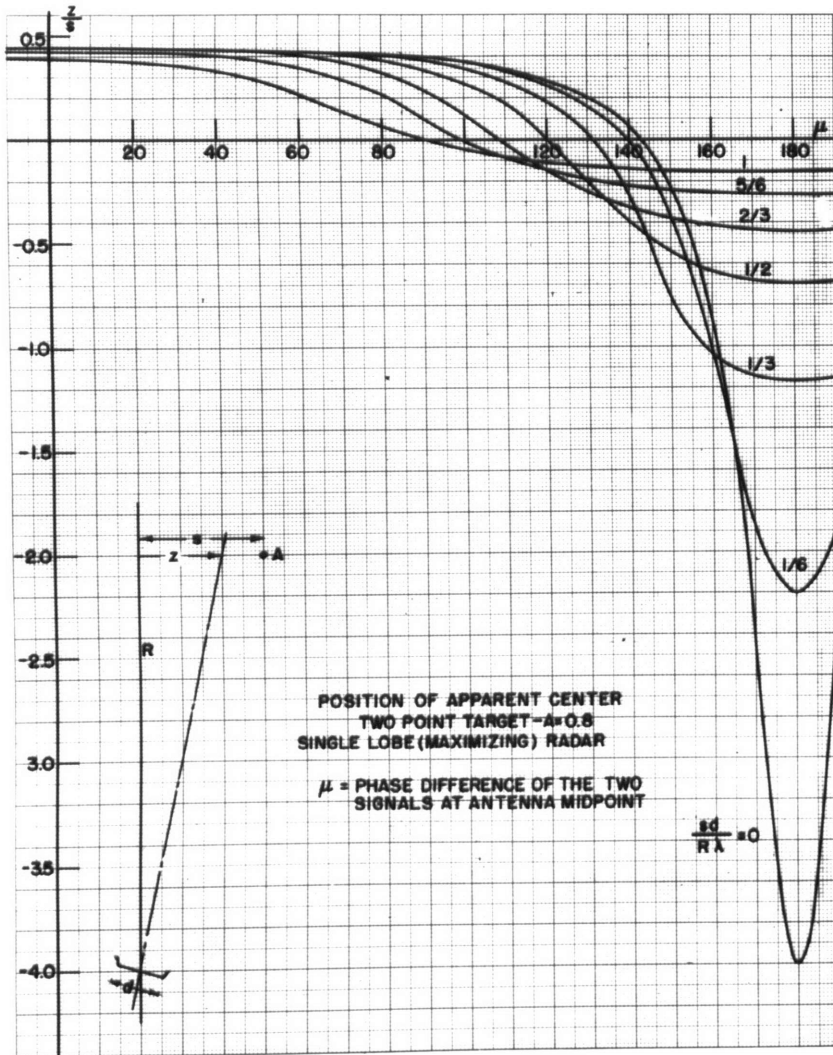


Fig. 2-3

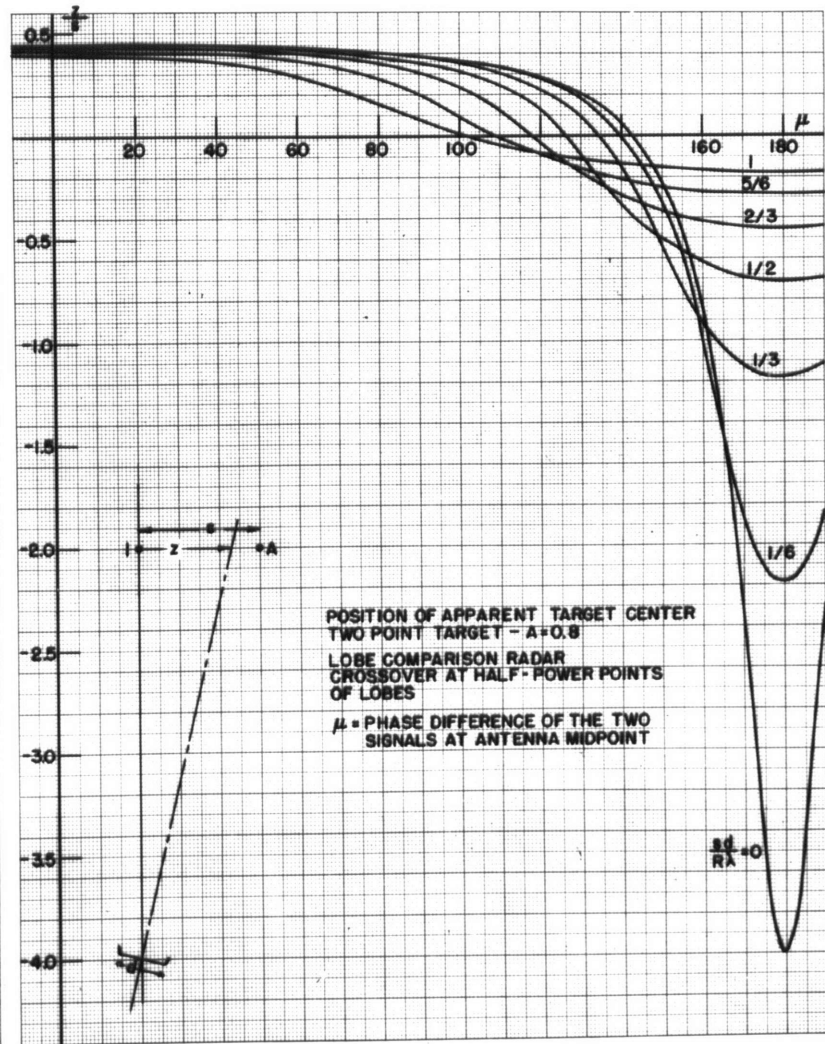


Fig. 2-4



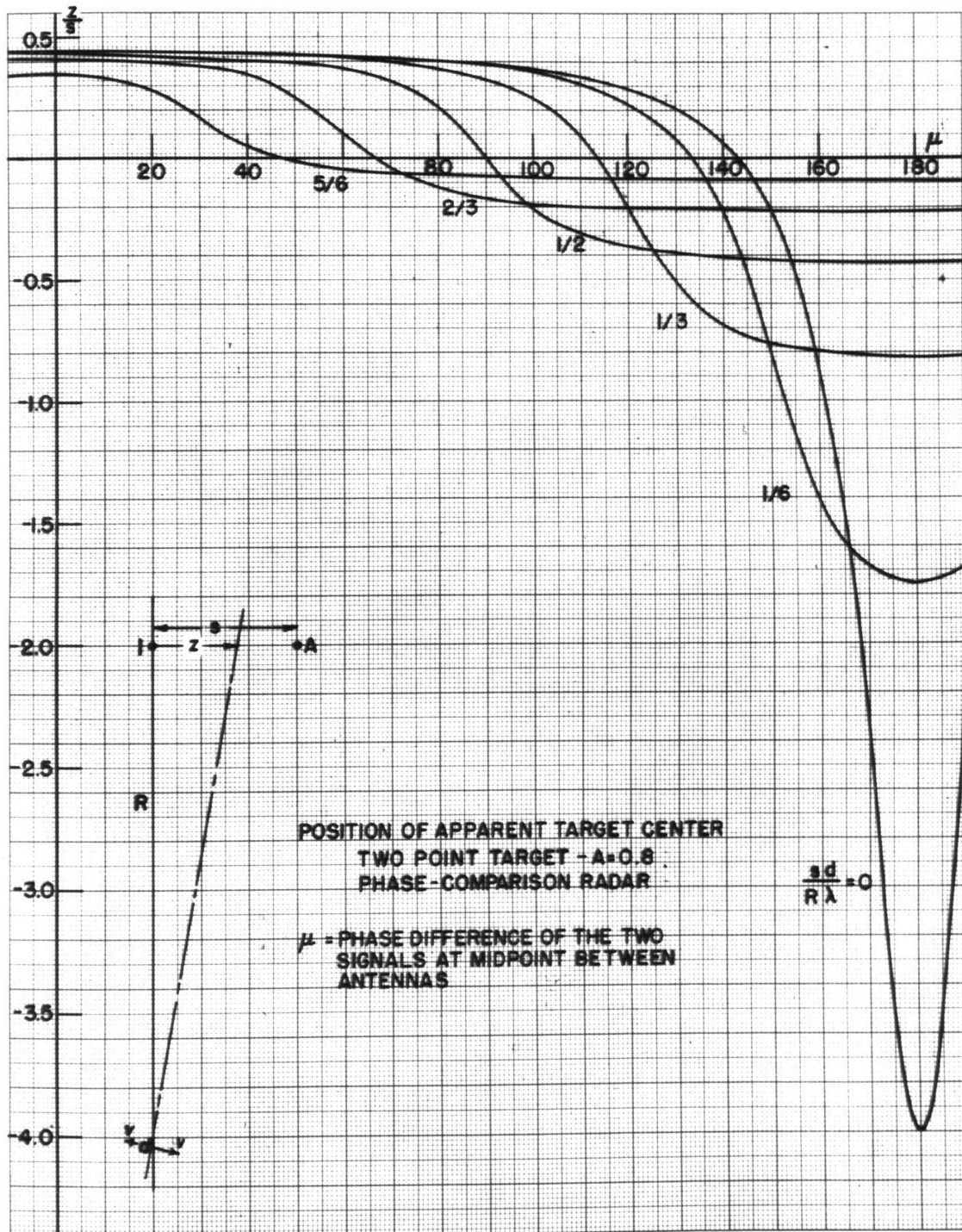


Fig. 2-5

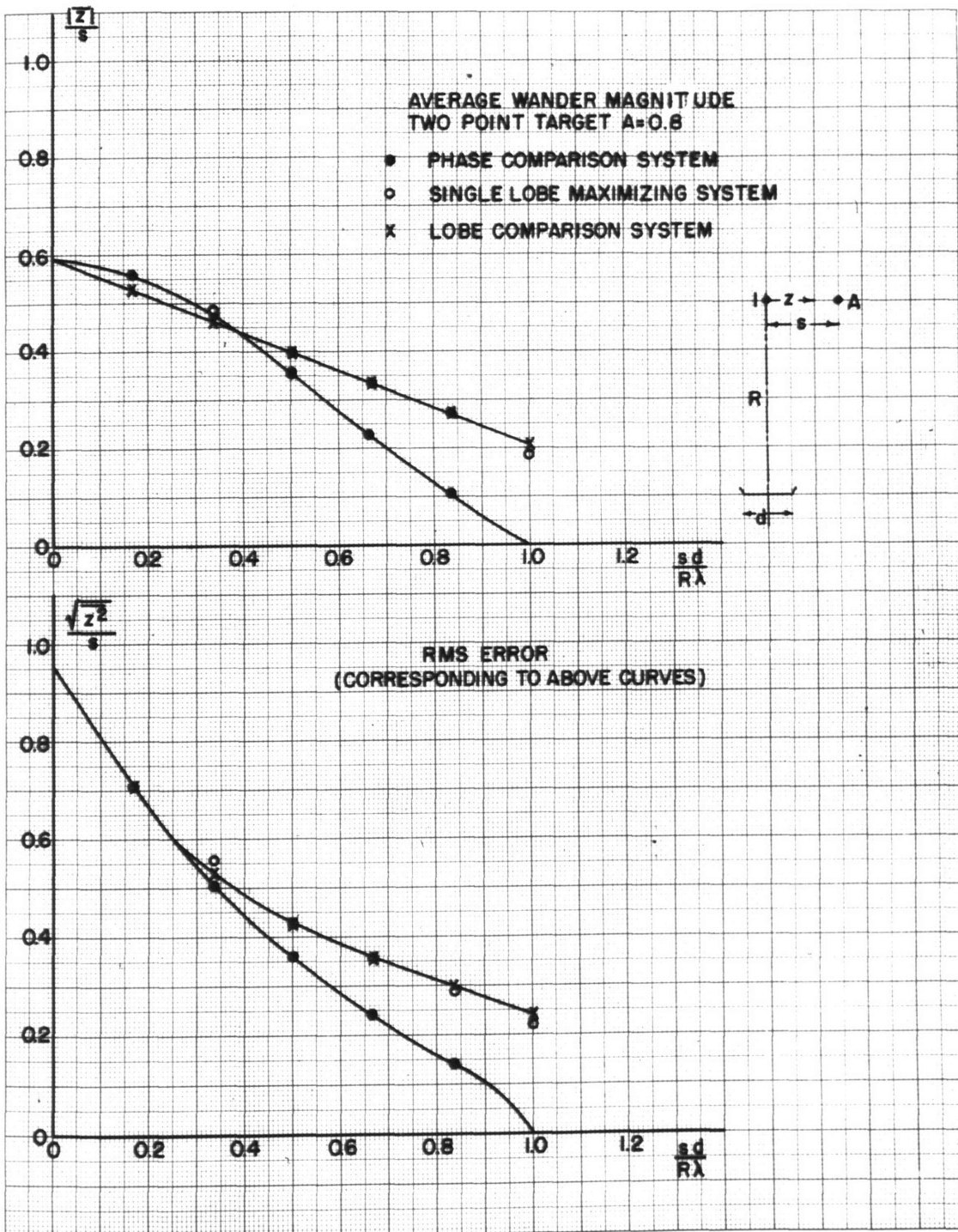


Fig. 2-6



[REDACTED]

A summary of these three families of curves is contained in Fig. 2-6, which shows the average magnitude and the rms of the wander measured by the three systems away from the position of the stronger point of the target. These data were obtained by graphical integration, with respect to  $\mu$ , of the curves of Fig's. 2-3, 2-4, and 2-5 and the squares of the curves.

The methods used in computing the curves of wander versus  $\mu$  are described in Appendix C.

### 2.22 Error-detector Output with a Two-point Target

The previous section illustrates the performance of the various types of radar systems when they are associated with an essentially instantaneous tracker, so that they can accurately follow the apparent center. It is also of interest to know the effects of wander when the radar remains stationary, which might correspond to the case with a tracker of infinite time-constant. With such a tracker, the radar would eventually orient in such a direction that the average error-detector output is zero. Unfortunately, it is a difficult task to find the position of the apparent center which corresponds to zero average output, except for the phase-comparison system with limiting. In the latter case, the position corresponds to that of the stronger point. For the other systems, this problem cannot be readily solved. However, a very similar problem which can be easily solved is the one in which the radar is oriented in the direction of the stronger point of the target. In this section there are presented curves showing the error-detector outputs of various phase-comparison and lobe-amplitude-comparison systems for a two-point target with the radar aimed at the stronger point. It is assumed that the lobes of the lobe-comparison system cross at their half-power (one way) points. The computations necessary for obtaining the curves are described

[REDACTED]

[REDACTED]

in Appendix C.

The outputs of linear error detectors of lobe-comparison radars with fast-acting agc and with slow-acting agc are shown by the curves of Fig's. 2-7 and 2-8 respectively. The fast agc is defined as one which is able to eliminate changes in the instantaneous mean of the amplitudes of the two lobe signals which are caused by changes in  $\mu$ . The slow agc merely holds constant the average for all  $\mu$  of this instantaneous mean. The nonuniform spacing of the curves corresponding to different values of the parameter  $\frac{sd}{RA}$  seems to reflect on the computational accuracy. However, many checks were made which indicate that the curves are approximately correct; apparently, the nonuniformities result from the manner in which the nonlinear lobe patterns enter the computations.

The outputs of the phase detectors of various phase-comparison radars are shown in Fig's. 2-9 and 2-10. In the case of the system with limiting, it was assumed that the output of the phase detector is proportional to the sine of the phase difference of the signals. For systems without limiting, it can be seen that the nature of the output depends on the type of phase detector that is employed. Twin-diode phase detectors, which are exemplified by the one used in the data-recording radar system described in Appendix F, have a peculiar unsymmetrical performance when the two signal inputs are unequal. This phenomenon is a result of nonlinearities in the process of taking the magnitudes of vector summations. It was assumed in all the computations for systems with no limiting that slow-acting agc circuits held constant the average signal level in each signal channel.

These families of curves are summarized in Fig. 2-11, which shows the average magnitude and rms of the error-detector outputs for the different

[REDACTED]

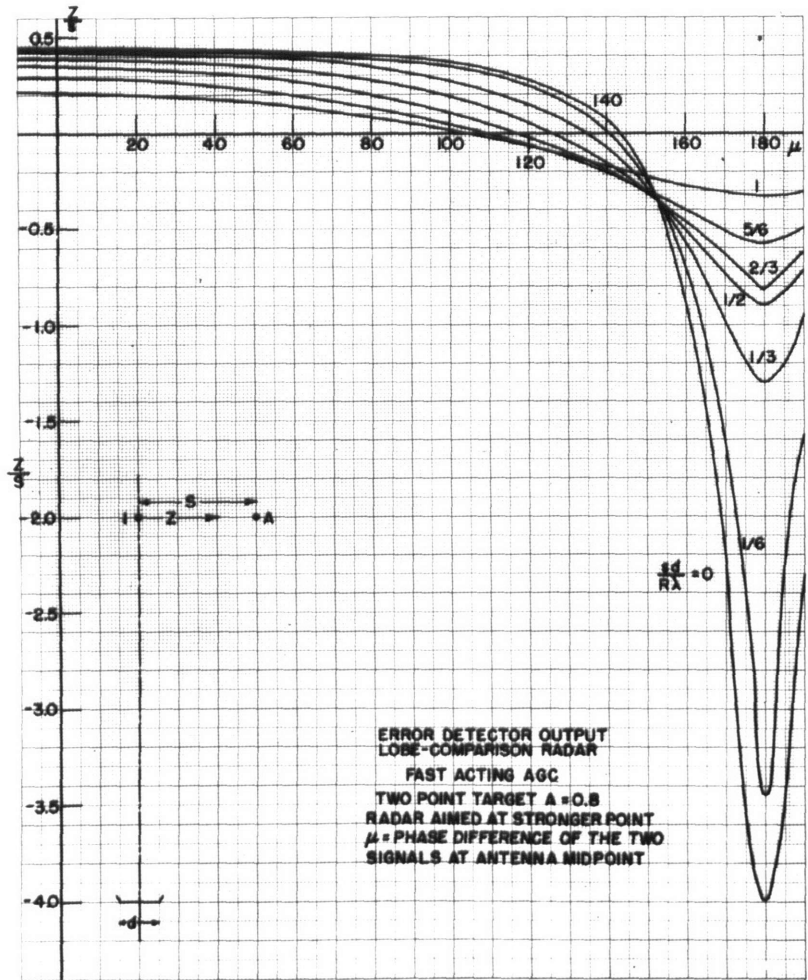


Fig. 2-7

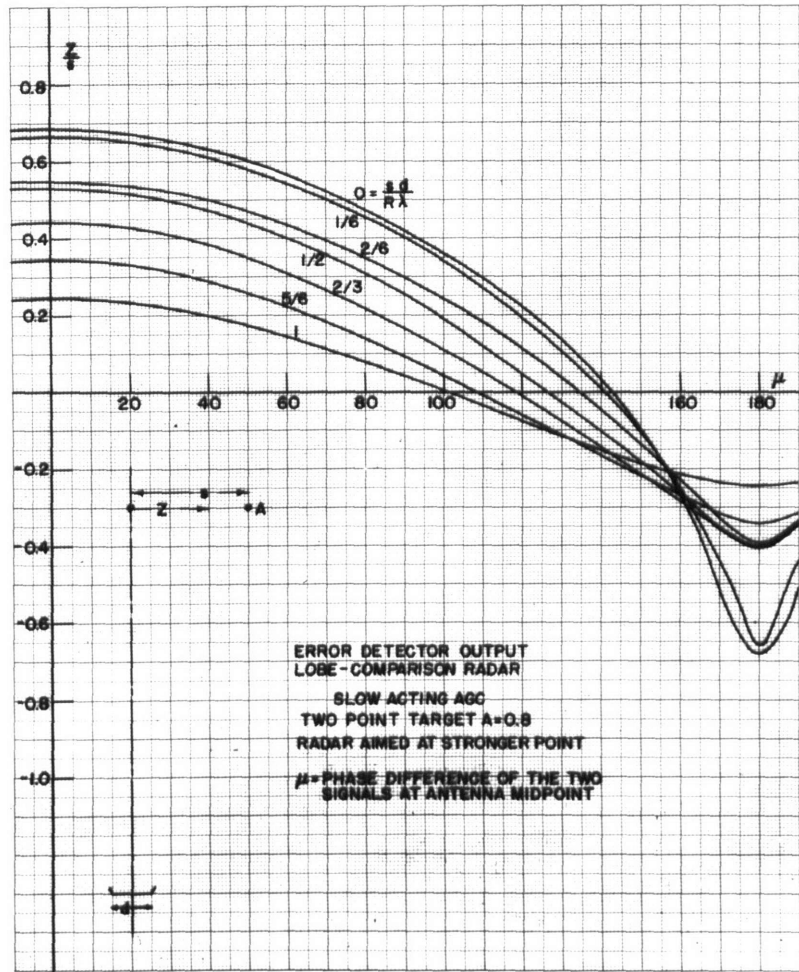


Fig. 2-8

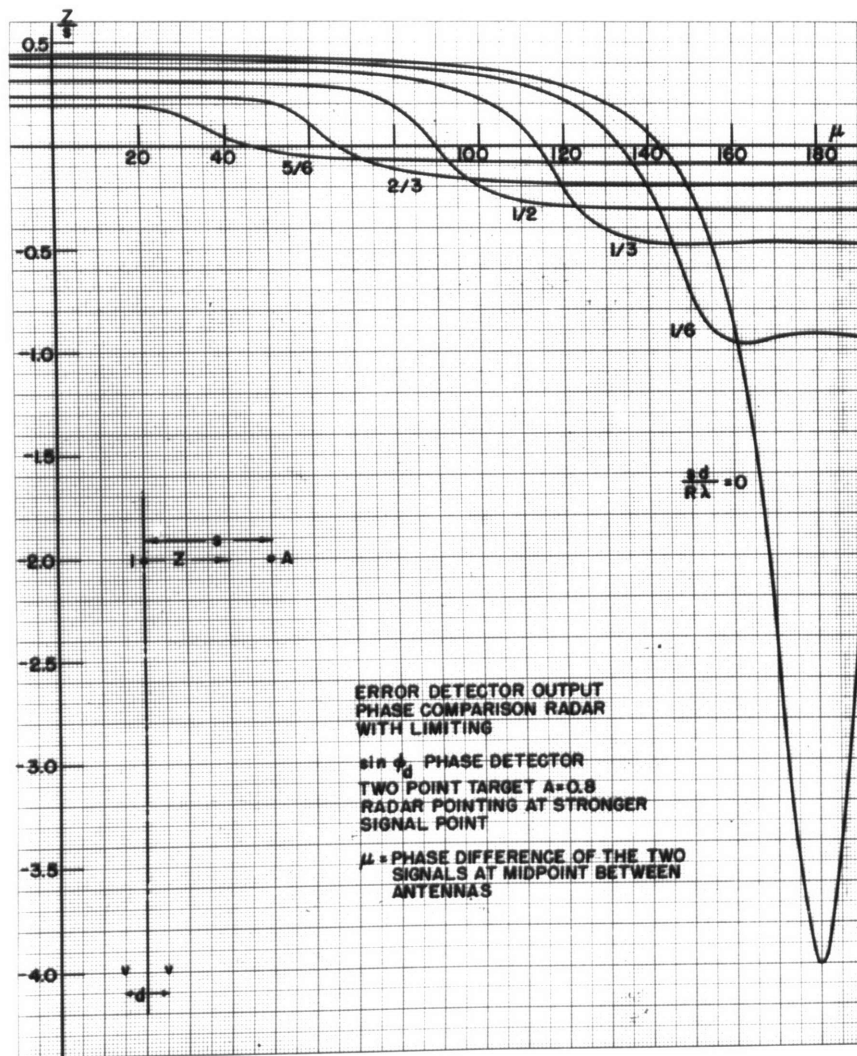


Fig. 2-9

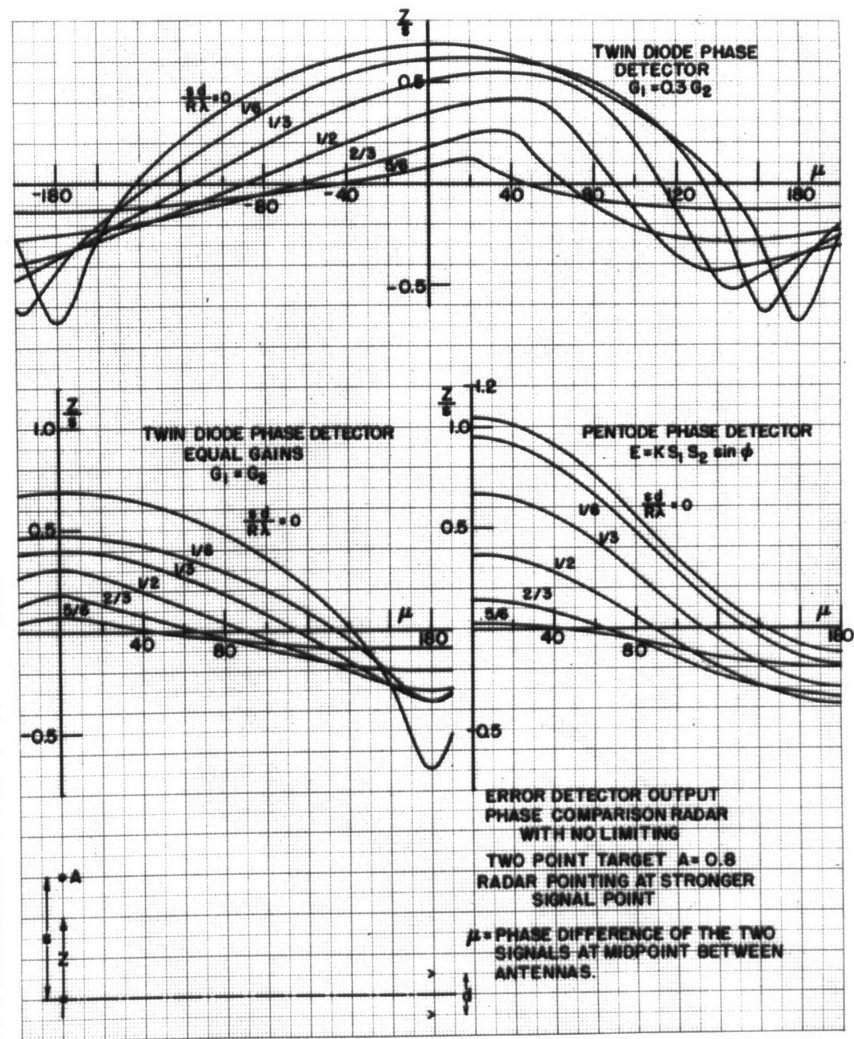


Fig. 2-10

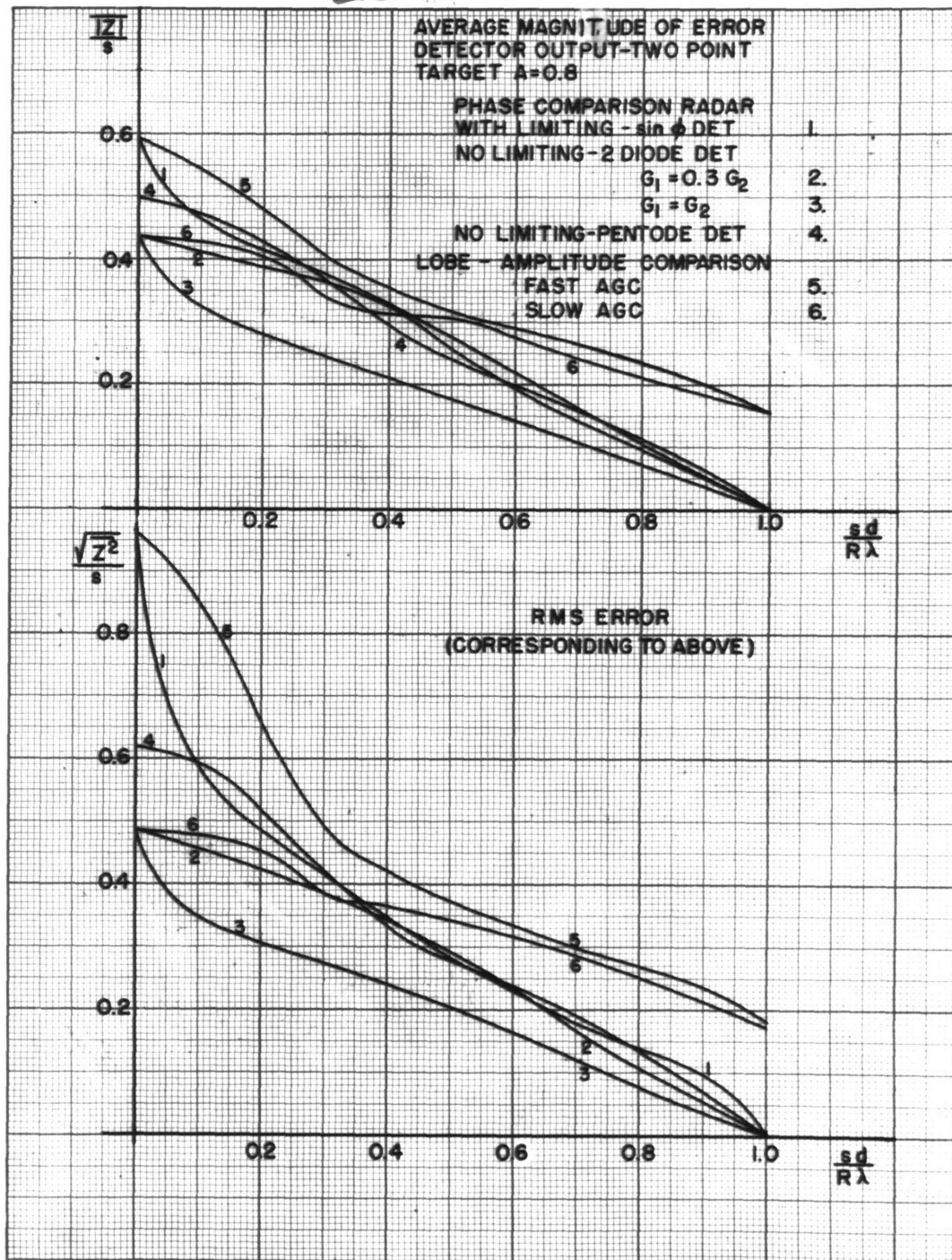


Fig. 2-11

systems. This figure was obtained in the same manner as was Fig. 2-6.

The results of this section were obtained for a set of conditions which, although possible, are for most cases somewhat artificial. Nevertheless, some important conclusions can be drawn from the results. In the first place, it can be seen that the spectral bandwidths of the outputs (assuming  $\mu$  increases uniformly with time) do not change significantly with range. Secondly, one can get an estimate of the magnitude of the noise produced by wander that is fed from the error detector into whatever control system might follow.

### 2.23 Comparison of Systems with a Two-point Target

It is now possible to form another comparison of the various types of direction-indicating systems similar to the one made in Sec. 2.16. On the basis of Fig's. 2-6 and 2-11 it can be said that the performance of the lobe-comparison systems is essentially the same as that of the phase-comparison systems at long range. By the time that the target is close enough so that the radar antenna aperture includes an appreciable portion of a lobe of the target's scattering pattern, the errors with the lobe-comparison systems are somewhat greater than those with the phase-comparison systems. There are also larger errors in systems with limiting (or fast agc) at long range than in systems without limiting; however, this difference quickly disappears with decreasing range.

It is interesting to consider qualitatively the behavior of the curves of Fig's. 2-6 and 2-11 for values of  $\frac{sd}{RA}$  greater than 1. First it should be noted that the curves for the phase-comparison systems go to zero when  $\frac{sd}{RA} = 1$ , or any integer, because the phase difference of the signals produced in the two antennas by either point is the same. Therefore the resultant



~~CONFIDENTIAL~~

signals in the two antennas have the same magnitude, and the phase difference is the same as is produced by either point. The maximum possible phase-detector output or angular wander does not depend on range, but only on the ratio of the strengths of the two point sources. Thus it can be said that the maximum possible wander is inversely proportional to range, when measured in terms of a linear dimension at the target. From these two ideas, it can be hypothesized that the shape of the curves for the phase-comparison systems with  $\frac{sd}{RA}$  greater than 1 is something resembling a plot of  $(1/x)\sin x$ .

For the lobe-comparison system, the actual strength of the signal received from the weaker point of the target would decrease with decreasing range, because that point is passing farther and farther from the main lobe of the antenna (presumably the system would invariably track closer to the stronger point). Thus the size of the angular errors themselves would decrease with decreasing range. As a result, the curves for the amplitude-comparison systems fall off with increasing  $\frac{sd}{RA}$  as  $1/x^2$ . At very short ranges, then, the errors in the lobe-comparison systems would be less than those in the phase-comparison systems.

### 2.3 PHASE-DETECTOR OUTPUT WITH A MULTI-POINT TARGET

Now that the analysis of the two-point target has been completed, it is appropriate to consider a target that is made up of an infinite number of point sources distributed at random within its boundary. These two extreme cases serve to bracket the problem of reflections from multi-point targets.

It is not possible to obtain an exact solution for the various systems with an infinite-point target. Nevertheless, an approximate solution for the output of a phase detector of a phase-comparison radar system can be attained. At long range, the phase-detector output of a phase-comparison system with

~~CONFIDENTIAL~~

limiting is exactly proportional to the wander of the apparent target center. Secondly, it was the output of a phase detector that was recorded for the experimental study of wander to be described, and it is desirable to know the size of discrepancies caused in some of these data by insufficiently great target range.

### 2.31 Probability Density of Phase-detector Output

The probability density function of the output of the phase detector of a phase-comparison system both with and without limiting is determined in the analysis to be described here. The phase detector of the system with limiting is such that its output is proportional to the sine of the phase difference of the resultant signals at the two antennas. In the system without limiting, the phase-detector output is assumed to be proportional to the product of the sine of the phase difference and the amplitude of one of the signals. This characteristic is typical of a twin-diode phase detector when one of the inputs is shifted by 90 degrees and is always substantially smaller than the other.

Let the signal in one of the antennas be given by

$$S_1 = \sum_{n=1}^N a_n e^{j\mu_n} \triangleq A_1 e^{j\phi_1}, \quad 2-19$$

where  $a_n$  and  $\mu_n$  are the amplitude and phase, respectively, of the signal from point  $n$  on the target and  $N$  is a large integer approaching infinity. The signal in the other antenna can then be expressed

$$\begin{aligned} S_2 &\triangleq A_2 e^{j\phi_2} = \sum_{n=1}^N a_n e^{j(\mu_n + kz_n)} = \sum_{n=1}^N a_n e^{j\mu_n} e^{jkz_n} \\ &= \sum_{n=1}^N a_n e^{j\mu_n} + \sum_{n=1}^N (e^{jkz_n} - 1) a_n e^{j\mu_n} \end{aligned}$$

$$\triangleq S_1 + D,$$





where

$$k \triangleq \frac{2\pi d}{\lambda R}$$

2-21

and  $z_n$  is the distance of the point  $n$  measured normal to the line-of-sight from the radar to the center of the target, as shown in Fig. 2-12. Because

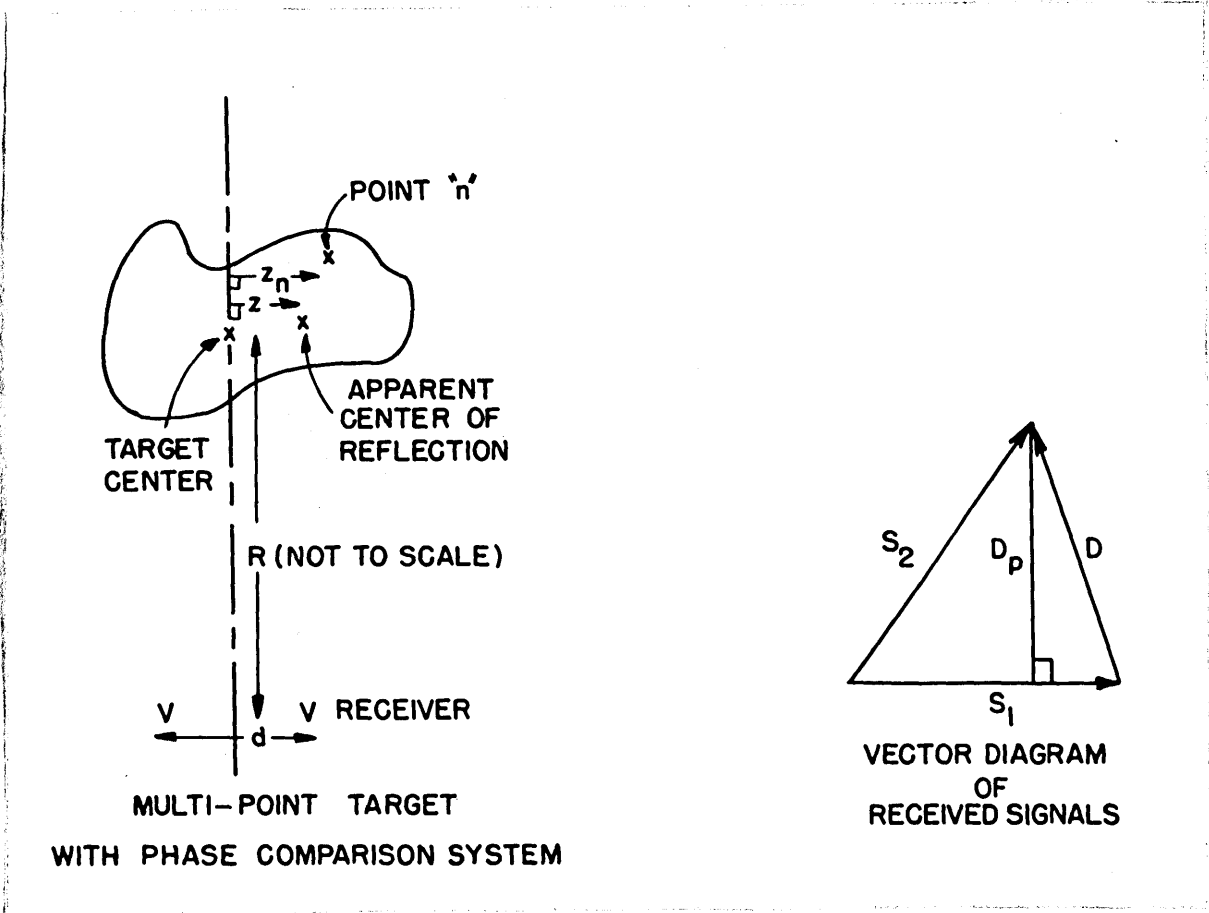


Fig. 2-12

Fig. 2-13

it has been assumed that the distribution of points on the target is random, there is no relation between the position coordinate  $z_n$  and the amplitude  $a_n$  or the phase  $\mu_n$  of any point  $n$ . As a result, the coefficient of any term in



the summation for D is uncorrelated with the equivalent coefficient in the summation for  $S_1$ , and D and  $S_1$  are statistically independent.

In the system with limiting, the output of the phase detector is  $\sin(\phi_2 - \phi_1)$ . It can be seen from Fig. 2-13 that

$$\begin{aligned} \sin(\phi_2 - \phi_1) &= \frac{\text{component of } S_2 \text{ out of phase with } S_1}{A_2} \\ &= \frac{D_p}{A_2} \triangleq \sin \phi_d \\ &= V_m, \end{aligned} \tag{2-22}$$

where  $D_p$  is defined as the component of D out of phase with  $S_1$ . It will be assumed that in the system without limiting a slow-acting agc is included, with the result that  $\sin \phi_d$  is multiplied by  $A_2/\overline{A_2}$ . Thus,

$$\frac{D_p}{A_2} \triangleq V_n \tag{2-23}$$

is the output of the phase detector when no limiting is employed.

Both D and  $S_2$  are made up of a very large number of independent components, none of which, it will be assumed, makes up a significant portion of the resultant. Therefore, both these quantities are normally distributed in two dimensions. The statistical independence of D and  $S_1$  has been demonstrated, with the result that  $D_p$  has a Gaussian distribution function

$$p(D_p) dD_p = \frac{1}{\sqrt{2\pi D_p^2}} e^{-D_p^2/(2\overline{D_p^2})} dD_p. \tag{2-24}$$

The amplitude  $A_2$  of  $S_2$  is the magnitude of a normal two-dimensional distribution, and has a standard Rayleigh distribution

$$p(A_2) dA_2 = \frac{2A_2}{A_2^2} e^{-A_2^2/\overline{A_2^2}} dA_2. \tag{2-25}$$

The magnitude of all practically significant values of  $D_p$  can be made

arbitrarily small compared with any significant values of  $A_2$  by choosing a sufficiently large target range, because  $D_p$  is inversely proportional to range at long range. At those ranges where  $D_p$  is always considerably smaller than  $A_2$ , the two quantities are statistically independent. The problem of finding the probability density of the phase-detector output then becomes the problem of finding the probability density of the quotient of two random variables whose individual probabilities are known. The solution to this problem is obtained in Appendix D, using a method outlined by Uspensky.<sup>25</sup> The resulting expression for the probability density function of the phase-detector output in the system with limiting is

$$p(v_m) dv_m = \frac{Q^2 dv_m}{2(v_m^2 + Q^2)^{3/2}}, \quad 2-26$$

where

$$Q^2 \triangleq \overline{|e^{jkz_n} - 1|^2}. \quad 2-27$$

At the long ranges considered in the last paragraph, the operation of the phase detector is restricted to the linear portion of its characteristic. With this restriction, the phase-detector output is completely proportional to the actual phase difference existing at the antennas, and therefore to the wander of the apparent target center. Also, at long range the value of  $k$  is small, with the result that  $Q^2$  is very nearly equal to  $\overline{(kz_n)^2} = k^2 \overline{z_n^2}$ . If these two facts are incorporated into Eq. 2-26, the resulting expression for the probability density function of the wander at long range is

$$p(z) dz = \frac{\overline{z_n^2} dz}{2(z^2 + \overline{z_n^2})^{3/2}}. \quad 2-28^*$$

---

\*This result agrees with one derived by Delano<sup>11</sup> on the basis of a lobe amplitude-comparison system.

In this expression, the normalization of the phase-detector output in terms of a linear displacement at the target is explained when it is realized that the output due to a unit displacement of a single-point target is  $k$ .

The above results are no longer valid when the range is sufficiently short that  $D_p$  may become appreciable compared with  $A_2$ . If  $D_p$  and  $A_2$  were still independent in such a case, it is obvious that there would be a finite probability of  $D_p > A_2$ . Eq. 2-22 and Fig. 2-13 show that this inequality is impossible. In order to resolve this dilemma let it be assumed that  $V_m = 1$  whenever the probability given in Eq. 2-26 calls for a value greater than unity.\* Thus,

$$p(V_m) dV_m = \frac{Q^2 dV_m}{2(V_m^2 + Q^2)^{3/2}}, \quad (-1 < V_m < +1)$$

$$P(V_m = -1) = P(V_m = +1) = \int_{+1}^{\infty} \frac{Q^2 dV_m}{2(V_m^2 + Q^2)^{3/2}} \cdot$$

2-29

The values of the rms and average magnitude of the phase-detector output computed from Eq's. 2-29 are always at least as great as the actual output. This is true because the type of nonlinear system characteristic implied by these equations is always equal to or greater than a sinusoidal system characteristic.

The phase-detector output of the system without limiting, given in

---

\*The validity of this assumption would be highly questionable were it not for the fact that at very short ranges, where the assumption introduces the greatest errors, there is good agreement between the results based on this assumption and those based on a different assumption which is valid at very short ranges, as described in the next section.

Eq. 2-23, has a probability density function of the same form as that of  $D_p$ , namely,

$$p(v_n) dv_n = \frac{1}{\sqrt{2\pi\overline{v_n^2}}} e^{-v_n^2/(2\overline{v_n^2})} dv_n \quad 2-30$$

where

$$\overline{v_n^2} = \frac{1}{(A_2)^2} \overline{D_p^2} = \frac{4}{\pi} \times \frac{\overline{D_p^2}}{A_2^2} = \frac{2Q^2}{\pi} \quad 2-31$$

### 2.32 Average Magnitude and RMS of Output

The values of the rms and the average magnitude of the output of the phase detector can be computed from the equations of the preceding section. For the system with limiting, the average magnitude, determined on the basis of Eq's. 2-29, is given by

$$\overline{|v_m|} = \int_0^1 \frac{Q^2 v_m dv_m}{(v_m^2 + Q^2)^{3/2}} + \int_1^\infty \frac{Q^2 dv_m}{(v_m^2 + Q^2)^{3/2}} \quad 2-32$$

and the mean squared value of the output is given by

$$\overline{v_m^2} = \int_0^1 \frac{Q^2 v_m^2 dv_m}{(v_m^2 + Q^2)^{3/2}} + \int_1^\infty \frac{Q^2 dv_m}{(v_m^2 + Q^2)^{3/2}} \quad 2-33$$

The mean squared value of the output of the phase detector of the system without limiting is given by Eq. 2-31. The average magnitude of this output is

$$\overline{|v_n|} = 2 \int_0^\infty v_n p(v_n) dv_n = \left(\frac{2}{\pi}\right)^{1/2} (\overline{v_n^2})^{1/2} = \frac{2Q}{\pi} \quad 2-34$$

As an example let us examine the values of these quantities for a target consisting of sources uniformly distributed in one dimension for a length  $L$ . It is shown in Appendix D that

$$Q^2 = 2\left(1 - \frac{\sin \frac{1}{2}kL}{\frac{1}{2}kL}\right) \quad 2-35$$

for such a target. The values of the rms and average magnitude of the phase-detector output that are obtained when this expression for  $Q^2$  is used in Eq's. 2-31 through 2-34 are plotted in Fig. 2-14. In these plots the outputs have been referred to a linear displacement at the target and normalized with respect to the length of the target by dividing all their values by  $kL$ .

The assumption made in connection with Eq's. 2-29 introduces a certain amount of error in the curves for the system with limiting. This error becomes more severe as the range decreases, because the probability  $P(V_m = \pm 1)$  is an inverse function of range. However, a different approximation can be made which is valid at very short ranges, when the target spans appreciably more than one lobe of the interference pattern of the receiving antennas. For these short ranges, it is assumed that any value of  $\phi_d$  is equally probable; this assumption is justifiable since any values of  $\phi_d$  may be adequately represented by values in the interval from  $-\pi$  to  $+\pi$ . In such a case the rms of the phase-detector output is just  $1/\sqrt{2}$ , and the average magnitude is  $0.636 = 2/\pi$ . The curves obtained by dividing these figures by  $kL$  are shown in Fig. 2-14 as the short-range approximations. The closeness of the curves drawn on the bases of the different assumptions indicates that the errors introduced by Eq's. 2-29, which are greatest for large values of  $\frac{L_d}{R\lambda}$ , are never very large.

There are a few details associated with Fig. 2-14 that are worthy of special mention. First there is the advantage which is apparently gained for long target ranges in not amplitude limiting prior to phase-detection. Obviously, this advantage is lost when the target comes in close. Furthermore, there are other phenomena, such as the one discussed in Sec. 2.52, which arise in a system without limiting that may make it desirable to

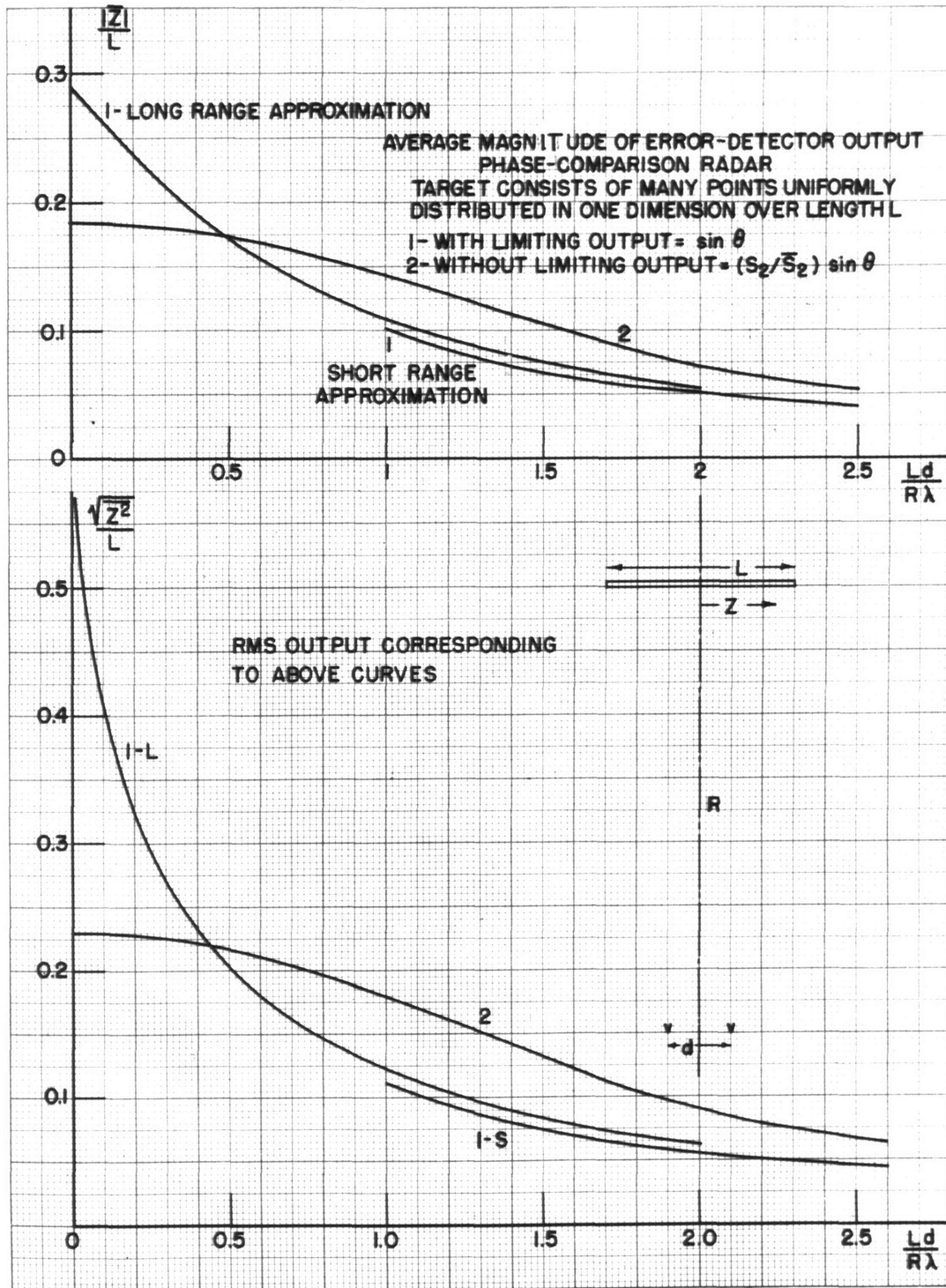


Fig. 2-14

~~CONFIDENTIAL~~

limit (or use a fast-acting agc) even at long ranges. In other words, it should not be concluded from Fig. 2-14 that it is undesirable to limit at long range.

The second point to be considered is that the curve of rms output with limiting tends to infinity with increasing range. The physical reason that it goes to infinity is that  $V_m$  is inversely proportional to  $A_2$  (Eq. 2-22), which has a Rayleigh distribution. In practice, it is doubtful that the occasional large outputs which give rise to this tendency could be measured, for a number of reasons. First, receiver thermal noise, whose effect is proportional to at least the first power of the range, reduces the ability of the radar to measure true angular wander at long range. Secondly, the sensitivity of the radar system in terms of feet at the target is inversely proportional to range. In the third place, these large outputs are always accompanied by weak signals, and the larger the output, the weaker the signal. On the basis of these three reasons and the design features representative of current radar practices, it has been determined that a value  $\frac{I_d}{RA} = 0.02$  is a very conservative lower limit for the region in which wander could be experimentally determined. Thus it is highly improbable that wander with a rms value greater than  $0.5L$  would ever be observed for a uniformly distributed target.

Finally, it should be mentioned that the output of the error detector of a lobe-comparison system should have properties similar to those of the output of a phase detector in a phase-comparison system for targets at moderately long ranges and beyond. For angular errors that are small compared with the lobewidths of the systems, the error-detector characteristics of both systems are very similar, with the result that the outputs under

~~CONFIDENTIAL~~



~~CONFIDENTIAL~~

identical conditions must be nearly the same. Probably a conservative lower limit to the ranges of good equivalence would be given by a value of  $\frac{Ld}{RA}$  in the vicinity of 0.2.

#### 2.4 RELATIONS BETWEEN SIGNAL AMPLITUDE AND WANDER

Any fundamental relationships which must necessarily exist between the amplitude of a signal from a target and the wander of its apparent center can be determined through appropriate use of Maxwell's equations. The completely general solutions to the equations are undoubtedly too vague to be practicable. However, a two-dimensional study of the electromagnetic field radiated by a rigid source can answer some of the questions regarding these relationships.

If a definite relationship could be established between signal amplitude and wander, the problems of the experimental determination of wander would be greatly simplified. It would then be possible to compute the various properties of wander, of which the measurement is difficult, knowing the properties of the amplitude of the signal, which can be recorded with relative ease. Unfortunately, no such definite relationship exists, because there is a solution to the equations which gives a very general expression for the amplitude without any wander whatever. However, the maximum possible wander which can accompany a given amplitude distribution can be determined.

The analyses presented here demonstrate the existence of the solution with no wander and show the relationship which exists between a given amplitude scattering pattern and the maximum wander associated with it. As a basis for the analyses it is assumed that the patterns of the amplitude and relative phase of the signal reflected by the target are fixed relative to the target. As the target rotates, so do the amplitude and phase patterns.

~~CONFIDENTIAL~~

The spectrum of the amplitude and wander measured by a radar receiver are then calculable from the amplitude and phase patterns when the target has a uniform rate of rotation with respect to the receiver. Such an assumption implies that the illuminating source has a fixed position relative to the target, and that the target is a perfectly rigid body. Although the assumption is obviously unjustifiable, the nature of the conclusions is such that their applicability is not seriously restricted.

#### 2.41 The Field at a Fixed Distance from a Target

In the two-dimensional problem considered in this analysis the electromagnetic field reflected from (or radiated by) the target can be expressed most conveniently in circularly cylindrical coordinates. At distances from the target which are large compared with the target and the wavelength the field can be represented by linear combinations of the elementary wave functions

$$\Psi_{nhk} = e^{jn\theta} H_n^{(1)}[(k^2 - h^2)^{\frac{1}{2}} R] e^{\pm jhz - j\omega t}, \quad 2-36$$

where  $R$ ,  $\theta$ , and  $z$  are the orthogonal coordinates and  $H_n^{(1)}$  indicates a Hankel function of the first kind and order  $n$ .<sup>26</sup> In this two-dimensional analysis, the field is invariant in the  $z$ -direction.

It is shown in Appendix E that the signal received by a linearly polarized antenna at a fixed  $R$  is given by

$$S = \sum_{n=-N}^N a_n e^{jn\theta} \triangleq A_S e^{j\phi_S} = S(\theta). \quad 2-37$$

This summation is essentially a Fourier series representation of the signal on a circle, with the target as its center, as a function of angular measurement along the circle. The limit  $N$  is in practice dependent on the size of the target measured in wavelengths.

The bounded sum can also be represented by a product of  $2N$  factors.

If we define

$$S(w) \triangleq \frac{a_N}{w^N} \prod_{n=1}^{2N} (w + w_n), \quad 2-38$$

where

$$w \triangleq r e^{j\theta}, \quad w_n \triangleq r_n e^{j\theta_n}, \quad 2-39$$

we obtain, for  $r = 1$ ,

$$S(\theta) = \frac{a_N}{e^{jN\theta}} \prod_{n=1}^{2N} (e^{j\theta} + w_n). \quad 2-40$$

It is demonstrated in Appendix E that Eq's. 2-37 and 2-40 are equivalent.

The positions of the  $w_n$ 's, which may be considered to be the zeros of  $S(-w)$ , in the complex  $w$ -plane are the significant quantities determining the behavior of  $S(\theta)$  in Eq. 2-40.

The amplitude and phase of  $S(\theta)$  can be separated by taking the natural logarithm of Eq. 2-40. The resulting expressions are

$$\ln A_S = \ln |a_N| + \frac{1}{2} \sum_{n=1}^{2N} \ln [1 + r_n^2 + 2r_n \cos(\theta - \theta_n)], \quad 2-41$$

$$\phi_S = \theta_{a_N} - N\theta + \sum_{n=1}^{2N} \theta_n + \sum_{n=1}^{2N} \tan^{-1} \left[ \frac{\sin(\theta - \theta_n)}{r_n + \cos(\theta - \theta_n)} \right]. \quad 2-42$$

### 2.42 Image Points in the $w$ -plane

The image point of any  $w_n$  in the complex  $w$ -plane is defined as that point with the same angle  $\theta_n$  and with a radius equal to the reciprocal of the radius  $r_n$  of the point  $w_n$ . In other words,  $w_1$  and  $w_2$  are said to be the image points of each other if  $\theta_1 = \theta_2$  and  $r_1 = \frac{1}{r_2}$ .

Very simple relationships exist between the amplitude functions and between the phase functions of  $w_n$ 's located at image points. If  $w_2$  is the image point of  $w_1$ , the amplitude functions associated with each are the same except for a constant factor, which can be absorbed in  $|a_N|$ . To demonstrate

CONFIDENTIAL

this similarity, substitute  $r_2 = 1/r_1$  and  $\theta_2 = \theta_1$  into the final term of Eq. 2-41, giving

$$\begin{aligned} \ln [1 + r_2^2 + 2r_2 \cos(\theta - \theta_2)] &= \ln \left[ 1 + \frac{1}{r_1^2} + \frac{2}{r_1} \cos(\theta - \theta_1) \right] \\ &= \ln [1 + r_1^2 + 2r_1 \cos(\theta - \theta_1)] + \ln \left[ \frac{1}{r_1^2} \right]. \end{aligned} \quad 2-43$$

The sum of the phase functions associated with each of a pair of image points is  $\theta$ , apart from a constant phase factor which can be absorbed in  $\theta_{a_N}$ . This relation is based on the fact that trigonometric manipulation yields the identity

$$\tan^{-1} \left[ \frac{\sin(\theta - \theta_1)}{r_1 + \cos(\theta - \theta_1)} \right] + \tan^{-1} \left[ \frac{\sin(\theta - \theta_1)}{1/r_1 + \cos(\theta - \theta_1)} \right] = \theta - \theta_1. \quad 2-44$$

Now let it be assumed that each  $w_n$  within the unit circle in the  $w$ -plane is paired with a first-order pole,  $\frac{1}{w}$ , at the origin of the  $w$ -plane. The phase introduced along the circle  $r = 1$  by the pole is just  $-\theta$ . The phase function of the  $w_n$  and the pole is therefore just the negative of the phase function of the image of  $w_n$ , while the amplitude function of the  $w_n$  and the pole is equal to that of the image of  $w_n$ .

It has just been shown that any zero of  $S(-w)$  can be moved to its image point without affecting the amplitude of  $S(\theta)$ , but with a very real change in the phase of  $S(\theta)$ . If the  $2N$  zeros are for the most part in different positions in the  $w$ -plane, as is most generally the case, there are approximately  $2N!$  different phase patterns associated with a given amplitude pattern.  $N$  is generally considerably greater than the maximum target dimension measured in wavelengths, with the result that there is, in practice, an extremely large number of phase patterns which can accompany a given amplitude-scattering pattern.

CONFIDENTIAL

2.43 Minimum Phase for a Given Amplitude Pattern

It is now possible to find a distribution of  $w_n$ 's in the  $w$ -plane which results in a phase function  $\phi_S(\theta) = 0$ , with one exception, for all  $\theta$  with any given amplitude function  $A_S(\theta)$ . The one exception occurs when  $A_S = 0$ , in which case a 180-degree phase discontinuity in  $\phi_S(\theta)$  is possible. If, on the other hand, we permit  $A_S$  to assume negative values, the 180-degree discontinuity is avoided, and the result has no restrictions.

Consider first the amplitude function associated with a pair of zeros,  $w_1$  and its image  $w_2$ . According to Eq's. 2-41 and 2-43,

$$\ln A_S = \ln |a_N| + \frac{1}{2} \ln \left[ \frac{1}{r_1^2} \right] + \ln [1 + r_1^2 + 2r_1 \cos(\theta - \theta_1)] , \quad 2-45$$

which gives for the amplitude function

$$\begin{aligned} A_S &= 2a_N \left[ \frac{1}{2}(r_1 + 1/r_1) + \cos(\theta - \theta_1) \right] \\ &\triangleq 2a_N [b_1 + \cos(\theta - \theta_1)] . \end{aligned} \quad 2-46$$

If  $S(w)$  is made up only of such factors as these, occurring in image pairs, the resulting amplitude function can be written

$$\begin{aligned} A_S &= 2a_N \prod_{n=1}^N [b_n + \cos(\theta - \theta_n)] \\ &= B_0 + \sum_{n=1}^N B_n \cos(n\theta - \theta'_n) . \end{aligned} \quad 2-47$$

The latter expression for  $A_S$  is a general Fourier series expansion in terms of  $\theta$ , which can adequately represent any two-dimensional amplitude scattering pattern encountered in practice.

The phase function associated with the  $N$  image pairs which determine Eq. 2-47 is

$$\phi_S = N\theta + \sum_{n=1}^N \theta_n , \quad 2-48$$

as can be seen from Eq's 2-42 and 2-44. If an  $N^{\text{th}}$  order pole is added at the origin of the  $w$ -plane, it adds  $-N\theta$  to the expression for the phase function, without affecting the amplitude pattern. The resulting phase function is simply a constant, which is completely irrelevant in the determination of wander.

The existence of an arbitrary amplitude pattern with no phase-front distortion has been demonstrated. It is not possible to say from the analyses presented here that the converse is true, namely, that an arbitrary phase pattern can exist with a constant amplitude pattern. However, the former relation is the one of interest in this research, for it shows that nothing definite can be said about the nature of wander from the measurement of the amplitude of the radar return from a target.

The probability density distribution of  $A_S$  is, in the case of highly complex targets, closely approximated by the Rayleigh distribution, as given in Eq. 2-25. If such is the case, the probability  $p(A_S=0) = 0$ , and the 180-degree phase discontinuities mentioned above are no longer possible. Then the wander of the apparent center becomes identically zero for the  $w_n$  distribution just considered.

#### 2.44 Maximum Wander with a Given Amplitude Pattern

The greatest possible phase pattern that might accompany a given amplitude scattering pattern can be found explicitly with the aid of the conclusions reached in Sec. 2.42. If it is assumed that all the  $w_n$ 's lie outside the unit circle of the  $w$ -plane, and that the pole at  $w = 0$  is removed,  $S(w)$  and  $\ln [S(w)]$  are analytical on and within the unit circle. The relationship between the amplitude and phase can then be found using a method of Wiener for determining the real and imaginary parts of a periodic function.

~~CONFIDENTIAL~~

With the above assumptions,  $\ln [S(w)]$  can be expanded in a Maclaurin series for  $r \leq 1$ ; thus,

$$\begin{aligned} \ln [S(w)] &= \ln A_S + j\phi_S = \ln a_N + \sum_{n=1}^{2N} \ln [w + w_n] \\ &= \sum_{k=0}^{\infty} c_k w^k . \end{aligned} \quad 2-49$$

On the unit circle,  $w^k$  can be written

$$w^k = e^{jk\theta} = \cos k\theta + j \sin k\theta . \quad 2-50$$

If the constants in the summation of Eq. 2-49 are split into their real and imaginary components,  $c_k = R[c_k] + jI[c_k]$ , the real and imaginary parts of  $\ln [S(w)]$  can be written

$$\ln A_S = \sum_{k=0}^{\infty} (R[c_k] \cos k\theta - I[c_k] \sin k\theta) \quad 2-51$$

$$\phi_S = \sum_{k=0}^{\infty} (R[c_k] \sin k\theta + I[c_k] \cos k\theta) . \quad 2-52$$

The angular pointing error produced in a radar system by  $\phi_S$  given in Eq. 2-52 is, according to the results of Sec. 2.1, proportional to  $\frac{1}{R} \frac{d\phi_S}{d\theta}$ .

The wander of the apparent center of the signal source is then directly proportional to  $\frac{d\phi_S}{d\theta}$ , which is given by

$$\frac{d\phi_S}{d\theta} = \sum_{k=0}^{\infty} k (R[c_k] \cos k\theta - I[c_k] \sin k\theta) . \quad 2-53$$

If  $\frac{d\theta}{dt}$  is constant, the relationship between the spectrum of wander, given in Eq. 2-53, and the spectrum of  $\ln A_S$ , given in Eq. 2-51, is very apparent.

It remains to be shown that the wander given by Eq. 2-53 is the maximum that can accompany any given amplitude function, as expressed in Eq. 2-51. To demonstrate this condition, it is necessary to prove merely that the total wander is reduced whenever any  $w_n$  is moved to its image point within

~~CONFIDENTIAL~~

the unit circle and a pole is added at the origin of the  $w$ -plane.

The phase function associated with any  $w_n$ , according to Eq. 2-42 is

$$\phi_S = \tan^{-1} \left[ \frac{\sin(\theta - \theta_n)}{r_n + \cos(\theta - \theta_n)} \right] . \quad 2-54$$

The derivative with respect to  $\theta$  of this function,

$$\frac{d\phi_S}{d\theta} = \frac{1 + r_n \cos(\theta - \theta_n)}{1 + r_n^2 + 2r_n \cos(\theta - \theta_n)} , \quad 2-55$$

always has its peak value when  $\theta = \theta_n + \pi$ . When  $r_n$  is substantially different from unity, this peak value is small and broad, and the resulting wander is not ever great. On the other hand, when  $w_n$  is close to the unit circle, the peak of  $\frac{d\phi_S}{d\theta}$  is very large and sharp. As a result, the significant wander produced by such a  $w_n$  is great over a small range of  $\theta$ ; for the remaining values of  $\theta$  the wander is substantially less important.

In all cases of practical importance the distribution of the  $w_n$ 's in the  $w$ -plane is more or less uniform with respect to  $\theta$ . Consequently, it is necessary to investigate the influence on wander of any  $w_n$  only in the vicinity of the peak it produces. When all  $r_n$ 's are greater than unity, all the peaks of wander are of the same sign, and all the peaks in a small range of  $\theta$  tend to add together. If a  $w_n$  is brought inside the unit circle (and a pole added at the origin), the effect on  $\phi_S$ , and therefore on  $\frac{d\phi_S}{d\theta}$ , is a change in sign, according to the conclusions of Sec. 2.42. The net result of moving a  $w_n$  to its image point inside the unit circle is thus shown to be a significant decrease in total wander in the vicinity of  $\theta = \theta_n + \pi$ , without any great change in wander for other values of  $\theta$ .

## 2.5 FURTHER STUDIES OF WANDER WITH PHASE-COMPARISON SYSTEMS

The presence of wander gives rise to some phenomena which are peculiar



to phase-comparison systems. These events must be studied before such systems can be designed to give the optimum performance of which they are capable. The first problem to be considered is that of bandwidth requirements in the measurement section of a phase-comparison system which is designed to operate with very short target ranges. Secondly, brief consideration is given to the possibility of deemphasizing the large values of wander which are accompanied by deep fades in signal amplitude through the use of partial limiting.

#### 2.51 Bandwidth Requirements with Targets at Short Range

When a target approaches close to a phase-comparison radar system, the possibility exists that the radar system may not be able to furnish any angular information on the position of that target. Such a condition is brought about by the presence of wander of the apparent center of the target. It may become serious when the physical angle subtended at the radar receiving antennas by the wander approaches or exceeds the angular width of a lobe of the interference pattern of the antennas.

To illustrate the manner in which wander can cause this blindness in phase-comparison systems, let it be assumed that the magnitude of the phase difference produced by the wander is inversely proportional to range. This assumption implies that the wander is constant in terms of feet at the target regardless of range; the wander caused by specular reflection from various target areas in succession is a good example of such wander. Furthermore, assume that the plot of wander as a function of time has a triangular waveshape, so that the wander is always uniformly increasing or decreasing with respect to time. Whenever the peak-to-peak phase difference caused by such wander is an integral multiple of  $2\pi$ , the output of any phase-detector

with a symmetrical characteristic has an average value of zero, regardless of the average phase difference. If a low-pass filter were to eliminate all but the average component of the phase-detector output, the output would be zero for all target positions. This example is an extreme case; in practice, a system would seldom go completely blind, but instead would seem to have a decreasing measurement sensitivity with decreasing range.

It is possible to avoid any chance of this blindness by means of proper system design. It can be seen from the diagrams of the various phase-comparison systems in Appendix B that the phase of the output is equal to the phase difference of the two inputs for every system, when no filtering exists in the frequency band of the information. The average value of the phase of the output must then equal the average phase-difference of the inputs. Thus the criterion for avoiding blindness in a phase-comparison system is the maintenance of adequate bandwidths in the measurement section, through the final nonlinear circuitry from which the angular information is obtained.

The bandwidths needed at various points in the measurement section of a system free from blindness may be substantially greater than the bandwidth of the wander. A short discussion will be given here indicating the increase in spectrum width that may exist at different points of a system. For mathematical convenience, a sinusoidal wander at a frequency  $\omega_w/2\pi$  will be assumed, giving a phase difference at the antennas of

$$\phi = \phi_0 \sin \omega_w t . \quad 2-56$$

The signal out of the phase detectors in a single-sideband-modulator system (or in the nulling-servo system if the servo is blocked) is roughly

$$\frac{\sin(\phi)}{\cos(\phi)} = \frac{\sin(\phi_0 \sin \omega_w t)}{\cos(\phi_0 \sin \omega_w t)} . \quad 2-57$$

Such a waveform (essentially a phase-modulated signal with a carrier frequency of zero) has a bandwidth approximately given by

$$BW = (\phi_0 + 1) \omega_w / 2\pi \text{ cps.}, \quad 2-58$$

where  $\phi_0$  is given in radians. The balanced mixers in the single-sideband-modulator system double this bandwidth. The bandwidth is preserved through the adder, for it can be readily ascertained that the bandwidth of the signal

$$\cos(\omega_r t - \phi) = \cos(\omega_r t - \phi_0 \sin \omega_w t) \quad 2-59$$

is again approximately

$$BW = 2(\phi_0 + 1) \omega_w / 2\pi. \quad 2-60$$

The outputs of the interferometer system and the Doppler-difference system have the same form as Eq. 2-59, with the result that the bandwidths in these systems are comparable with those given above. In the nulling-servo system, it is necessary that the servomechanism be capable of following variations only up to the highest frequency present in the wander. Then the phase detector will always be operating on a linear portion of its characteristic.

The bandwidths determined by substituting in Eq's. 2-58 and 2-60 the maximum values of  $\phi_0$  and  $\omega_w$  encountered in actual cases may be as high as a few hundred cps. For example, if a 30-foot peak value of wander at 30 cps were measured with a X-band system with an 18-inch antenna spacing, the bandwidth determined by Eq. 2-60 would be 220 cps for the target at 1000 feet. However, in all probability the bandwidths so computed are appreciably larger than those which would be required in practice, for a number of reasons. In the first place, the energy in the wander is usually spread out over the entire spectrum up to the maximum frequency, and is concentrated principally about zero frequency. The sinusoidal wander assumed in the

calculations is a bit unreal in that it concentrates all the energy at one frequency. Another difference between sinusoidal wander and the more random wander encountered in practice is that the probability density distribution of the former has maxima at the peak values of wander instead of at the mean value, as does the latter.

Secondly, the bandwidth computations were based on the assumption of wander with a constant magnitude measured in terms of feet at the target, regardless of range. This assumption implies that the wander results from true motion of the actual center of reflection. Considerably less bandwidth may be required if the wander is caused by interference between the signals from two or more stationary points, as is more probably the case. Consider, for instance, the two-point target analyzed in Sec. 2.2. The phase-detector outputs plotted in Fig. 2-9 do not show any significant increases in bandwidth as the range decreases. If the long-range wander in this plot were produced by true motion of a reflecting area, there would be a remarkable increase in bandwidth for values of  $\mu$  near 180 degrees. It can be concluded, therefore, that the computations based on a constant magnitude of wander at the target give larger values of signal bandwidth within a system than will probably exist in practice.

Finally, it is not necessary in all cases that the signal which would exist at any point in an idealized system be completely reproduced at the corresponding point in an actual system, in order that the average value of phase difference be measurable. As an illustration of this fact, consider a nulling-servo system in which the servo bandwidth is inadequate to follow completely the changes in phase difference at the antennas. Even though a phase lag may develop in the phase-shifter output due to servo sluggishness,

as long as the lag is less than about 60 degrees, the phase-detector operation continues to be essentially linear. Whenever the operation is linear, there is no chance of the system going blind.

#### 2.52 Reduction of Large Errors with Partial Amplitude Limiting

The difference in phase of the signals received from a target by the two antennas of a phase-comparison system may occasionally deviate from its average value by an extraordinary amount. The wander associated with such a deviation can indicate that the apparent center of reflection is far outside the physical boundary of the target. An example of this condition is shown in Fig. 2-5 of Sec. 2.21 on the wander of the apparent center of a two-point target. The existence of large deviations in the position of the apparent center of a multi-point target is also possible, as is evident from inspection of Eq. 2-29.

These large errors in apparent position are almost invariably accompanied by a substantial reduction in the received-signal strength. In the case of the two-point target, the wander peaks occur when the signals from the two points are out of phase at the receiver, giving a resultant signal only 0.2 as large as the signal from the stronger point. The large errors indicated by Eq. 2-28 are for the most part due to the presence of  $A_2$  in the denominator of Eq. 2-22, as can be realized from a study of the probability distribution functions of  $D_p$  and  $A_2$ , given in Eq's. 2-24 and 2-25.

The output of the error-detector in a phase-comparison system has an undesired component due to wander. The rms value of this component is increased greatly by the occasional large output which accompanies a spike of wander, provided complete amplitude limiting precedes the error detector. However, if incomplete limiting is used, then all readings of phase difference

taken during deep signal fades are multiplied by the strength of the signal, while those taken with normal signal strength are unaffected. In this manner the deleterious effects of the large excursions of the apparent center are substantially reduced.

The nature of the large errors is such that it would be very possible to employ partial limiting in an idealized system. The probability of the presence of these errors in any practical situation is small, because the probability distribution of the magnitude of the received signal is generally something approaching a Rayleigh distribution. For such a distribution, the probability that the instantaneous signal amplitude is less than half the rms value of the amplitude is only 0.22. Furthermore, since the target is constantly in motion, even when these errors arise, they will last for only a short time. Therefore, it is possible to reduce the influence of these errors on the output through the use of partial limiting (or no limiting at all) in conjunction with a slow-acting automatic gain control.

It is probably undesirable to use no amplitude limiting in a phase-comparison system. In the first place, the gain of the radar system to true angular errors changes with variations in the error-detector sensitivity, which is proportional to signal amplitude. Changes in the radar-system gain would affect the sensitivity and stability of any overall system of which the radar was a part.

Secondly, the undesired noise in the error-detector output can actually be increased when limiting is removed if the radar axis is not pointed directly at the target. The desired output, which is proportional to aiming error, from a system without limiting is multiplied by the instantaneous magnitude of the received signal. A study is made in Appendix D of the

**CONFIDENTIAL**

error-detector output of a system without limiting for the multi-point target, considered as in Sec. 2.3, at long range. It is shown that the mean squared value of the jitter in the output, in terms of a linear coordinate at the target is given by

$$\overline{(Z - z_0)^2} = 0.272 z_0^2 + 0.637 \overline{z_n^2}, \quad 2-61$$

where  $z_0$  is defined as the distance of the center of the target away from the axis of the antenna system of the radar. The probability density distribution of the output is determined in the appendix, and is plotted for various values of  $z_0/(\overline{z_n^2})^{1/2}$  in Fig. 2-15. It can be seen from this plot and from Eq. 2-61 that the dispersion of the output about its correct value increases considerably with increasing  $z_0$  for a system without limiting. If the system had perfect amplitude limiting, the dispersion of the output would be independent of  $z_0$  for all operating conditions within the linear range of the phase-detector characteristic.

The use of partial limiting, with the knee of the limiter characteristic corresponding to an input of perhaps 0.3 to 0.5 of the average value of the input, is a possible means for minimizing the jitter in the error-detector output. Probably the chief difficulty involved in the use of partial limiting is a practical one. The design and construction of limiters with no change in phase shift in the operating region near the knee of their characteristics is a very exacting task, particularly if the limiters are intended for pulsed i-f signals.

If the problems of building limiters for partial limiting prove overwhelming, it is probably preferable to use complete limiting rather than no limiting. The occasional large errors which exist with limiting are troublesome only at long ranges, because at short ranges system nonlinearities

**CONFIDENTIAL**

CONFIDENTIAL

PROBABILITY DENSITY FUNCTION  
 OF PHASE-DETECTOR OUTPUT  
 FOR VARIOUS CONSTANT AIMING ERRORS  
 PHASE-COMPARISON SYSTEM-NO LIMITING  
 MULTI-POINT TARGET AT VERY LONG RANGE

Z = OUTPUT REFERRED TO A LINEAR  
 COORDINATE AT THE TARGET

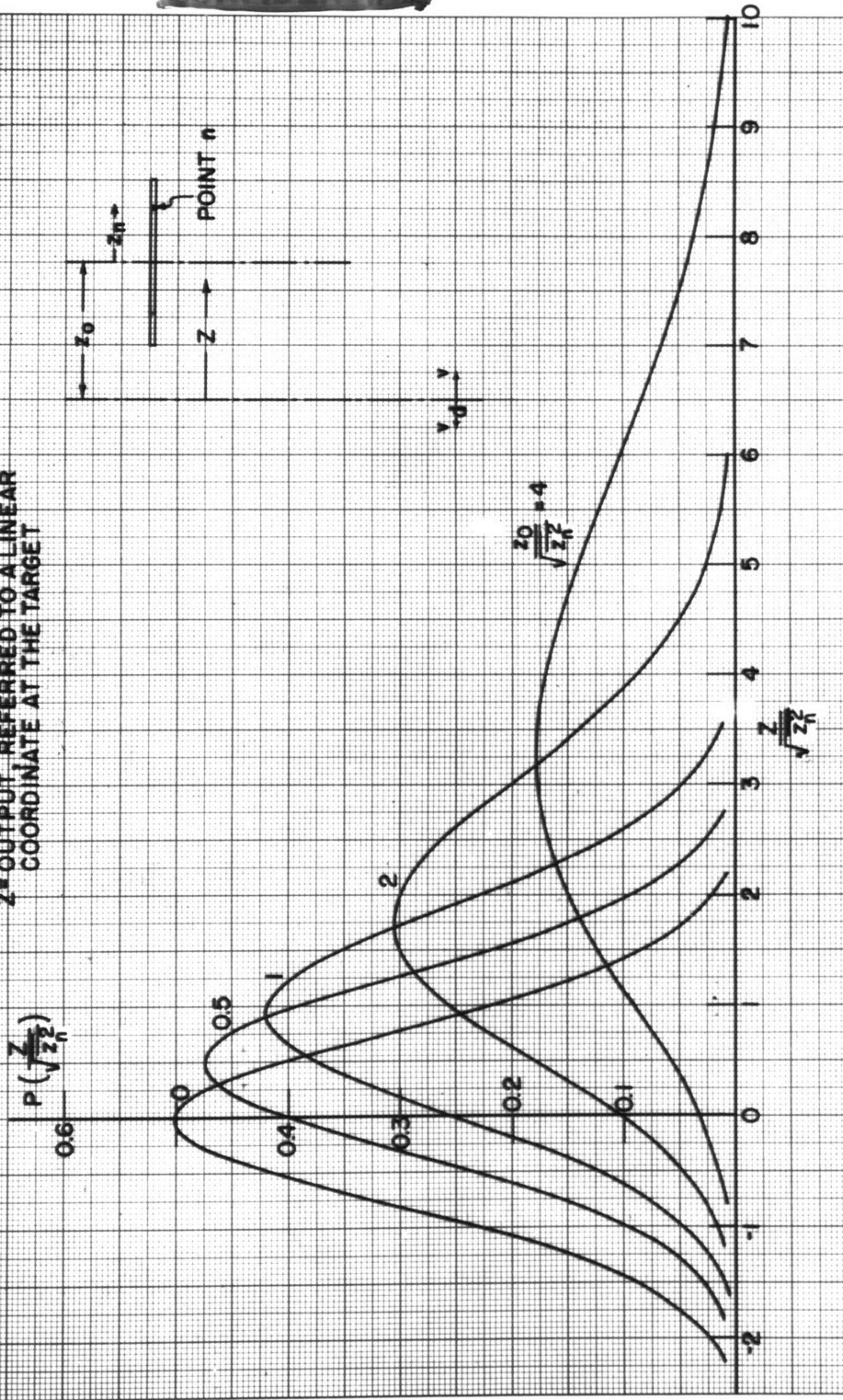
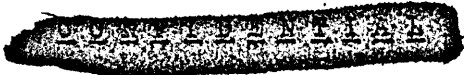


FIG. 2-15





severely limit the magnitude of errors that can take place. In many applications, the excess noise introduced by amplitude fluctuations in systems without limiting will be greater than that caused by the occasional large peaks of wander.



### 3. THE EXPERIMENTAL DETERMINATION OF WANDER

An experimental program was conducted for the purpose of acquiring data on the nature of target-echo fluctuations from a variety of aircraft in flight. The principal value of the program lies in the spectra of wander of the apparent radar center which were obtained from data records made during a number of flight tests. Received-signal amplitudes were also recorded during the tests, and their spectra are presented along with the wander spectra.

A phase-comparison system with amplitude limiting was used to measure the wander as a function of time. The changes in average phase-difference due to target maneuvers were removed, with the result that the phase-detector output was due to wander and thermal noise alone. With such a system, the output of the phase detector is directly proportional to the wander, provided that the target range is sufficiently great to insure that the phase differences due to the wander are always within the limits of linear phase-detector operation. The output of the phase detector was recorded to obtain the desired wander data. It is shown in Sec. 2.15 of the previous chapter that the wander thus measured would likewise be obtained from lobe-comparison systems with targets at long range.

Two separate series of flight tests for recording wander data were conducted. The first series was held at the Naval Aviation Ordnance Test Station, Chincoteague, Virginia, during the summer of 1949, using many of the major radar components from the Meteor S-band Model-II pulse seeker.<sup>27</sup> Many shortcomings were later found in the results of these tests, particularly in the phase records. The second set of tests was made during the winter of

[REDACTED]

1950-1951 from the roof of the Research Laboratory of Electronics at M. I. T., using X-band pulse equipment. These tests were considerably more successful than the S-band tests, and provided an appreciable quantity of satisfactory data on wander.

Because of the greater significance of the results of the X-band tests, these tests will be described first and in greater detail. The S-band tests are considered next; while the results are not accurate, nevertheless some interesting comparisons can be made between echo fluctuations at S-band and X-band frequencies.

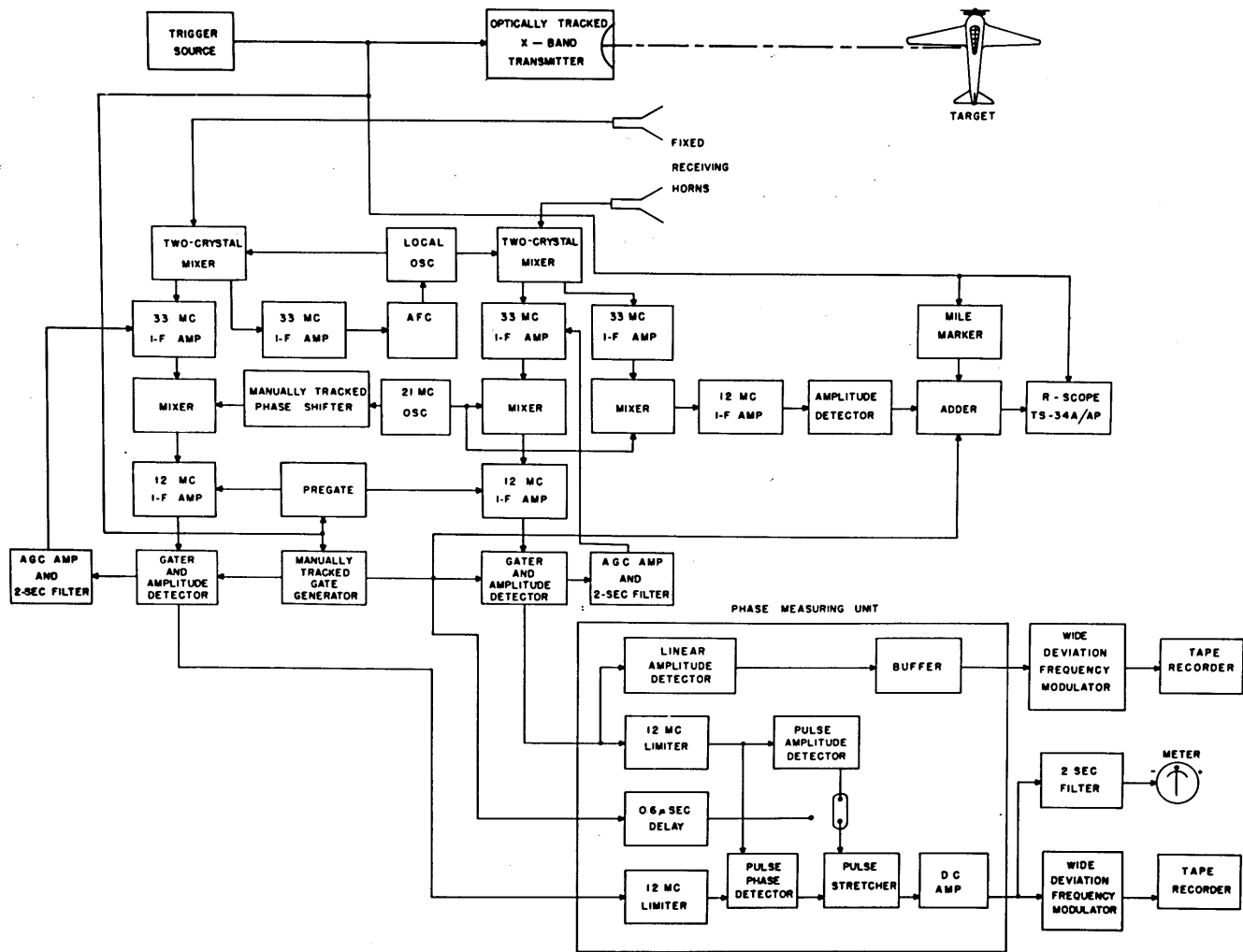
### 3.1 X-BAND WANDER TESTS

Records of phase difference between the echo-signals received by two adjacent antennas, and of the amplitude of one of the signals, were made and analyzed in this experimental investigation. The two X-band antennas, which had roughly a 40-degree beamwidth between half-power points, were rigidly mounted with a spacing of 5 feet. The line joining the antennas was approximately normal to the average direction to the targets as they flew over various prescribed courses. This antenna spacing gave a system sensitivity of 300 degrees electrical phase difference per degree of rotation of the line-of-sight, or 1.6 degrees phase difference for a 1-foot lateral displacement of the apparent target center at 2 miles range. Such a value of system sensitivity was chosen as a compromise between the need for a large region of linearity with targets at close range and the desirability of overcoming the effects of thermal noise at longer ranges.

#### 3.11 Equipment for Obtaining Data

A block diagram of the pulse-radar system with which the data were measured is shown in Fig. 3-1, and a photograph of the receiving and measuring

[REDACTED]



RADAR SYSTEM  
FOR  
RECORDING TARGET NOISE DATA

Fig. 3-1

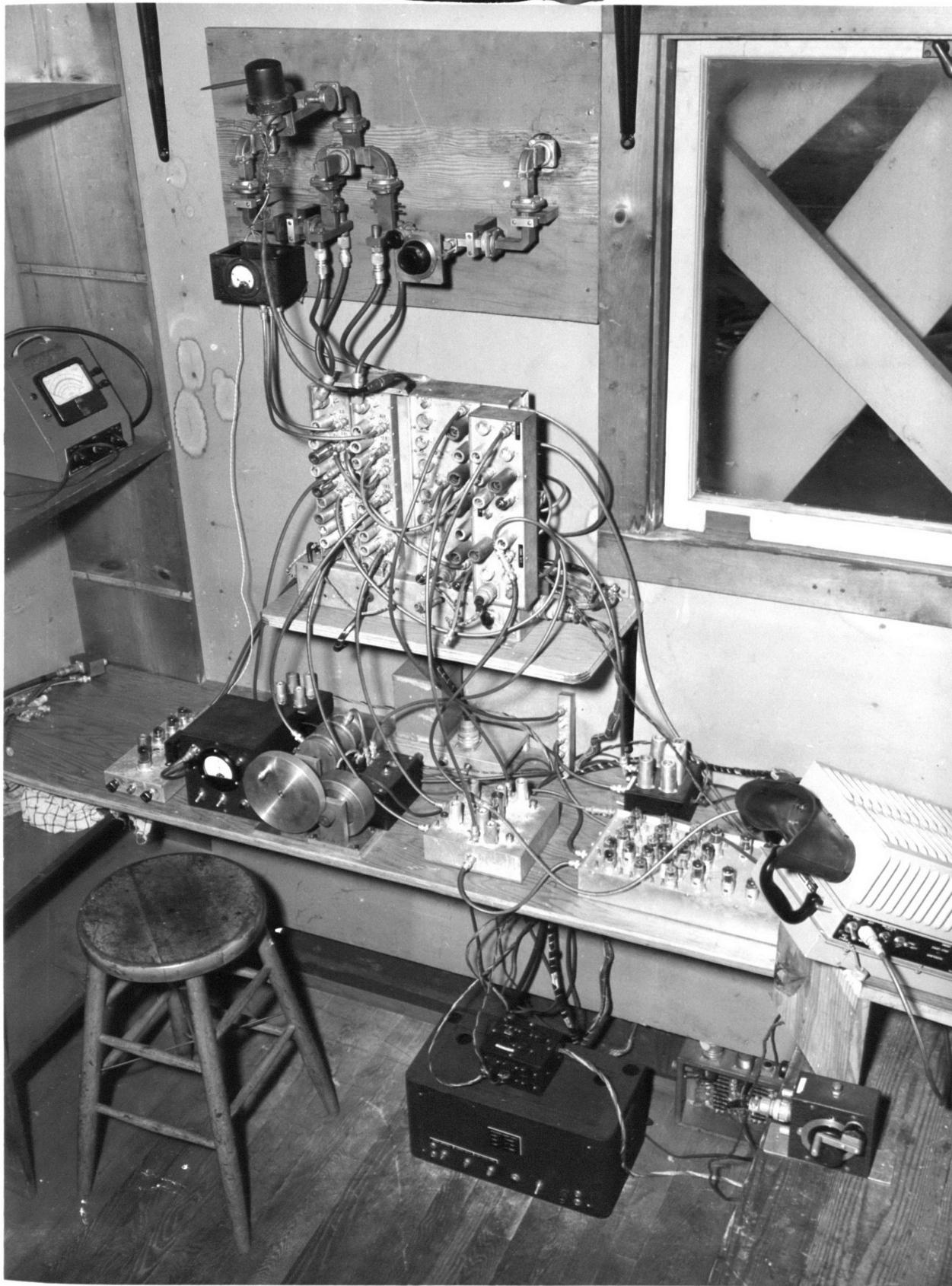


Fig. 3-2 Receiving and Measuring Sections of Radar System

sections is shown in Fig. 3-2. The transmitter, located atop a tower adjacent to the receiving equipment, produced 1-microsecond pulses of r-f energy with a peak power of 40 kw and at a repetition frequency of 900 pps. The transmitting antenna consisted of a 30-inch paraboloid with a horizontally polarized feed. The antenna was aimed manually at the target with the aid of a boresighted ring sight attached to it. The maximum range of the system with a medium sized target was about 6 miles.

The axes of the fixed receiving antennas were tilted at an angle of 22 degrees above the horizon, in order that good signals could be received from targets at long range while ground reflections were appreciably attenuated. The large changes in the difference of phases of the received signals which result from changes in target position were removed with a manually-driven continuous phase-shifter. A meter with a 0.2 second time constant was used in the output of the phase detector to provide the necessary error indication for the operator of the phase shifter. A large inertia wheel was connected to the shaft of the phase-shifter, with the result that the highest frequency at which the phase-shifter shaft could be oscillated was about 0.3 cps. As a consequence of the presence of the inertia wheel, the highest frequency component in any extraneous errors that might be introduced in the phase-shifter tracking was 0.3 cps.

The range gate, which had a duration of 1.3 microseconds, was kept on the target by manual tracking. The operator of the gate-tracking unit had a range-scope display with marks every mile as a gate-position indicator. During the tests, the target range was frequently read off the R-scope and recorded. A dual potentiometer was used as the control for the range-gate position. One section was required in the range-gate circuit; the other

~~CONFIDENTIAL~~

section was used to obtain the product of range and phase difference.

The time constant of the closed-loop response of the automatic gain control was about 0.3 second. It was necessary to maintain a long time-constant in order to avoid detrimental effects of phase-shift change with gain change in the i-f amplifiers. As long as such phase-shift changes were slow, they could be removed with the manually driven phase-shifter.

The phase-difference and amplitude data were recorded on magnetic tape moving at 7.5 inches per second, using separate frequency modulators and Magnecorder tape recorders. The frequency modulators had a maximum deviation of 70 percent of the center frequency of 4 kcps, which made it unnecessary to incorporate any wow compensation. The overall signal bandwidth of the record-playback equipment was greater than 100 cps, which was the half-power bandwidth of the measurement outputs of the radar system. The cutoff characteristics of the recorders and the measurement circuits were quite sharp, with the result that played-back data requires no amplitude compensation for frequency components below 80 cps.

Schematic diagrams and more thorough descriptions of the various circuits used in the radar and recording equipment are presented in Appendices F and H.

### 3.12 Description of Recorded Data

The two types of data normally recorded in these tests were obtained from the phase measuring unit of the radar system. The output of the pulse phase detector was stretched, amplified, and then multiplied by range in the tracking control of the range-gate generator. When a strong echo was being received, the voltage thus obtained was proportional to the wander of the apparent target center. The signal-amplitude record was obtained directly from an amplitude detector with an output proportional to one of the inputs

~~CONFIDENTIAL~~

**CONFIDENTIAL**

to the phase measuring unit. Slow amplitude fluctuations were removed by the agc prior to the amplitude detector, so that only those fluctuations above 0.5 cps were recorded.

A calibration was obtained for the wander records from a fixed land target at a range of 1.28 miles. The transmitting antenna and range gate were set on the target, and the manual phase-shifter spun through a number of complete revolutions. The phase-detector output, which was simply a reproduction of the voltage vs. phase characteristic, was then recorded. From a knowledge of the target range, antenna spacing, phase-detector characteristic, and peak phase-detector output, the desired calibration can be computed for any data taken with the recorder gain set at the value used in recording the calibration. As an example of the calibration procedure, assume that the system has a 5-foot antenna spacing with a transmitter frequency of 9375 mcps. The system sensitivity is then 2.53 degrees of electrical phase change per foot of lateral displacement of the target at 1.28 miles. If the phase-detector characteristic were linear from -90 to +90 degrees, the peak-to-peak output would correspond to  $180/2.53 = 71$  feet. From a plot of the characteristic, the difference between the actual peak-to-peak value and that of a triangular characteristic can be determined; in Fig. 3-3, the actual characteristic has a 22-percent smaller value. Thus the peak-to-peak voltage of this calibration record corresponds to 55 feet.

Three types of courses were flown during the tests by the various targets at an elevation of 1500 feet and a usual speed of 160 mph. A radial course along the perpendicular bisector of the line joining the antennas provided fixed head-on and tail-on views. A straight crossing course flown parallel to the line joining the antennas at a range of 2 miles gave a slowly

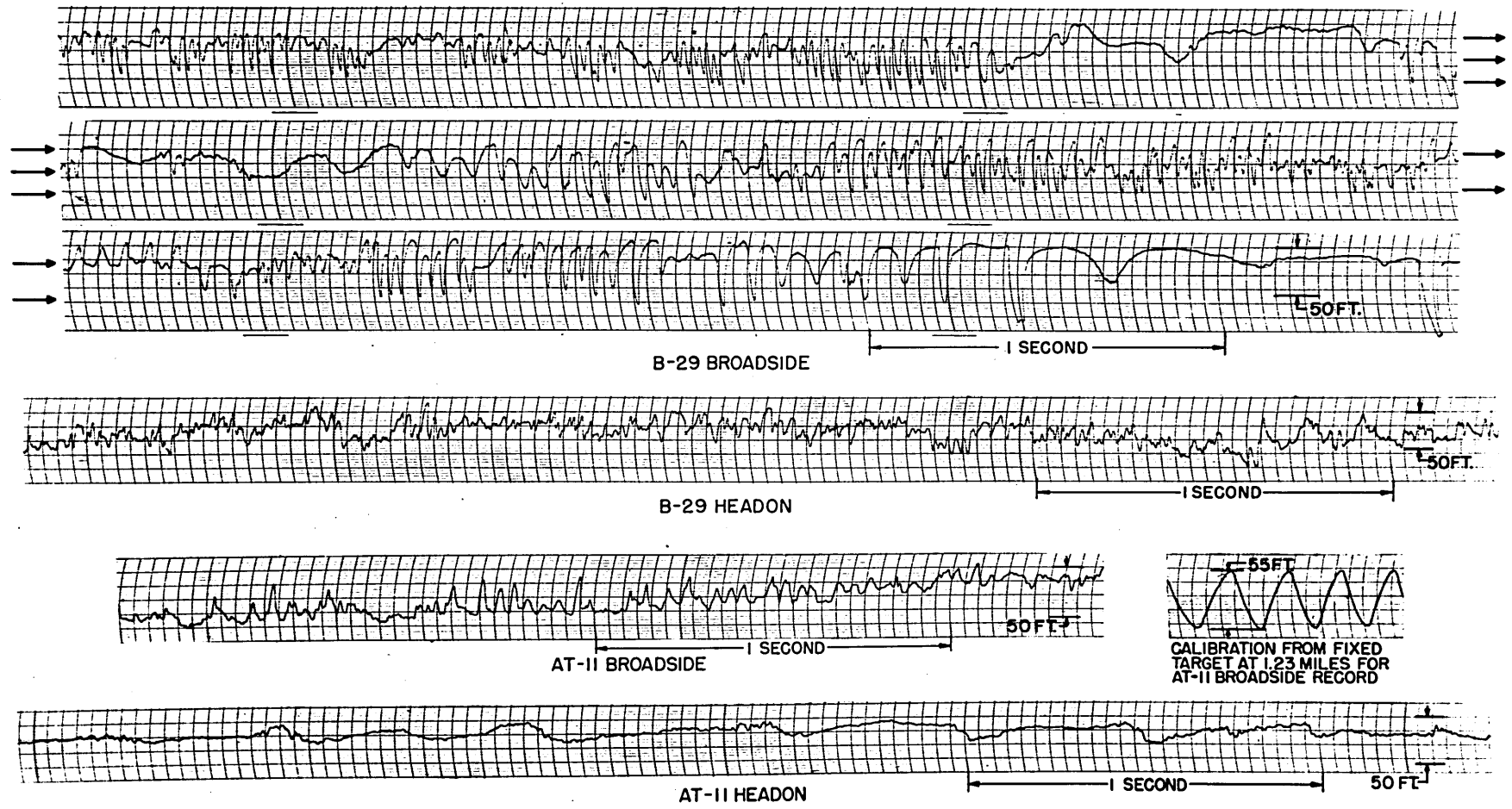
**CONFIDENTIAL**



changing broadside view of the targets. The circular course, which had a radius of 1.5 miles centered 3.5 miles from the radar along the perpendicular bisector, was to provide a continuously changing aspect of a maneuvering target. However, the only usable data from this course for most of the targets were obtained from the near- and far-broadside portions. Nevertheless, these data are very useful for comparing the spectra from maneuvering and non-maneuvering targets. Relatively long minimum ranges in the courses with broadside aspects were selected in preference to smaller ranges (with which lower system sensitivity could be used) in order to provide as much usable data from each run as possible.

The above-mentioned courses were used with six different types of aircraft. In addition, some special tests were made. Circularly polarized receiving antennas were used in one test in place of the linearly polarized ones normally used. The limiters of the phase measuring unit were bypassed in another test. Finally, data were obtained from two targets flying in close parallel formation on the radial and crossing courses. Table 3-1 is a summary of the types of aircraft for which data on fluctuations in amplitude and on wander were obtained.

Samples of typical data recorded during these tests are shown in Fig. 3-3. These pen-recorder copies were made from the magnetic tape originals recorded during the tests. Several points concerning these data are worthy of special mention. First, it should be noted that the magnitude of the wander is substantially greater for the broadside target aspect than for the head-on aspect. With the B-29 broadside, the wander occasionally exceeded the linear portion of the phase-detector characteristic, which corresponds to 90 feet (peak-to-peak) at 2 miles. As might be predicted, the ratio of



WANDER OF APPARENT RADAR CENTER OF B-29 AND AT-11 AIRCRAFT

Fig. 3-3

**CONFIDENTIAL**

- Single Propellor - AT-6 (Navy SNJ) - Additional data with circularly polarized receiving antennas
- Two Propellors - B-26 (Navy JD) - Additional data with no limiting  
- Simultaneous recording of amplitude and phase
- AT-11 (Navy SNB)
- C-46
- Four Propellors - B-29
- Jet Propelled - F-84
- Multiple Target - TBM - Two aircraft in close formation

Table 3-1 - Targets Used in Flight Tests

magnitudes of head-on wander to broadside wander was less for the AT-11 than for the B-29. (The spacing between nacelles of the 34-foot long AT-11 is 12 feet, whereas the B-29 outboard nacelles are separated by 62 feet and the length of the B-29 is 96 feet.) The gradual shift in one direction of the AT-11 broadside data is not significant; it is caused by inadequate tracking of the phase shifter in the radar receiver. Finally, the radical changes from time to time in the spectral character of the wander from the broadside B-29 should be noted. The changes can probably be attributed to yawing of the target; they were noted for other aircraft, particularly the C-46, and seemed to be most pronounced on windy days.

### 3.13 Method of Data Analysis

An elaborate procedure was used to reduce the data recorded during the flight tests. The data were first edited and copied, in order to obtain complete sections of good data for the various viewing aspects of the different targets. Then the data were analyzed with an electronic spectrum

**CONFIDENTIAL**

~~CONFIDENTIAL~~

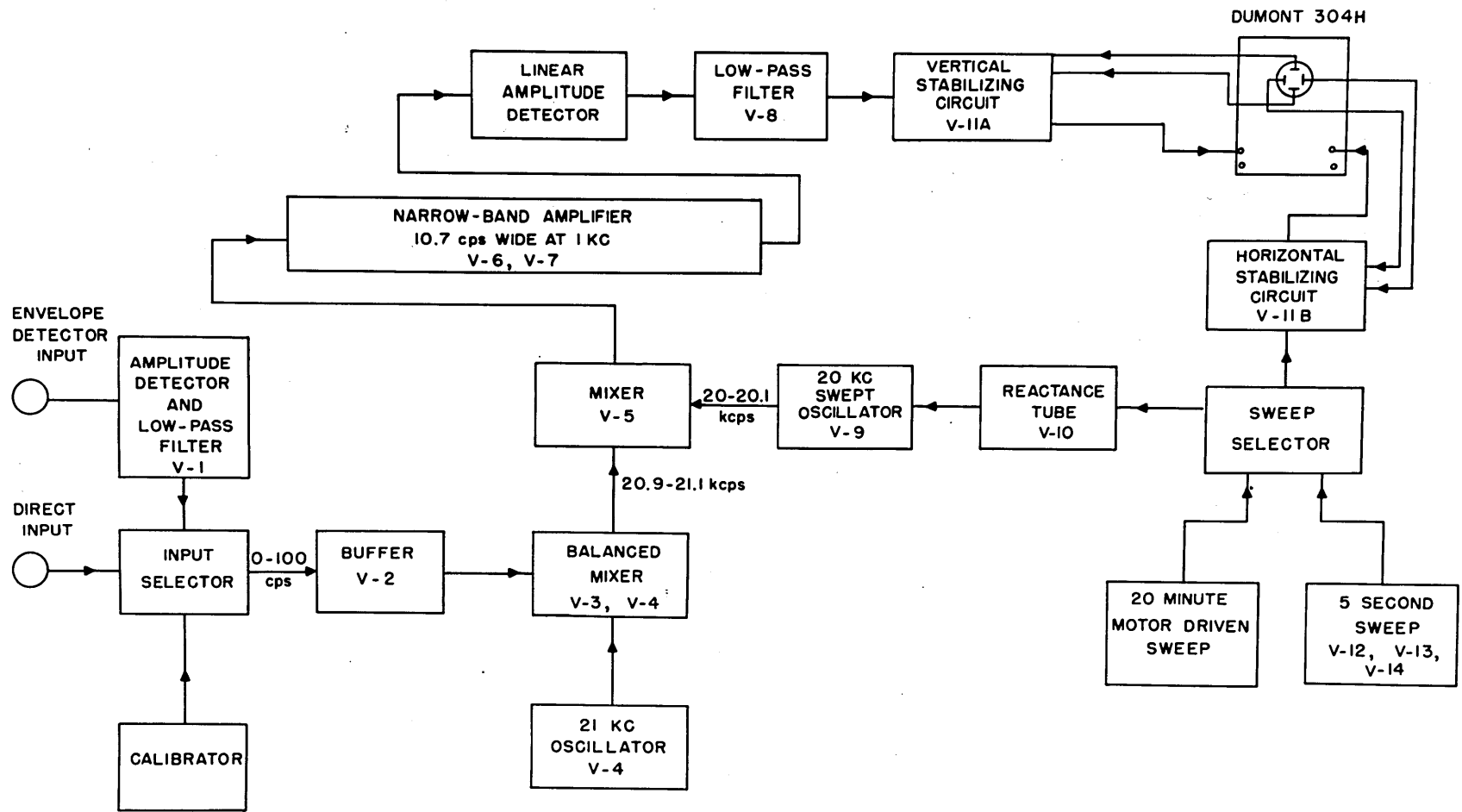
analyzer, which produced the desired frequency spectra.

The spectrum analyzer is essentially a narrow-band amplifier whose center frequency is in effect swept over the frequency band of the data to be analyzed. A block diagram of the analyzer is shown in Fig. 3-4. The analyzer has a resolution of 10 cps and, as operated in these tests, a sweep bandwidth of 140 cps. The center frequency was swept uniformly over the 140-cps band at a rate of 5.6 cps per minute. With such a slow sweep rate, the center frequency remained at essentially the same frequency for a complete playing of most sections of data that were analyzed. The low-pass filter on the output of the amplitude detector following the narrow-band amplifier selected the average value of the voltage density at any frequency. The average value was then displayed as the vertical deflection of the oscillograph spot. A schematic diagram and description of special circuits used in the analyzer are presented in Appendix G.

The first step in the data editing procedure was to select, after examination of both the amplitude and wander records, those sections of data with acceptable signal return and phase-shifter tracking. Copies were then made of all such sections. The copies were then usually cut into two or more shorter sections corresponding to different intervals of range, target aspect, or signal strength. The two ends of each of these subsections were spliced together, and the closed loop thus formed was used as a continuous source of data for the analyzer. Spectra were made with the loops played back at twice the recording speed; the resulting spectra had a bandwidth of 70 cps with a resolution of 5 cps.

After a study was made of all the spectra obtained in this manner, all the acceptable data for each kind of run with a given target was assembled

~~CONFIDENTIAL~~



0 - 200 cps SPECTRUM ANALYZER BLOCK DIAGRAM

Fig. 3-4

**CONFIDENTIAL**

and spliced together. The composite records thus formed were made into loops and played back at twice normal speed into the spectrum analyzer. Copies were then made of the composite records onto magnetic tape moving at 1.5 inches per second, using a carrier frequency of 400 cps. Then the copies were likewise formed into loops, played back at 15 inches per second, and analyzed. From these analyses, average spectra with 5-cps and 1-cps resolutions were obtained for the various aspects of the different targets. Fig. 3-5 is a photograph of the spectrum analyzer and playback equipment as operated with a continuous loop of tape. On the left are the tape recorder and the continuous-tape storing reel. The analyzer and power supply are on the right. The unit directly under the clock is the wide-band FM modulator and demodulator.

The spectrum analyzer was calibrated for the wander analyses with the aid of the calibration records described in the second paragraph of Sec. 3.12. An example will be used to describe the method. Assume that it is desired to set the analyzer so that a  $3 \text{ ft}/\sqrt{\text{cps}}$  spectral density gives a 1-inch deflection, with the data sped up by a factor of 2. It was determined from measurements that the effective noise bandwidth of the narrow-band amplifier is 10.75 cps. For the data supplied at twice normal speed, this is a noise bandwidth of 5.38 cps. Therefore, it can be said that a sinusoid with a rms value corresponding to  $3 \times \sqrt{5.38} = 6.95$  feet would give the same deflection as a flat spectral density of  $3 \text{ ft}/\sqrt{\text{cps}}$ . An adjustable source of sinusoidal voltage can be set at this value by comparison with the signal obtained from the calibration record played back at twice the recording speed. A similar method can be used for the analyses with a data speedup of 10; however, it should be remembered that the calibration record should be

**CONFIDENTIAL**

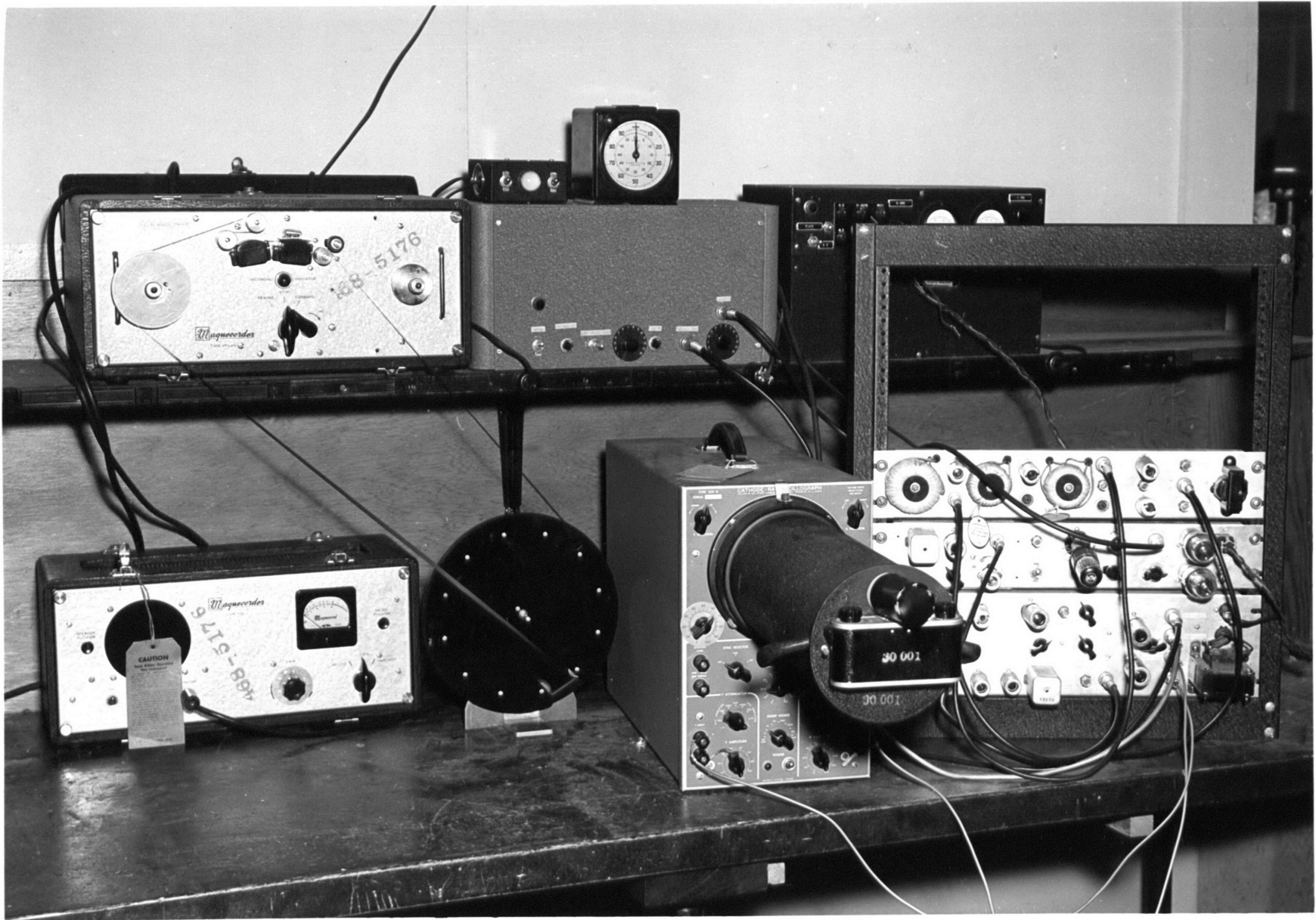


Fig. 3-5 Spectrum Analyzer and Playback Equipment

processed in the same manner as the data to be analyzed, because the level of the output of the playback equipment varies with changes in tape speed.

Details of the copying and editing procedure are presented in Appendix H, along with a description of the recording, playback, and copying equipment.

### 3.14 Spectra of Data on Single Targets

In this section are presented the spectra obtained from the data on wander and amplitude fluctuations measured with the various targets. The spectra are usually shown in pairs. The upper of each pair is the wander spectrum and the lower is the spectrum of the corresponding record of amplitude fluctuations. The horizontal scales of both types of spectra are linear with respect to frequency, the calibration being either 4 or 20 cps per large division, as is specified for each pair.

The vertical scales of the wander spectra are calibrated in feet/ $\sqrt{\text{cps}}$ . The value read off one of these curves at any frequency is the rms value of all the frequency components of wander within a 1-cps bandwidth centered at that frequency. In other words, if a given piece of data were passed through a filter with a 1-cps bandwidth, the rms value of the output of the filter would be the ordinate of the spectrum of the data at the center frequency of the filter. The ordinates of any of these spectra are larger by a factor of  $\sqrt{2}$  than the ordinates of the voltage spectrum computed by taking the square root of the Fourier transform of the autocorrelation function of the same original data. This difference arises from the fact that a Fourier transform of an autocorrelation function extends over all frequencies from  $-\infty$  to  $+\infty$ , whereas the spectra obtained here extend only over positive frequencies. The mean squared value of any data equals the integral of the Fourier transform of the autocorrelation of the data from  $-\infty$  to  $+\infty$ , or the



integral of the square of the spectrum as presented here from 0 to  $+\infty$ .

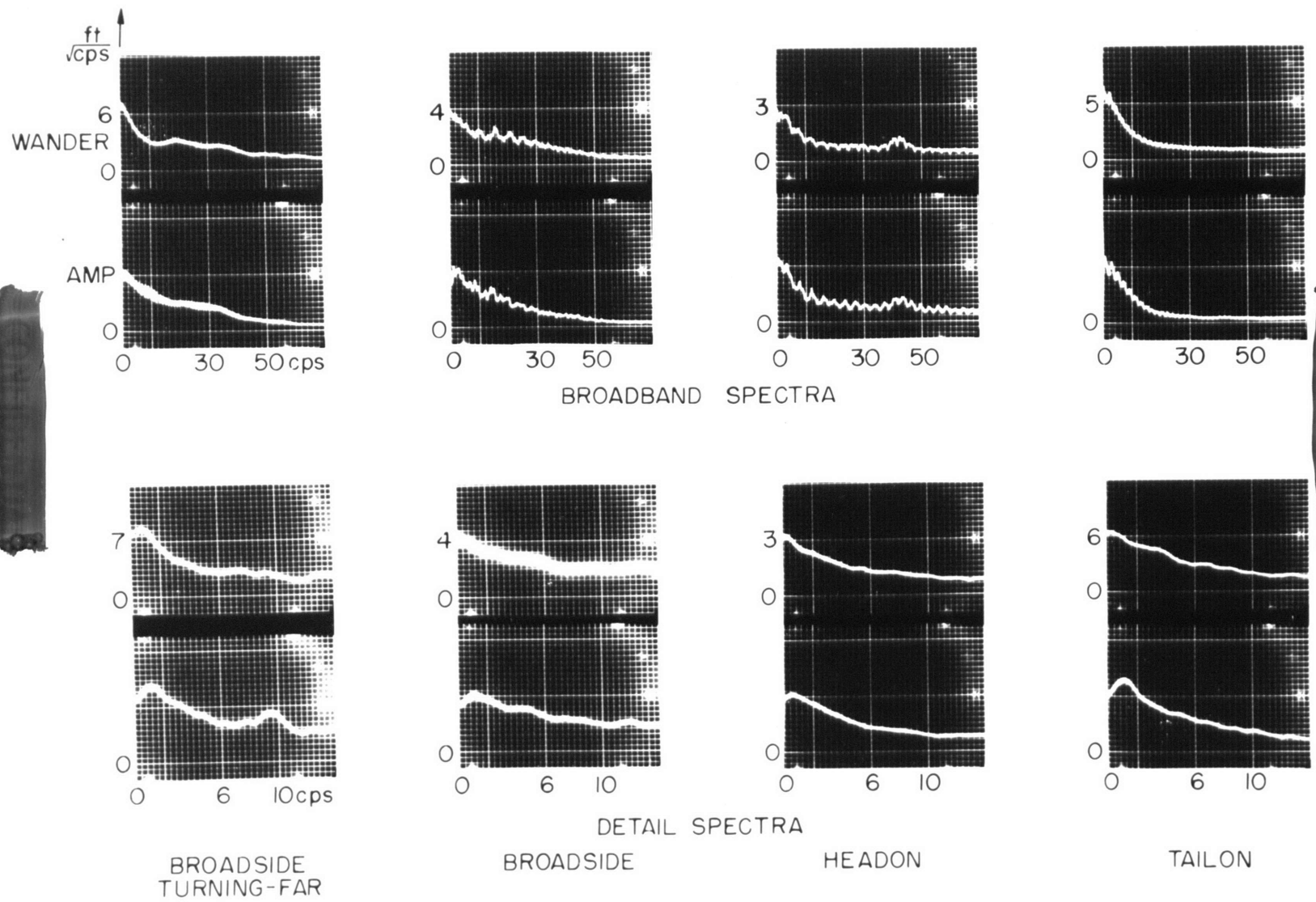
The vertical scales of the amplitude spectra are in relative voltage density; there is no absolute calibration for these records.

Spectra obtained by analyzing the composite of all the data for each of a number of different aspects of B-29, AT-11, C-46, B-26, and AT-6 targets are shown in Fig's. 3-6 through 3-10, respectively. The average length of data from which these spectra were taken was approximately 2 minutes. The fine structure in many of the broad-band low-resolution spectra is not significant; it is present because the time-constant of the analyzer was not sufficiently great to take the average over the entire length of the long records from which these spectra were made.

Similar spectra for the data from head-on and tail-on aspects of a jet-propelled F-84B aircraft are shown in Fig. 3-11. The total length of data for these spectra was considerably smaller than that for most of the previous spectra, because the target flew the prescribed courses at 300 mph in this case, instead of the usual 160 mph. For the same reason, the phase-shifter tracking was inadequate on the circular and crossing courses, with the result that no broadside data was successfully recorded from this target.

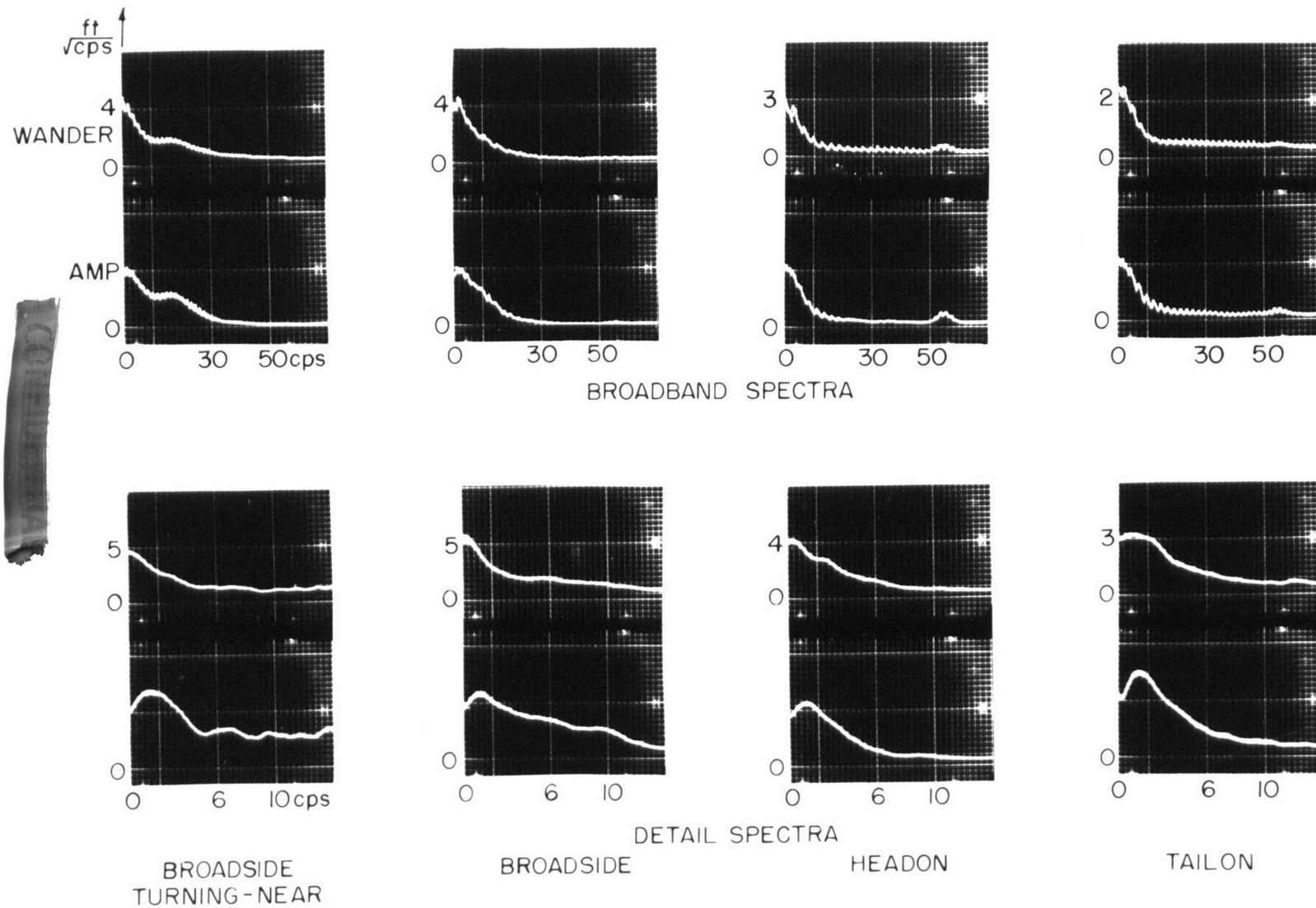
The spectra of data obtained from successive runs of a given target over the same course are not identical, though they are usually quite similar. This phenomenon is illustrated by the broad-band spectra presented in Fig. 3-12, which were made of data taken on separate runs of a B-26 on the radial course and of an AT-11 on the crossing course.

That the spectrum of short sections of wander data can change considerably during a run is obvious from the reproduction of the B-29 broadside data shown in Fig. 3-3. The broad-band spectra shown in Fig. 3-13 indicate the



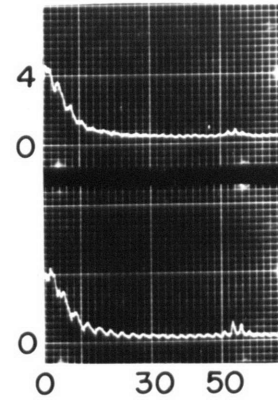
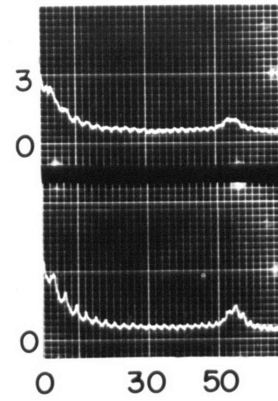
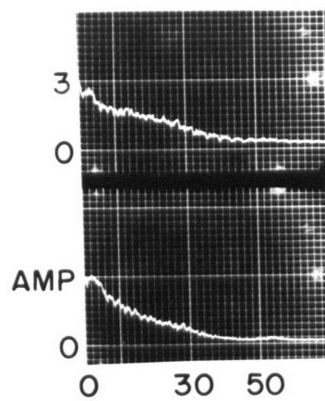
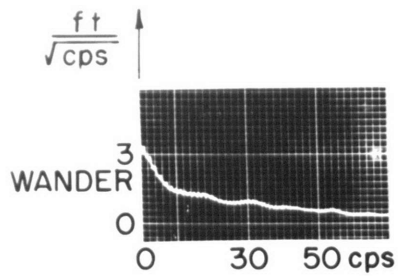
SPECTRA OF WANDER AND SIGNAL AMPLITUDE WITH B-29 TARGET

Fig. 3-6

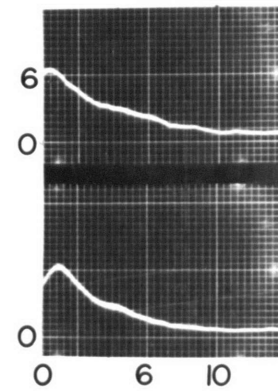
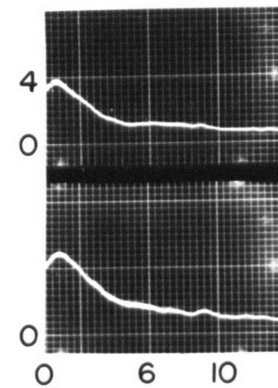
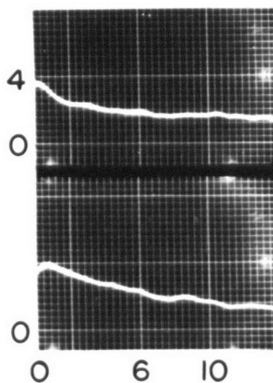
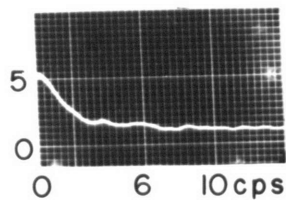


SPECTRA OF WANDER AND SIGNAL AMPLITUDE WITH AT-11 TARGET

Fig. 3-7



BROADBAND SPECTRA



DETAIL SPECTRA

BROADSIDE  
TURNING-NEAR

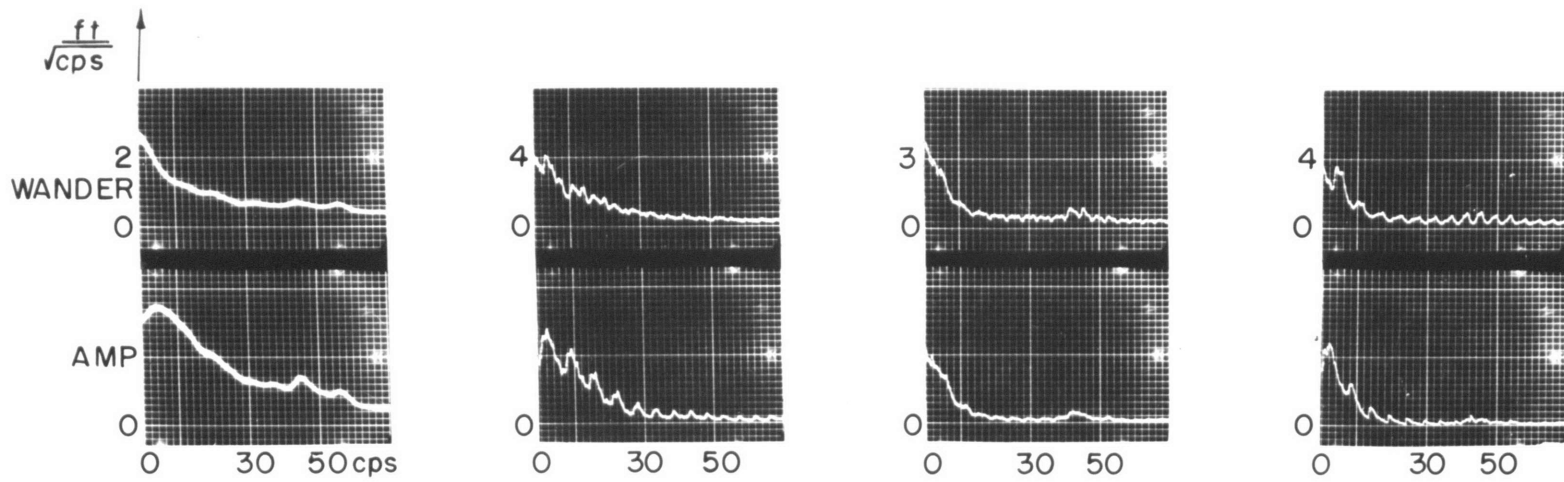
BROADSIDE

HEADON

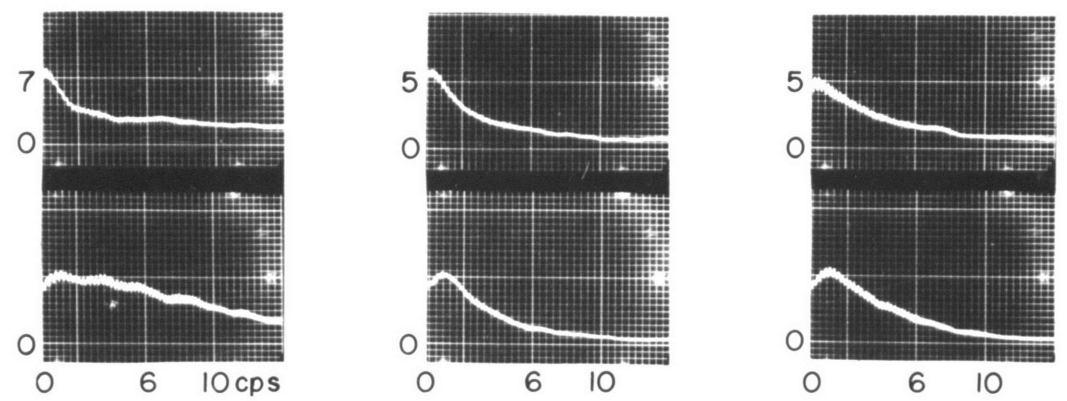
TAILON

SPECTRA OF WANDER AND SIGNAL AMPLITUDE WITH C-46 TARGET

Fig. 3-8



BROADBAND SPECTRA



DETAIL SPECTRA

BROADSIDE  
TURNING-FAR

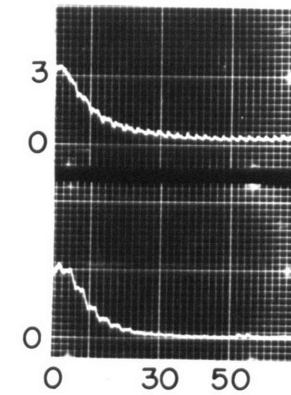
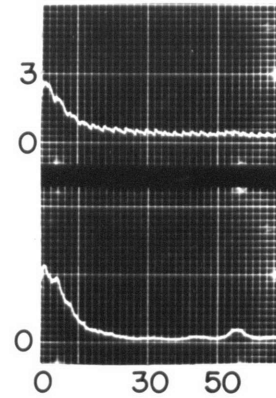
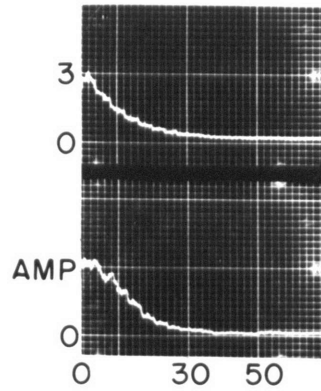
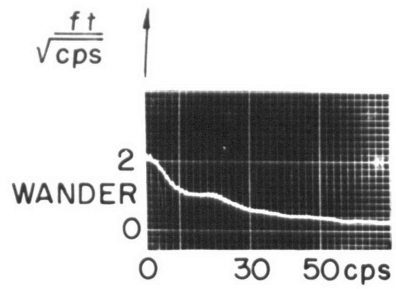
BROADSIDE

HEADON

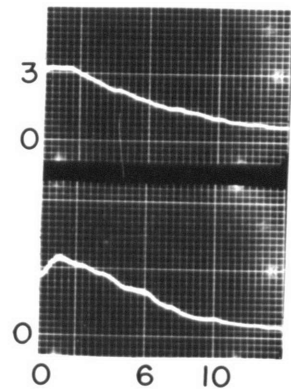
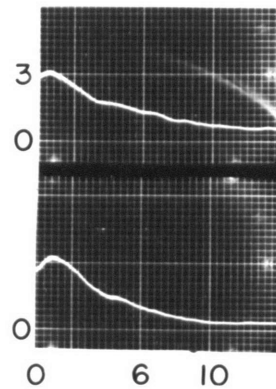
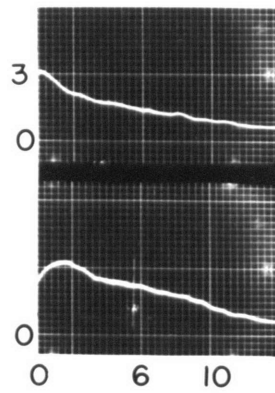
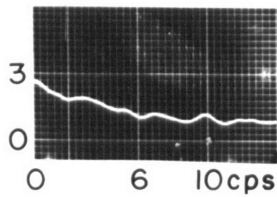
TAILON

SPECTRA OF WANDER AND SIGNAL AMPLITUDE WITH B-26 TARGET

Fig. 3-9



BROADBAND SPECTRA



DETAIL SPECTRA

BROADSIDE  
TURNING NEAR

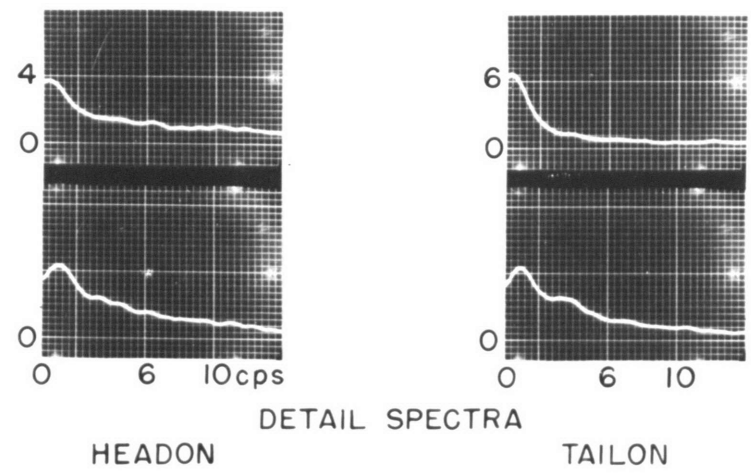
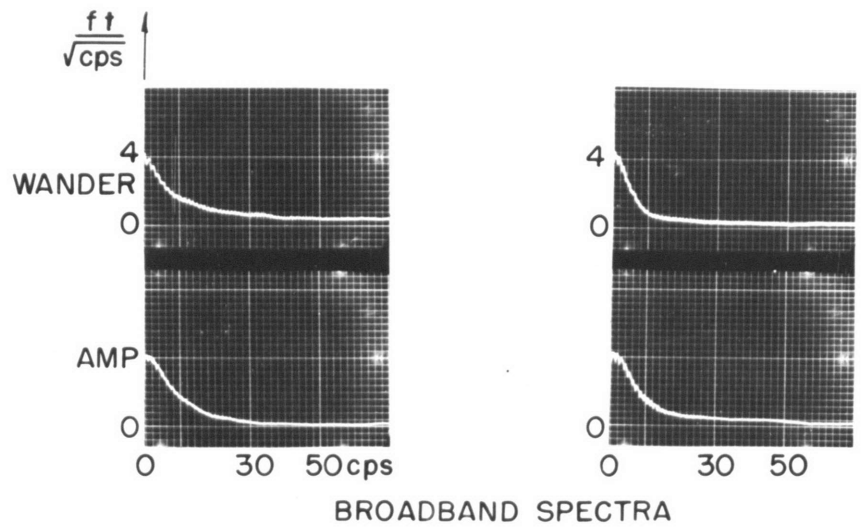
BROADSIDE

HEADON

TAILON

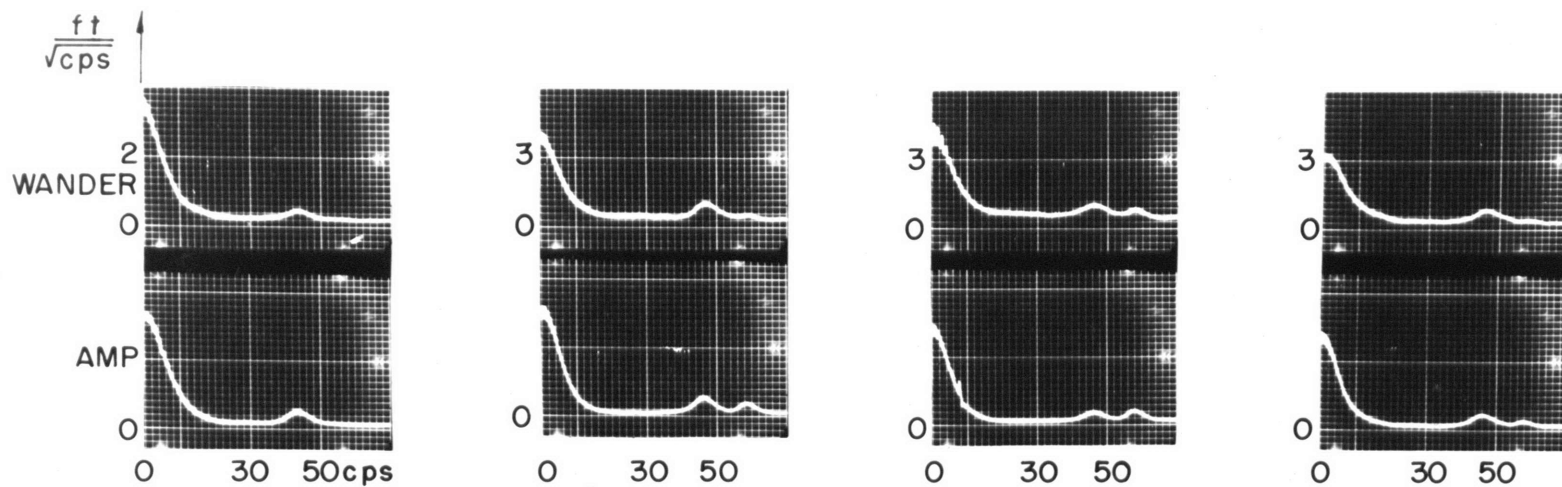
SPECTRA OF WANDER AND SIGNAL AMPLITUDE WITH AT-6 TARGET

Fig. 3-10

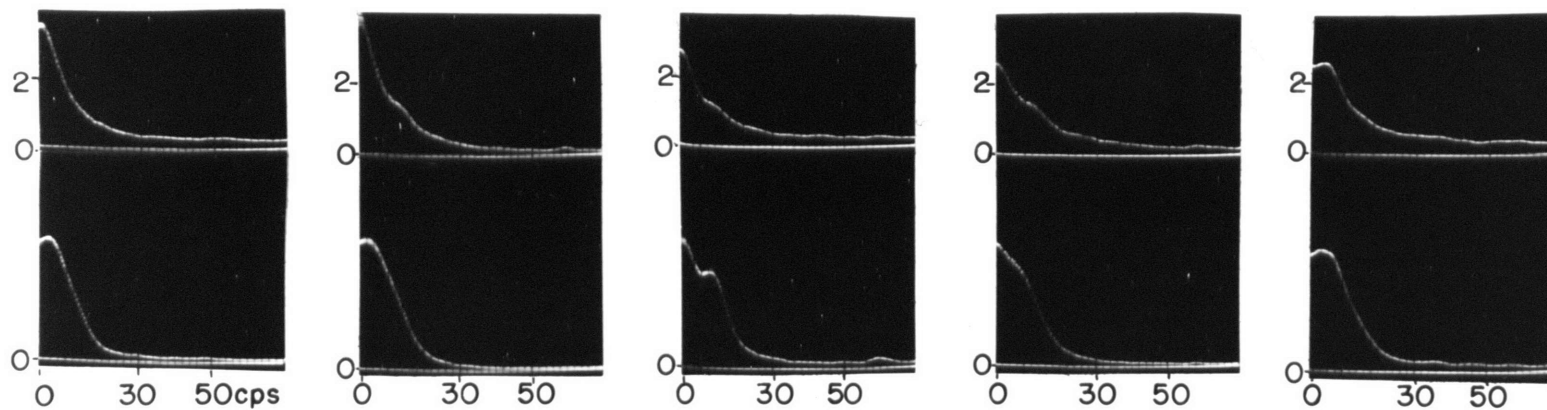


SPECTRA OF WANDER AND SIGNAL AMPLITUDE WITH F-84 TARGET

Fig. 3-11



B-26 HEADON

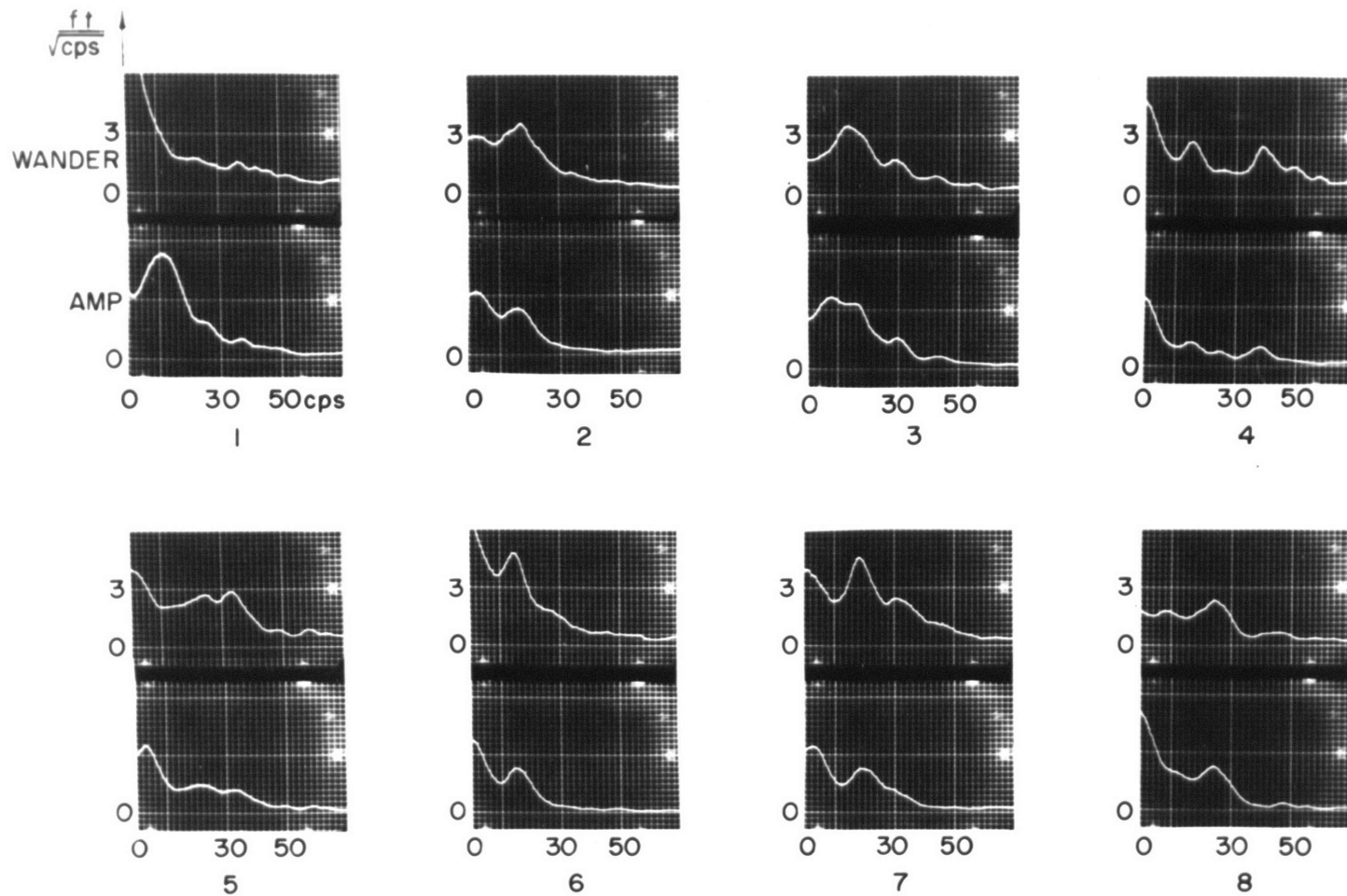


AT-II BROADSIDE

BROADBAND SPECTRA OF DATA FROM SUCCESSIVE SIMILAR RUNS

Fig. 3-12





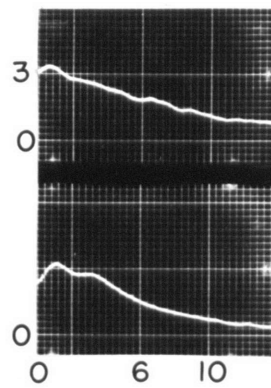
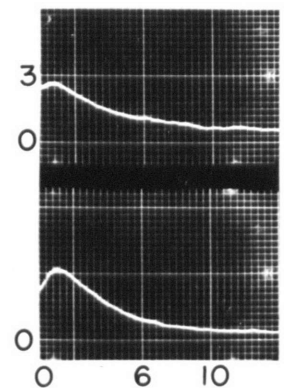
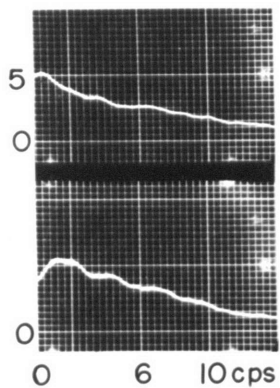
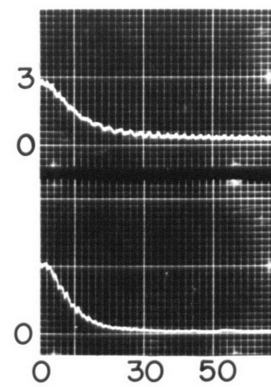
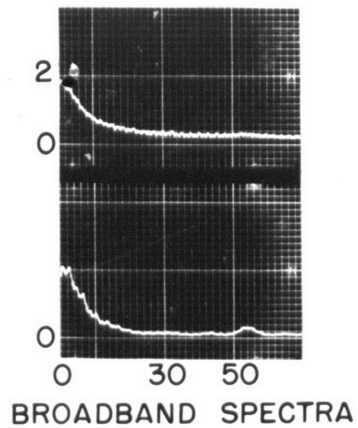
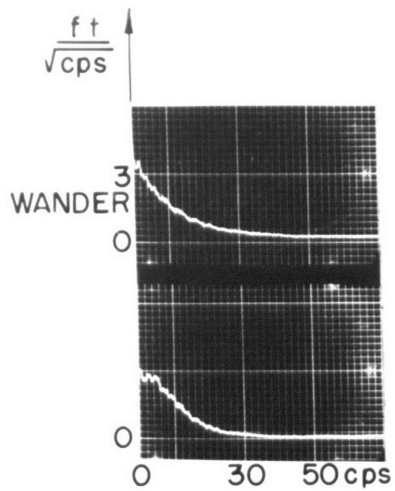
BROADBAND SPECTRA OF SUCCESSIVE 3-SECOND SECTIONS OF DATA FROM  
BROADSIDE B-29 TARGET

Fig. 3-13

changes which can be expected in such a case. These spectra were made from successive 3-second sections of a record of B-29 broadside data. Changes of comparable magnitude could be expected from the broadside aspects of many other types of aircraft. On the other hand, data obtained with head-on and tail-on aspects apparently do not have such violent changes in spectral character.

A complex reflection body, such as an aircraft target, can introduce appreciable depolarization in the reflection of a linearly polarized incident wave. A study of the importance of such depolarization was made by recording data with an AT-6 target on the radial and crossing courses after the linearly polarized receiving antennas had been replaced with circularly polarized ones. Spectra of the composite data recorded with the circularly polarized antennas are shown in Fig. 3-14. With the exception of the absolute calibration of the wander spectra of the broadside aspect, the corresponding spectra in Fig's. 3-10 and 3-14 are practically the same. It was found during the flight test in which all the data on the AT-6 was recorded that equally good error signals for the operator of the phase shifter were obtained with both types of antennas. On the basis of these tests it can be said that no serious system limitations result from the use of circularly polarized receiving antennas in place of linearly polarized ones when the transmitted signal is linearly polarized.

The limiters of the phase measuring unit were bypassed during one flight test with a B-26 aircraft. This test was held for the purpose of investigating the possible reduction of the large wander errors which are accompanied by deep fades in signal strength, as considered in Sec. 2.52. The spectra of the data recorded during these tests are shown in Fig. 3-15.



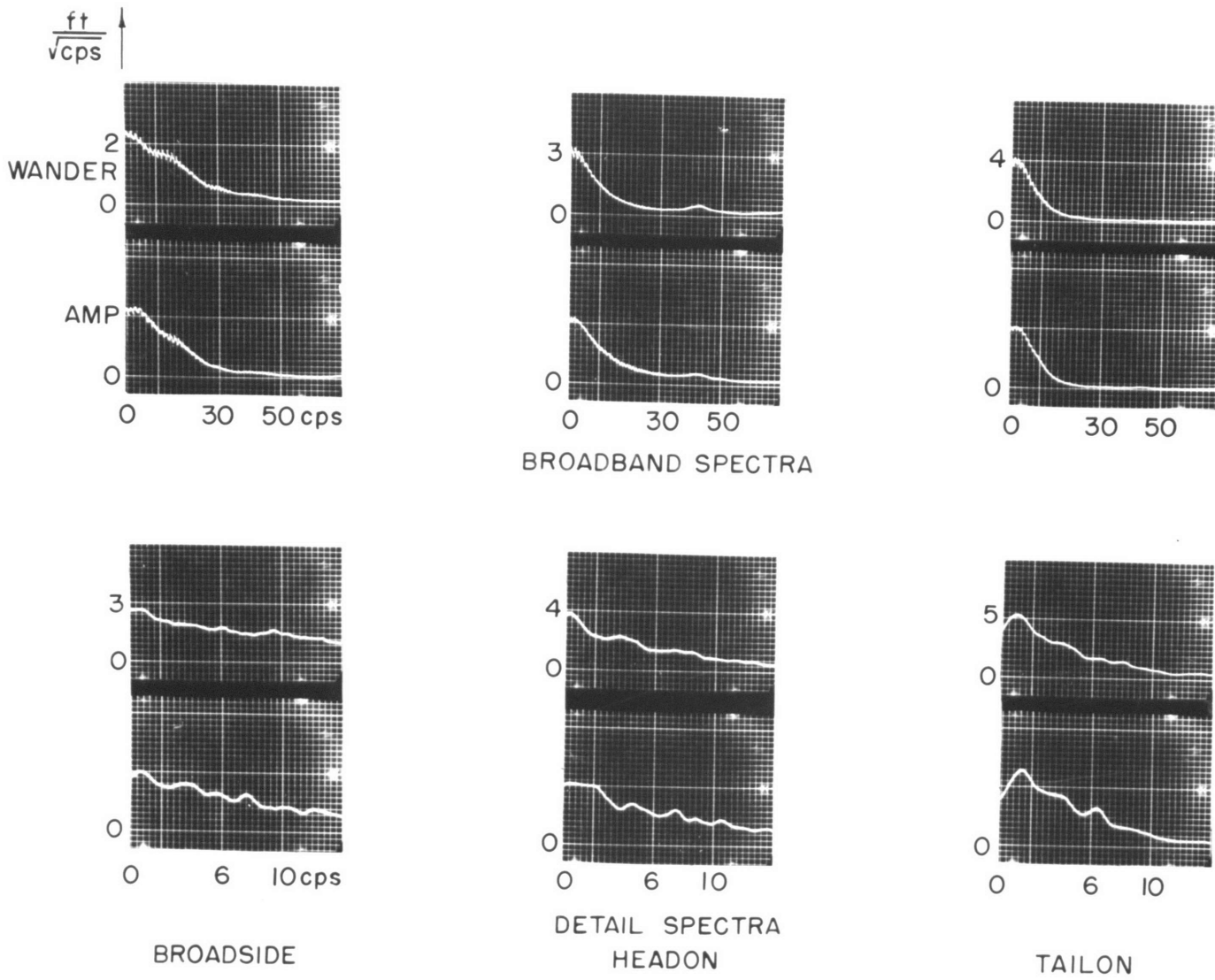
BROADSIDE

DETAIL SPECTRA  
HEADON

TAILON

SPECTRA OF WANDER AND SIGNAL AMPLITUDE WITH AT-6 TARGET  
AND CIRCULARLY POLARIZED RECEIVING ANTENNAS

Fig. 3-14



SPECTRA OF DATA RECORDED WITH NO LIMITING-B-26 TARGET

Fig. 3-15

[REDACTED]

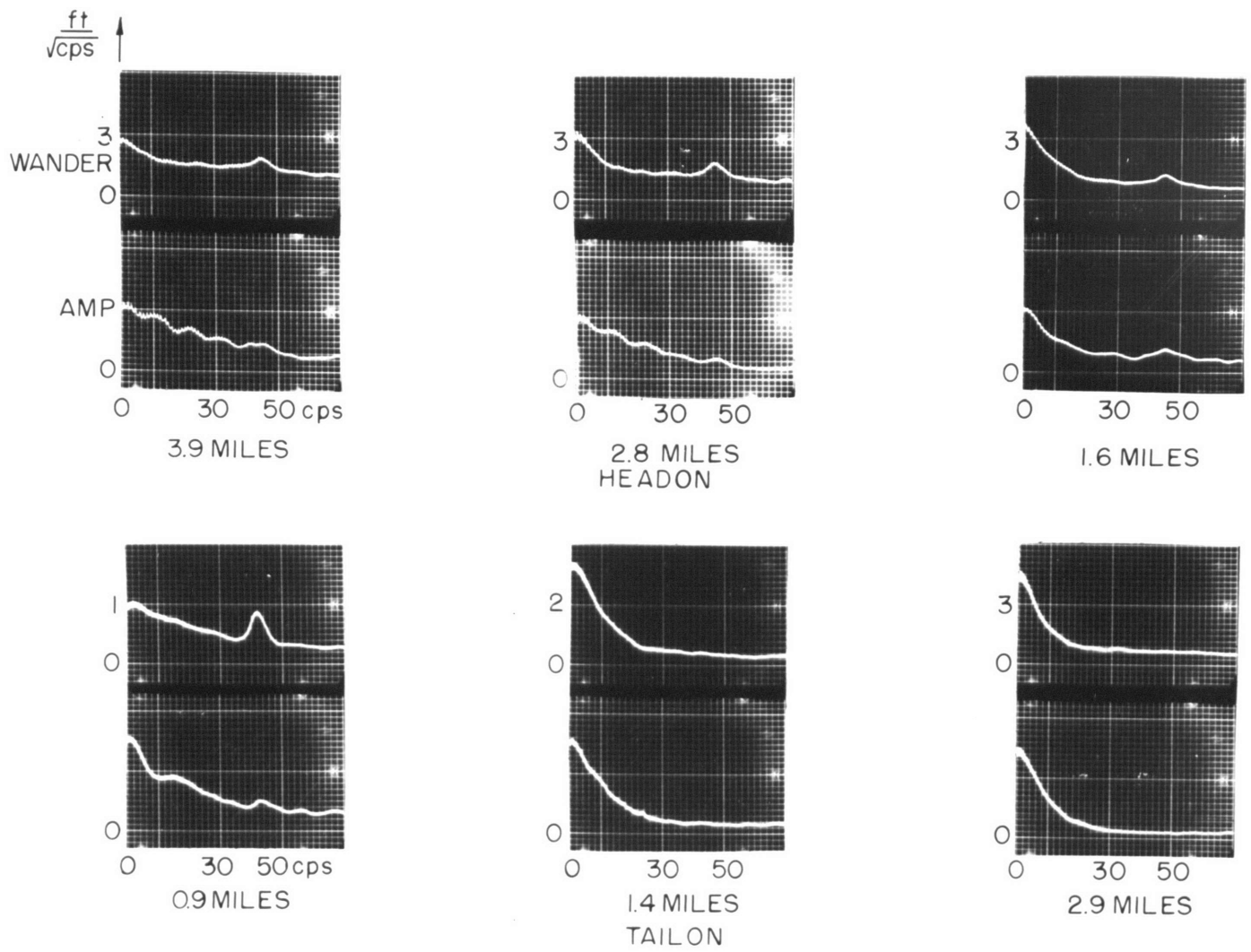
From a comparison of these spectra with the corresponding ones in Fig. 3-9, it can be seen that there is somewhat less wander without limiting than with the system in normal operation. This reduction in wander is to be expected, because the occasional large peaks are eliminated. However, it was noted during the flight test that the indication of the tracking meter on the output of the phase detector was erratic, and that it was very difficult for the operator of the phase shifter to obtain a steady, consistent error signal. It was surmised from these observations that it is probably inadvisable to operate a system completely without limiting, as was also concluded in Sec. 2.52.

It is to be expected that the spectrum of the phase-detector output due to wander varies when the target range becomes so short that the wander exceeds the linear portion of the system characteristic. The spectra shown in Fig. 3-16, which were made from data recorded with the B-29 target on head-on and tail-on runs, illustrate the sort of spectrum changes that can be expected. It can be seen that the spectrum bandwidth becomes broader and that the zero-frequency ordinate decreases with decreasing range, as might be predicted from the analysis presented in Sec. 2.51.

### 3.15 Multiple-target Data

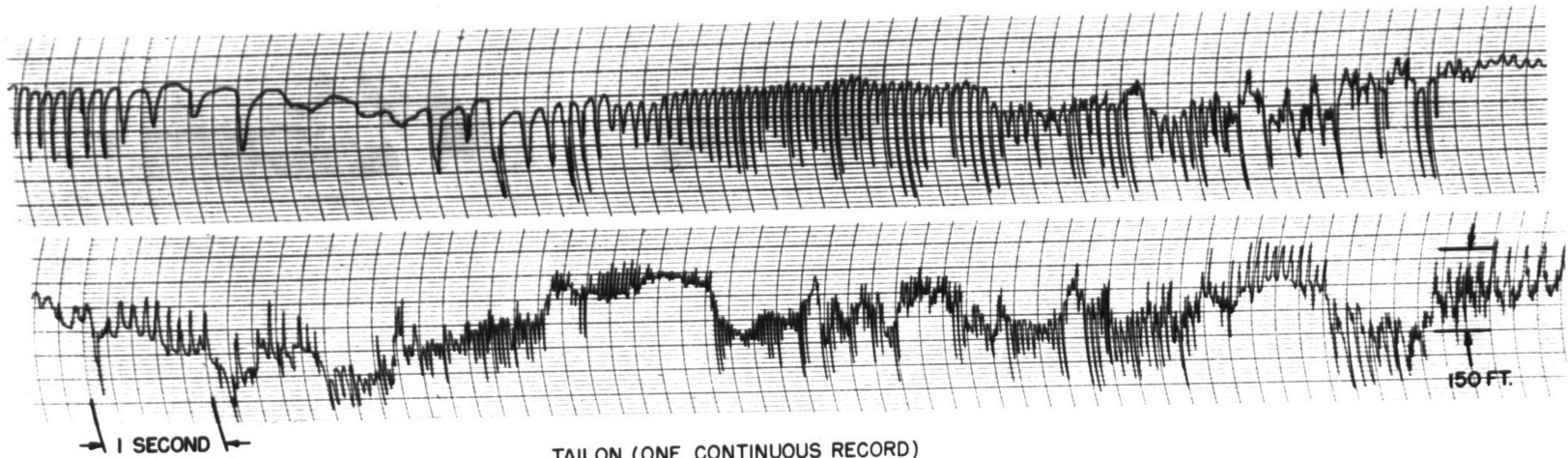
Two single-engine TBM aircraft flying in close formation over the radial and crossing courses served as the target in one flight test. The two aircraft flew in such formations that the line between them was always roughly normal to the line-of-sight from the radar. In order to reduce the possibility of non-linear system operation, the system sensitivity was reduced by decreasing the spacing of the receiving antennas from 5 feet to 20 inches. Pen-recorder copies of typical wander data recorded during this test are shown in Fig. 3-17. Spectra of the composite of all the amplitude

[REDACTED]

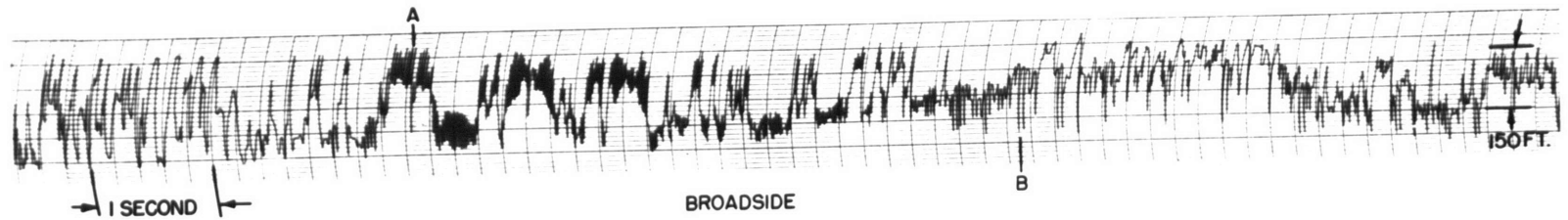


BROADBAND SPECTRA OF DATA WITH B-29 TARGET AT VARIOUS RANGES

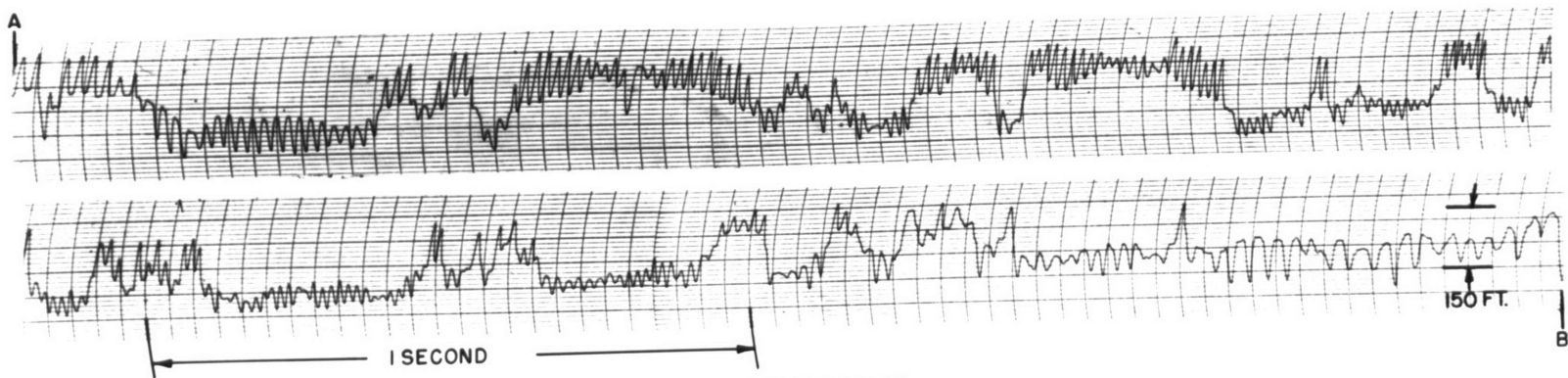
Fig. 3-16



TAILON (ONE CONTINUOUS RECORD)



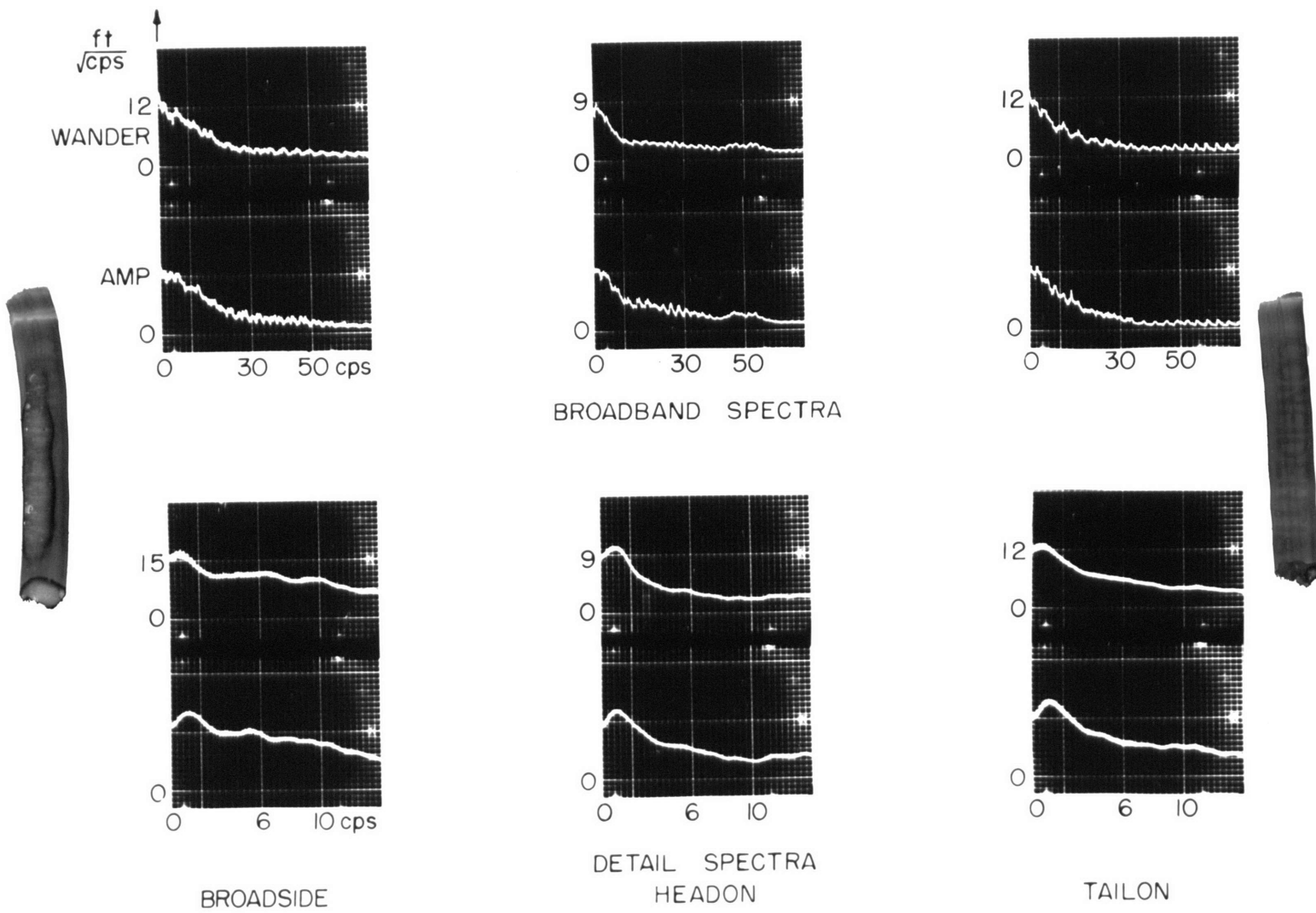
BROADSIDE



EXPANDED BROADSIDE

WANDER OF THE APPARENT RADAR CENTER OF MULTIPLE TARGET

Fig. 3-17



SPECTRA OF WANDER AND SIGNAL AMPLITUDE WITH MULTIPLE TARGET  
2-TBM AIRCRAFT IN CLOSE FORMATION

Fig. 3-18



and wander records for various aspects are presented in Fig. 3-18. As might be expected, the ordinates of the wander spectra for the two airplanes are considerably greater than those for single targets. Normally the centers of the targets were about 60 feet apart for all the runs.

A number of interesting features can be observed in the records of wander shown in Fig. 3-17. The first is the behavior of the predominant frequency, which at any time is the difference in Doppler frequencies of the two reflected signals. As the airplanes perform slight maneuvers relative to one another, the difference frequency varies, occasionally going to zero, as in the first part of the tail-on record.

The capture of the average phase, and consequently of the apparent radar center, by the stronger of the two signals can be seen in both records, particularly in the detail of the broadside data. As the signals change in relative amplitude, the average position of the apparent center jumps from one target to the other; in the meantime fluctuations in the position take place at the Doppler-difference frequency. It can also be seen, particularly in the latter portion of the tail-on data, that the interference between the two signals tends to repel the apparent center off target on the side away from the weaker point during times when the signals are out of phase, as indicated by the periodic spikes of wander. This effect is not as apparent in the detail of the broadside data, because the Doppler-difference frequency was so high that the system was unable to reproduce the spikes faithfully.

The fact that the spikes of wander all have the same sign at the beginning of the tail-on record is not significant, because at this point the two aircraft were so close to the radar that the wander exceeded the linear portion of the radar-system characteristic. This section is included

mainly to illustrate the zero-frequency beat between the signals.

### 3.16 Discussion of Spectra

Probably the most important quantities which can be determined from the frequency spectra presented in the preceding two sections are the zero-frequency ordinates of the wander spectra. These figures can be determined from the narrow-band high-resolution spectra with greater accuracy than from the wide-band spectra. For the single targets, the values of the low-frequency density of wander lie between the extremes of 2.5 and 8 ft/ $\sqrt{\text{cps}}$ , with an average value of approximately 4.5 feet (rms) in a 1-cps bandwidth.

The bandwidths of the spectra and the rms values of wander can also be evaluated from the spectra. Except for periodic wander components at propeller blade frequencies, the highest frequency components were obtained from the broadside aspect of the B-29 target. For this case, the wander spectrum extends out to 50 cps and has a quarter-power point at about 25 cps. On the average, the frequency of the quarter-power point is in the vicinity of 10 cps. The rms value of any wander spectrum can be computed by taking the square-root of the integral with respect to frequency of the square of the spectrum. This was done for Fig's. 3-6 through 3-11 and 3-18, using the detail spectra for frequencies below 10 cps and the broadband spectra above 10 cps. The results are listed in Table 3-2.

The presence of a predominant frequency component in many of the spectra of both amplitude and wander with the AT-11 broadside has a very interesting connotation; such an effect is just what would be expected from a target with two principal reflecting areas. This component is evident at 16 cps in the broadside-turning data in Fig. 3-7, and at lower frequencies in at least three of the AT-11 spectra in Fig. 3-12. In the circular course, from which



<u>Target</u>	<u>Broadside Turning</u>	<u>Broadside</u>	<u>Head-on</u>	<u>Tail-on</u>
B-29	23 ft	13 ft	8 ft	15 ft
AT-11	10	8.4	6.9	6.1
C-46	9.2	9.5	8.0	11
B-26		12	9.0	9.0
AT-6	7.0	6.8	6.6	8.1
F-84			7.7	8.5
Two-TBM		47	23	29

Table 3-2 - RMS Wander of Apparent Radar Center

the broadside-turning data were obtained, the rate-of-change of viewing aspect was about 2.9 degrees per second. With a transmitted frequency of 9375 mcps, the spacing of two points which would be necessary to give the observed 16-cps beat is 17 feet. The frequency is lower in the spectra in Fig. 3-12 because the relative turning rate of the aircraft is smaller than in the circular course. The reason for the differences among the latter spectra is probably the variable yawing rate of the target.

It should be mentioned that on the runs along the crossing course, from which the broadside data were obtained, the targets presented a slowly changing aspect to the radar, since they flew on a straight course. As a result, the broadside wander spectra are somewhat broader, and their zero-frequency ordinates lower, than those that would be obtained from truly constant broadside views of the targets.

A set of curves from which a comparison can be made of the results of various wander studies was prepared by Dr. R. C. Seamans, Jr. as part of a separate research project<sup>28</sup> and is presented in Fig. 3-19. The ordinates



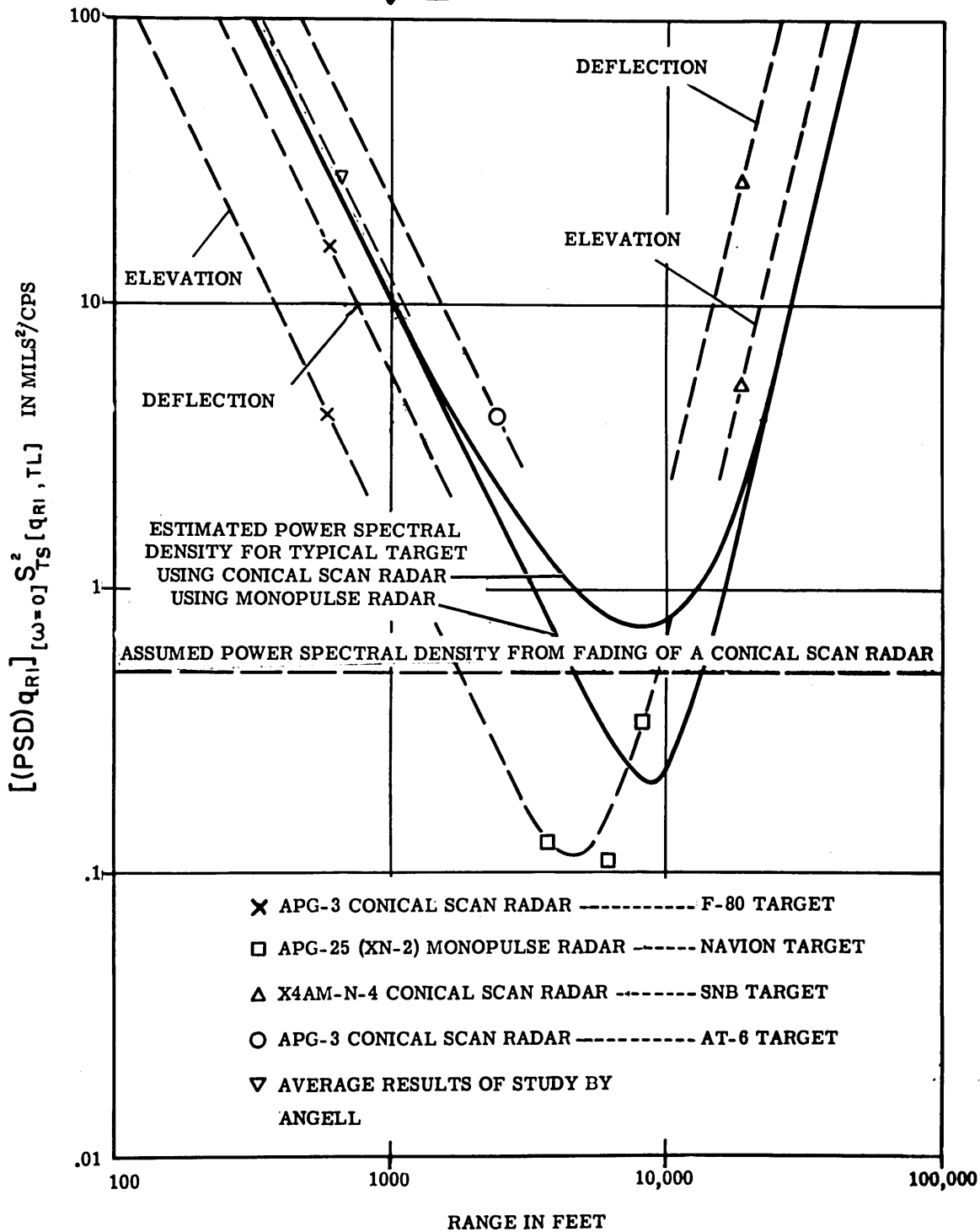


FIG I-1 POWER SPECTRAL DENSITY OF RADAR INTERFERENCE AS A FUNCTION OF TARGET RANGE

Courtesy Dr. R. C. Searns, Jr.

Fig. 3-19

**CONFIDENTIAL**

of this plot show the power spectral densities at zero frequency of the angular deviations caused by target-echo fluctuations and thermal noise. At short ranges the curves have a negative slope of 6 decibels per octave, because at these ranges the principal source of jitter is wander, which is constant in terms of feet at the target. At long ranges, the curves have a positive slope of 12 decibels per octave, due to the effects of threshold noise. The values of the power spectral density were computed for the different tracking systems from the standard deviation of the measured tracking errors and from the frequency response of the tracker. These values are determined on the basis of the Fourier transform of the autocorrelation function, and are therefore half the square of the figures read off spectra such as those presented in Sec. 3.14.

Errors in the wander spectra may have been produced by any one or more of a number of sources. Probably the most serious errors arose from insufficient accuracy in the manual tracking of the phase shifter. Tracking inaccuracies occasionally caused large low-frequency errors, which, as mentioned in Sec. 3.11, were almost always of a frequency below 0.3 cps. Any data sections in which these errors were appreciable were removed by editing before the data were analyzed. In obtaining the detail spectra, a single-section high-pass R-C filter was used to reject data below 0.3 cps. The combined effects of the high-pass filter and the tracking errors are insignificantly small above 1 cps in the high-resolution spectra of wander.

Another effect of inadequate phase-shifter tracking was a reduction in the size of the region of linear system operation. With correct tracking, the response characteristic of the phase detector was symmetrical and almost triangular. When a tracking error existed, the limiting size of wander

**CONFIDENTIAL**

~~CONFIDENTIAL~~

fluctuations that could be measured in the direction of the error was correspondingly reduced. Consequently, the measured wander would be smaller than it should be, because the spikes of wander would be missing. All sections of data in which the tracking obviously caused non-linearities were removed during the editing process, although it is almost certain that many sections with slight non-linearities were not noticed and eliminated.

Other errors were caused in some of the records when the wander exceeded the linear portion of the phase-detector characteristic. The spacing of the receiving antennas was such that the linear region corresponded to 90 feet peak-to-peak displacement at 2 miles range. Although the resulting system sensitivity was nearly optimum for the smaller targets, it was obviously too great for the B-29 on the crossing course. Therefore, the wander spectra for the B-29 presented in Fig. 3-6 may indicate lower spectral densities than actually exist; however, the spectra in Fig. 3-16, showing phase-detector outputs for different ranges, suggest that measurements made at 2-miles range are not far from correct.

There are many other possible sources of errors which may have been present to a small extent. First is the  $\cos \beta$  factor, where  $\beta$  is the angle between the line-of-sight and the center line of the antenna system. All the wander measurements are affected by this factor; however, the largest values of  $\beta$  for which measurements were made was about 20 degrees, for which the factor is 0.94. On the average, the errors in wander measurement produced by this cause were substantially less than 2 percent.

Because the receiving antennas had a broad beamwidth, appreciable angular errors could have been produced by reflections of the target-echo return off nearby objects, particularly the ground. However, in the direction

~~CONFIDENTIAL~~

~~CONFIDENTIAL~~

in which the antennas were aimed was a building, about 250 feet distant, with a flat roof at almost exactly the level of the antennas. This building served as a shield for ground reflections until the elevation angle of the target was so high that the ground reflections could no longer give trouble.

Finally, there were two possible sources of differential phase shift in the radar receiver. The limiters in the phase measuring unit had phase delays which changed with changes in the signal levels at the inputs. Although the limiters were adjusted to have a differential phase shift of less than 2 degrees when both inputs varied together within a range of 26 decibels, phase differences as great as 15 degrees could arise when the signals varied independently. Similarly, differential phase shifts could arise in the i-f amplifiers due to Miller effect when the agc voltages varied independently, even though the amplifiers were aligned to have very small differential phase shifts when their gains were equal. Fortunately, both these sources of error are serious only at short ranges, where the phase differences due to wander are very great, because at long ranges both received signals are always nearly equal. The errors due to Miller effect were restricted to very low frequencies by the low-pass filter in the agc circuits.

### 3.2 S-BAND TESTS

During the flight-test part of the S-band experimental program simultaneous recordings were made of the amplitudes and of the difference in phases of the signals received from various radar targets by two adjacent antennas. For these tests the antennas were mounted five feet apart on a movable platform which was continuously aimed in the direction of the geometrical center of the target by means of optical tracking. Some of the

~~CONFIDENTIAL~~

**CONFIDENTIAL**

data thus obtained were analyzed using the spectrum analyzer described in Sec. 3.13 and Appendix G.

### 3.21 Data Recording Setup

The equipment used for recording data during the flight tests was basically the same as that used for the X-band tests, except that manual aiming of the receiving antenna system was used in place of manual tracking of a continuous phase shifter to remove the large phase changes resulting from changes in target position. A block diagram of the equipment is shown in Fig. 3-20.

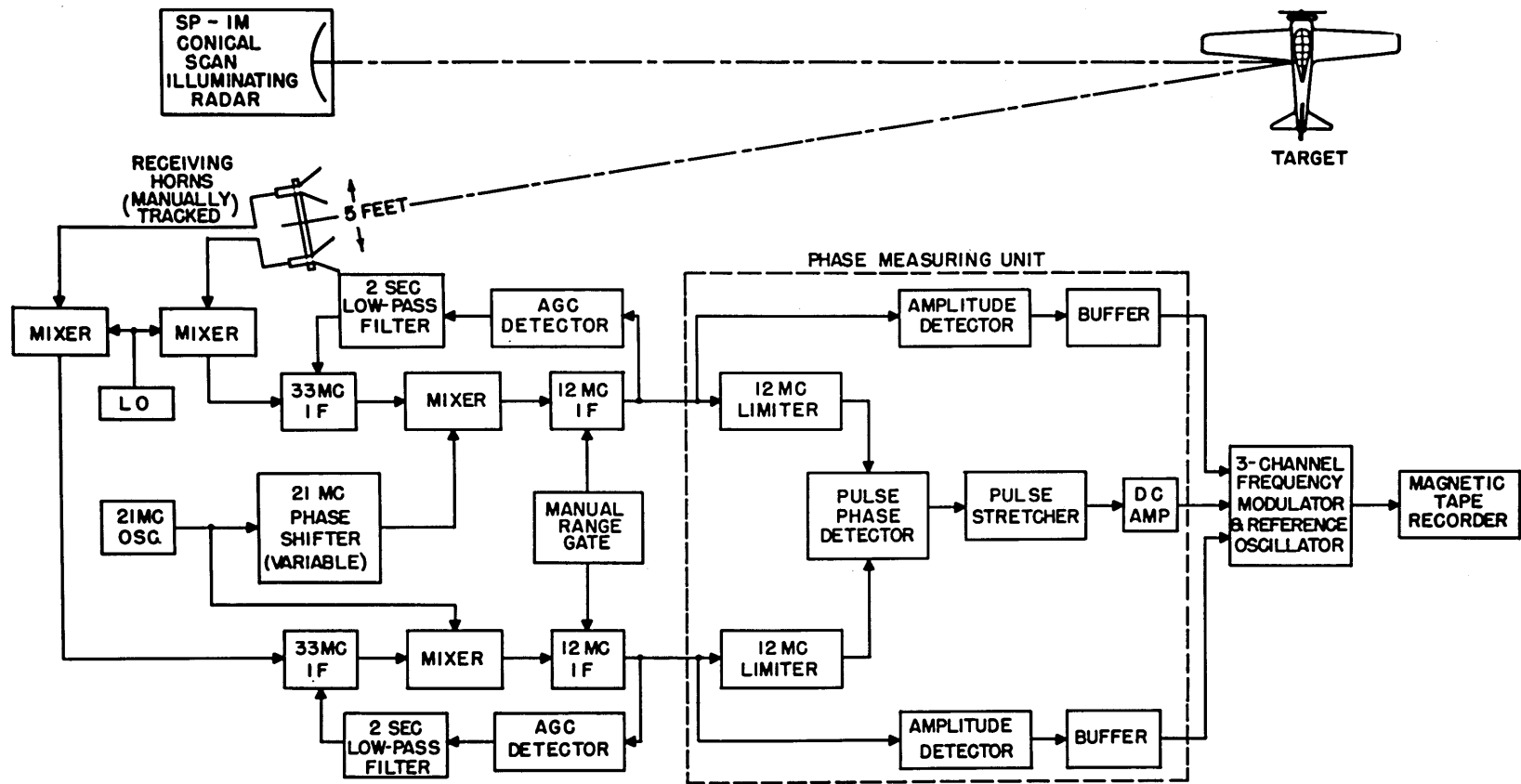
The transmitter was a Navy type SP-1M conical scan radar, which had a peak power output of 700 kilowatts with a pulse repetition frequency of 600 pps and a 1-microsecond pulse duration. The transmitting antenna, which had a 3.6-degree beamwidth in both planes, was fed by a mutated linearly polarized feed; hence the polarization of the transmitted signal did not change during the scan cycle. The scanning frequency was 24 cps.

The i-f amplifiers and agc circuits were the same as those used in the X-band tests. The range-gate generator was similar to the one described in Appendix F, the chief differences being that a 2.0-microsecond gate was used in these tests and that no means was provided for multiplying the phase-detector output by range. The signal gating was accomplished in the i-f amplifiers, instead of in a separate gating circuit, as was done in the X-band tests.

The same phase measuring unit was employed in both series of tests; however, in these tests, the pulse stretcher was triggered by an amplitude detector operating on the output of one of the limiters. This method of triggering made the system more susceptible to ground clutter than did the method of triggering with the range gate, as used in the X-band tests.

**CONFIDENTIAL**





S-BAND DATA RECORDING SETUP

Fig. 3-20

Because of this greater sensitivity to ground clutter, it was necessary to reduce the average signal levels at the inputs to the limiters to one fourth their optimum values.

The maximum range of the measurement radar was about 5 miles on a medium sized aircraft. Because the targets were flown at an elevation of 1500 feet and the transmitting antenna could not be elevated to angles greater than 30 degrees, almost no data were obtained for target ranges of less than a mile.

A single three-channel recording system was used during these tests.\* Three carriers, with average frequencies of 3, 7, and 11 kcps were frequency modulated with a maximum deviation of about 4 percent by the three quantities to be recorded. The three carriers were then combined and recorded, along with a fourth unmodulated reference carrier of 15 kcps, on magnetic tape moving at 15 inches per second. The transcriber consisted of three similar electronic circuits from which were obtained three voltages, each of which was proportional to the ratio of the frequencies of one of the modulated carriers and the reference.

The radar receiving equipment and the recorder were mounted on a platform truck which was wheeled into the field adjacent to the SP-1M radar site during the flight tests. Electrical power was obtained from two gasoline-driven generators.

### 3.22 Spectra of S-band Data

Data were recorded for various types of Navy airplanes, including

---

\*The three-channel recording and playback equipment was developed by Mr.

C. R. Hurtig of the Research Laboratory of Electronics at M. I. T.

~~CONFIDENTIAL~~

single-, twin-, and four-engine as well as the FH-1 jet aircraft. The same three kinds of courses were flown by the targets in these tests as in the X-band tests.

The data were edited and analyzed by a procedure similar to the one described in Sec. 3.13 for the X-band tests. First, pen-recorder copies were made of all the data. From these copies it was possible to determine those sections of data which would be usable. Two magnetic-tape copies were then made of the data onto tapes moving at 15 and 1.5 inches per second, using the wide-deviation FM equipment described in Appendix H for making the copies. Both these copies were then cut into the desired sections, according to the usability of the data and the target aspect represented by the data. The various sections of the copies were then spliced into loops, played back at 15 inches per second, and analyzed with the same spectrum analyzer that was used for reducing the X-band data.

The method of operating the analyzer in obtaining the spectra of the S-band data was somewhat different and less efficient than the method that was worked out for the X-band data. In the former method, the bandwidth of the output of the amplitude detector was made comparable with that of the tuned amplifier. The sweep rate was made as fast as possible, limited only by the transient response of the tuned amplifier and the amplitude detector. With a random input to the analyzer, no two sweeps gave the same pattern. The average, or, more exactly, the most probable, pattern was obtained by photographing 700 sweeps of the analyzer using a very slow camera, stopped down so far that no individual sweep showed up. It was determined empirically that 700 sweeps (requiring 1 hour) was about the minimum number that gave good averaging with a data input approximating a stationary time series.

~~CONFIDENTIAL~~

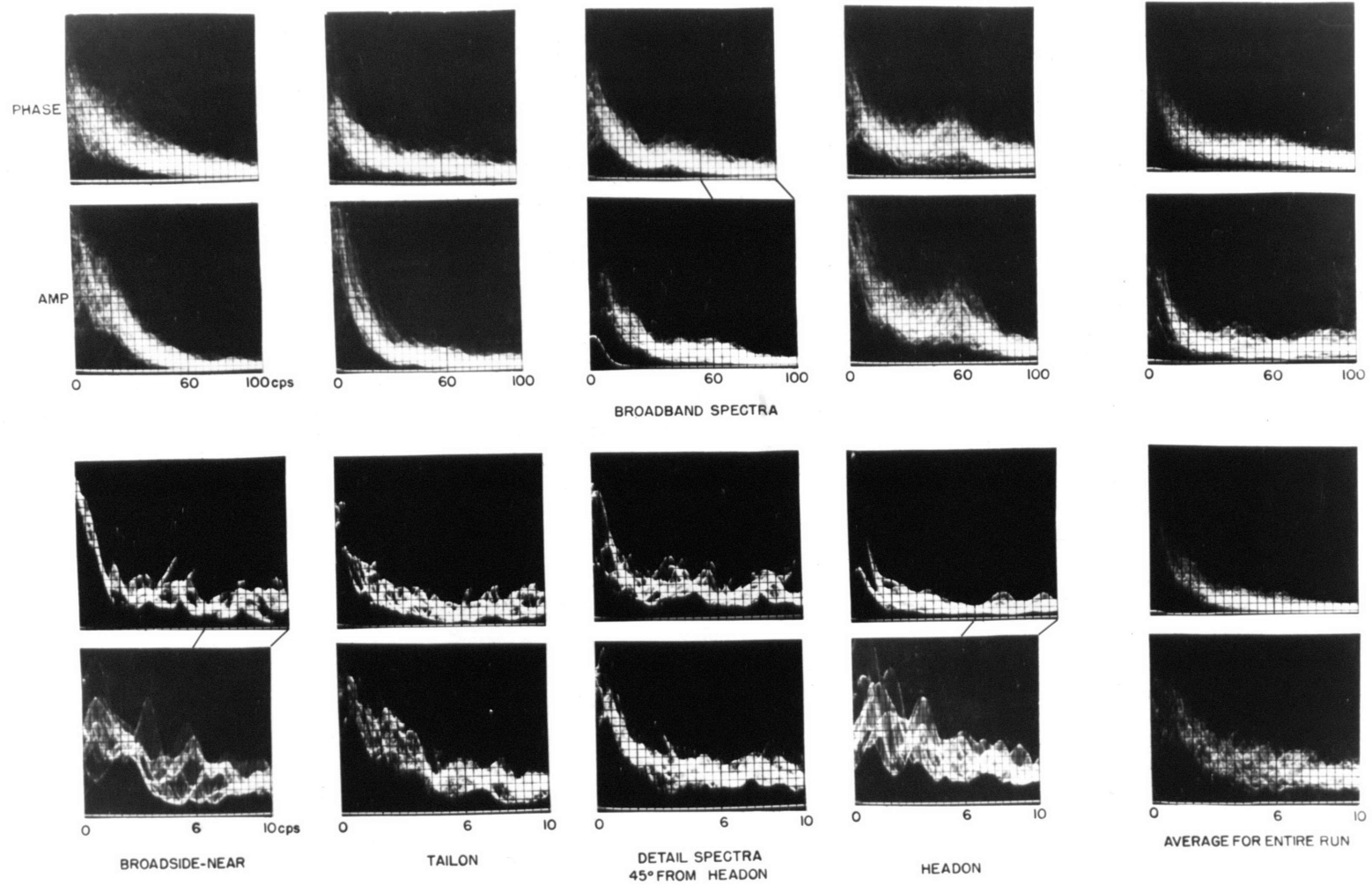
[REDACTED]

In Fig's. 3-21 and 3-22 are shown voltage spectra of data taken with a four-engine PB4Y-2 and with a single-engine F6F aircraft. The data for the PB4Y-2 were taken with the target on a circular course. The first four sets of spectra were obtained for various aspects presented to the radar by the target. The fifth set represents the average spectra for this type of flight and was obtained by splicing together all the usable data from the run. The F6F data were obtained from various portions of the radial and the circular courses.

Several features of the spectra are worthy of special note. First is the appearance of propellor modulation in the spectra for head-on aspects. For the F6F, very pronounced propellor modulation and its second harmonic are evident in the amplitude spectra at 48 and 96 cps. It seems that propellor modulation can be substantially more severe at S-band than at X-band. The presence of substantial energy at 24 cps in some spectra is caused by lobing of the transmitting radar (incidentally at half the propellor blade frequency of the F6F). Secondly, it can be seen that the widths of the spectra for the broadside aspects are greater than for other aspects. This phenomenon can be explained by the fact that both the target reflecting area and the turning rate of the target relative to the radar are maximum when the target is at the broadside-near point of the circular course.

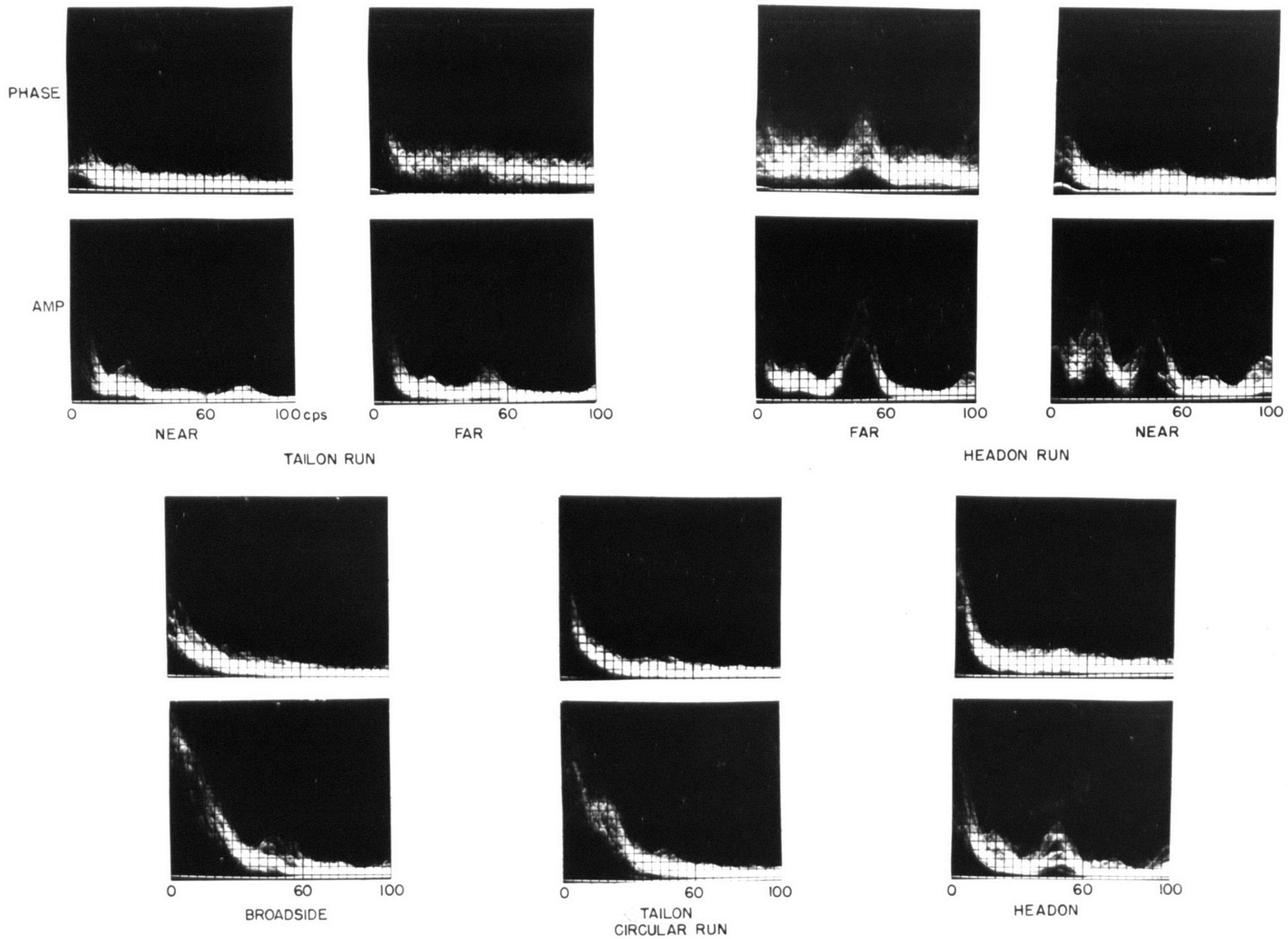
It is a significant fact that the widths of the spectra are different in the cases of a turning and a non-maneuvering target. For the tail-on aspect of the F6F target, the half-voltage point of the amplitude spectrum from the circular course occurs at 18 cps, whereas it is at a very low frequency (less than 5 cps) in the corresponding spectrum from the radial course. In the fourth place, from the phase records of the F6F radial flight, it is

[REDACTED]



SPECTRA OF S-BAND DATA WITH PB4Y-2 TARGET ON CIRCULAR COURSE

Fig. 3-21



SPECTRA OF S-BAND DATA WITH F6F TARGET

Fig. 3-22

[REDACTED]

easy to see how the thermal noise adds an essentially flat spectrum to that of the phase jitter caused by the target and imperfections in the equipment. Finally, the peculiar appearance of many of the detail spectra of the FB4Y-2 data is a result of the short sections of data from which the spectra were made. For the shortest sections the speed-up data are far from stationary, since the period of the data is only 0.8 second.

Most of the phase spectra, particularly the detail ones, exhibit very large low-frequency components of jitter. These components were caused not only by fluctuations in the target echo, but also by inaccuracies in the tracking of the receiving antenna platform and by drift in the i-f amplifiers, as considered in the succeeding section. In fact, for much of the data, the latter causes predominate. When, after part of the data had been analyzed, the seriousness of these low-frequency errors was realized, the process of data reduction was halted in favor of expediting the X-band tests for obtaining more satisfactory data.

### 3.23 Discussion of S-band Data

While most of the amplitude data recorded during these tests can be relied upon as representative, very little of the phase data can be considered to be free from extraneous errors. A study of the pen-recorder copies of the data indicated that perhaps the only moderately reliable phase data was obtained from the broadside-near portion of the circular course with the FB4Y-2 target. The value of most of the phase records was diminished by a number of sources which existed in the equipment and the operating procedure.

The most serious errors in the phase records resulted from the manual-tracking technique employed in removing the average phase difference due to target motion. Although care was taken in aiming the antenna system to keep

[REDACTED]

[REDACTED]

the tracking smooth, very low frequency errors of considerable magnitude arose due to tracking inaccuracies. As a result of these errors, most of the wide-band spectra of the phase jitter are unreliable below 20 cps. (The speed-ups gave detailed spectra which are probably valid down to 2 cps.) Other low-frequency phase errors may have been introduced by slowly changing gains in the i-f amplifiers.

Additional errors in the phase records results from the limiters in the phase measuring unit. It was found that the difference in phase shifts through the limiters varied somewhat with input level to the limiters. Extreme care had been taken in the design of the limiters to avoid such differential phase shifts, and tests prior to field measurements indicated satisfactory performance. However, laboratory tests on the phase measuring unit after the completion of the flight tests indicated that differential phase changes as great as 8 degrees might have accompanied a change of 20 decibels in input level. It was thought that this effect might be responsible for the similarity between the spectra of corresponding amplitude and phase records from some of the flights. However, many samples of data taken with a single-engine aircraft flying head-on have substantial propellor modulation in the amplitude records with no sign of it in the phase records, indicating that the cross modulation of the phase signal by amplitude variations was not serious.

Another deficiency of the amplitude limiters was an indirect result of the presence of short-range ground clutter. As mentioned in Sec. 3.21, it was necessary to decrease the dynamic range of amplitudes over which the limiters would function by reducing the signal levels at the inputs to the limiters to one fourth their optimum values. As a result, phase measurements were not accurate during signal fades greater than 10 decibels, and partial

[REDACTED]



modulation of phase readings by the signal amplitude may have resulted occasionally. With the limiters in this condition, it would be rare that large spikes of phase difference, such as those arising with a two-point target (see Sec. 2.21), would be observed in the recorded data.

Although it was not in itself a source of error, the limitation on the minimum range obtainable in the field setup, mentioned in Sec. 3.21, did restrict the quality of the phase data that was obtained. At a 1-mile range, the system sensitivity was only 1.1 degrees of phase difference per foot lateral displacement of the apparent target center. As a result, for some of the records, the phase jitter due to target echo fluctuations was smaller than the jitter due to thermal noise and system errors.

Another deficiency in the phase records was the lack of an absolute calibration of the magnitude of the phase jitter at the time of recording. Even though the data were not multiplied by target range to make them constant in terms of feet at the target, the wander could have been determined through a knowledge of magnitude of the phase jitter and from the notes that were made on target range as a function of time. Only a rough approximation to an absolute calibration could be made from the antenna swings (which ran the phase detector through its characteristic) which were used to mark the beginning and end of each run.

#### 4. CONCLUSIONS

The most important results of this study of errors in angle radar systems are summarized in the six conclusions presented in this chapter.

A. The phenomenon of wander of an apparent target center can be attributed to either of two causes. The more easily understood cause exists when the reflected signal at any time comes from one principal area of the target and when that area moves about on the target as a function of time. Usually, however, the wander is produced by interference between signals of comparable magnitude reflected simultaneously from two or more distinct areas of the target. When the wander originates in the former manner, the apparent center always remains within the physical boundary of the target. If the wander is brought about by changing phases of interfering signals, the apparent center of reflection can pass well outside the limits of the target.

B. The position of the apparent center of a target with but a single predominant reflecting area is the same regardless of the type of direction-indicating system in use and is independent of range, because any system will point to that area as the center of reflection. However, when the wander is produced by interference, this statement is true only for target ranges that are great enough to insure completely linear system operation, that is, for ranges at which the wander spans at most a very small portion of a lobe of the pattern of the receiving-antenna system. For shorter ranges, different magnitudes of wander may be measured by phase-comparison and lobe-comparison systems, although the differences are generally small. For a given system and a given target, the average magnitude of wander due to interference decreases appreciably when the target approaches the radar at short range. Similarly, for a given target at a particular intermediate or short range,

the magnitude of wander decreases with decreasing antenna lobe-width, and consequently with increasing receiving-antenna aperture.

C. The zero-frequency ordinate of a spectrum of wander measured with a given radar system depends on the type of target, its turning rate relative to the radar, and the target aspect presented to the radar. In general, larger targets give greater ordinates, and the greater the turning rate, the smaller the ordinate. For the X-band system used in this research, the values of low-frequency densities of wander measured with single-aircraft targets on typical courses varied between 2.5 and 8 feet in a 1-cps bandwidth, with an average of about  $4.5 \text{ feet}/\sqrt{\text{cps}}$ . The bandwidths of the wander spectra measured with this system were generally less than 10 cps, although in some cases frequency components higher than 40 cps were observed.

D. The wander of the apparent radar center of two targets flying in close formation is considerably greater than that of either target. It was observed experimentally that at times the position of the apparent center may vary rapidly over distances greater than the separation of the targets. At other times, the apparent center may tend to lock on one, then the other, target in a random manner, all the time oscillating to some extent at the Doppler-difference frequency of the signals reflected from the two targets. Spectra of the wander of two single-engine aircraft in close formation were measured with zero-frequency ordinates as great as  $15 \text{ ft}/\sqrt{\text{cps}}$ , and with bandwidths to the half-voltage point as large as 20 cps.

E. Very large deviations of the position of the apparent radar center occasionally take place when wander is caused by interference among a multiplicity of signals from fixed points on a target. In practice, these large deviations, which may be substantially greater than the maximum

[REDACTED]

dimension of the target, are almost invariably accompanied by deep fades in the amplitude of the received signal and are of short duration. Consequently, the large error signals which these deviations might produce in the error-detector output of a direction-indicating radar system can be suppressed through the use of a slow-acting automatic gain control, and in the case of a phase-comparison system, through the use of partial limiting. However, other results of partial limiting, which are definitely detrimental to system performance, make its application of questionable value.

F. Care must be taken in the design of phase-comparison systems in order to avoid the possibility of the system going blind when the target range is so short that the receiving antennas span an appreciable fraction of a lobe of the scattering pattern of the target. At such ranges, the possibility exists that the average of the output of a phase detector is zero, regardless of the target position. However, such blindness can be completely avoided if the measurement section of the radar has an adequately wide bandwidth. Bandwidths as great as, and possibly much wider than, that of the wander spectrum are needed in many cases in order to insure linear system operation.

[REDACTED]

## 5. RECOMMENDATIONS FOR FURTHER RESEARCH

The foregoing treatment of various phenomena associated with wander of the apparent center of reflection of radar targets is by no means exhaustive, and many aspects of the problem merit further investigation. Although the nature of the subject of wander is such that completely explicit and comprehensive solutions cannot be given, nevertheless many specific, feasible questions can be formulated. In particular, some of the effects of wander associated with phase-comparison systems, which at present are quite obscure, can undoubtedly be understood if they are studied in an appropriate manner. This chapter is devoted to a discussion of some of the more important unsolved problems of wander and possible methods for treating them.

### 5.1 BANDWIDTH REQUIREMENTS OF PHASE-COMPARISON SYSTEMS

It was demonstrated in Sec. 2.51 that a phase-comparison system with too narrow a bandwidth in the measurement circuits can go blind when a target approaches the radar. It was also shown that if this bandwidth is greater than  $(\phi_0 + 1)f_w$ , where  $\phi_0$  is the maximum phase difference in radians and  $f_w$  is the highest frequency associated with the wander, the possibility of such blindness is avoided. In practice, however, it may be very difficult to obtain this bandwidth. In addition, this requirement of wide bandwidth may be in direct contradiction to the requirements for optimum performance at ranges where the signal strength is close to that of thermal noise. Therefore, it would be desirable to determine how much relaxation of bandwidth requirements could be made before serious deterioration of short-range system performance would be encountered.

There are a number of reasons for suspecting that the bandwidth requirement repeated above is substantially greater than would be needed in practice.

For one thing, this requirement was established on the basis of true motion of a single area of reflection. When the wander is produced by interference, the situation is not nearly as severe. The curves of phase-detector output with a two-point target given in Sec. 2.22 show that there is essentially no increase in bandwidth as range is decreased. In the second place, the sinusoidal wander assumed in computing the requirement is unduly pessimistic, because it represents a function for which the largest excursions have the greatest probability.

Thirdly, it is not necessary to have complete reproduction of all the rapid wander fluctuations in order to obtain a good measurement of the average position of the apparent radar center. For example, with the nulling-servo system, the servo can lag the input phase difference by as much as 60 degrees or more without introducing appreciable non-linearity into the phase-detector operation. Finally, it is possible that for phase-rate measurement, such as can be obtained with a single-sideband-modulator system followed by a frequency discriminator, less bandwidth is needed than that required for a positional phase-comparison system.

There are a number of ways in which this problem could be approached. It would be possible to conduct a series of flight tests using different bandwidths in the measurement section of a phase-comparison system. Such an approach is costly, empirical, and apt to be inconclusive, because of the multitude of extraneous factors which are bound to enter; flight tests have their greatest value in confirming more rigorously determined results.

An analysis based on a continuous, random distribution of points over a target, such as that assumed in Sec. 2.31, could yield some very definite information on bandwidth requirements. A time-varying wander could be

**CONFIDENTIAL**

introduced by assuming a uniform, slow rotation of the target about its center. If the target is then given a uniform angular velocity with respect to the radar, the necessary conditions are set up for studying the effects of wander on the ability of an idealized phase-comparison system to measure the motion of a target.

Some attempts were made during the course of this research to perform such an analysis as that just described. It was found that the analysis soon gets involved in substantial amounts of mathematical statistics. It is felt that considerably greater success with reasonable effort would be obtained in an experimental study using a simulated target. An adequate simulation for many targets could be obtained with a reasonable amount of apparatus in the following manner.

Construct five or six similar oscillators with different frequencies adjustable over the same band of approximately 30 cps. (The center frequency of the band should probably be about 10 kcps, in order to maintain adequate stability of the frequency differences.) These frequencies are set to correspond to the Doppler frequencies (referred to a different center frequency) from 5 or 6 points on a rigid, uniformly rotating target. The statistics of the vector sum of 5 or 6 random components are very similar to those of the sum of many components, so that little would be gained by using more than 6 oscillators. The outputs of the oscillators, which may be of different amplitudes, are added directly to form one signal input to the radar. The other input is formed by passing the 5 or 6 outputs through separate, adjustable phase delays, and adding the delayed signals. The delays are set to be proportional to the Doppler frequencies of the corresponding signals, because phase difference and Doppler frequency are both linearly

**CONFIDENTIAL**

[REDACTED]

related to the position of the source on the target. Decreasing range is simulated by increasing in proportional amounts all the various phase delays. Either signal input can then be put through a continuous phase shifter driven at a constant rate, in order to reproduce the effects of a constant angular rate-of-change of the line-of-sight.

The performance of the system under test would be indicated by its ability to measure the constant phase-rate introduced by the continuous phase shifter.

## 5.2 OPTIMUM LIMITING LEVEL

The large excursions in the position of an apparent target center which occur occasionally as a result of interference between signals from two or more areas of a target are generally accompanied by deep fades in the strength of the received signal. Consequently, it is possible to suppress the detrimental effects on the error-detector output caused by these large spikes of wander by allowing the output level from the error detector to be dependent on signal level. However, it was indicated in Sec. 2.52 that the rms noise out of an error detector can actually be larger without limiting than with limiting at times when system aiming errors exist, suggesting that it is desirable to use some form of limiting.

Partial limiting can be used to deemphasize the largest errors, which are accompanied by the weakest signals. With partial limiting, all signals with amplitudes greater than a certain level are limited, while those below that level are passed linearly. This limiting level is governed by the ratio of the input voltage to the limiter which corresponds to the knee of the limiter characteristic to the average input voltage. It is necessary to determine the most acceptable limiting level, for which the noise output

[REDACTED]



from the error detector due to target echo fluctuations is a minimum. The target simulator described in the preceding section could be used very readily in such a determination.

An analytical study, even though approximate, should be made in order to determine the influence of partial limiting on the performance of phase-rate measuring systems. It is very difficult to predict this influence on the basis of phase measuring system performance, because of the manner in which partial limiting affects both the rms value and the spectrum bandwidth of an error-detector output.

### 5.3 PROPERTIES OF WANDER IN WIDE-BAND SYSTEMS

It is known that a phase-comparison system with a wide bandwidth in the measurement section is linear in the sense that the phase of the output with respect to the reference signal is equal to the phase difference of the input signals. However, the average magnitude of the phase of the output is not always inversely proportional to the range of a particular target. If the wander results from interference of many signals from a target, the magnitude of wander usually decreases with decreasing range, as is suggested by the curves of Sec. 2.21 for a two-point target. On the other hand, when the wander is caused by glint, or true motion of a single reflecting area, the average magnitude of the phase of the output is exactly proportional to target range.

A knowledge of the manner in which wander decreases with decreasing range is highly desirable in determining system bandwidths, as considered in Sec. 5.1, apart from its academic interest. An extension of the analysis used in Sec. 2.3 for computing the phase-detector output with a multi-point target could supply the desired information. However, the mathematics thus

involved might well be unfeasible, so that an experimental approach would prove more fruitful. To this end, the target simulator described in Sec. 5.1 would be very useful, particularly when used in conjunction with a nulling-servo phase-comparison system. It would merely be necessary to feed the simulator outputs into the system inputs and note the behavior of the servo output (with adequate bandwidth throughout the system).

An experimental flight-test setup could also be instrumented for studying wander with phase-comparison systems. It would be necessary to use equipment for measuring phase (not the sine of the phase difference), for which the nulling-servo system with wide bandwidth is well suited. An abnormally large receiving-antennas spacing should be employed, in order to guarantee that short-range conditions can be obtained, that is, to insure that the receiving antennas span at least a substantial portion of a lobe-width of the target's scattering pattern.

#### 5.4 WANDER WITH LOBE-COMPARISON SYSTEMS AND TARGETS AT SHORT RANGE

The wander of an apparent target center as measured with a lobe-comparison system usually decreases as the target approaches the radar, as is illustrated by the results for a two-point target presented in Sec. 2.21. These results show that the manner in which the wander changes with range is not the same as with a phase-comparison system. Therefore, a separate study is required of the magnitudes and spectra of wander and of the error-detector output with a lobe-comparison system as functions of target range.

It is believed that the present need for this investigation is probably less intense than the need for additional study of wander with phase-comparison systems. For one thing, lobe-comparison systems do not go completely blind at short ranges, as can the phase-comparison systems. Secondly, in

many applications, smaller antenna apertures are used in lobe-comparison systems than in equivalent phase-comparison systems, with the result that short-range conditions are encountered at greater actual target ranges with the latter systems.

Any study of wander at short ranges with lobe-comparison systems that would be appreciably more general than that of Sec. 2.21 should be based on an experimental procedure. The non-linearities encountered with short target ranges cause the mathematics associated with even a uniform aperture to become hopelessly complicated.

#### 5.5 DOPPLER FREQUENCIES IN TARGET ECHOES

The Doppler frequency of the signal reflected from a target towards the radar receiver is an indication of the rate of change of the apparent range to the target. The position of the apparent center of a target can fluctuate in range in much the same manner as it does in angle. These range fluctuations cause the Doppler signal to spread out over a band of frequencies. In fact, the frequency components in the spectrum of the Doppler signal must extend over at least as great a bandwidth as that of the wander measured with a phase-comparison system, because the phase differences associated with wander are produced by the differences between two nearly equal Doppler signals.

The bandwidths of Doppler spectra from radar targets are of interest in the design of Doppler radar systems, such as the c-w phase-comparison system described in Appendix B. These bandwidths can be determined experimentally with a relatively small amount of equipment. For a laboratory setup, the target simulator described in Sec. 5.1 could be employed. It would merely be necessary to amplitude-limit either output from the simulator and feed the result to a spectrum analyzer. With a c-w transmitter and receiver, tests

could be made on actual targets by studying the beat between the received signal and spillover from the transmitter. Just such data from aircraft targets in flight was recorded in conjunction with this research program using X-band equipment consisting of a transmitter and receiver plus an amplitude detector. However, the data was recorded on magnetic tape, and the wow of the recorder had a spectrum comparable with that of the data. As a result, no conclusions were drawn from those data.

#### 5.6 PROBABILITY DENSITY DISTRIBUTION OF WANDER

The probability distribution of the position of the apparent center of reflection of a target is necessary information in determining the performance of non-linear radar systems. For systems that are completely linear, the spectrum or autocorrelation function of the wander is all that is required, aside from the system transfer function, in computing the output; however, in practice, the first probability function, or even the first joint probability, may be desired.

If the wander is caused by interference among the signals from a very large number of points on a target, the distribution function of the wander when the target is at very long range has the form given in Eq. 2-28 in Sec. 2.31. Actual distribution functions may be considerably different from this, because targets are not always at very long range and may appear to have a very small number of principal reflecting areas. Experimentally determined data, such as that obtained with the X-band system in this research, can be analyzed either manually, from copies such as those shown in Fig. 3-3, or electronically, using apparatus developed especially for the purpose.

## APPENDIX A

## POINTING ERRORS DERIVED FROM SIGNAL DISTRIBUTION AT RECEIVER

The analyses used in obtaining the results described in Sec. 2.1, on a comparison of radar systems based on the distribution of the reflected signal at the receiver, are presented in this appendix. In these analyses it is assumed that the expression for the resultant signal received by a uniform aperture is

$$S = \int_{-\frac{1}{2}d}^{\frac{1}{2}d} A(x) e^{j[\phi(x) + \frac{2\pi\beta}{\lambda} x]} dx \triangleq \int_{-\frac{1}{2}d}^{\frac{1}{2}d} A(x) e^{jG(x)} dx, \quad 2-2$$

and that the expressions for the signals received by the two lobes of a lobe-comparison system are

$$S_{a,b} = \int_{-\frac{1}{2}d}^{\frac{1}{2}d} A(x) e^{j[\phi(x) + \frac{2\pi(\beta \pm \beta_q)}{\lambda} x]} dx \\ \triangleq \int_{-\frac{1}{2}d}^{\frac{1}{2}d} A(x) e^{j[G_{a,b}(x)]} dx. \quad 2-3$$

A-1 Direction Indication of Single-lobe System

The condition by which a single-lobe system determines the direction of an apparent target center is given by

$$\frac{dA_S}{d\beta} = 0. \quad 2-4$$

If  $\phi_S$  is the phase of  $S$ , as defined in Eq. 2-1, the magnitude of  $S$ ,  $A_S$ , can be found by integrating the projection onto  $S$  of the integrand of Eq. 2-2,

giving

$$A_S = \int_{-\frac{1}{2}d}^{\frac{1}{2}d} A(x) \cos[\phi(x) + \frac{2\pi\beta}{\lambda} x - \phi_S] dx. \quad A-1$$

The derivative of this expression with respect to  $\beta$  yields the final result

$$\frac{dA_S}{d\beta} = \int_{-\frac{1}{2}d}^{\frac{1}{2}d} A(x) \left( \frac{d\phi_S}{d\beta} - \frac{2\pi}{\lambda} x \right) \sin\left[\phi(x) + \frac{2\pi\beta}{\lambda} x - \phi_S\right] dx = 0. \quad 2-5$$

A relation containing a double integral but no undetermined quantity such as  $\phi_S$  can also be derived to satisfy Eq. 2-4. First let S be split into its real and imaginary components

$$\begin{aligned} S &= \int_{-\frac{1}{2}d}^{\frac{1}{2}d} A(x) e^{jG(x)} dx \\ &= \int_{-\frac{1}{2}d}^{\frac{1}{2}d} A(x) \cos[G(x)] dx + j \int_{-\frac{1}{2}d}^{\frac{1}{2}d} A(x) \sin[G(x)] dx \\ &\triangleq R[S] + j I[S]. \end{aligned} \quad A-2$$

It is evident that

$$A_S^2 = R^2[S] + I^2[S], \quad A-3$$

and that Eq. 2-4 is satisfied when

$$R[S] \frac{dR[S]}{d\beta} + I[S] \frac{dI[S]}{d\beta} = 0. \quad A-4$$

The derivatives of  $R[S]$  and  $I[S]$  are

$$\frac{dR[S]}{d\beta} = - \frac{2\pi}{\lambda} \int_{-\frac{1}{2}d}^{\frac{1}{2}d} x A(x) \sin[G(x)] dx \quad A-5$$

$$\frac{dI[S]}{d\beta} = \frac{2\pi}{\lambda} \int_{-\frac{1}{2}d}^{\frac{1}{2}d} x A(x) \cos[G(x)] dx. \quad A-6$$

Substituting from Eq's. A-2, A-5, and A-6 into Eq. A-4 gives the relation

$$\begin{aligned} & - \int_{-\frac{1}{2}d}^{\frac{1}{2}d} A(y) \cos[G(y)] dy \int_{-\frac{1}{2}d}^{\frac{1}{2}d} x A(x) \sin[G(x)] dx \\ & + \int_{-\frac{1}{2}d}^{\frac{1}{2}d} A(y) \sin[G(y)] dy \int_{-\frac{1}{2}d}^{\frac{1}{2}d} x A(x) \cos[G(x)] dx \end{aligned}$$

$$\begin{aligned}
 &= \int_{-\frac{1}{2}d}^{\frac{1}{2}d} \int_{-\frac{1}{2}d}^{\frac{1}{2}d} x A(x) A(y) (\sin[G(y)] \cos[G(x)] - \cos[G(y)] \sin[G(x)]) dx dy \\
 &= \int_{-\frac{1}{2}d}^{\frac{1}{2}d} \int_{-\frac{1}{2}d}^{\frac{1}{2}d} x A(x) A(y) \sin[G(y) - G(x)] dx dy = 0 .
 \end{aligned} \tag{2-6}$$

### A-2 Direction Indication of Lobe-comparison System

When a lobe-comparison system is pointed in the direction of an apparent target center, the amplitudes of the signals received from the targets by two lobes a and b are equal. That is,

$$A_{S_a} - A_{S_b} = 0 . \tag{2-7}$$

The quantities  $A_{S_a}$  and  $A_{S_b}$  can be found in terms of  $\phi_{S_a}$  and  $\phi_{S_b}$ , the phases of  $S_a$  and  $S_b$  respectively, by the same method used in obtaining Eq. A-1, which

gives

$$A_{S_{a,b}} = \int_{-\frac{1}{2}d}^{\frac{1}{2}d} A(x) \cos\left[\phi(x) + \frac{2\pi(\beta \pm \beta_q)}{\lambda} x - \phi_{S_{a,b}}\right] dx . \tag{A-7}$$

When Eq's. A-7 are substituted into Eq. 2-7, the result is

$$\begin{aligned}
 &\int_{-\frac{1}{2}d}^{\frac{1}{2}d} A(x) \cos\left[\phi(x) + \frac{2\pi(\beta + \beta_q)}{\lambda} x - \phi_{S_a}\right] dx \\
 &\quad - \int_{-\frac{1}{2}d}^{\frac{1}{2}d} A(x) \cos\left[\phi(x) + \frac{2\pi(\beta - \beta_q)}{\lambda} x - \phi_{S_b}\right] dx \\
 &= -2 \int_{-\frac{1}{2}d}^{\frac{1}{2}d} A(x) \sin\left[\phi(x) + \frac{2\pi\beta}{\lambda} x - \frac{\phi_{S_a} + \phi_{S_b}}{2}\right] \sin\left[\frac{2\pi\beta_q}{\lambda} x + \frac{\phi_{S_a} - \phi_{S_b}}{2}\right] dx \\
 &= 0 .
 \end{aligned} \tag{A-8}$$

Eq. 2-9 of Sec. 2.12 can be obtained from this expression by multiplying the latter by  $-\frac{1}{2}$ .

A double-integral expression equivalent to Eq. 2-9 and containing no

undetermined constants can be obtained in a manner similar to that by which Eq. 2-6 was derived. Eq. 2-7 is satisfied by the condition

$$R^2[S_a] + I^2[S_a] - (R^2[S_b] + I^2[S_b]) = 0. \quad 2-8$$

The real and imaginary components of  $S_a$  and  $S_b$ , which can be obtained from Eq's. 2-3, have forms very similar to those of the components of  $S$ , given in Eq. A-2. One can write

$$\begin{aligned} R^2[S_a] + I^2[S_a] &= \int_{-\frac{1}{2}d}^{\frac{1}{2}d} \int_{-\frac{1}{2}d}^{\frac{1}{2}d} A(x) A(y) \cos[G_a(x)] \cos[G_a(y)] dx dy \\ &\quad + \int_{-\frac{1}{2}d}^{\frac{1}{2}d} \int_{-\frac{1}{2}d}^{\frac{1}{2}d} A(x) A(y) \sin[G_a(x)] \sin[G_a(y)] dx dy \\ &= \int_{-\frac{1}{2}d}^{\frac{1}{2}d} \int_{-\frac{1}{2}d}^{\frac{1}{2}d} A(x) A(y) \cos[G_a(y) - G_a(x)] dx dy, \end{aligned} \quad A-9$$

and

$$R^2[S_b] + I^2[S_b] = \int_{-\frac{1}{2}d}^{\frac{1}{2}d} \int_{-\frac{1}{2}d}^{\frac{1}{2}d} A(x) A(y) \cos[G_b(y) - G_b(x)] dx dy. \quad A-10$$

The result obtained by substituting Eq's. A-9 and A-10 into Eq. 2-8 is

$$\begin{aligned} &\int_{-\frac{1}{2}d}^{\frac{1}{2}d} \int_{-\frac{1}{2}d}^{\frac{1}{2}d} -2 A(x) A(y) \sin \frac{1}{2}[G_a(y) + G_b(y) - G_a(x) - G_b(x)] \\ &\quad \times \sin \frac{1}{2}[G_a(y) - G_b(y) - G_a(x) + G_b(x)] dx dy \\ &= \int_{-\frac{1}{2}d}^{\frac{1}{2}d} \int_{-\frac{1}{2}d}^{\frac{1}{2}d} -2 A(x) A(y) \sin[G(y) - G(x)] \sin\left[\frac{2\pi\beta_0}{\lambda}(y-x)\right] dx dy \\ &= -2 \int_{-\frac{1}{2}d}^{\frac{1}{2}d} \int_{-\frac{1}{2}d}^{\frac{1}{2}d} A(x) A(y) \sin[G(y) - G(x)] \sin\left[\frac{2\pi\beta_0 y}{\lambda}\right] \cos\left[\frac{2\pi\beta_0 x}{\lambda}\right] dx dy \\ &\quad + 2 \int_{-\frac{1}{2}d}^{\frac{1}{2}d} \int_{-\frac{1}{2}d}^{\frac{1}{2}d} A(x) A(y) \sin[G(y) - G(x)] \cos\left[\frac{2\pi\beta_0 y}{\lambda}\right] \sin\left[\frac{2\pi\beta_0 x}{\lambda}\right] dx dy \end{aligned}$$



$$= 4 \int_{-\frac{1}{2}d}^{\frac{1}{2}d} \int_{-\frac{1}{2}d}^{\frac{1}{2}d} A(x) \sin\left[\frac{2\pi\beta_0 x}{\lambda}\right] A(y) \cos\left[\frac{2\pi\beta_0 y}{\lambda}\right] \sin(G(y) - G(x)) dx dy$$

$$= 0 , \quad \text{A-11}$$

of which the final equality is the same as Eq. 2-10.

### A-3 Direction Indication with First-order Aperture Illumination

The following material is a graphical computation of the apparent direction of a signal source which produces first-order illumination of the antenna aperture of various types of radar direction-indicating receiving systems. The first-order illumination implies that the expressions for the signal from the source are

$$\phi(x) = u_1 x , \quad A(x) = v_0 + v_1 x , \quad \text{2-18}$$

where  $x$  is a linear coordinate along the aperture, measured from the center of the aperture.

The resultant signal received by a uniform aperture with illumination given by Eq. 2-18 is, according to Eq. 2-2,

$$S = \int_{-\frac{1}{2}d}^{\frac{1}{2}d} (v_0 + v_1 x) e^{j(u_1 + \frac{2\pi\beta}{\lambda})x} dx . \quad \text{A-12}$$

Obviously, it is sufficient to solve Eq. A-12 with  $u_1 = 0$ , because solutions for other values of  $u_1$  can be obtained by merely increasing  $\beta$  by  $\frac{u_1 \lambda}{2\pi}$ .

For  $u_1 = 0$ ,

$$S = + \int_{-\frac{1}{2}d}^{\frac{1}{2}d} v_0 \cos\left[\frac{2\pi\beta x}{\lambda}\right] dx + \int_{-\frac{1}{2}d}^{\frac{1}{2}d} v_1 x \cos\left[\frac{2\pi\beta x}{\lambda}\right] dx$$

$$+ j \int_{-\frac{1}{2}d}^{\frac{1}{2}d} v_0 \sin\left[\frac{2\pi\beta x}{\lambda}\right] dx + j \int_{-\frac{1}{2}d}^{\frac{1}{2}d} v_1 x \sin\left[\frac{2\pi\beta x}{\lambda}\right] dx$$

$$= v_0 d \frac{\sin H}{H} + j \frac{1}{2} v_1 d^2 \left( \frac{\sin H}{H^2} - \frac{\cos H}{H} \right)$$

$$= v_0 d \left[ \frac{\sin H}{H} + j \frac{v_1 d}{2v_0} \left( \frac{\sin H}{H^2} - \frac{\cos H}{H} \right) \right], \quad \text{A-13}$$

where  $H \triangleq \frac{\pi d}{\lambda} \beta$ .

The magnitude of  $S$ ,  $A_S$  is found from the relation

$$A_S = (R^2[S] + I^2[S])^{\frac{1}{2}}. \quad \text{A-14}$$

Plots of  $A_S$  as a function of  $H$ , for various values of the parameter  $\frac{v_1 d}{2v_0}$ , are shown in Fig. A-1. These plots were normalized on the basis of constant total power incident upon the aperture. The total incident power is proportional to

$$\begin{aligned} \int_{-\frac{1}{2}d}^{\frac{1}{2}d} A^2(x) dx &= \int_{-\frac{1}{2}d}^{\frac{1}{2}d} (v_0 + v_1 x)^2 dx = v_0^2 d + v_1^2 \frac{d^3}{12} \\ &= v_0^2 d \left( 1 + \frac{1}{3} \left[ \frac{v_1 d}{2v_0} \right]^2 \right). \end{aligned} \quad \text{A-15}$$

The normalization of each curve was achieved by setting

$$v_0 d = \left( 1 + \frac{1}{3} \left[ \frac{v_1 d}{2v_0} \right]^2 \right)^{-\frac{1}{2}}. \quad \text{A-16}$$

The direction in which a single-lobe (searchlight radar would indicate the apparent position of the source corresponds to the value of  $H$  for which  $A_S$  is maximum. For  $0 < \frac{v_1 d}{2v_0} < \sqrt{3}$ , this value is zero, indicating that the radar points normal to the phase front. For other values of the parameter, the values of  $H$  corresponding to the maxima of  $A_S$  were read off the plots. It should be noted that because the plots were symmetrical about  $H = 0$ , either positive or negative values of  $H$  could be used. The abscissas of the maxima for non-negative  $H$  were the basis for the curves of Fig. 2-2 for the single-lobe system.

The error-detector output of a lobe-comparison system which measures the difference in magnitude of the two received signals can be determined

**CONFIDENTIAL**

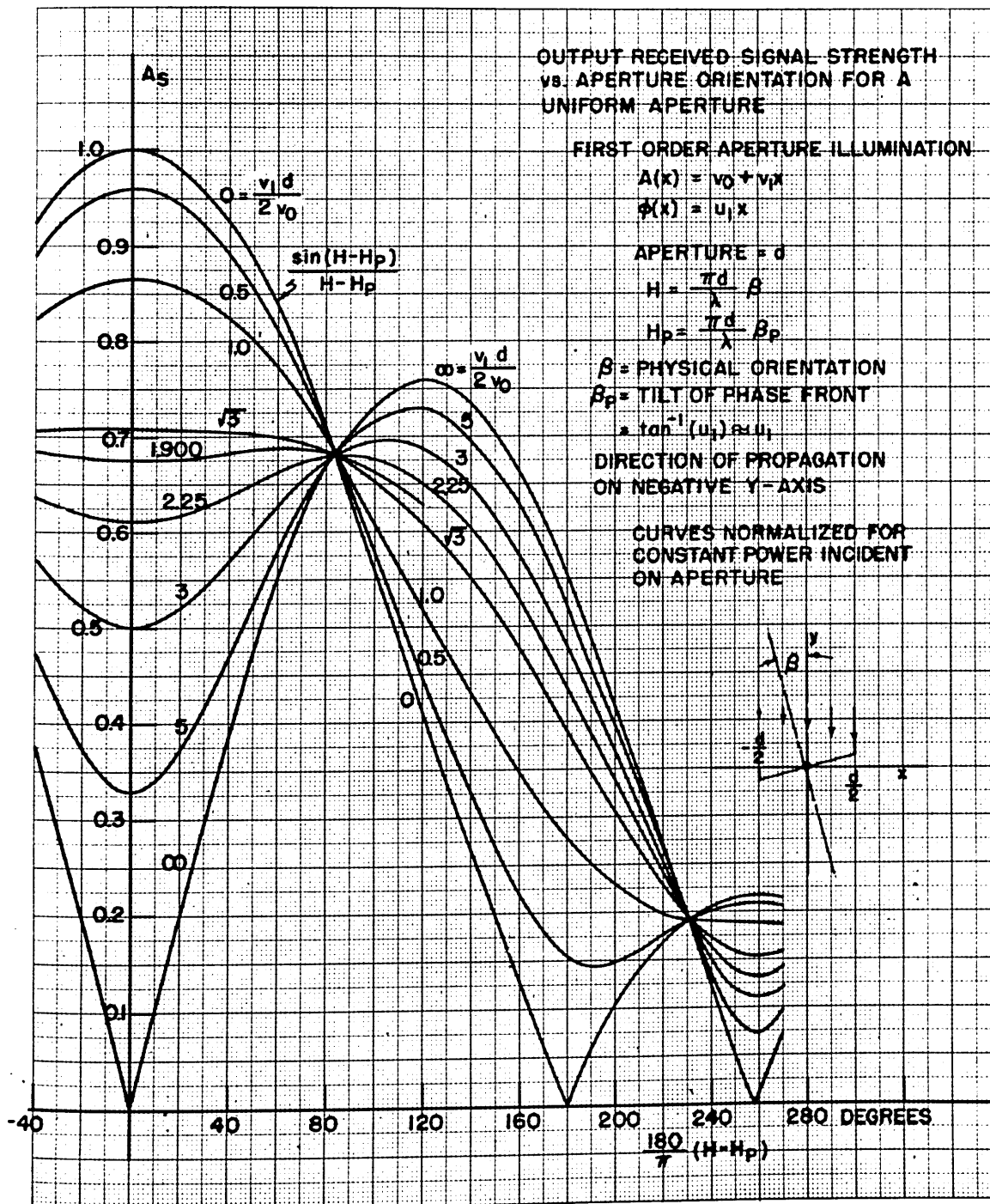


Fig. A-1

**CONFIDENTIAL**

CONFIDENTIAL

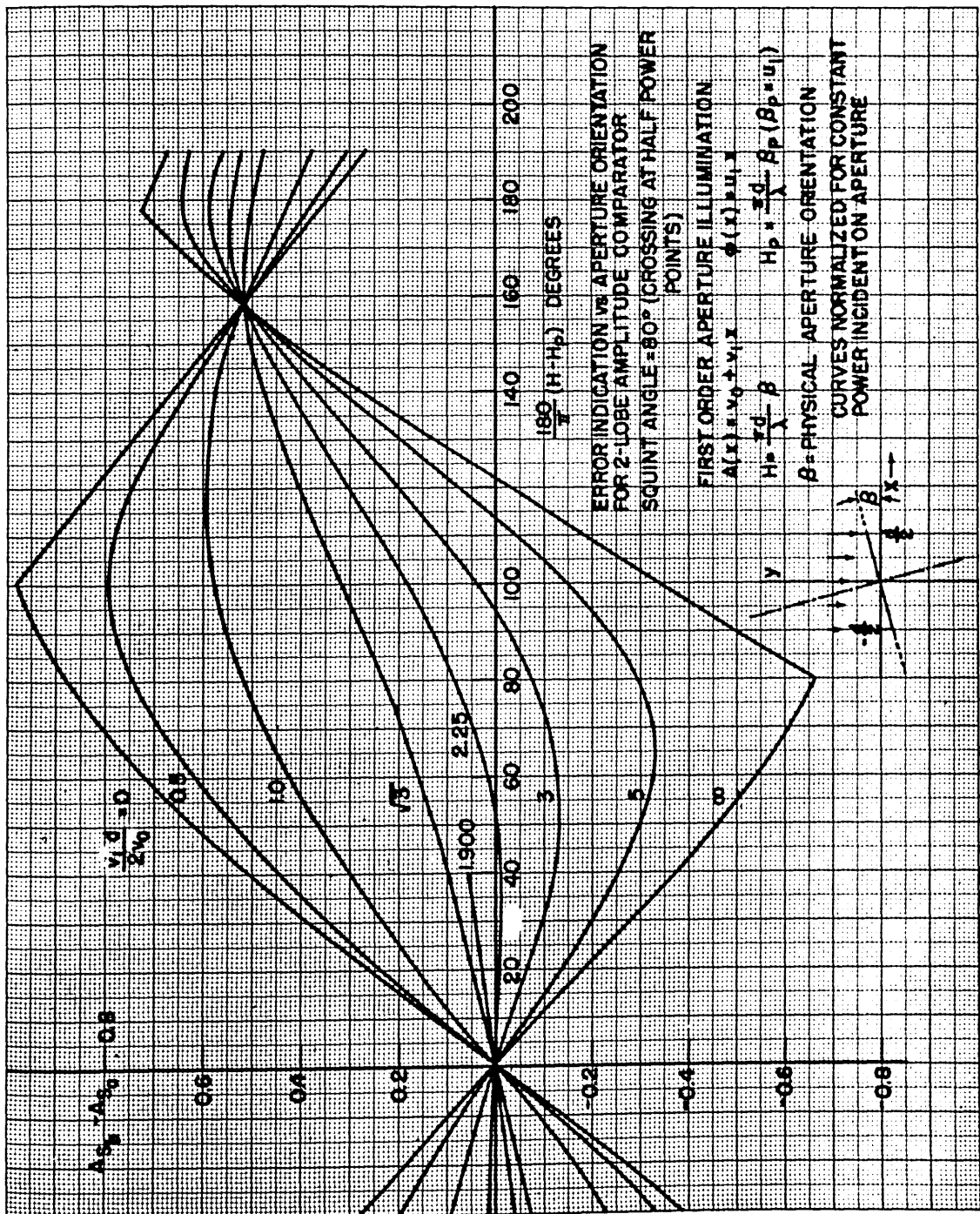


FIG. A-2

from Fig. A-1. Each of the curves of Fig. A-2 was plotted by reading the difference of the ordinates of the corresponding curve in Fig. A-1 for abscissas separated by 160 degrees (of H). Therefore, these curves are for a lobe-comparison system with a normalized squint angle of 80 degrees, which gives a crossover at the 0.707 points of the lobes, as can be seen from the curve of Fig. A-1 for  $\frac{v_1 d}{2v_0} = 0$ .

The curves of Fig. A-2 all go through the origin, with the result that there is never an error signal when the antenna is pointed normal to the phase front. However, for those curves which have a negative slope when  $H = 0$ , this is an unstable point, and the antenna would eventually swing to the direction corresponding to a zero-point with a positive slope. Again, it should be noted that either positive or negative values of H are equally possible. The curves in Fig. 2-2 for the lobe-comparison system were drawn from the positive values of H corresponding to the zero-crossings with positive slope in Fig. A-2.

For the phase-comparison system, the computation of direction is considerably more straightforward. According to Eq. 2-13, when  $A(x)$  has the same sign at both antennas, the system indicates the true normal to the phase front. When  $A(x)$  changes sign between the antennas, which is equivalent to saying that  $|\frac{1}{2}v_1 d| > |v_0|$ , the antenna must turn away from the normal to the phase front by an amount sufficient to introduce a phase change of  $\pm \pi$ . This reorientation corresponds to an angular error of  $\beta = \frac{\lambda}{2d}$ , or  $H = \frac{1}{2}\pi$ .

## APPENDIX B

## DESCRIPTIONS OF VARIOUS PHASE-COMPARISON SYSTEMS

In this appendix are presented brief descriptions of four different types of phase-comparison systems which have been used in similar applications. Expressions for the signals existing at various points of the systems are shown on the block diagrams. It can be seen that the outputs of all the systems are equivalent, as mentioned in Sec. 2.14, provided that the bandwidths of the signals are not restricted anywhere in the systems.

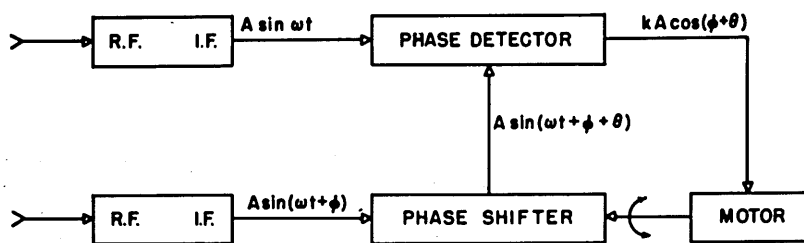
B-1 Nulling Servo System

Fig. B-1 is a block diagram of the receiving section of a phase-comparison radar system which uses a servo driving a phase shifter in such a manner as to keep constant the output of a phase detector. The system employs separate r-f and i-f sections with a common local oscillator for the two antennas. A phase shifter is inserted (either directly or indirectly) in the circuits associated with one antenna, and is driven by a motor which is controlled from the output of the phase detector on the i-f amplifier outputs. The phase-difference at the phase detector is thus held fixed, and the angular rotation of the phase shifter is proportional to the phase difference of the received signals.

An entirely electronic system with essentially the same block diagram is currently under development in the guidance group of Project Meteor at M. I. T. This system uses electronic equivalents of the phase shifter and its mechanical drive. Substantially wider bandwidths can be obtained, if needed, with the electronic system.

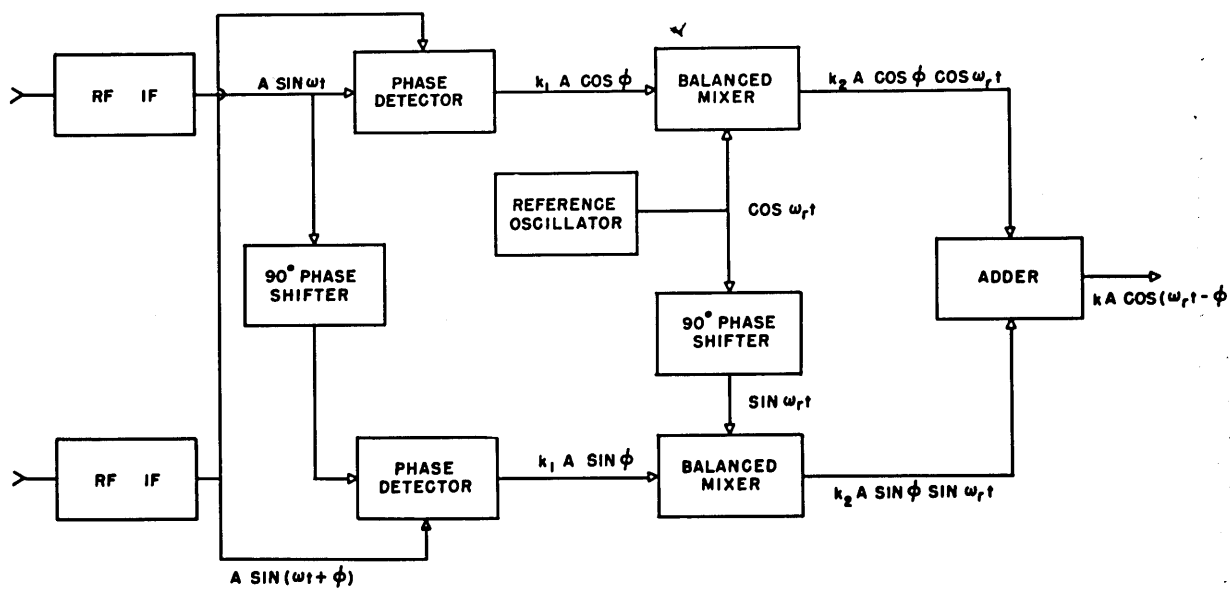
B-2 Single-sideband-modulator System

The single-sideband-modulator system employs two r-f and i-f sections,



BLOCK DIAGRAM OF SYSTEM WITH NULLING SERVO

Fig. B-1



BLOCK DIAGRAM OF SYSTEM WITH SINGLE-SIDEBAND MODULATOR

Fig. B-2

[REDACTED]

which can be the same as those for the nulling servo system except that no phase shifter is needed. Two phase detectors are used, as shown in the block diagram in Fig. B-2, to form part of a single-sideband modulator. The expressions shown on the diagram indicate the signals available at different points. The output, as shown on the diagram, consists of a signal whose amplitude is proportional to that of the received signals and whose phase relative to a fixed reference equals the phase difference of the received signals.

### B-3 Interferometer System\*

The interferometer system, shown in block form in Fig. B-3, differs from the previous two systems in that only a single i-f section is required. One of the received signals is shifted in phase at a constant known rate in the r-f section. The two signals are then added and amplified. The detected envelope of the sum is a waveform of which the principal component is a sine wave with an amplitude proportional to that of the received signals, and with a phase relative to a fixed reference frequency equal to the phase difference of the received signals. This system is unique among those considered in this report in that the output also contains components produced by amplitude modulation of the received signal, when the amplitude modulation contains frequencies near that of the principal component of the envelope.

### B-4 Doppler-difference System

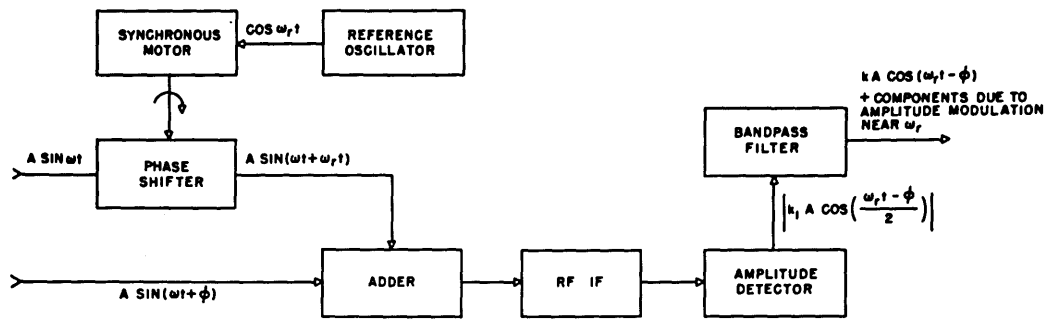
This system differs from the three other systems that were described in that it uses continuous-wave signals, whereas the others employ pulsed

---

\*Developed by the Defense Research Laboratory of the University of Texas.

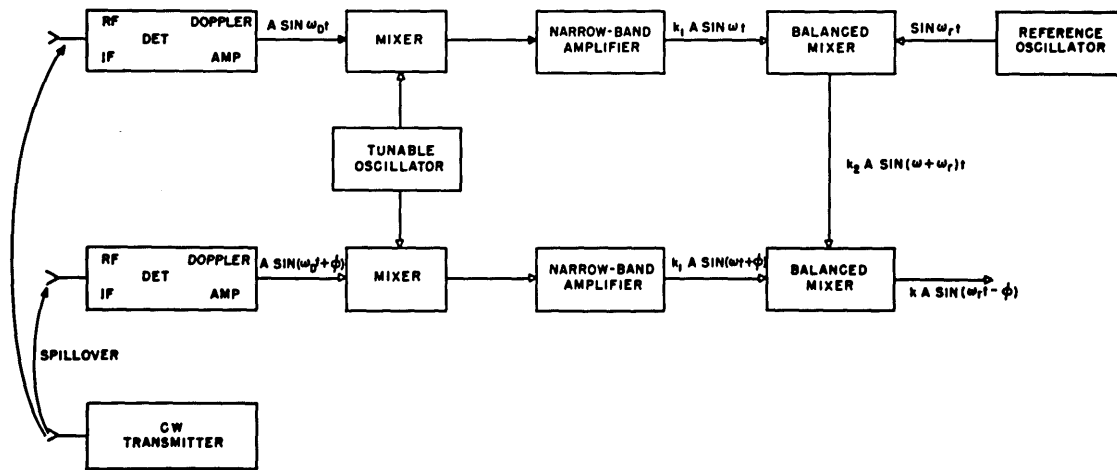
[REDACTED]





BLOCK DIAGRAM OF INTERFEROMETER SYSTEM

Fig. B-3



BLOCK DIAGRAM OF DOPPLER-DIFFERENCE SYSTEM

Fig. B-4

signals. In the Doppler-difference system, the echo return received by two antennas beats with spillover from the transmitter. Envelope detection of the outputs of the two i-f amplifiers gives signals with amplitudes proportional to the strength of the radar echoes at each antenna. The detector outputs may be considered to be of equal frequency (the Doppler frequency due to target motion) with varying phase difference, the phase difference being a function of the angular position of the target.

Fig. B-4 shows a block diagram of the system. As in the interferometer and single-sideband-modulator systems, the output is a sine wave with its amplitude proportional to the amplitude of the echo and with a phase, relative to a fixed reference frequency, equal to the phase difference of the received signals.

~~CONFIDENTIAL~~

APPENDIX C

ANALYSIS OF A TWO-POINT TARGET

The computations described in this appendix are based on the assumption of a two-point target, in which the two points are omnidirectional sources with relative signal strengths of 1.0 and 0.8. The separation of the two points is  $s$ , with the line joining the points normal to the line-of-sight from the radar. The aperture of the receiving antenna system is called  $d$ , which is the spacing of the antennas of the phase-comparison system or the size of the antenna of the single-lobe or lobe-comparison systems. It is assumed that the axis of the antenna system remains approximately parallel to the line-of-sight at all times, a condition requiring that  $d/\lambda$  is much greater than unity. It is furthermore postulated that  $R$ , the range from the radar to the target, is much greater than both  $d$  and  $s$ .

C-1 Position of Apparent Target Center

Phase-comparison Radar - When the axis of the radar receiver is aimed directly at the stronger point of the target, the phase difference of the received signals is exactly proportional to the lateral displacement of the apparent center of reflection measured away from the position of the stronger point. Therefore, the position of the apparent center can be determined by calculating the phase difference of the received signals with the two antennas equidistant from the stronger point.

Let the antenna system be aimed at the stronger point, and let the phase of the signal received from that point be zero. Then, in accordance with Eq's. 2-19 and 2-20 of Sec. 2.31, the two resultant received signals can be written

$$S_1 \triangleq A_1 e^{j\phi_1} = 1 + 0.8 e^{j\mu_1} ,$$

C-1

~~CONFIDENTIAL~~

$$S_2 = A_2 e^{j\phi_2} = 1 + 0.8 e^{j(\mu_1 + \frac{2\pi d}{\lambda R} s)} \quad C-2$$

The difference in phase of the signals from the two points at the midpoint between the antennas is

$$\mu \triangleq \frac{1}{2}(\mu_1 + \mu_2 + \frac{2\pi d}{\lambda R} s) = \mu_1 + \frac{\pi d}{\lambda R} s \quad C-3$$

The phase difference of the signals received by the two antennas from the weaker point is

$$\Delta\mu = 2\pi \frac{sd}{R\lambda} \quad C-4$$

where the quantity  $\frac{sd}{R\lambda}$  is equal to the fraction of a lobe width of the scattering pattern of the target that is spanned by the receiving antenna system.

The quantity to be determined is  $\phi_1 - \phi_2$ . This determination can be made conveniently with the aid of a table of the functions

$$\phi_1 = \tan^{-1} \left[ \frac{A \sin \mu_1}{1 + A \cos \mu_1} \right] \quad C-5$$

$$\phi_2 = \tan^{-1} \left[ \frac{A \sin(\mu_1 + 2\pi \frac{sd}{R\lambda})}{1 + A \cos(\mu_1 + 2\pi \frac{sd}{R\lambda})} \right] \quad C-6$$

where A is the ratio of the strength of the weaker point source to that of the stronger source. For any values of the parameter  $\frac{sd}{R\lambda}$  and the independent variable  $\mu$ ,  $\mu_1$  can be found from Eq. C-3 and  $\phi_1 - \phi_2$  read from the tables. The data for the curves of Fig. 2-5 were found in this manner for 10-degree increments of  $\mu$  and for values of  $\frac{sd}{R\lambda}$  equal to  $\frac{1}{6}$ ,  $\frac{1}{3}$ ,  $\frac{1}{2}$ ,  $\frac{2}{3}$ , and  $\frac{5}{6}$ .

In order to normalize the wander of the apparent target center in terms of the spacing of the two points of the target it is necessary to divide  $\phi_1 - \phi_2$  by an appropriate quantity. The phase difference introduced by the displacement  $s$  of the radar center of a target is just  $\Delta\mu$ . Therefore, dividing  $\phi_1 - \phi_2$  by  $\Delta\mu$  (both quantities in either radians or degrees) gives the desired normalization.

When  $R = \infty$ , both  $\phi_1 - \phi_2$  and  $\Delta\mu$  are zero, so that a different method

must be used for computing the position of the apparent target center. As R approaches infinity, the ratio of  $\phi_1 - \phi_2$  to  $\Delta\mu$  becomes, in the limit, just  $\frac{d\phi}{d\mu}$ , which can be evaluated from Eq. C-5, giving

$$\frac{d\phi}{d\mu} = \frac{A^2 + A \cos \mu}{1 + A^2 + 2A \cos \mu} \quad \text{C-7}$$

The plot of this equation is the curve for  $\frac{sd}{R\lambda} = 0$  in Fig. 2-5 of Sec. 2.21. According to Sec. 2.15, this curve is also applicable in the cases of lobe-comparison and single-lobe systems.

Single-lobe Radar - The position of the apparent radar center of a two-point target, as determined by a single-lobe radar, can be computed by means of a graphical analysis. Although this method is straightforward, it is considerably more laborious than the computations for the phase-comparison radar. In brief, the method used here is to plot the strength of the received signal for any target configuration as a function of antenna orientation, and to read off the plot the direction of the antenna axis for maximum signal strength.

According to Eq. 2-2 of Sec. 2-1, the expression for the signal received from the two-point target by a uniform aperture is

$$\begin{aligned} S &= \int_{-\frac{1}{2}d}^{\frac{1}{2}d} e^{j\frac{2\pi\beta}{\lambda}x} dx + 0.8 e^{j\mu} \int_{-\frac{1}{2}d}^{\frac{1}{2}d} e^{j\frac{2\pi[\beta - (s/R)]}{\lambda}x} dx \\ &= \left[ \frac{\sin H}{H} + e^{j\mu} \times 0.8 \frac{\sin(H - H_s)}{H - H_s} \right] \times d \\ &\triangleq [K_1 + e^{j\mu} K_2] \times d, \end{aligned} \quad \text{C-8}$$

where

$$H_s \triangleq \pi \frac{sd}{R\lambda} \quad \text{C-9}$$

and  $\beta$  is measured with respect to the line-of-sight to the stronger point,

positive  $\beta$  being in the direction towards the weaker point. The relative magnitude of the received signal is

$$\frac{1}{d} A_S = [K_1^2 + K_2^2 + 2K_1K_2 \cos \mu]^{\frac{1}{2}}, \quad \text{C-10}$$

which can be conveniently evaluated with adequate accuracy for this purpose using a sheet of polar-coordinate graph paper and a pair of dividers.

For any given  $H_s$  and  $\mu$ , the value of  $H$  for which  $A_S$  is maximum can be found by plotting Eq. C-10 for a number of different values of  $H$  in the vicinity of that for the maximum and reading off the plot the value of  $H$  at the maximum. In order to normalize the results in terms of the target dimension, it is necessary to divide the values of  $H$  corresponding to the maxima of  $A_S$  by  $H_s$ , since  $H_s$  is the standardized angle subtended by the target.

The curves of Fig. 2-3 for six values of  $\frac{sd}{R\lambda}$  between 1/6 and 1 were plotted by using the above method for 10-degree increments of the independent variable  $\mu$ .

Lobe-comparison Radar - The method used for computing the position of the apparent target center measured with a lobe-comparison radar is similar to the method used for the single-lobe system. For given target conditions, the strengths of the signals received by the two lobes are plotted as functions of antenna orientation, and the direction for which the two strengths are equal is read off the plot.

The signals received by the two lobes are, according to Eq's. 2-3 and C-8, given by

$$S_a = \left[ \frac{\sin(H + H_q)}{H + H_q} + e^{j\mu} \times 0.8 \frac{\sin(H + H_q - H_s)}{H + H_q - H_s} \right] \times d, \quad \text{C-11}$$

$$S_b = \left[ \frac{\sin(H - H_q)}{H - H_q} + e^{j\mu} \times 0.8 \frac{\sin(H - H_q - H_s)}{H - H_q - H_s} \right] \times d. \quad \text{C-12}$$

~~CONFIDENTIAL~~

The magnitudes of  $S_a$  and  $S_b$  can be evaluated with the aid of a table of the function  $\frac{\sin H}{H}$  and a 'vector-magnitude computer' consisting of a sheet of polar graph paper and a pair of dividers. For any given  $\mu$  and  $H_s$ , the value of  $H$  for which plots of the magnitudes of  $S_a$  and  $S_b$  as functions of  $H$  intersect is the standardized direction of the apparent center of the target. This standardized direction can be normalized in terms of the target dimension by dividing by  $H_s$ , as in the case of the single-lobe radar.

Each of the six curves of Fig. 2-4 for values of  $\frac{sd}{R\lambda}$  between  $1/6$  and  $1$  were plotted for 10-degree increments of  $\mu$  using this method of computation with an assumed value of  $H_q = 80$  degrees, as in Appendix A. For each point on any of the curves, it was usually found necessary to make six evaluations of the magnitude of  $S_a$  or  $S_b$  in order to get the desired accuracy in the result.

#### C-2 Error-detector Output with Radar Pointing at Stronger Point

The output of the error-detector of a phase-comparison or a lobe-comparison system which is aimed at the stronger point of the two-point target can be determined using methods similar to those described in Sec. C-1. In this section, the methods used for computing the error-detector outputs of a variety of phase-comparison and lobe-comparison systems are described.

Phase-comparison Radar with Limiting - The output of the phase-detector of a system in which both received signals are amplitude limited prior to phase detection is very nearly equal to  $\sin(\phi_1 - \phi_2)$ . The values of  $\phi_1 - \phi_2$  for various values of  $\mu$  and  $\frac{sd}{R\lambda}$  were determined in Sec. C-1. It is merely necessary to find the sine of these angles to find the phase-detector output. The output can then be normalized in terms of the target dimension by dividing the output by  $\Delta\mu$  (expressed in radians).

The curves of Fig. 2-9 for  $\frac{sd}{R\lambda} = \frac{1}{6}, \frac{1}{3}, \frac{1}{2}, \frac{2}{3}$ , and  $\frac{5}{6}$  were computed in this

~~CONFIDENTIAL~~

manner. The curve for  $\frac{sd}{RA} = 0$  is the same as the corresponding curve for the plot of the position of the apparent target center.

Phase-comparison Radar without Limiting - When the outputs of the two i-f amplifiers of a phase-comparison radar system are fed directly into the phase detector without being amplitude limited, the nature of the phase-detector output depends to a certain extent on the type of phase detector in use. Three different types of phase-detector configurations will be considered in these analyses.

Almost all phase-detector circuits are such that when both signal inputs have fixed amplitudes, the output is roughly equal to the cosine of the phase difference of the inputs. If one input is shifted by  $\frac{1}{2}\pi$ , the output is then nearly a sinusoidal function of the phase difference. It will be assumed that such a phase shift of one input is used in each of the systems considered here.

A system employing a twin-diode phase detector and unequal gains in the i-f amplifiers will be considered first. Such a phase detector may be constructed using any of a variety of circuits, but the principle of operation is essentially the same for all of them; the output of the phase detector is equal to the difference in the magnitudes of the vector sum and the vector difference of the two inputs to the phase-detector. A typical circuit for such a phase-detector was used in the phase measuring unit with which the experimental data of this research were obtained, and is described in Appendix F, Sec. F-11.\*

---

\*In actual operation, this phase detector was used with equal gains in the i-f amplifier, which does not affect its circuit in any way.



According to the above description, the phase-detector output is

$$V_n = |S_1 + g S_2 e^{j\frac{1}{2}\pi}| - |S_1 - g S_2 e^{j\frac{1}{2}\pi}|, \quad C-13$$

where  $g$  is the ratio of gains of the i-f amplifiers. For the actual computation, it was assumed that  $g = 0.3$ . When the values of  $S_1$  and  $S_2$ , given in Eq's. C-1 and C-2, are substituted in Eq. C-13, the result is

$$V_n = \left| 1 + 0.3 e^{j\frac{1}{2}\pi} + 0.8 e^{j\mu} + 0.24 e^{j(\frac{1}{2}\pi + \mu + \Delta\mu)} \right| - \left| 1 - 0.3 e^{j\frac{1}{2}\pi} + 0.8 e^{j\mu} - 0.24 e^{j(\frac{1}{2}\pi + \mu + \Delta\mu)} \right|. \quad C-14$$

The necessary vector additions in evaluating Eq. C-14 for  $\Delta\mu = \frac{1}{3}\pi, \frac{2}{3}\pi, \pi, \frac{4}{3}\pi$ , and  $\frac{5}{3}\pi$ , and 10-degree increments of  $\mu$  were performed graphically as indicated in Fig. C-1. The magnitudes of the two vector sums were read off with the aid of a pair of dividers and subtracted to give the desired results.

It can be noted in the results, which are plotted in the upper part of Fig. 2-10, that the output for any positive  $\mu$  is usually different from the output for  $-\mu$ , except when  $\frac{sd}{R\lambda} = 0$ . This phenomenon is brought about by the unsymmetrical manner in which  $\mu$  affects the vector sums shown in Fig. C-1.

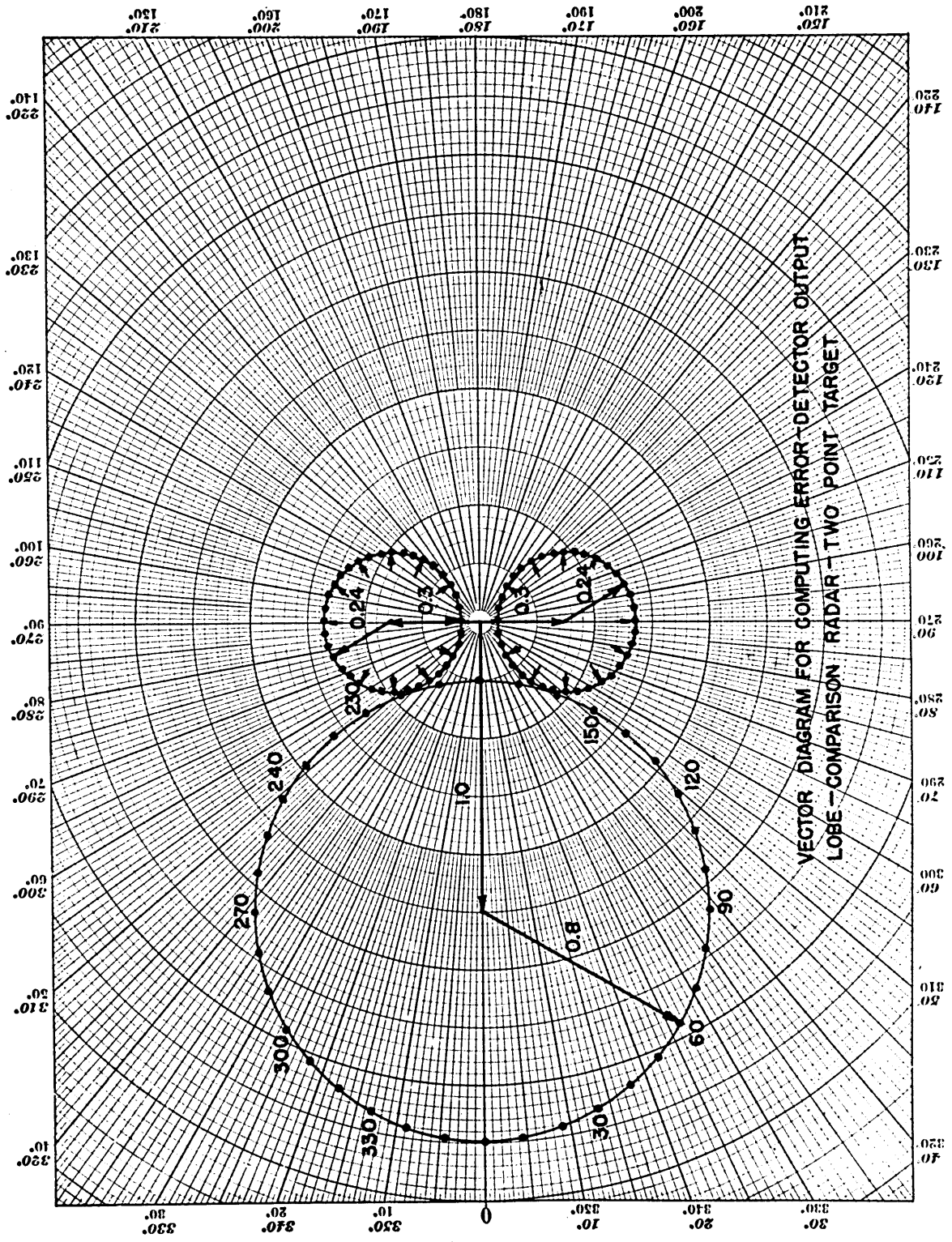
The data obtained by the above method were normalized in terms of the target dimension in accordance with the following reasoning. At very long range, the two received signals have the same magnitude, and the phase difference between them is very small. That is,

$$S_2 = S_1 e^{j d\phi}. \quad C-15$$

If now an ideal target is assumed which consists of a single source at a distance  $g$  from the axis of the receiving-antenna system, the phase-detector output due to that target, from Eq. C-13 is

$$V_n = 2g \Delta\mu = 4\pi g \frac{sd}{R\lambda}, \quad C-16$$

since the slow-acting agc, which it is assumed that the radar possesses, will eventually adjust the magnitudes of the received signals to unity. With



NO. 3124. POLAR CO-ORDINATE.

CODER BROS COMPANY, INC. NORWOOD MASSACHUSETTS  
PRINTED IN U.S.A.

Fig. C-1

a two-point target, with signals from the two points having levels of 1.0 and 0.8, the average magnitude of the received signal in either channel, taken over all  $\mu$ , is 1.168, as can be determined from Eq. C-37 in the treatment of the lobe-comparison error detector. Therefore, the slow-acting agc will tend to divide all the results computed above by this figure of 1.168. As a result, it is necessary to divide all the figures of phase-detector output by the quantity  $4\pi g \times 1.168 \times \frac{sd}{R\lambda}$  to reduce them to terms of target dimensions.

The phase-detector output with  $R = \infty$  is merely

$$V_n = 2g \, d\phi \times A_{S_1} . \quad C-17$$

The expression for the normalized output is

$$Z = \frac{d\phi}{d\mu} \times \frac{1}{A_{S_1}} \times A_{S_1} = \frac{d\phi}{d\mu} \times \frac{1}{1.168} \times A_{S_1} . \quad C-18$$

According to a discussion in Sec. C-1,  $\frac{d\phi}{d\mu}$  is the expression for the wander of the apparent center of the target at infinite range, such as is plotted in Fig. 2-5. The plot of phase-detector output for  $\frac{sd}{R\lambda} = 0$  can be found from Fig. 2-5 by multiplying the ordinates of the corresponding curve by the factor  $\frac{1}{1.168} \times A_{S_1}$ .

The second type of phase-comparison system to be considered is one using a twin-diode phase detector and equal gains in the i-f amplifiers. The output of the phase detector of this system is also given by Eq. C-13, with  $g = 1$ . When the values of  $S_1$  and  $S_2$  from Eq's. C-1 and C-2 are substituted into this equation, the resulting expression for the output is

$$V_n = \left| 1 + e^{j\frac{1}{2}\pi} + 0.8 e^{j\mu} [1 + e^{j(\frac{1}{2}\pi + \Delta\mu)}] \right| \\ - \left| 1 - e^{j\frac{1}{2}\pi} + 0.8 e^{j\mu} [1 - e^{j(\frac{1}{2}\pi + \Delta\mu)}] \right| . \quad C-19$$

The magnitudes of the vector summations contained in Eq. C-19 were evaluated

in the same manner as was Eq. C-14, using the graphical technique with appropriate circles drawn on polar graph paper.

The data were normalized in terms of the target dimension by dividing them by the factor  $4\pi \times 1.168 \times \frac{sd}{R\lambda}$ , as described above.

The normalized curve for  $\frac{sd}{R\lambda} = 0$  is the same as that computed for the system with unequal gains in the i-f amplifiers.

The third type of phase-comparison system is one using a pentode phase detector, for which there is no basic difference whether the gains of the i-f amplifiers are equal or not. In this system, the two received signals are applied (at an intermediate frequency) to two grids of a pentode, which serves essentially as a mixer. The pentode plate current is given by

$$\begin{aligned} i_b &= I_b [1 + m_1 A_{S_1} \cos(\omega_r t + \phi_1)] [1 + m_2 A_{S_2} \cos(\omega_r t + \phi_2)] \\ &= I_b [1 + m_1 A_{S_1} \cos(\omega_r t + \phi_1) + m_2 A_{S_2} \cos(\omega_r t + \phi_2) \\ &\quad + \frac{1}{2} m_1 m_2 A_{S_1} A_{S_2} \cos(2\omega_r t + \phi_1 + \phi_2) \\ &\quad + \frac{1}{2} m_1 m_2 A_{S_1} A_{S_2} \cos(\phi_1 - \phi_2) ] , \end{aligned} \tag{C-20}$$

where the last term is the desired quantity. If the other terms are removed by means of appropriate filtering and balancing, and one of the inputs is shifted in phase by  $\frac{1}{2}\pi$ , the output of the pentode phase detector can be written

$$V_n = A_{S_1} A_{S_2} \sin(\phi_1 - \phi_2) . \tag{C-21}$$

The phase-detector output due to an ideal, single-point target a distance  $s$  away from the axis of the receiving-antenna system is  $\sin(2\pi \frac{sd}{R\lambda})$ , which for very large  $R$  is equal to  $\Delta\mu$ . The phase-detector output with the two-point target is

$$V_n = \frac{1}{(1.168)^2} A_{S_1} A_{S_2} \sin(\phi_1 - \phi_2) , \tag{C-22}$$

since, as described previously, the slow-acting agc tends to divide both signals by the long-time average of the amplitudes. When this output is normalized in terms of the target dimension the resulting expression is

$$Z = \frac{1}{(1.168)^2} A_{S1} A_{S2} \frac{\sin(\phi_1 - \phi_2)}{\Delta\mu} .$$

C-23

The values of  $(1/\Delta\mu) \sin(\phi_1 - \phi_2)$  were computed in determining the error-detector output of the phase-comparison radar with limiting. The magnitudes of the two amplitudes can be determined for any  $\mu$  and  $\Delta\mu$  by means of the law of cosines, as explained in conjunction with Eq. C-10.

The curve for the normalized output with  $\frac{sd}{R\lambda} = 0$  was computed by multiplying the results of Eq. C-18 by  $A_{S1}/1.168$ .

The curves for the outputs of the latter two types of phase detectors are shown in the bottom two sets of Fig. 2-10.

Lobe-comparison Radar - The output of the error detector of a lobe-comparison system with a fast-acting agc is different from that of a corresponding system with a slow-acting agc. The difference between the results with fast or slow agc corresponds very closely to the difference between the results with phase-comparison systems having limiting or no limiting. It is assumed that the fast-acting agc is capable of eliminating any amplitude fluctuations caused by changes in  $\mu$ , thereby holding constant the instantaneous mean of the amplitudes of the signals in the two lobes.\* The slow-acting agc merely holds constant the long-time average, taken over all possible values of  $\mu$ , of the mean value of the two amplitudes. Therefore, with

---

\*The highest frequency to which the agc can respond must necessarily be lower than the scan frequency of a sequential lobing system.

a fast-acting agc, the error-detector output is

$$2 \frac{A_{S_a} - A_{S_b}}{A_{S_a} + A_{S_b}}, \quad \text{C-24}$$

and with a slow agc,

$$2 \frac{A_{S_a} - A_{S_b}}{A_{S_a} + A_{S_b}}. \quad \text{C-25}$$

With the radar antenna aimed at the stronger point of the two-point target, the expressions for the signals in the two lobes are, according to Eq's. C-11 and C-12,

$$S_a = \left[ \frac{\sin H_q}{H_q} + e^{j\mu} \times 0.8 \frac{\sin(H_q - H_s)}{H_q - H_s} \right] \times d, \quad \text{C-26}$$

$$S_b = \left[ \frac{\sin H_q}{H_q} + e^{j\mu} \times 0.8 \frac{\sin(H_q + H_s)}{H_q + H_s} \right] \times d, \quad \text{C-27}$$

since  $H = 0$ . The constant factor  $d$  is subsequently dropped from these expressions, with no loss of generality.

The error-detector output can be normalized in terms of the target dimension by first computing the output due to an ideal, single-point target at a distance  $s$  from the axis of the antenna system. For either slow- or fast-acting agc, the expression for this quantity is

$$\text{Output} = 2 \frac{\frac{\sin(H_q - H_s)}{H_q - H_s} - \frac{\sin(H_q + H_s)}{H_q + H_s}}{\frac{\sin(H_q - H_s)}{H_q - H_s} + \frac{\sin(H_q + H_s)}{H_q + H_s}}. \quad \text{C-28}$$

At very long range,  $H_s$  is very much less than unity, with the result that

$$\begin{aligned} \frac{\sin(H_q - H_s)}{H_q - H_s} &= \left[ \frac{\sin H_q - H_s \cos H_q}{H_q} \right] \left[ 1 + \frac{H_q}{H_s} \right] \\ &= \frac{\sin H_q}{H_q} + \frac{H_s \sin H_q}{H_q^2} - \frac{H_s \cos H_q}{H_q} + \frac{H_s^2 \cos H_q}{H_q^2}, \end{aligned} \quad \text{C-29}$$

and

$$\frac{\sin(H_q + H_s)}{H_q + H_s} = \frac{\sin H_q}{H_q} - \frac{H_s \sin H_q}{H_q^2} + \frac{H_s \cos H_q}{H_q} - \frac{H_s^2 \cos H_q}{H_q^2} \quad C-30$$

The substitution of Eq's. C-29 and C-30 into Eq. C-28 gives

$$\text{Output} = 2 H_s \left[ \frac{\sin H_q - H_q \cos H_q}{H_q^2} \right] \left[ \frac{H_q}{\sin H_q} \right] = 2 H_s \left[ \frac{1 - H_q \cot H_q}{H_q} \right], \quad C-31$$

where it has been assumed that  $\frac{H_s^2 \cos H_q}{H_q^2}$  can be neglected in comparison with  $\frac{\sin H_q}{H_q}$ . If  $H_q = 80$  degrees, as in Appendix A, Eq. C-31 becomes

$$\text{Output} = 1.081 H_s. \quad C-32$$

The error-detector output due to the two-point target becomes, after normalization in terms of the target dimension,

$$Z = \frac{1}{0.540 H_s} \times \frac{A_{S_a} - A_{S_b}}{A_{S_a} + A_{S_b}} \quad C-33$$

for the system with a fast-acting agc, or, for the system with a slow agc,

$$Z = \frac{1}{0.540 H_s} \times \frac{A_{S_a} - A_{S_b}}{A_{S_a} + A_{S_b}} \quad C-34$$

The curves of Fig. 2-7 were plotted for the system with the fast-acting agc and a squint angle of  $H_q = 80$  degrees. Points on the curves were computed for 10-degree increments of  $\mu$ . The curves for  $H_s = 30^\circ, 60^\circ, 90^\circ, 120^\circ, 150^\circ,$  and  $180^\circ$  were determined by finding the values of  $A_{S_a}$  and  $A_{S_b}$ , which can be obtained from Eq's. C-26 and C-27 by the method used for evaluating Eq's. C-11 and C-12, and substituting them into Eq. C-33. For  $H_s = 0$ , the curve is the same as the corresponding curve for the wander of the apparent radar center, shown in Fig. 2-4, because at long range the system is completely linear in that error-detector output is proportional to wander.

For the system with the slow-acting agc, it is necessary to compute the average, taken over all  $\mu$ , of the mean value of the signal amplitudes received by the two lobes. The average of the mean is equal to the mean value of the average amplitude of each of the two signals taken over all  $\mu$ .

The expression for either received signal, given in Eq's. C-26 and C-27, can be abbreviated, as in Eq. C-8, giving the form

$$S_a = \left[ \frac{\sin H_q}{H_q} + e^{j\mu} \times 0.8 \frac{\sin(H_q - H_s)}{H_q - H_s} \right] = K_1 + e^{j\mu} K_2, \quad C-35$$

where  $K_1$  and  $K_2$  can be found from a table of  $\frac{\sin H}{H}$ . According to Eq. C-10, the magnitude of S is

$$A_S = [K_1^2 + K_2^2 + 2K_1K_2 \cos \mu]^{1/2} = K_1 \left[ 1 + \frac{K_2^2}{K_1^2} + 2 \frac{K_2}{K_1} \cos \mu \right]^{1/2}. \quad C-36$$

The average value of  $A_S$ , taken over all  $\mu$ , is

$$\begin{aligned} \overline{A_S} &= \frac{K_1}{\pi} \int_0^\pi \left[ 1 + \frac{K_2^2}{K_1^2} + 2 \frac{K_2}{K_1} \cos \mu \right]^{1/2} d\mu \\ &= \frac{2K_1}{\pi} \int_0^{1/2\pi} \left[ \left( 1 + \frac{K_2}{K_1} \right)^2 - 4 \frac{K_2}{K_1} \sin^2 \left( \frac{1}{2}\mu \right) \right]^{1/2} d\left( \frac{1}{2}\mu \right) \\ &= \frac{2}{\pi} (K_1 + K_2) \int_0^{1/2\pi} \left[ 1 - \frac{4 K_1 K_2}{(K_1 + K_2)^2} \sin^2 \left( \frac{1}{2}\mu \right) \right]^{1/2} d\left( \frac{1}{2}\mu \right). \end{aligned} \quad C-37$$

The final form of this equation is a complete elliptical integral, values of which can be found in mathematical tables.<sup>30</sup>

For any given values of  $H_q$  and  $H_s$ , the quantities  $\overline{A_{S_a}}$  and  $\overline{A_{S_b}}$  can be computed from Eq. C-37, and then be added to find the denominator of Eq. C-34. After this is done, the curves of Fig. 2-8 can be computed in the same way as the curves of Fig. 2-7 were found, with the exception of the curve for  $H_s = 0$ . The latter curve is the same as the corresponding curve for the



~~CONFIDENTIAL~~

the phase-comparison radar with the twin-diode phase detector (without limiting), because in each case the output is proportional to the product of the wander of the apparent target center and the ratio of the instantaneous to the average signal strength.

~~CONFIDENTIAL~~

## APPENDIX D

PHASE-DETECTOR OUTPUT WITH A MULTI-POINT TARGET

In this appendix there are presented the mathematical analyses which were used in computing some properties of the output of the phase detector of a phase-comparison system caused by a multi-point target. It is assumed that the target is made up of a very large number of isotropic sources, distributed at random within the finite dimensions of the target in such a way that the amplitude and phase of any source is independent of its position. The amplitudes of the sources are such that no one source contributes an appreciable part of a total received signal. The maximum dimension of the target is assumed to be very small compared with the range from the target to the radar.

D-1 Phase-detector Output with Limiting

If the signal received by one antenna of a phase-comparison system is expressed as

$$S_1 = \sum_{n=1}^N a_n e^{j\mu_n} \triangleq A_1 e^{j\phi_1}, \quad 2-19$$

the signal received by the other antenna is

$$\begin{aligned} S_2 &\triangleq A_2 e^{j\phi_2} = \sum_{n=1}^N a_n e^{j(\mu_n + kz_n)} \\ &= \sum_{n=1}^N a_n e^{j\mu_n} + \sum_{n=1}^N (e^{jkz_n} - 1) a_n e^{j\mu_n} \\ &\triangleq S_1 + D, \end{aligned} \quad 2-20$$

where

$$k \triangleq \frac{2\pi d}{\lambda R} \quad 2-21$$

and  $z_n$  is the distance of the point  $n$  from the axis of the antenna system of the radar. As explained in Sec. 2.31,  $D$  and  $S_1$  are statistically independent.

CONFIDENTIAL

When amplitude limiting is employed prior to phase detection, the phase-detector output is

$$V_m \triangleq \sin(\phi_2 - \phi_1) = \frac{D_p}{A_2}, \quad 2-22$$

where  $D_p$  is the component of  $D$  that is 90 degrees out of phase with  $S_1$ .

According to Sec. 2.31, the probability density functions for  $D_p$  and  $A_2$  are

$$p(D_p) dD_p = \frac{1}{\sqrt{2\pi D_p^2}} e^{-D_p^2/(2D_p^2)} dD_p, \quad 2-24$$

$$p(A_2) dA_2 = \frac{2A_2}{A_2^2} e^{-A_2^2/(A_2^2)} dA_2. \quad 2-25$$

The mean-squared values of  $D_p$  and  $A_2$  can be determined from Eq. 2-20. Because each of these quantities is made up of  $N$  independent components, the mean-squared values are

$$\overline{D_p^2} = \frac{1}{2} \overline{D^2} = \frac{1}{2} N (a_n^2 |e^{jkzn} - 1|^2) = \frac{1}{2} N (a_n^2) |e^{jkzn} - 1|^2, \quad D-1$$

$$\overline{A_2^2} = N (a_n^2). \quad D-2$$

For extremely long ranges,  $D_p$  and  $A_2$  are statistically independent, because  $A_2$  is practically equal to  $A_1$ , which is independent of  $D_p$ . For these cases, the probability density of  $V_m$  can be computed exactly. The value of  $p(V_m) dV_m$  can be found by differentiating the total probability  $P(V_{mt})$  of finding the phase-detector output between 0 and  $V_{mt}$ . The total probability can be computed by summing the infinitesimal probabilities of all possible  $\frac{D_p}{A_2}$  lying between 0 and  $V_{mt}$ .<sup>25</sup> That is,

$$P(V_{mt}) = \int_0^{V_{mt}} p(V_m) dV_m = \int_0^\infty p(D_p) \left[ \int_{A_2=D_p/V_{mt}}^\infty p(A_2) dA_2 \right] dD_p. \quad D-3$$

The integration of  $p(D_p)$  need only extend between the limits 0 and  $\infty$ , and not from  $-\infty$  to  $+\infty$ , because  $A_2$  is always positive.

The integral of  $p(A_2)$  can be evaluated directly from Eq. 2-25, giving

$$\int_{A_2=D_p/V_{mt}}^{\infty} p(A_2) dA_2 = \frac{1}{A_2^2} \int_{D_p/V_{mt}}^{\infty} e^{-A_2^2/(A_2^2)} 2A_2 dA_2 = e^{-D_p^2/(V_{mt}^2 A_2^2)} \quad D-4$$

Substituting Eq's. 2-24 and D-4 into Eq. D-3 gives

$$P(V_{mt}) = \frac{1}{\sqrt{2\pi D_p^2}} \int_0^{\infty} e^{-\left[\frac{1}{2D_p^2} + \frac{1}{V_{mt}^2 A_2^2}\right] D_p^2} dD_p \quad D-5$$

$$\begin{aligned} &= \frac{1}{\sqrt{2\pi D_p^2}} \times \frac{\pi^{\frac{1}{2}}}{2\left[\frac{1}{2D_p^2} + \frac{1}{V_{mt}^2 A_2^2}\right]^{\frac{3}{2}}} \\ &= \frac{1}{2} \left[1 + \frac{2 D_p^2}{V_{mt}^2 A_2^2}\right]^{-\frac{1}{2}} \quad D-6 \end{aligned}$$

Eq. D-6 can be further reduced by substituting the mean-squared values of  $D_p$  and  $A_2$  from Eq's. D-1 and D-2, with the result that

$$P(V_{mt}) = \frac{1}{2} \left[1 + \frac{|e^{jkz_n} - 1|^2}{V_{mt}^2}\right]^{-\frac{1}{2}} = \frac{1}{2} \left[1 + \frac{Q^2}{V_{mt}^2}\right]^{-\frac{1}{2}} \quad D-7$$

Differentiating this expression with respect to the variable  $V_m$  gives

$$p(V_m) dV_m = -\frac{1}{4} \frac{-2 \frac{1}{V_m^3} Q^2}{\left[1 + \frac{Q^2}{V_m^2}\right]^{3/2}} dV_m = \frac{Q^2 dV_m}{2(V_m^2 + Q^2)^{3/2}} \quad 2-26$$

The quantity  $V_m$  can be standardized in terms of a linear coordinate at the target. The output due to a displacement  $Z$  of an ideal, single-point target at very long range is, according to Eq's. 2-20 and 2-22,

$$\text{Output} = k \times Z \quad D-8$$

Therefore, the phase-detector output, expressed in terms of a linear coordinate at the target, has a probability density

$$p(Z) dZ = \frac{(Q/k)^2 dZ}{2[Z^2 + (Q/k)^2]^{3/2}} \quad D-9$$

~~CONFIDENTIAL~~

D-2 Average Magnitude and RMS of Output

The average values of the magnitude and the square of the phase-detector output with amplitude limiting can be computed from the probability function of the output. For any range, this function is approximated by

$$p(V_m) dV_m = \frac{Q^2 dV_m}{2(V_m^2 + Q^2)^{3/2}}, \quad (-1 < V_m < +1) \quad 2-29$$

$$P(V_m = -1) = P(V_m = +1) = \int_{+1}^{\infty} \frac{Q^2 dV_m}{2(V_m^2 + Q^2)^{3/2}}.$$

Since this function is symmetrical about  $V_m = 0$ , the average magnitude of the output can be written

$$\overline{|V_m|} = \int_0^1 \frac{Q^2 V_m dV_m}{(V_m^2 + Q^2)^{3/2}} + \int_1^{\infty} \frac{Q^2 dV_m}{(V_m^2 + Q^2)^{3/2}}, \quad 2-32$$

and the mean-squared value

$$\overline{V_m^2} = \int_0^1 \frac{Q^2 V_m^2 dV_m}{(V_m^2 + Q^2)^{3/2}} + \int_1^{\infty} \frac{Q^2 dV_m}{(V_m^2 + Q^2)^{3/2}}. \quad 2-33$$

According to Eq. D-8, the average magnitude of the output can be normalized in terms of a linear coordinate at the target by dividing the value computed in Eq. 2-32 by  $k$ . When the indicated integrations are performed, and the division made, the resulting expression is

$$\overline{|Z|} = \frac{1}{k} [1 + Q - (1 + Q^2)^{1/2}]. \quad D-10$$

The corresponding expression for the mean-squared value of the output, which must contain a normalizing factor of  $1/k^2$ , is

$$\overline{Z^2} = \frac{1}{k^2} [1 + Q^2 \ln\left(\frac{1 + [1 + Q^2]^{1/2}}{Q}\right) - (1 + Q^2)^{1/2}]. \quad D-11$$

For a system without amplitude limiting, the probability density

~~CONFIDENTIAL~~

function of the phase-detector output is

$$p(V_n) dV_n = \frac{1}{\sqrt{2\pi V_n^2}} e^{-V_n^2/(2V_n^2)} dV_n, \quad \text{D-30}$$

where

$$\overline{V_n^2} = \frac{2Q^2}{\pi}. \quad \text{D-31}$$

The mean squared value of  $V_n$  can be normalized in terms of a linear coordinate at the target by dividing Eq. D-31 by  $k^2$ , giving

$$\overline{z^2} = \frac{2Q^2}{\pi k^2}. \quad \text{D-12}$$

From Eq's. D-34 and D-8, the normalized value of the average magnitude of the wander is found to be

$$|\overline{Z}| = \frac{2Q}{\pi k}. \quad \text{D-13}$$

### D-3 Results for a Uniformly Distributed Target

The values of the average magnitude and root-mean-square of the phase-detector output can now be computed for a target consisting of a large number of sources uniformly distributed in one dimension over a distance  $L$ . As can be seen from inspection of Eq's. D-10 through D-13, it is only necessary to compute the value of  $Q$  as a function of range and substitute it in the equations.

Because the uniformly distributed target is symmetrical about its center, the center will be chosen as the reference from which the position  $z_n$  of each source  $n$  is measured. This choice implies that the axis of the receiving antenna system is pointed at the center of the target. The problem of finding  $Q$  then becomes the problem of finding the mean squared magnitude of  $e^{jkz_n} - 1$  for  $z_n$  uniformly distributed from  $-\frac{1}{2}L$  to  $+\frac{1}{2}L$ . The solution to this problem is

$$\begin{aligned}
 Q^2 &\triangleq \overline{|e^{jkz_n} - 1|^2} && 2-27 \\
 &= \frac{1}{L} \int_{-\frac{1}{2}L}^{\frac{1}{2}L} |e^{jkz_n} - 1|^2 dz_n = \frac{1}{L} \int_{-\frac{1}{2}L}^{\frac{1}{2}L} ([\cos(kz_n) - 1]^2 + \sin^2[kz_n]) dz_n \\
 &= \frac{1}{kL} \int_{-\frac{1}{2}kL}^{\frac{1}{2}kL} 2[1 - \cos(kz_n)] d(kz_n) \\
 &= 2 \left[ 1 - \frac{\sin(\frac{1}{2}kL)}{\frac{1}{2}kL} \right] . && 2-35
 \end{aligned}$$

The plots of Fig. 2-14 were made from data obtained by substituting  $Q$  from Eq. 2-35 into Eq's. D-10 through D-13. Standardization of the results in terms of the length of the target was obtained by dividing the values of the average magnitude and rms of the output by  $L$ .

#### D-4 Phase-detector Output with Errors in Aiming

The above results for phase-detector output due to multi-point targets do not apply in all cases when the radar antenna system is not aimed directly at the center of the target. In the following analyses, some of the properties of the output of a phase detector are computed for a target off the axis of the antenna system. It is assumed that the target is at very long range, so that the phase-detector operation is restricted to its linear region. Consequently, the results also apply to the output of the error detector of a lobe-comparison system.

If the signal received by one antenna is

$$S_1 = \sum_{n=1}^N a_n e^{j\mu_n} , \quad 2-19$$

the signal received by the other antenna is

$$\begin{aligned}
 S_2 &= \sum_{n=1}^N a_n e^{j(\mu_n + k[z_0 + z_n])} = e^{jkz_0} \sum_{n=1}^N a_n e^{j(\mu_n + kz_n)} \\
 &= (S_1 + D) e^{jkz_0} , && D-14
 \end{aligned}$$

where  $z_0$  is the distance from the center of the target to the axis of the radar antenna system and  $z_n$  is the distance from the point  $n$  to the line through the center and parallel to the radar axis.

Because it has been postulated that the range is very great,  $k$  is very much less than unity, and all terms containing powers of  $k$  higher than the first can be neglected. Therefore, Eq. D-14 can be written

$$S_2 = (S_1 + D)(1 + jkz_0) = S_1 + jkz_0 S_1 + D. \quad D-15$$

The term  $jkz_0 D$  can be dropped because  $D$  itself is made up only of terms containing  $k$  to the first and higher powers.

For a system with amplitude limiting, the output of the phase detector is

$$V_m = \frac{\text{component of } S_2 \text{ out of phase with } S_1}{A_2 = A_1}, \quad 2-22$$

where  $A_2$  equals  $A_1$  by virtue of the long target range. Substituting Eq. D-15 into Eq. 2-22 gives

$$V_m = \frac{kz_0 A_1 + D_p}{A_1} = kz_0 + \frac{D_p}{A_1}. \quad D-16$$

This equation shows that the phase-detector output with amplitude limiting is the linear sum of the output due to wander and the output due to the aiming error.

For a system without amplitude limiting, this highly desirable linear superposition no longer exists. With such a system, the phase-detector output is given by

$$V_n = \frac{\text{component of } S_2 \text{ out of phase with } S_1}{A_2 = A_1} \quad 2-23$$

$$= \frac{kz_0 A_1 + D_p}{A_1}$$

$$= kz_0 \frac{A_1}{A_1} + \frac{D_p}{A_1} \triangleq V_1 + V_2. \quad D-17$$



Because  $A_1$  and  $D_p$  are statistically independent, the mean-squared value of  $V_n$  is equal to the sum of the mean-squared values of  $V_1$  and  $V_2$ .

The probability density distribution of  $V_1$  has the same form as that of  $A_1$ , since the two quantities are proportional. Thus,

$$p_1(V_1) dV_1 = \frac{2V_1}{V_1^2} e^{-V_1^2/(\overline{V_1^2})} dV_1, \quad D-18$$

where

$$\overline{V_1^2} = (kz_0)^2 \frac{\overline{A_1^2}}{(\overline{A_1})^2}. \quad D-19$$

The probability density distribution of  $V_2$  is exactly the same as that of  $V_n$  given in Eq. 2-30, namely,

$$p_2(V_2) dV_2 = \frac{1}{\sqrt{2\pi\overline{V_2^2}}} e^{-V_2^2/(2\overline{V_2^2})} dV_2, \quad D-20$$

where

$$\overline{V_2^2} = \frac{2z_0^2}{\pi} = \frac{2}{\pi} k^2 \overline{z_n^2}. \quad D-21$$

The mean value of  $A_1$  can be computed from its probability density distribution, giving

$$\begin{aligned} \overline{A_1} &= \int_0^{\infty} A_1 p(A_1) dA_1 = \int_0^{\infty} \frac{2A_1^2}{A_1^2} e^{-A_1^2/(\overline{A_1^2})} dA_1 \\ &= \frac{2}{\overline{A_1^2}} \times \frac{(\overline{A_1^2})^{3/2}}{4} \times \sqrt{\pi} = (\pi/4)^{1/2} (\overline{A_1^2})^{1/2}. \end{aligned} \quad D-22$$

When this result is substituted into Eq. D-19, the expression for the mean-squared value of  $V_1$  becomes

$$\overline{V_1^2} = \frac{4}{\pi} k^2 z_0^2. \quad D-23$$

The mean-squared value of  $V_n$ , which is the sum of Eq's. D-21 and D-22, can be normalized in terms of a linear coordinate at the target by dividing by  $k^2$ , giving

$$\overline{z^2} = \frac{4}{\pi} z_0^2 + \frac{2}{\pi} \overline{z_n^2} = \overline{(z - z_0)^2} + z_0^2. \quad D-24$$

The desired normalized output is  $z_0$ . The mean-squared value of the jitter in the output is therefore

$$\overline{(z - z_0)^2} = \left(\frac{4}{\pi} - 1\right) z_0^2 + \frac{2}{\pi} \overline{z_n^2} = 0.272 z_0^2 + 0.637 \overline{z_n^2}. \quad D-25$$

The probability density distribution of  $Z$  can be computed by a method analogous to that used in obtaining Eq. D-3. The probability that  $V_n$  has a definite value is the sum of all possible joint probabilities giving

$V_1 + V_2 = V_n$ , which can be written

$$p(V_n) = \int_0^{\infty} p_1(V_1) p_2(V_n - V_1) dV_1, \quad D-26$$

since  $V_1$  is never negative. In this expression the differential  $dV_n$  has been omitted for convenience. If Eq's. D-18 and D-20 are substituted into Eq. D-25, the result is

$$\begin{aligned} p(V_n) &= \frac{1}{V_1^2} \left[ \frac{2}{\pi V_2^2} \right]^{\frac{1}{2}} \int_0^{\infty} V_1 e^{-V_1^2 / (\overline{V_1^2})} e^{-(V_n - V_1)^2 / (2\overline{V_2^2})} dV_1 \\ &= C_0 \int_0^{\infty} V_1 e^{-C_1 V_1^2 + C_2 V_1} dV_1, \end{aligned} \quad D-27$$

where

$$C_0 \triangleq \frac{1}{V_1^2} \left[ \frac{2}{\pi V_2^2} \right]^{\frac{1}{2}} e^{-V_n^2 / (2\overline{V_2^2})}, \quad C_1 \triangleq \frac{1}{V_1^2} + \frac{1}{2\overline{V_2^2}}, \quad C_2 \triangleq \frac{V_n}{V_2^2}. \quad D-28$$

If a new variable  $X$  is chosen such that

$$V_1 \triangleq \frac{C_2}{2C_1} + X \triangleq C_3 + X, \quad D-29$$

Eq. D-26 becomes

$$\begin{aligned}
 p(V_n) &= C_0 \int_{-C_3}^{\infty} x e^{+(\frac{1}{2}C_2C_3 - C_1x^2)} dx + C_0C_3 \int_{-C_3}^{\infty} e^{+(\frac{1}{2}C_2C_3 - C_1x^2)} dx \\
 &= C_0 e^{\frac{1}{2}C_2C_3} \times \frac{1}{2C_1} e^{-\frac{1}{2}C_2C_3} + C_0C_3 e^{\frac{1}{2}C_2C_3} \int_{-C_3}^{\infty} e^{-C_1x^2} dx \\
 &= \frac{C_0}{2C_1} [1 + (2\pi)^{\frac{1}{2}} C_4 e^{\frac{1}{2}C_4^2} \int_{-\infty}^{C_4} \frac{e^{-\frac{1}{2}x_1^2}}{(2\pi)^{\frac{1}{2}}} dx_1] \quad \text{D-29}
 \end{aligned}$$

where

$$\begin{aligned}
 C_4^2 \triangleq C_2C_3 &= \frac{C_2^2}{2C_1} = \frac{V_n^2}{2V_2^2} [(V_2^2)/(V_1^2) + \frac{1}{2}]^{-1} \\
 &= \frac{\pi}{2} \frac{Z^2}{z_n^2} \times \frac{z_0^2}{z_n^2} \times [(z_0^2)/(z_n^2) + 1]^{-1}, \quad \text{D-30}
 \end{aligned}$$

$$x_1^2 \triangleq 2C_1 x^2. \quad \text{D-31}$$

The final integral of Eq. D-29 is evaluated in mathematical tables.<sup>31</sup>

If  $V_n$  in Eq. D-29 is normalized in terms of a linear coordinate at the target, the resulting probability density distribution for the phase-detector output without limiting is

$$p(Z) dZ = C_5 [1 + (2\pi)^{\frac{1}{2}} C_4 e^{\frac{1}{2}C_4^2} \int_{-\infty}^{C_4} \frac{e^{-\frac{1}{2}x_1^2}}{(2\pi)^{\frac{1}{2}}} dx_1] dZ \quad \text{D-32}$$

where

$$\begin{aligned}
 C_5 \triangleq \frac{kC_0}{2C_1} &= \frac{1}{2}k [1 + (V_1^2)/2(V_2^2)]^{-1} \times \left[ \frac{2}{\pi V_2^2} \right]^{\frac{1}{2}} e^{-V_n^2/2(V_2^2)} \\
 &= \frac{1}{2} [1 + z_0^2/(z_n^2)]^{-1} \times (z_n^2)^{-\frac{1}{2}} \times e^{-\pi Z^2/4(z_n^2)}. \quad \text{D-33}
 \end{aligned}$$

The distributions for various values of the parameter  $z_0^2/(z_n^2)$  are plotted in Fig. 2-15. As is to be expected, for small values of the parameter, the distribution is similar to a Gaussian curve, while for large values, the shape of the distribution approaches that of a Rayleigh distribution.

~~CONFIDENTIAL~~

APPENDIX E

GENERAL EXPRESSIONS FOR THE SIGNAL SCATTERED BY A TARGET

Derivations are presented in this appendix of the general expressions, used in Sec. 2.4 on "Relations Between Signal Amplitude and Wander", for the distribution of the electromagnetic signal reflected from a target. The expressions are obtained only for the two-dimensional case, which is sufficiently general for the intended purpose.

E-1 Fourier Series Representation of the Signal

It is desired to find the expression for the field along a circle whose center is at the center of the target and whose radius is very large compared with the target and with the wavelength. The solutions to Maxwell's field equations in circularly cylindrical coordinates can be readily adapted to this two-dimensional problem. On such a circle, the total field can be represented by linear combinations of elementary wave functions

$$\psi_{nhk} = e^{jn\theta} H_n^{(1)}[(k^2 - h^2)^{\frac{1}{2}} R] e^{\pm jhz - j\omega t}, \quad 2-36$$

where  $R$ ,  $\theta$ , and  $z$  are the orthogonal cylindrical coordinates and  $H_n^{(1)}$  indicates a Hankel function of the first kind and order  $n$ .<sup>26</sup> Since the problem here involves only two dimensions  $R$  and  $\theta$ , the field does not depend on  $z$ , so that  $h = 0$ . In the same reference it is shown that, for  $h = 0$ ,

$$E_r = \frac{j\omega}{R} \sum_{n=-\infty}^{\infty} n b_n \psi_n, \quad E_\theta = -j\omega \sum_{n=-\infty}^{\infty} b_n \frac{\partial \psi_n}{\partial R}, \quad E_z = k^2 \sum_{n=-\infty}^{\infty} a_n \psi_n. \quad E-1$$

When  $R$  is very large,  $E_r$  becomes negligibly small and

$$\frac{\partial \psi_n}{\partial R} = jk \psi_n.$$

Therefore the received signal is proportional to the sum of the elementary wave functions.

~~CONFIDENTIAL~~

When  $R$  is very much greater than  $n$ ,

$$H_n^{(1)}[kR] = \left[ \frac{2}{\pi kR} \right]^{\frac{1}{2}} e^{j(kR - \frac{2n+1}{4} \pi)} \quad E-2$$

A pattern with a term  $e^{jn\theta}$  can only be generated by a physically realizable source whose maximum dimension is of the order of magnitude of  $n\lambda$  or greater. For a target of finite size, then,  $n$  is bounded, and the signal for large  $R$  can be written

$$S = \sum_{n=-N}^N c_n e^{jn\theta} \left[ \frac{2}{\pi kR} \right]^{\frac{1}{2}} e^{jkR} e^{-j\frac{\pi}{4}} e^{-j\omega t} e^{-j\frac{n\pi}{2}} \quad E-3$$

For a given very large  $R$ , the signal at some time  $t$  such that

$$e^{jkR} e^{-j\frac{\pi}{4}} e^{-j\omega t} = 1 + j0$$

is given by

$$\begin{aligned} S(\theta) &= \sum_{n=-N}^N c_n \left[ \frac{2}{\pi kR} \right]^{\frac{1}{2}} e^{-j\frac{n\pi}{2}} e^{jn\theta} \\ &\triangleq \sum_{n=-N}^N a_n e^{jn\theta} \end{aligned} \quad 2-37$$

E-2 Multiple Product Equivalent of Fourier Series

Let the function  $S(w)$  of the complex variable  $w$  be defined by

$$S(w) \triangleq \frac{a_N}{w^N} \prod_{n=1}^{2N} (w + w_n) \quad 2-38$$

where

$$w \triangleq r e^{j\theta}, \quad w_n \triangleq r_n e^{j\theta_n} \quad 2-39$$

On the unit circle in the  $w$ -plane,  $r = 1$ , and

$$S(w) = S(\theta) = \frac{a_N}{e^{jN\theta}} \prod_{n=1}^{2N} (e^{j\theta} + w_n)$$

If the multiple product in Eq. 2-40 is expanded, the resulting expression for  $S(\theta)$  is

~~CONFIDENTIAL~~

$$\begin{aligned}
 s(\theta) &= \frac{a_N}{e^{jN\theta}} [e^{j2N\theta} + (w_1 + w_2 + \dots + w_n)e^{j(2N-1)\theta} \\
 &\quad + (w_1w_2 + w_1w_3 + \dots + w_2w_3 + \dots + w_{2N-1}w_{2N})e^{j(2N-2)\theta} \\
 &\quad + (\dots)e^{j(2N-3)\theta} + \dots \\
 &\quad + (w_1w_2 \dots w_{2N})] \\
 &= a_N [e^{jN\theta} + (w_1 + \dots)e^{j(N-1)\theta} + (w_1w_2 + \dots)e^{j(N-2)\theta} \\
 &\quad + \dots + (w_1w_2 \dots w_N + \dots) + \dots \\
 &\quad + (w_1w_2 \dots w_{2N})e^{-jN\theta}] .
 \end{aligned}
 \tag{E-4}$$

The variable  $\theta$  enters into the second set of terms in Eq. E-4 in exactly the same way as it does into Eq. 2-37. There are  $2N+1$  undetermined constants  $a_n$  in Eq. 2-37. In Eq. 2-40 there are  $2N$  constants  $w_n$  and one multiplier  $a_N$ , which is the same as  $a_N$  in Eq. 2-37. The coefficients of corresponding terms in Eq's. 2-37 and E-4 can be equated, giving  $2N$  independent simultaneous equations, which are adequate for finding the  $2N$  constants  $w_n$ . Therefore, it has been demonstrated that Eq's. 2-37 and 2-40 are equivalent.

~~CONFIDENTIAL~~

## APPENDIX F

## RADAR EQUIPMENT FOR RECORDING DATA

The equipment used in obtaining experimental data on wander of the apparent radar center of aircraft targets and on the amplitude fluctuations of the radar echo is described in this appendix.

Block diagrams of the overall X-band and S-band systems are shown in Fig's. 3-1 and 3-20, respectively. In the following sections, schematic diagrams of the various component blocks of the systems are presented, along with descriptions of special features and design techniques associated with many of the units.

F-1 I-F Amplifier

The i-f amplifiers were the same units that were used in the flight tests of the Meteor Model-II pulse seeker.<sup>27</sup> The input stage of these amplifiers is a 33 mcps cascode circuit with a noise figure of about 1.6 decibels. The following stages of amplification are grouped into three staggered doubles, giving an overall half-power bandwidth of 2.0 mcps. The center frequency is changed from 33 mcps to 12 mcps at the middle of the second double, by mixing with a 21 mcps signal. A schematic diagram of the amplifier is shown in Fig. F-1.

For the X-band wander tests, the two measurement i-f amplifiers were carefully aligned to have the minimum possible difference in their phase-delay characteristics. The alignment was made with the amplifier gains at about 10 decibels less than maximum, which was the most probable gain setting as anticipated for the tests. First, one of the amplifiers was aligned to have the desired frequency response. Then the same input, obtained from a wobulated signal generator, was applied to both amplifiers. Identical





**CONFIDENTIAL**

amplitude detectors were used in the outputs of both amplifiers. The difference between the outputs of the detectors was used as an indication for aligning the second amplifier. It was found that the amplitude-frequency characteristics could be balanced within one percent over the entire pass-band. Since both the amplifiers were minimum-phase networks, the difference in phase delay through them could be computed from a knowledge of the difference between the amplitude-frequency characteristics and either characteristic. For these amplifiers, the maximum difference in phase delay was about 0.8 degree for a one percent difference in the pass-bands. Over the entire range of gain settings expected in the tests, the amplitude unbalance rarely exceeded 2 percent, indicating a maximum phase differential of less than 2 degrees.

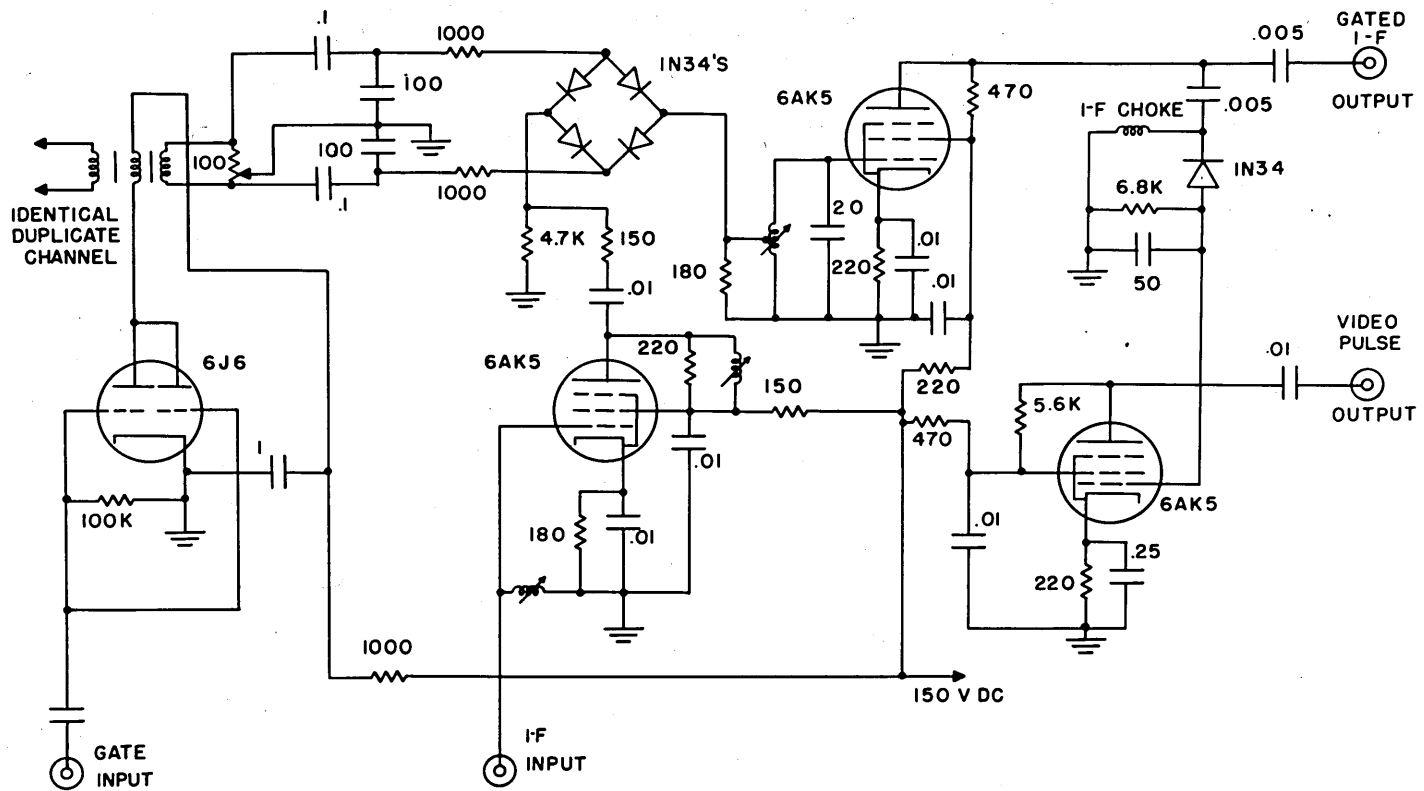
#### F-2 Gater and Amplitude Detector

A balanced gating circuit employing a ring of four 1N34 germanium diodes was used to render the system insensitive except during the time of the return of the desired echo. It was necessary to use a balanced circuit in order to avoid undesirable transients in tuned circuits following the gater. A pulse amplitude detector was included in the unit, following the gating circuit, in order to furnish a video pulse for the agc amplifier. Fig. F-2 is a schematic diagram of the gater and the amplitude detector.

The bandwidth of the gating circuit and the following buffer amplifier was kept greater than 6 mcps, so that spurious differential phase shifts would be tolerably small. Residual differential phase shifts were compensated by appropriate adjustment of the limiters of the phase measuring unit.

The attenuation through the gating circuit during the "off" time between pulses is more than 50 decibels greater than that during pulses.

**CONFIDENTIAL**



2 - CHANNEL BALANCED GATER

Fig. F-2

### F-3 Automatic Gain Control

The agc unit consists of a video pulse amplifier and pulse amplitude detector, followed by a low-pass filter with a 4-second time constant and an output buffer stage. A schematic of the unit is shown in Fig. F-3.

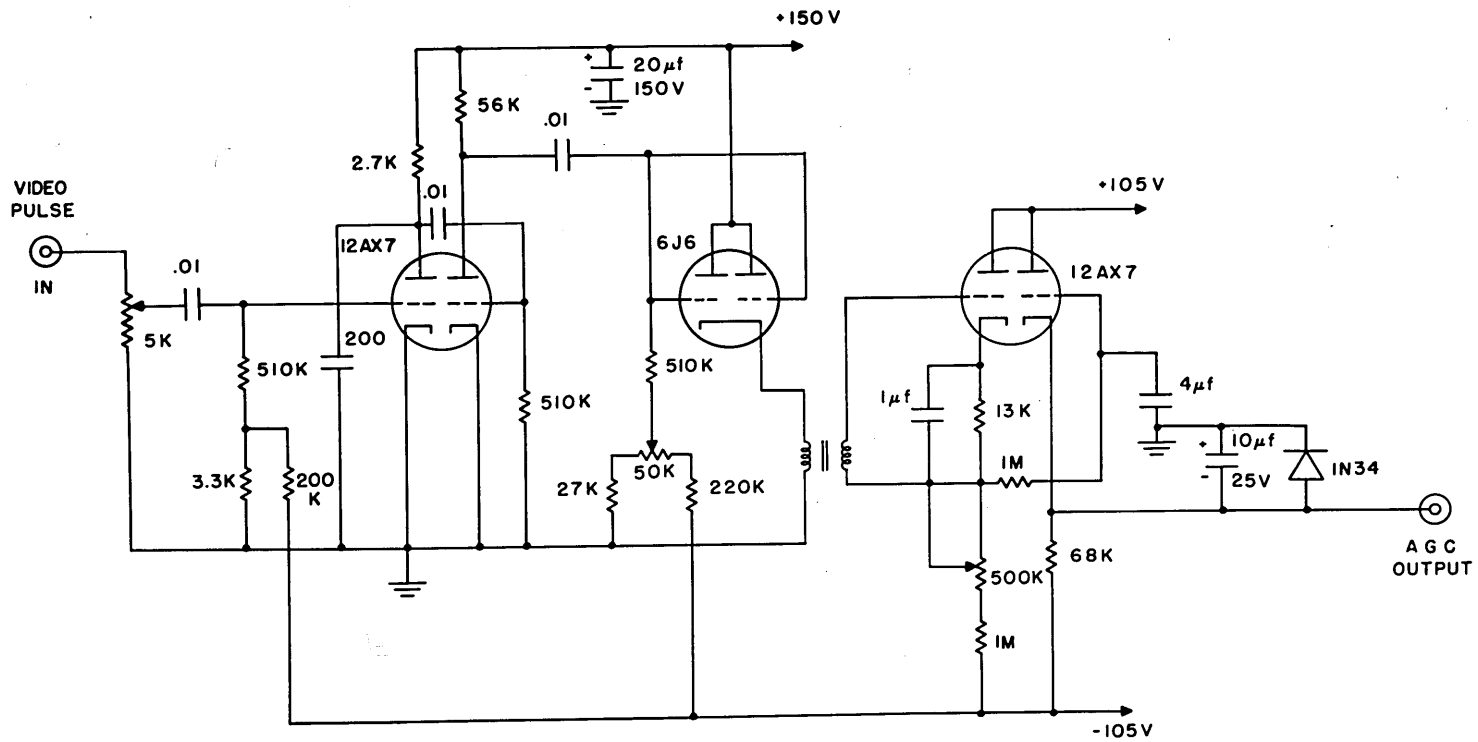
### F-4 Automatic Frequency Control

The automatic frequency control provides a direct voltage to the repeller of the klystron which is the local oscillator in the receiver, in order to keep the frequency of the klystron just 33 mcps away from the frequency of the transmitter. The afc unit consists of a 33-mcps i-f amplifier and frequency discriminator, which is followed by a direct-coupled amplifier which drives the repeller. A schematic of the unit is shown in Fig. F-4.

### F-5 Manually Tracked Range-gate Generator

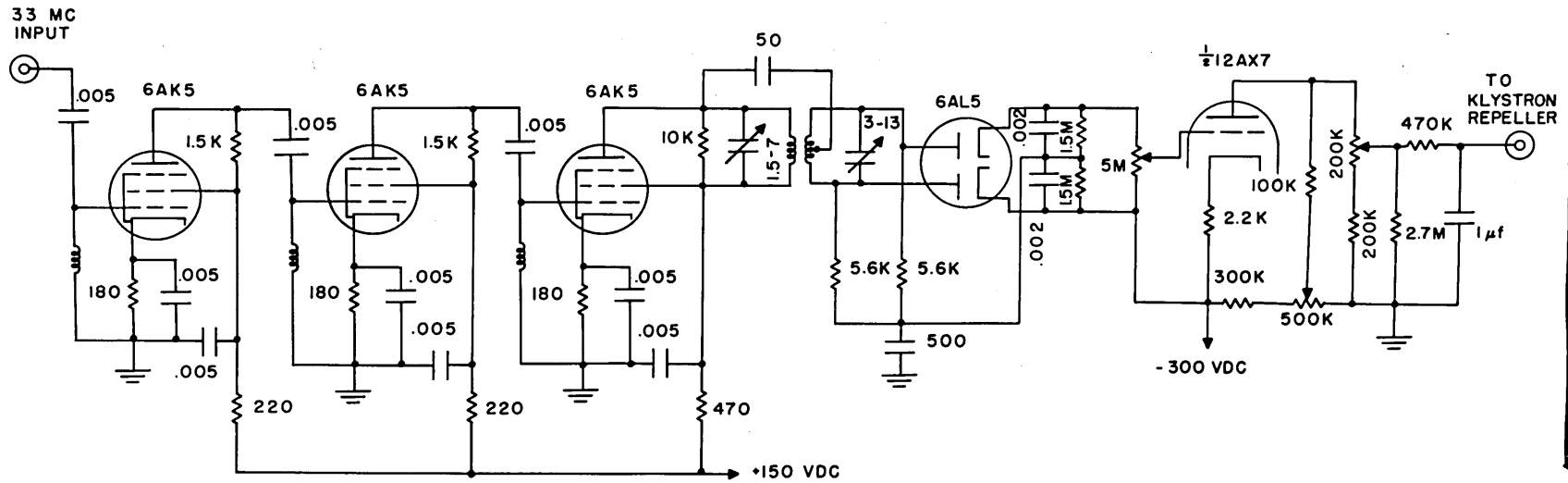
The range-gate generator for producing the pulses to operate the gater was manually adjusted to provide the proper delay in the range gate. The generator was triggered by a video pulse which was obtained directly from the transmitter over coaxial cable. The output of the generator was a 1.3-micro-second pulse having a flat top. The pulse could be delayed with respect to the trigger by any time between 0 and 70 microseconds, corresponding to target ranges between 0 and 6 miles. A schematic diagram of the unit is shown in Fig. F-5.

The adjustable time delay in the unit was achieved by comparing a manually controlled direct voltage with the saw-tooth voltage output from a phantastron. The phantastron was triggered by the input from the transmitter. A small voltage change at the output of the comparison diode occurred at the time when the direct voltage and the saw-tooth were equal. This change was used to fire the blocking oscillator which generated the range gate.



A G C AMPLIFIER AND FILTER

Fig. F-3



AUTOMATIC FREQUENCY CONTROL

Fig. F-4

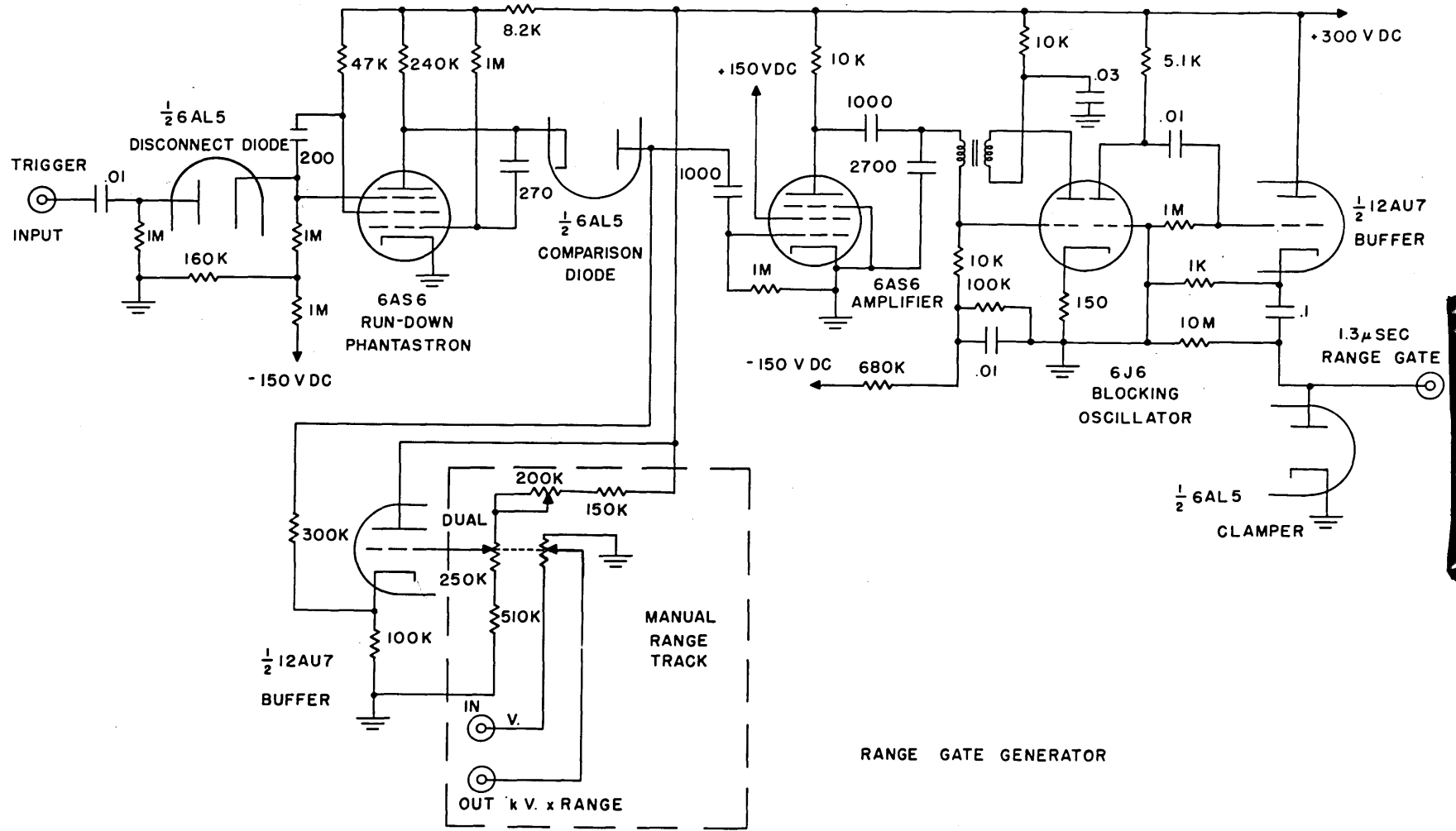


Fig. F-5

Because the phantastron output was a linear sawtooth, the magnitude of the manually controlled direct voltage was a linear function of target range. Therefore, it was possible to use a dual linear potentiometer in the manual control in order to multiply the output voltage from the phase measuring unit by range. An additional rheostat was needed in order to make the zero position of the dual potentiometer coincide with zero time delay.

#### F-6 Pregater

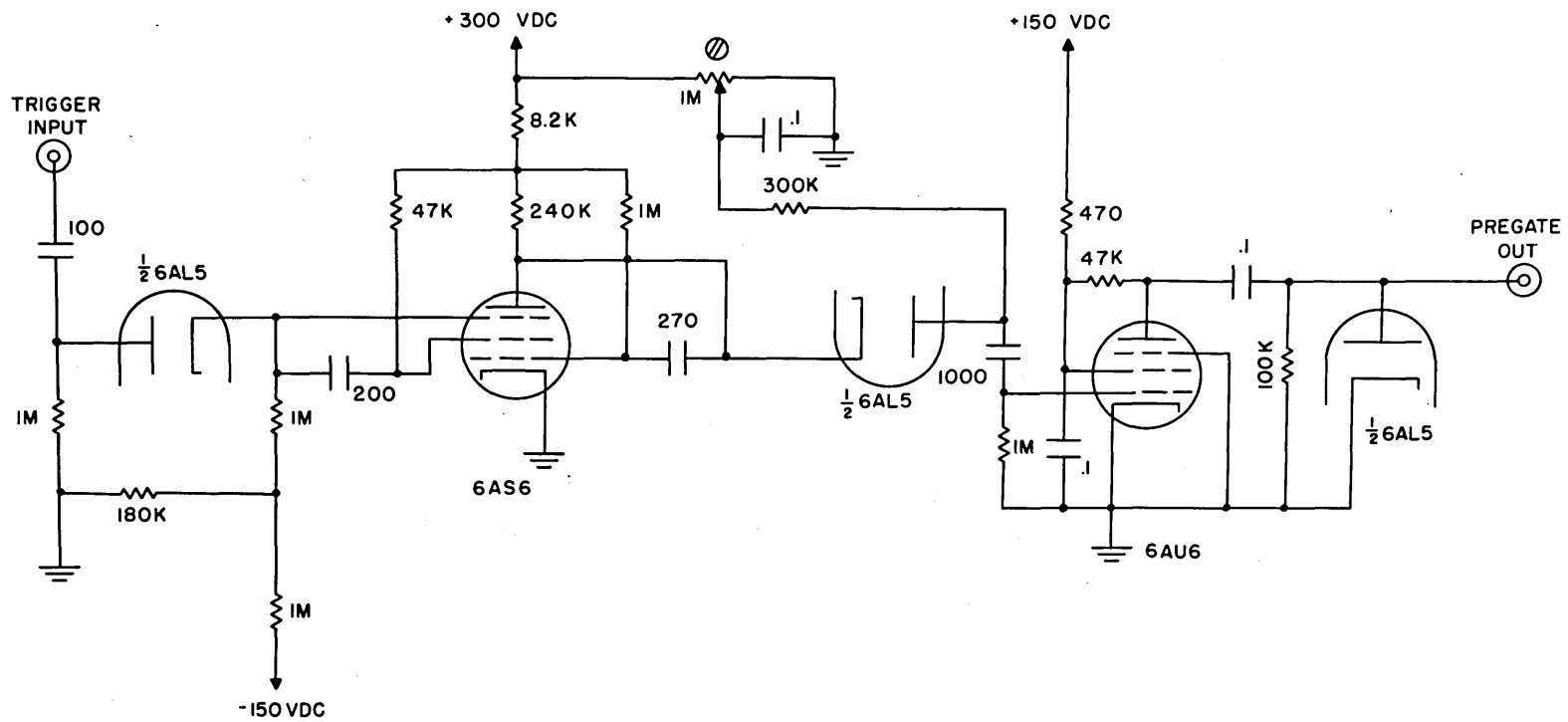
The pregater was used to generate a second range gate for removing from the inputs to the gater the strong signals due to nearby ground clutter. The second range gate, which was applied to the suppressor grids of the pentodes in the next-to-last stage of the i-f amplifiers, had a duration of 90 microseconds (8 miles) and an adjustable starting time. The circuit for obtaining the variable starting time was the same as the circuit for producing the delay in the range-gate generator. In operation the delay in the pregater was set at 7 microseconds, so that all echoes from targets within 0.6 miles were excluded. The schematic of the pregater is shown in Fig. F-6.

#### F-7 21-Mcps Oscillator

A crystal-controlled oscillator was used as the source of 21-mcps signals for the variable phase-shifter and the mixers in the i-f amplifiers. Three separate cathode followers are used as buffers for the three identical outputs. It was necessary to use separate buffers in order to obtain sufficient signal strength (0.5 volt) at the 21-mcps inputs of the i-f amplifiers, which had an impedance of 90 ohms. The schematic of the oscillator is shown in the lower part of Fig. F-7.

#### F-8 Mile Marker

The mile marker is a circuit for generating 1-microsecond pulses every



PREGATER  
 GIVING  
 10-MILE GATE WITH ADJUSTABLE  
 STARTING TIME

6-6



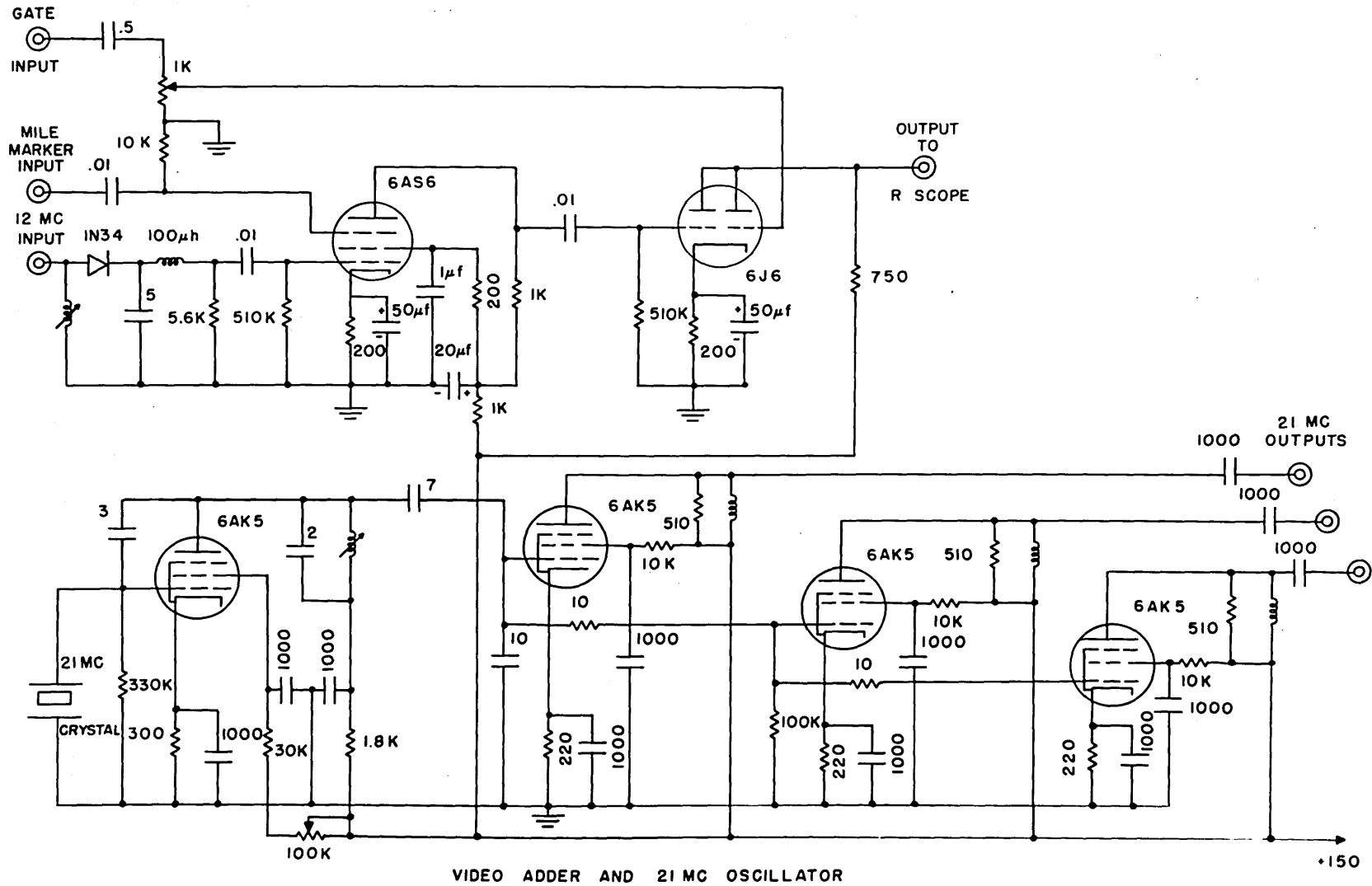


Fig. F-7

10.74 microseconds for a 100-microsecond interval following each firing of the r-f transmitter. These pulses were used to provide pips corresponding to 1-mile intervals on the range scope. A schematic diagram of the unit is shown in Fig. F-8.

The first twin triode of the mile marker is a one-shot multivibrator which produces a single 100-microsecond pulse that is started by the input trigger. The input trigger is the same video pulse from the transmitter that is used to trigger the range-gate generator. The first section of the second twin triode is an amplifier for the 100-microsecond pulse, which is applied with negative polarity to the grid of the second section. This triode has a dissipationless L-C tank with a resonant frequency of 93.1 kcps connected in its cathode circuit. During the pulse, the tank is unloaded, because the triode is cut off. The infinite Q of the tank is obtained by means of a Q-multiplier using half of the third twin triode. In the final stages, the sinusoidal tank voltage is amplified, squared, and differentiated, in order to obtain the desired output pulses. A switch in the output circuit is incorporated to furnish either positive or negative markers.

#### F-9 Video Adder

A video adding circuit was used to combine the three inputs to the vertical amplifier of the TS-34 range scope. The inputs were the range gate, the mile-marking pulses, and the output of the i-f amplitude detector. The amplitude detector was included in the adding circuit, of which a schematic diagram is shown in the upper part of Fig. F-7.

#### F-10 12-Mcps Limiter and Amplitude Detector of Phase Measuring Unit

Amplitude limiters were needed in the phase measuring unit to remove the fluctuations in the amplitudes of the 1-microsecond pulses from the i-f

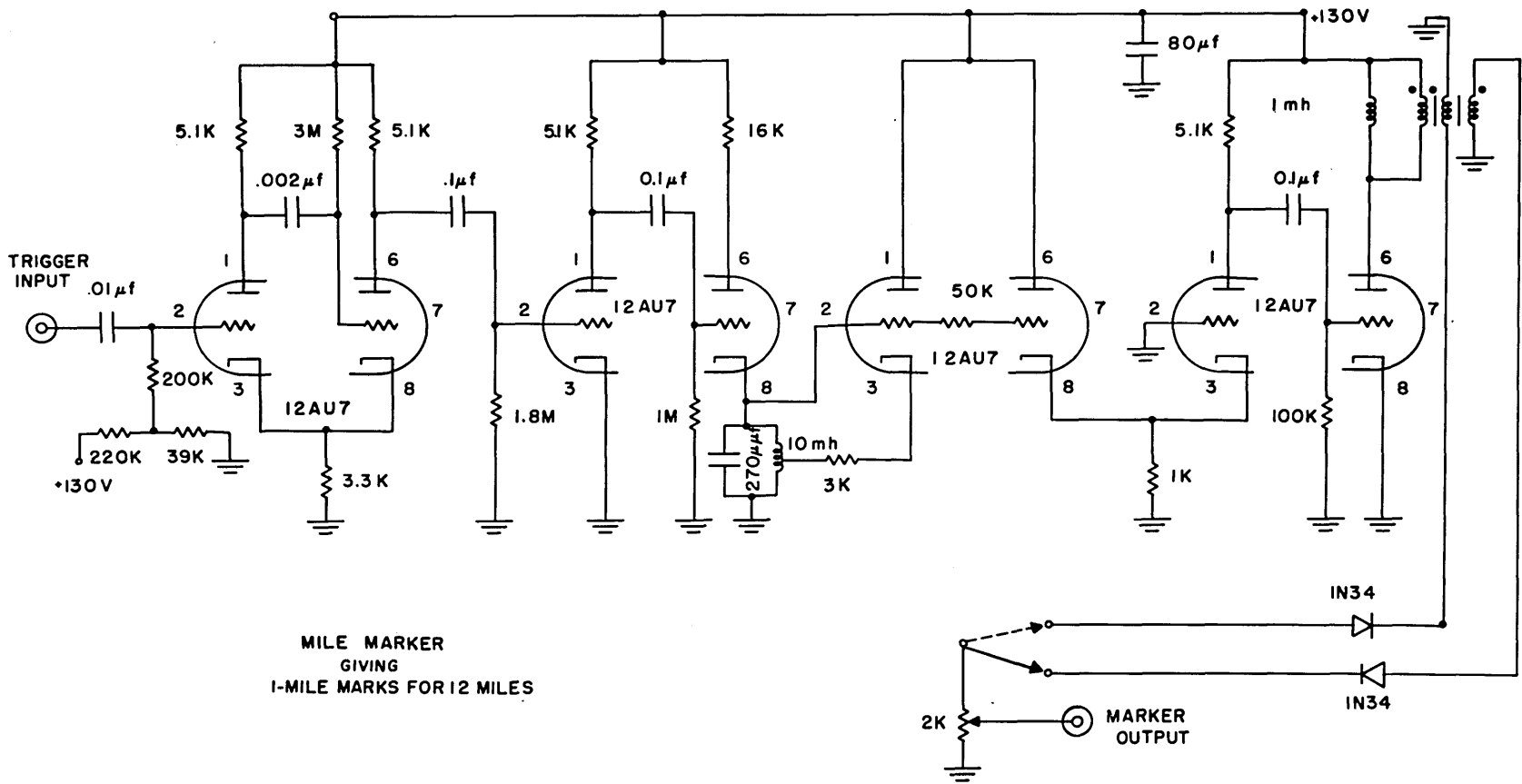


Fig. F-8

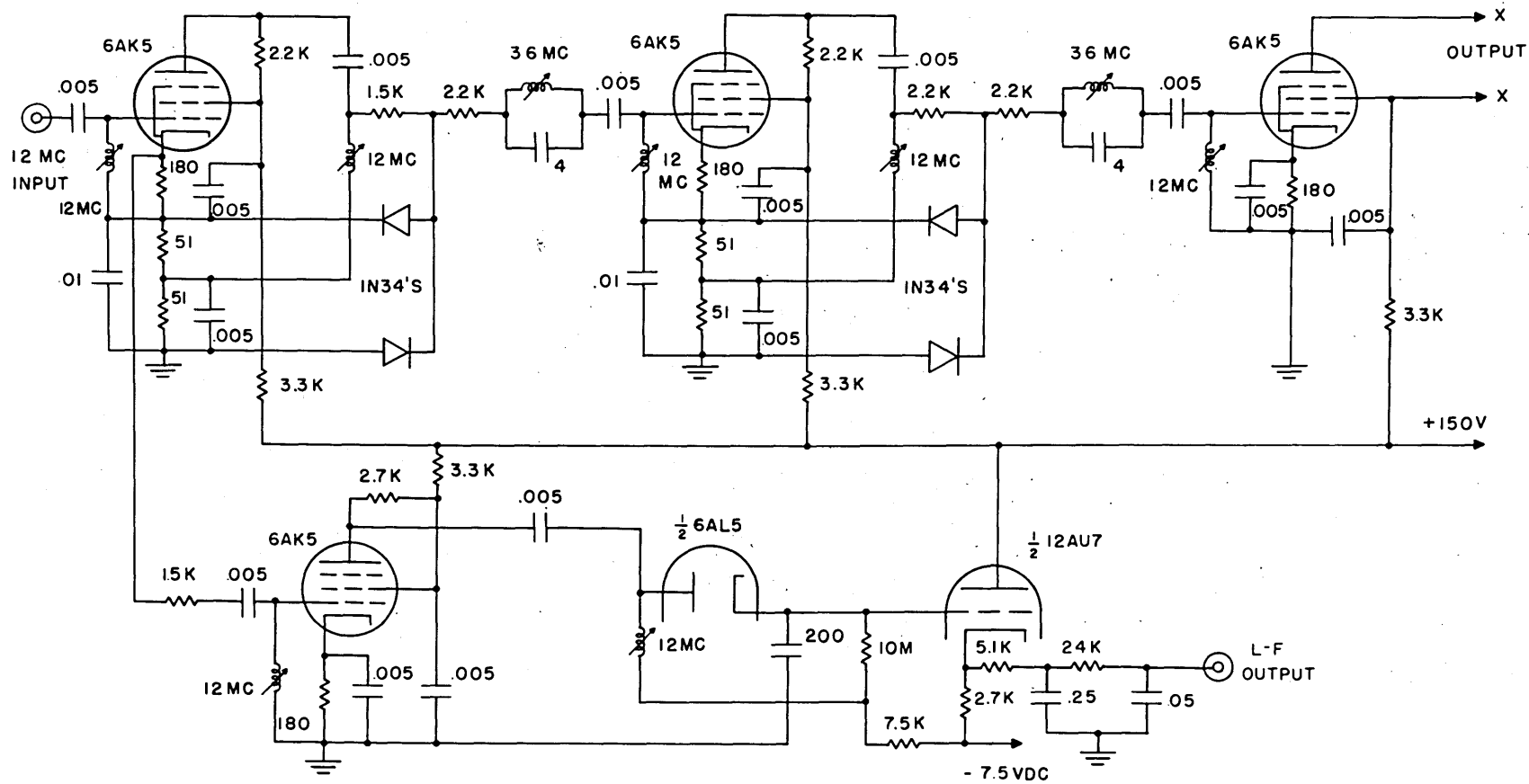
[REDACTED]

amplifiers, prior to phase detection. It was required that the difference in the phase delays through the two limiters be very small. However, it was not sufficient that the two limiters have the same phase-delay vs. input-amplitude characteristic, because the signal levels into the limiters were not necessarily equal. Each limiter had to be such that only very small variations in phase delay accompanied changes in input level over a voltage range of 20 to 1 (26 decibels). An amplitude detector was included with each limiter for the purpose of furnishing a direct voltage proportional to the pulsed signal amplitude at the input to the limiter. A schematic of the limiter and amplitude detector is shown in Fig. F-9.

Biased diodes were chosen as the basic elements in the limiters, because of the restrictions imposed by the nature of the pulsed signals. Since the duty cycle of the input was of the order of .001, the circuit could not be designed around any principle of charge retention, such as in grid limiting with class-C tube operation. Furthermore, bandwidths greater than 2 mcps were desired, because the pulses had a duration of only one microsecond. In the final design of the limiters, the pentode amplifiers were operated class A-1. Bias voltages for the diodes were obtained from the cathode circuits of the pentodes. The capacitance at the junction of each pair of diodes was kept at a minimum by means of isolating resistors and careful wiring layout; these precautions were necessary because the bandwidth of the circuit at this point had to be sufficiently great to permit the generation of a 12-mcps square wave.

A 36-mcps trap was needed to eliminate the third harmonic generated by the diodes. The amount of third harmonic that the diodes generate is a function of the signal level at the input to the limiter. Without the trap, the third harmonic was shifted in phase relative to the fundamental by the tuned circuit at the grid of the following tube. Consequently the zero-crossings

[REDACTED]



LIMITER, LINEAR AMPLITUDE DETECTOR AND BUFFER OF PHASE MEASURING UNIT

Fig. F-9

[REDACTED]

of the resultant wave at the grid could be shifted by varying the input level to the limiter, unless the third harmonic was eliminated.

Two stages of limiting were needed in each channel in order to obtain performance over the desired range of signal levels of 26 decibels.

Tests on the complete limiters showed that with careful adjustment the maximum differential phase delay could be kept in the neighborhood of 1 to 2 degrees when both inputs were equal and varied over the range from 0.1 to 2.0 volts rms. The change in phase delay through each limiter was higher, about 10 degrees maximum. This change was not thought to be serious, because under those conditions when the signals in the two channels are appreciably different, the phase differences associated with wander can be as great as 90 degrees or more.

When overall tests were made on the combination of the gater and the limiters, it was found that the maximum differential phase delay in the two channels could be kept under 3 degrees when both inputs were equal.

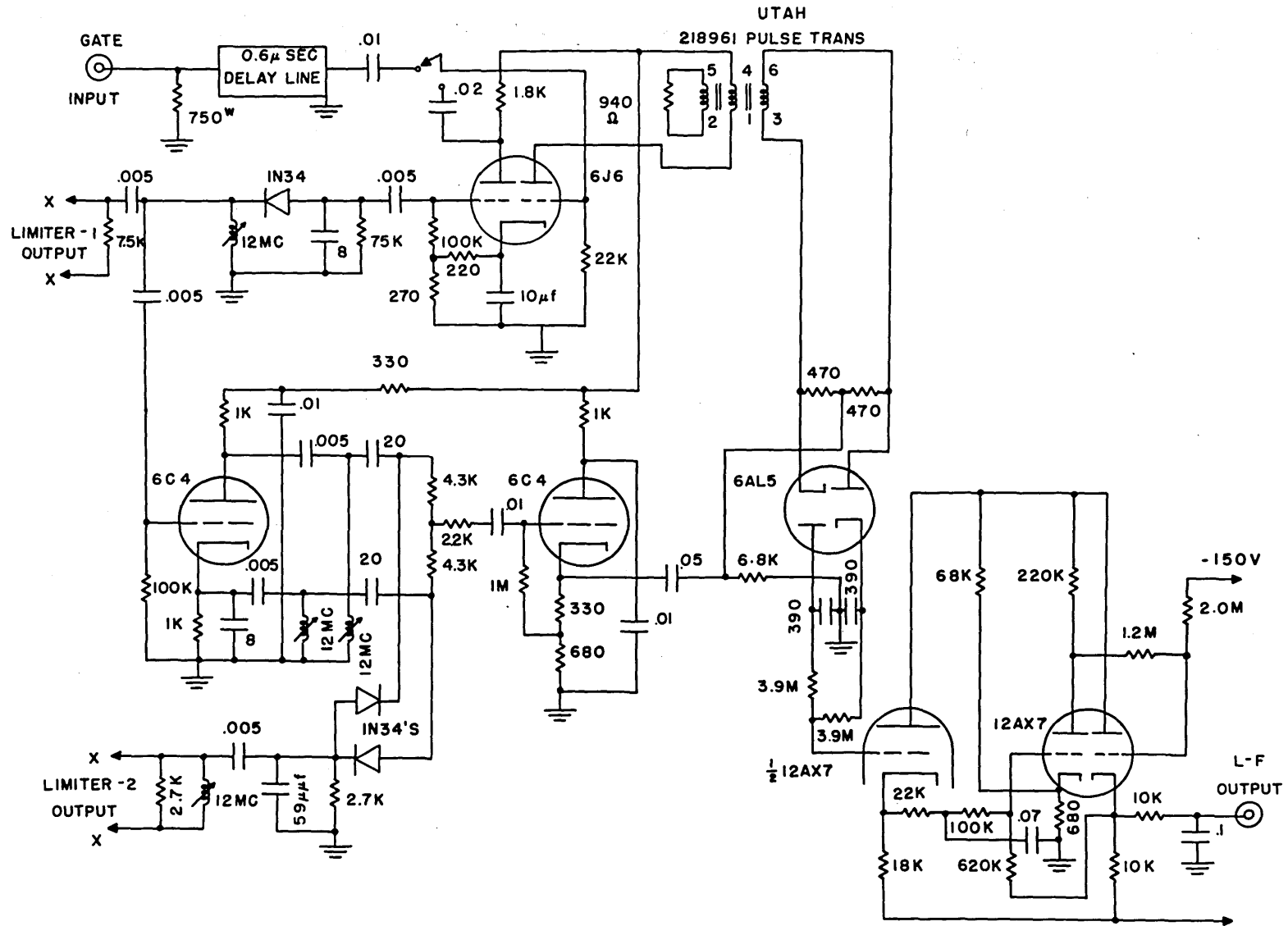
#### F-11 12-Mcps Pulse Phase Detector of Phase Measuring Unit

The phase detector of the 12-mcps phase measuring unit was built around a 6C4 triode phase splitter and a pair of 1N34 germanium diodes. The output of the phase detector was a pulse whose height was approximately equal to the cosine of the phase difference of the inputs. A circuit diagram of the phase detector is contained in the lower left part of the schematic in Fig. F-10.

The functions of phase detection and pulse stretching were kept separate in the phase measuring unit in order to insure that adequate bandwidth was maintained in the phase measurements without introducing distortion due to diagonal clipping in the diode circuits.

A capacitance of 59  $\mu\text{f}$  was added to the input which connects directly

[REDACTED]



PHASE DETECTOR, PULSE STRETCHER AND D-C AMPLIFIER  
OF PHASE MEASURING UNIT

Fig. F-10

[REDACTED]

to the two diodes, in order to equalize the bandwidths of the two inputs, and eliminate phase errors due to drift in the intermediate frequency. The input to the diodes has a much lower impedance than the input to the 6C4, which draws no grid current.

The levels of the two inputs to the phase detector were adjusted to give a characteristic of output vs. phase difference that was as near to a triangular waveform as could be obtained.

#### F-12 Pulse Stretcher and D-C Amplifier of Phase Measuring Unit

The function of this part of the phase measuring unit was to convert the video pulses from the phase detector into the direct voltage required by the recording equipment. The schematic diagram of the stretcher and amplifier is presented in the upper and right-hand portions of Fig. F-10.

The pulse stretcher, which was built around a 6J6 twin triode and a 6AL5 twin diode, operates in the following manner. At the same time that the desired pulse, of voltage  $V_d$ , comes out of the phase detector, a fixed amplitude pulse of similar duration, and of magnitude  $V_b$ , is produced in the output of the 6J6 amplifier. The latter pulse, which is called a bias pulse, causes both halves of the 6AL5 to conduct. During the pulse, the two capacitors on the output side of the 6AL5 are charged to voltages equal to  $V_d + \frac{1}{2}V_b$  and  $V_d - \frac{1}{2}V_b$ , respectively. Between pulses, one capacitor discharges into the other through the two 3.9 megohm resistors, so that the average of the two capacitor voltages remains constant at  $V_d$ , unless one of the diodes conducts. This possibility can be prevented if the bias pulse amplitude is made considerably larger than the maximum pulse from the phase detector. In order to prevent distortion when the amplitude of the desired pulse is varying at a high frequency (say 50 cps), it is necessary to insure that both diodes

[REDACTED]



conduct during every pulse. Satisfactory operation in this respect can also be guaranteed by keeping the pulse out of the 6J6 amplifier considerably larger than the pulse from the phase detector.

Two different methods were used for obtaining the bias pulse. In the S-band tests the pulse was obtained from an amplitude detector on one of the limiter outputs. It was found that with this method the pulse stretcher was occasionally triggered by ground clutter which occasionally appeared at the limiter outputs despite the range gater. In the second method, used in the X-band tests, the bias pulse was derived from the range gate directly, thereby eliminating any possibility of triggering on ground clutter. The range gate was passed through a 0.6-microsecond delay line, in order to compensate for the delay of the signal in the limiters and the associated tuned circuits.

The direct-coupled amplifier consisted of an input cathode follower, a triode amplifier, and an output cathode follower, with considerable negative feedback around the last two stages. Stable power supplies of +150, -7.5 and -150 vdc were required by the amplifier. The overall voltage gain of the amplifier was 5.

## APPENDIX G

## SPECTRUM ANALYZER

A swept-frequency spectrum analyzer was designed and constructed for reducing the data on wander and amplitude fluctuations recorded during the flight tests. The analyzer was adjusted to process data in a frequency bandwidth of 140 cps with a resolution of 10 cps. A block diagram of the analyzer is presented in Fig. 3-4 of Sec. 3.13. A schematic diagram of the entire analyzer is shown in Fig. G-1, which was laid out in roughly the same manner as the block diagram.

G-1 Special Circuits

Some of the circuitry used in the spectrum analyzer is rather unique in its design or characteristics. The more significant of these special circuits are described here.

The balanced mixer at the input to the analyzer was designed to have good balance stability over periods of an hour or more. The mixer includes a twin diode 6AL5 (V-3) and half a twin triode 12AU7 (V-4). The triode serves as a phase splitter for the carrier frequency of 20 kcps. The diodes are arranged in series between the two outputs of the phase splitter in such a manner that they both conduct simultaneously over half of each cycle of the carrier. During the conduction period, both diodes tend to connect (through 10 kilohm resistors) the low-frequency signal input to ground, thus serving as a chopper for the input signal. The low frequencies are then filtered from the chopped signal, leaving the desired sidebands with suppressed carrier. With the 6AL5 shock mounted, it was found that the drift in balance was generally less than 80 decibels below the signal from either output of the phase splitter over a period of one hour or more. In other words, in the



period of an hour, the maximum unbalance corresponded to an input of about 0.2 millivolts. It is suspected that the chief reason for this good stability is the presence of the 10-kilohm resistors in series with both diodes, their purpose being to mask variations in the forward impedance of the diodes.

The feedback stabilizers around the direct-coupled Dumont 304H Oscillograph were used to reduce the slow drift in the centering of the oscillograph pattern. The stabilizers provided equal attenuations between each deflecting plate of either pair and the corresponding input, while simultaneously inverting the signal from the appropriate plate. With the stabilizers in use, and with the oscillograph run off a regulated power line, the drift in the centering was less than 0.05 inches per hour.

The 5-second sweep circuit was designed to provide a linear, periodic sweep voltage with a period which could be varied between 1 and 15 seconds. A 4- $\mu$ f paper capacitor was charged through an adjustable resistance from the output of a cathode-coupled amplifier. The input of the amplifier was connected directly to the capacitor. The gain of the amplifier was adjusted to be exactly unity, with the result that the voltage across, and therefore the current through, the charging resistor was always constant. From the cathode of the cathode-coupled amplifier was taken the sweep output, and also a voltage which fired a single-shot multivibrator when the output reached a certain level. The multivibrator output was used to trigger a thyatron, which discharged the capacitor and caused the cycle to repeat. The maximum change in slope of the output waveform was less than two percent when the circuit was correctly adjusted.

#### G-2 Operational Procedure

A brief description of the methods of operating the analyzer is pre-

CONFIDENTIAL

sented here. Different methods were used for processing the S-band and the X-band data; for most applications, the latter method is highly preferable.

In the former method, the analyzer was swept as fast as possible. The sweep rate was limited only by the bandwidth of the narrow-band tuned amplifier. The optimum sweep rate was determined empirically by first noting the peak value of the spectrum of a sinusoidal input with the analyzer swept very slowly, and then increasing the sweep speed until the peak of the spectrum dropped about two percent. After the sweep rate was adjusted, the horizontal sweep length was set. Next the frequency scale of the sweep was set, using the internal calibration signal with the INPUT SEL switch set on CAL. This calibration signal is a half-wave rectified 60-cps wave, containing components at frequencies of 0, 60, and 120 cps. The tuning capacitor on the swept oscillator and the SWEEP  $\Delta F$  control, which regulates the sweep voltage applied to the reactance tube, were adjusted to place the three calibrating frequencies at the desired abscissas on the oscillograph face.

The next step in the adjustment, after the sweep controls were set, was to balance the mixer. First the BUFFER SWITCH was set either to connect or eliminate the buffer; in all the data reductions of this research program, the buffer was used. When the buffer is used, the gain control, a 50-kilohm potentiometer across the output of the switch, is set to the minimum gain consistent with the input to be analyzed, in order to minimize the effects of drift in the buffer. Then, with the INPUT SEL switch set to BAL, the resistive and capacitive balance controls were adjusted to minimize the vertical deflection of the oscillograph trace at zero frequency. Next the vertical position of the pattern was set to the desired point. The vertical gain control, in the cathode of the first triode section of V-8, was set so

CONFIDENTIAL

[REDACTED]

that the maximum signal which could be passed through the narrow-band amplifier without distortion gave a 2-inch deflection of the trace.

Finally, it was necessary to set the 1-megohm potentiometer controlling the level of the signal into the buffer. This adjustment was performed with the desired input signal applied to the DIRECT INPUT jack and with the INPUT SEL switch on DIR. The setting was considered correct when the spot on the oscillograph screen occasionally (perhaps once in five sweeps) went off scale in the vertical direction. After this control was set, the analyzer was ready for operation.

In the preferred method of operation, which was used for the X-band data, the analyzer was swept across the desired range of frequencies only once, a process requiring about 20 minutes. The first step in setting up the analyzer for this type of operation was to set the horizontal sweep length, after which the SWEEP  $\Delta F$  control was adjusted, using the calibrating signal, to give the desired frequency scale. Then the SWEEP SELECTOR switch was turned to its middle position, which connected the motor-driven sweep generator. The motor-driven potentiometer was turned manually until the oscillograph spot was at the point corresponding to zero frequency (or approximately 0.1 inches away, to compensate for the lag in the 15-second filter). The frequency vernier on the swept oscillator was adjusted to bring the zero-frequency peak of the spectrum to the abscissa where the spot was located. Next the INPUT SEL switch was set to BAL, and the mixer balanced using the two controls for the purpose, after which the vertical positioning of the pattern was set.

With the desired data supplied to the analyzer, the sweep potentiometer was manually set at the frequency of maximum spectral density in the data. Then the SWEEP SELECTOR was turned to its third position, which connected

[REDACTED]

**CONFIDENTIAL**

a 15-second filter in the vertical amplifier of the analyzer. The 1-megohm input potentiometer was adjusted so that the maximum steady-state deflection of the spot was approximately one inch for the amplitude spectra, or for the wander spectra, so that the desired calibration in  $\text{ft}/\sqrt{\text{cps}}$  was obtained. Finally, the sweep potentiometer was set to the starting position, the motor started, and the spectrum photographed.

**CONFIDENTIAL**

## APPENDIX H

## DATA RECORDING AND EDITING

The equipment and techniques employed in recording and editing the X-band data on wander and amplitude fluctuations will be described in this appendix. The method of editing the S-band data was fundamentally the same, although it was considerably more elaborate and less practicable. Only the recording equipment for the X-band data will be described, because it is felt that in view of its far greater compactness, dependability, and ease of operation, this equipment is much more useful in practice than the multi-channel equipment used for the S-band data.

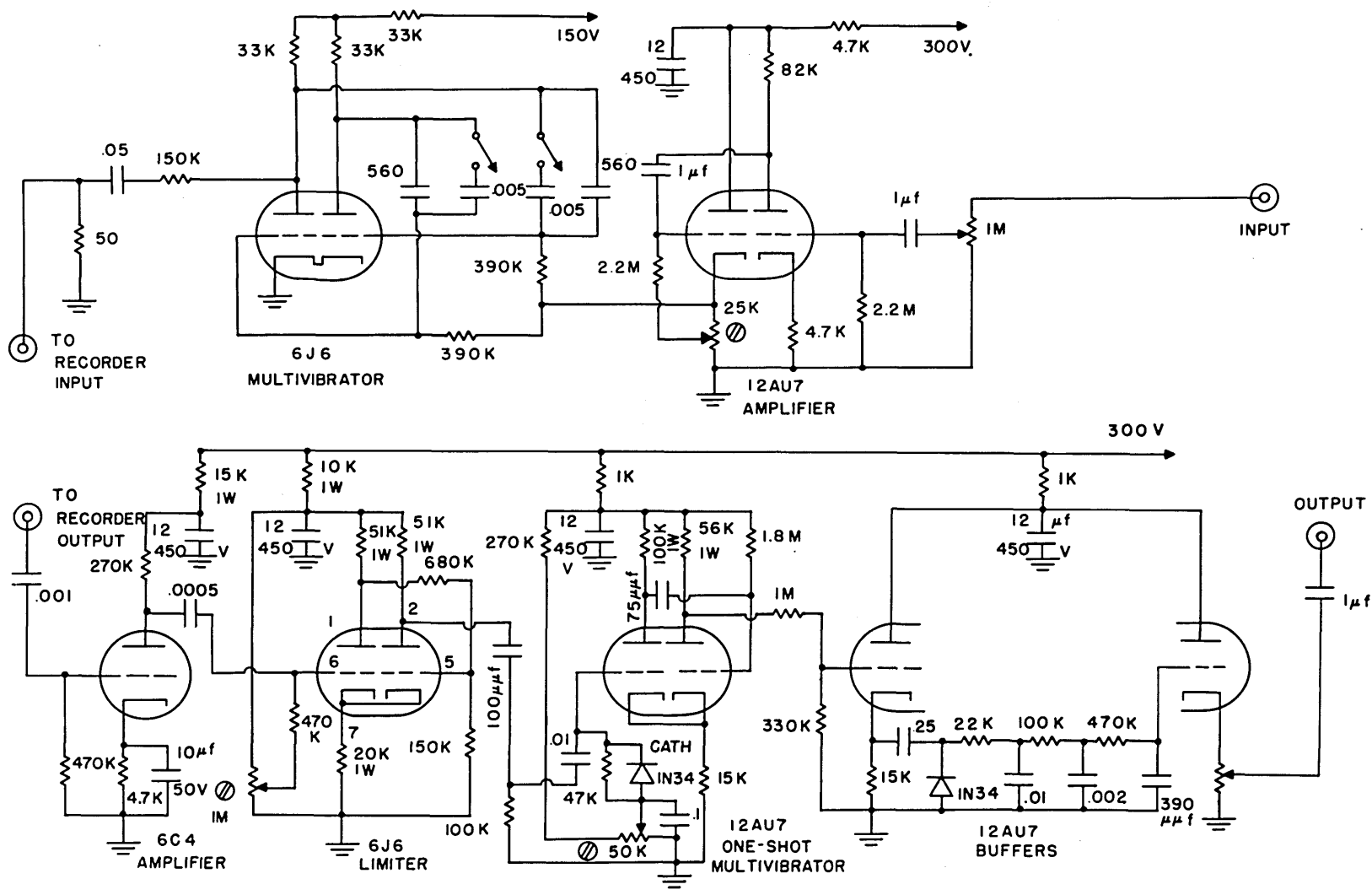
H-1 Recording and Playback Equipment\*

The original records of the flight-test data were made on magnetic tape using wide-band frequency modulators. Separate modulating circuits were required for the wander data and for the amplitude data. A schematic diagram of either of the modulators is shown in the upper part of Fig. H-1. The frequency-modulating unit consists simply of a capacitance-coupled amplifier with a lower half-power frequency of about 0.1 cps and a symmetrical, plate-coupled multivibrator. The grid resistors of the multivibrator are returned to the output of the amplifier. The average voltage out of the amplifier can be adjusted to set the center frequency of the carrier to a nominal value of 4 kcps. The peak deviation of the instantaneous carrier frequency was  $\pm 70$  percent of the center frequency. The attenuated output of the multivibrator was recorded onto magnetic tape moving at 7.5 inches per second,

---

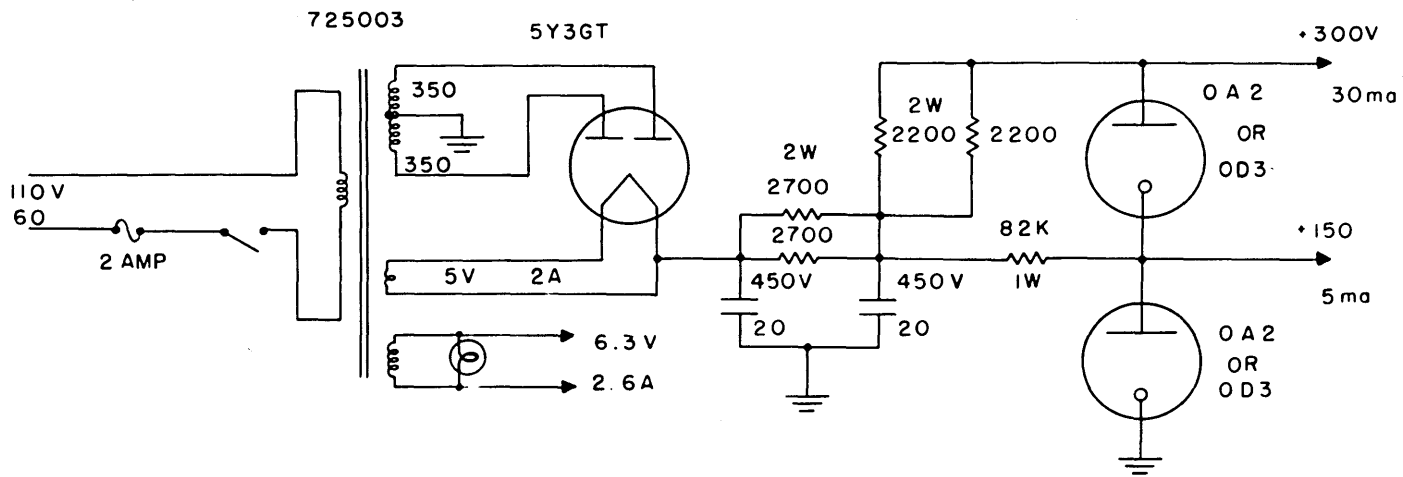
\*Credit is due Mr. P. E. Green, of the Research Laboratory of Electronics, for the basic design of the wide-band frequency modulator and demodulator.





FREQUENCY MODULATOR AND DEMODULATOR FOR RECORDING

Fig. H-1



POWER SUPPLY  
FOR  
FM DATA SPEEDUP SYSTEM

Fig. H-2


using a separate Magnecorder tape recorder for each type of data.

The frequency demodulator is essentially an electronic frequency meter based on the principle of cycle counting. A schematic of the demodulator is presented in the lower part of Fig. H-1. After the input to the demodulator is amplified in the first stage, it is amplitude limited in the second stage, which is in principle a positive-feedback amplifier with infinite gain. The square-wave output from the limiter is differentiated and used to trigger a one-shot multivibrator, which produces one 40-microsecond pulse for each cycle of the input to the demodulator. The base of the multivibrator output waveform is clamped at ground potential by a diode. A low-pass filter is used to extract the average value of the clamped waveform, which is directly proportional to the number of pulses per unit time, and therefore to the frequency of the input to the demodulator.

The overall bandwidth of the signal channel from the input of the modulator to the output of the demodulator is slightly greater than 100 cps. The maximum-signal-to-noise ratio of the entire channel is greater than 50 decibels.

The only adjustment in the modulator is the center-frequency control, which never required resetting during the flight tests. In the demodulator, there are two adjustments, namely, the limiter control and the pulse width control. The former control was found to require attention once during the 6-month period of data reductions, the latter control needed no attention.

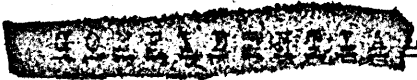
A switch was included in the modulator for lowering the average carrier frequency by a factor of 10. The lower frequency was used when the data was copied onto tape moving at 1.5 inches per second.

  
H-2 Editing Procedure

It was necessary to edit the data recorded during the flight tests in order to eliminate those sections which were not considered satisfactory. The two chief reasons for rejecting data were weak signal strength (the recorders were left on during a run even though the target may have been temporarily lost) and poor phase-shifter tracking.

The first step in selecting the data to be analyzed was to examine all the data visually. To this end, a cathode-ray oscillograph with a long-persistence (P-7) screen was used with a slow (1 inch per second) horizontal sweep speed. First the amplitude records were examined, and all regions with good signal strength noted. (The maximum system gain was not great enough to bring thermal noise up to the level of normal signal strength, so that it was easy to note when a target had been acquired.) Then the phase records were inspected, and all intervals with good tracking of the phase shifter noted. It was also possible to determine from the phase records when ground clutter was troublesome, because ground clutter produced a much different type of phase jitter from that of an aircraft. From these notes and the notes made during the flight test of target range and aspect, the sections of data that were to be analyzed were determined.

The next step was to make copies, on magnetic tape, of all the accepted data. Two Magnecorder tape recorders were used in the copying process, along with the frequency demodulator. The output of the playback machine was fed into the demodulator. The input for the recording Magnecorder was obtained from the output of the limiter in the demodulator. In this way amplitude fluctuations in the carrier from the original records were eliminated, without substantially increasing the random noise in the records. Copies were also



CONFIDENTIAL

made of the calibrations at the ends of each phase record. After the copying was completed, the copies were cut into the desired sections. Each section was spliced into a loop, to serve as a continuous source of data for the analyzer, and analyzed. The copies were played back at twice normal speed for these analyses, thus producing spectra with a 5-cps resolution over a 70-cps frequency band.

After all the individual sections of data had been analyzed, all the accepted data for a given target aspect with each aircraft were spliced together. The composite tapes were analyzed in the same manner as the individual sections. The spectra thus obtained are the broadband ones shown in Fig's. 3-6 through 3-11, 3-14, 3-15, and 3-18. When this process was completed, slow-speed copies were made of the composite records and the calibration tapes onto tape moving at 1.5 inches per second. For this purpose, the composite records were played back into the demodulator, and the demodulator output was filtered by a low-pass filter with a 20-cps half-power frequency. The filtered output was used as the source of signal for the frequency modulator, operated now with a 400-cps center frequency. The slow-speed copies were played back at 15 inches per second into the frequency demodulator and analyzed. The spectra thus obtained, having a 1-cps resolution over a bandwidth of 14 cps, are the detail spectra shown in the figures mentioned above.

CONFIDENTIAL

## APPENDIX J

## BIOGRAPHICAL NOTE

James B. Angell was born on December 25, 1924 in Staten Island, New York. He was graduated from grade school and the Tottenville High School on Staten Island, after which he attended Drake Business College in Perth Amboy, New Jersey for six months. He started at the Massachusetts Institute of Technology in September 1941, and received the degrees of Bachelor of Science and Master of Science from the Cooperative Course in Electrical Engineering in February 1946. During this period, he worked for four months each at the General Radio Company, Western Electric Company and Bell Telephone Laboratories.

On March 1, 1946 Angell joined the staff of the Research Laboratory of Electronics as a Research Assistant in Electrical Engineering, a position which he has held to the present time. During this period he was associated with the guidance group of Project Meteor, and was engaged principally in system analysis and the design of radar circuit components.

Angell is a member of Eta Kappa Nu, Tau Beta Pi, and Sigma Xi, an associate member of the American Institute of Electrical Engineers and the Institute of Radio Engineers, and a colleague in the American Guild of Organists.

## REFERENCES - I

- 1 - Chu, L.J., The Seeker Problem of Guided Missiles, Meteor Report No. 3, Mass. Inst. of Tech., Sept 15, 1946, Confidential.
- 2 - Meade, J. E., Hastings, A. E., and Gerwin, H. L., Noise in Tracking Radars, Naval Research Laboratory Report No. 3759, Nov. 15, 1950, Confidential.
- 3 - Keen, R., Wireless Direction Finding, Fourth Edition, Iliffe and Sons, Ltd., 1947
- 4 - Heiligtag, T., Causes of Errors in Direction Finding, Jahrbuch der Drahtlosen Telegraphie und Telephonie (Berlin), Vol. 21, 1923 pp. 77ff.
- 5 - Ridenour, L. N., Radar System Engineering, Radiation Laboratory Series, New York, 1947.
  - A - Section 3.7
  - B - Section 3.9
- 6 - Lawson, J. L., Detection of Propellor and Sambo Modulations, Radiation Laboratory Report S-10, May 16, 1944, Restricted.
- 7 - Lawson, Ashby, and Martin, Modulation of Radar Signals from Airplanes, Radiation Laboratory Report No. 914, March 28, 1946.
- 8 - Muchmore, R. B., and Weiss, L. H., Radar Echo Scintillation from P-80 and A-20 Airplanes, Hughes Aircraft Company Technical Memorandum No. 212, Nov. 30, 1948, Secret.
- 9 - Smith, R. N., and Hammel, J. E., Resolution of Individual Targets in a Formation of Aircraft by a Radar Set, Boeing Airplane Company Document No. D9068, March 31, 1948, Confidential.
- 10 - James, H. M., Nichols, N. B., and Phillips, R. S., Theory of Servo-mechanisms, Radiation Laboratory Series, Vol. 25, New York, 1947
  - A - Sections 6.6 to 6.10
  - B - Chapters 6, 7, and 8

[REDACTED]

REFERENCES - II

- 11 - Delano, R. H., Angular Scintillation of Radar Targets, Hughes Aircraft Company Technical Memorandum No. 233, April 24, 1950, Secret.
- 12 - Weiss, H. K., Analysis of Tracking Errors, Ballistics Research Laboratory Report No. 649, September 11, 1947, Confidential.
- 13 - Campbell, E. J., Radar Tracking Analysis, Radiation Laboratory Report No. 495, February 5, 1944, Restricted.
- 14 - Phillips and Boyd, Analysis of Tracking Errors of the MK56X System, Radiation Laboratory Report No. 884, March 1, 1946.
- 15 - Campbell, E. J., Analysis of Over-water Tracking, Radiation Laboratory Report No. 695, Feb. 12, 1945.
- 16 - Crout, P. D., and Bothwell, F. E., A Theoretical Treatment of Radar Target Return, Part 1, Radiation Laboratory Report No. 719, August 31, 1945, Restricted.
- 17 - Stibitz, G. R., Effect of Noise Interference on Radar Angle, Fairchild Engine and Airplane Corp. Report No. 1503, Sept. 29, 1948, Confidential.
- 18 - FM/CW Radar and Antiaircraft Missile Guidance, Raytheon Mfg. Co. Progress Report for the Period 1 October - 30 November 1950, Secret.
- 19 - Wiener, N., The Extrapolation, Interpolation and Smoothing of Stationary Time Series, John Wiley and Sons, New York, 1949.
- 20 - System and Radar Noise Analysis of Two-beam Command Guidance for MX-800, M. W. Kellogg Co. Report No. SPD 129, Dec. 1, 1947, Secret.
- 21 - Page, R. M., Accurate Angle Tracking by Radar, Naval Research Laboratory Report No. RA 3A 222A, Dec. 28, 1944, Confidential.
- 22 - Hearn, C. E., A General Analysis and Comparison of Monopulse Tracking Radars - - Thumper Project, General Electric Co. Report No. TR 55360, Nov. 10, 1947, Secret.
- 23 - Straiton, A. W., Brooks, F. E., LaGrone, A. H., and Tolbert, C. W., Operational Characteristics of Angle Separation Equipment, University



CONFIDENTIAL  
REFERENCES - III

- of Texas Electrical Engineering Research Laboratory Report No. 24,  
Jan. 17, 1949.
- 24 - Hamlin, E. W., Seay, P. A., and Gordon, W. E., A New Solution to the Problem of Vertical Angle-of-arrival of Radio Waves, Journal of Applied Physics, Vol. 20, March 1949, pp. 248-251.
- 25 - Uspensky, J. V., Introduction to Mathematical Probability, New York, 1937  
Chapter XIII, Sec. 6.
- 26 - Stratton, J. A., Electromagnetic Theory, New York, 1941.  
Chapter VI, Sec. 6.6, p. 360.
- 27 - Cookson, A. E. and Renhult, W. B., Jr., The Model II Pulse Seeker,  
Meteor Report No. 58, Mass. Inst. of Tech., July 12, 1950 Confidential.
- 28 - Seamans, R. C., Jr., Comparison of Automatic Tracking Systems for Interceptor Aircraft, M. I. T. Instrumentation Laboratory Doctorate Thesis, June 1951, Confidential.
- 29 - Davenport, W. B., Jr., A Study of Speech Probability Distributions,  
M. I. T. Research Laboratory of Electronics Report No. 148,  
August 25, 1950.
- 30 - Burington, R. S., Handbook of Mathematical Tables and Formulas,  
Sandusky, Ohio, 1940, p. 263
- 31 - Burington, p. 257.
- CONFIDENTIAL